

The University of Maine

DigitalCommons@UMaine

Electronic Theses and Dissertations

Fogler Library

Spring 5-2021

Nanocellulose Conduits for Enhanced Regeneration of Peripheral Nerve Injuries

Nicklaus R. Carter

nicklaus.carter@maine.edu

Follow this and additional works at: <https://digitalcommons.library.umaine.edu/etd>



Part of the [Biological Engineering Commons](#), [Biomaterials Commons](#), and the [Other Biomedical Engineering and Bioengineering Commons](#)

Recommended Citation

Carter, Nicklaus R., "Nanocellulose Conduits for Enhanced Regeneration of Peripheral Nerve Injuries" (2021). *Electronic Theses and Dissertations*. 3351.

<https://digitalcommons.library.umaine.edu/etd/3351>

This Open-Access Dissertation is brought to you for free and open access by DigitalCommons@UMaine. It has been accepted for inclusion in Electronic Theses and Dissertations by an authorized administrator of DigitalCommons@UMaine. For more information, please contact um.library.technical.services@maine.edu.

NANOCELLULOSE CONDUITS FOR ENHANCED REGENERATION OF PERIPHERAL NERVE INJURIES

By

Nicklaus Carter

B.S. University of Maine, 2015

A DISSERTATION

Submitted in Partial Fulfillment of the

Requirements for the Degree of

Doctor of Philosophy

(in Biomedical Engineering)

The Graduate School

The University of Maine

May 2021

Advisory Committee:

David J. Neivandt, Professor of Chemical and Biomedical Engineering, Advisor

Douglas Bousfield, Professor of Chemical Engineering

Benjamin Harrison, Assistant Professor of Biomedical Science

Caitlin Howell, Assistant Professor of Biomedical Engineering

Paul Sweetnam, Founder and CSO of Redux Therapeutics

Copyright 2021 Nicklaus Carter

NANOCELLULOSE CONDUITS FOR ENHANCED REGENERATION OF PERIPHERAL NERVE INJURIES

By Nicklaus Carter

Dissertation Advisor: Dr. David J. Neivandt

An Abstract of the Dissertation Presented
in Partial Fulfillment of the Requirements for the
Degree of Doctor of Philosophy
(in Biomedical Engineering)
May 2021

ABSTRACT

Peripheral neuropathy is estimated to afflict 20 million people in the United States. Most cases of neuropathy result from physical injuries and trauma arising from automobile accidents and war. Peripheral nerves have the intrinsic ability to regenerate over time, bridging the injury gap. However native regeneration is limited to a distance of only a few millimeters. Current methods utilized to assist in the regeneration of peripheral nerves over distances exceeding those amenable to native repair include nerve autografts and allografts, and implantation of conduits. Nerve autografts are regarded as the most effective method but require a second surgical site to access a donor nerve. Allografts are similar to autografts except the donor nerve is from another individual and the patient therefore requires a prolonged regimen of immunosuppressant medication. Conduits currently on the market have equal or lower success rates relative to nerve autografts. Issues that arise with the use of the current generation of conduits involve foreign body reaction, and the potential need for second surgeries to remove the conduit. It is proposed that a biocompatible material such as nanocellulose may serve as a viable alternative conduit construction material. The current work determined means by which conduits comprising cellulose nanofibrils may be produced and evaluated their efficacy in regeneration after a sciatic nerve injury in a murine model. Development of a GMP compliant process to produce such cellulose nanofibril conduits was completed and a tolerability study was conducted in non-human primates.

ACKNOWLEDGEMENTS

First, I would like to thank Dr. David Neivandt for his dedication and advisement that began back in the first year of my undergraduate college experience. As an instructor he was devoted to ensuring his students would succeed in the program. As an advisor he has been both persistent and supportive through every step of my graduate school experience. I attribute much of my successes in college to his mentorship.

I would like to express my appreciation to those serving on my thesis committee Dr. Douglas Bousfield, Dr. Benjamin Harrison, Dr. Caitlin Howell, and Dr. Paul Sweetnam for continually providing support for me during my research through numerous insightful discussions.

I also would like to thank our collaborators at various organizations such as the Eggan Laboratory of Harvard University (Dr. Kevin Eggan, Dr. Maura Charlton, and Dr. Joanie Mok), Nano Terra (Dr. Paul Sweetnam), and the Southwest National Primate Research Center. Without these collaborations this research would not have been possible.

I am very grateful to those of The Process Development Center at the University of Maine, Mike Bilodeau, Mark Paradis, Dr. Donna Johnson, Keith Hodgins, and Nick Hill for their patience and assistance in learning several processes and techniques of the paper industry.

It was my pleasure to work with and train a lot of great students during this research and as such express my gratitude to Marley Dewey, Conor Millard, Roxanne Castillo, Mary Bourque, Izzie Grant, and Julia Towne.

Last but not least, I would like to thank my family and friends for always keeping the pressure on and providing plenty of support over the years. I am grateful to all who have been a part of this process and assisted in making this a reality.

TABLE OF CONTENTS

ABSTRACT	iii
ACKNOWLEDGEMENTS	iv
TABLE OF FIGURES.....	ix
TABLE OF TABLES.....	xi
TABLE OF EQUATIONS.....	xii
CHAPTER ONE PERIPHERAL NERVOUS SYSTEM ANATOMY, PHYSIOLOGY AND NATIVE REPAIR MECHANISMS	1
1.1 PERIPHERAL NERVOUS SYSTEM.....	1
1.2 PERIPHERAL NERVE ANATOMY.....	1
1.3 ACTION POTENTIALS AND PROPAGATION	2
1.4 SALTATORY CONDUCTION	4
1.5 WALLERIAN DEGENERATION	5
1.6 AXONAL REGENERATION	7
1.7 LIMITATIONS OF NATIVE PERIPHERAL NERVE REGENERATION	8
CHAPTER TWO SURGICAL INTERVENTIONS TO PROMOTE PERIPHERAL NERVE REPAIR	10
2.1 FREQUENCY AND SEVERITY OF PERIPHERAL NERVE INJURIES	10
2.2 CURRENT APPROACHES TO PERIPHERAL NERVE REPAIR.....	11
2.2.1 NEURORRHAPHY	11
2.2.2 GRAFTS.....	12
2.2.3 CONDUITS	12
2.3 LIMITATIONS OF CURRENT METHODS OF PERIPHERAL NERVE REPAIR	15
2.3.1 NEURORRHAPHY	16
2.3.2 GRAFTS.....	16
2.3.3 CONDUITS	17
2.4 DESIRED PROPERTIES OF NEURAL CONDUITS	21
2.5 TESTING OF THE EFFICACY OF CONDUIT ENTUBULATION FOR PERIPHERAL NERVE REPAIR	23
2.6 THE POTENTIAL OF CELLULOSE NANOFIBER FOR NEURAL CONDUIT PRODUCTION	24
CHAPTER THREE EXPERIMENTAL METHODS	26
3.1 PULP PREPARATION	26
3.2 CONFIGURATION OF CONTINUOUS REFINEMENT VIA A SUPERMASSCOLLOIDER	26
3.3 SMC OPERATION	29
3.4 CNF SLURRY CHARACTERIZATION.....	31

3.5 CNF MORPHOLOGICAL DETERMINATION/DEVELOPMENT OF CALIBRATION CURVES.....	32
3.6 SHEET FORMATION	34
3.7 CNF SHEET THICKNESS MEASUREMENTS	35
3.8 TENSILE STRENGTH MEASUREMENTS	35
3.9 AIR PERMEABILITY MEASUREMENTS	36
3.10 OXYGEN PERMEABILITY MEASUREMENTS.....	36
3.11 DIFFUSION COEFFICIENT OF GLUCOSE IN A CELLULOSE NANOFIBER SHEET.....	37
3.12 CNF SHEET POROSITY	40
3.13 CNF SHEET TOPOGRAPHY	41
3.14 CONDUIT FORMATION.....	41
3.15 PACKAGING	42
3.16 ETHYLENE OXIDE STERILIZATION	43
3.17 CELL CULTURE AND CELL GROWTH STUDIES.....	44
3.18 CONDUIT IMPLANTATION.....	45
3.19 GRIP STRENGTH ANALYSIS OF MICE	47
3.20 END OF LIFE ANALYSIS.....	47
3.21 SLIDE PREPARATION AND STAINING	49
CHAPTER FOUR CELLULOSE NANOFIBER SHEET CHARACTERIZATION AND NEURAL CONDUIT DEVELOPMENT	52
4.1 CNF SHEET CHARACTERIZATION	52
4.1.1 SHEET THICKNESS	52
4.1.2 TENSILE STRENGTH TESTING.....	53
4.1.3 SURFACE PROFILOMETRY MEASUREMENTS	53
4.1.4 CNF SHEET TRANSPARENCY	55
4.1.5 AIR PERMEABILITY OF CNF SHEETS.....	56
4.1.6 MERCURY POROSIMETRY OF CNF SHEETS	57
4.1.7 OXYGEN PERMEABILITY OF CNF SHEETS	58
4.2 CNF CONDUIT DEVELOPMENT	59
4.3 CONDUIT SEAL EMPLOYING NON-MECHANICAL MEANS	59
4.4 EVALUATION OF CONDUIT SEAL INTEGRITY.....	60
4.5 EVALUATION OF THE EFFECT OF CNF SHEET THICKNESS ON CONDUIT INTEGRITY	62
4.6 MECHANICAL INTERLOCKING CNF CONDUITS.....	64
4.7 EVALUATION OF THE STABILITY OF MECHANICALLY INTERLOCKED CNF CONDUITS	65

4.8 CONCLUSION	66
CHAPTER FIVE CELLULAR COMPATIBILITY WITH CELLULOSE NANOFIBER AND <i>IN VIVO</i> STUDIES	68
5.1 CELLULAR PROLIFERATION ON, AND COMPATIBILITY WITH, CELLULOSE NANOFIBER SHEETS	68
5.2 INTRODUCTION TO <i>IN VIVO</i> STUDIES	71
5.3 MURINE STUDY ONE: SCIATIC NERVE TRANSECTION WITH NO TISSUE RESECTION	71
5.4 MURINE STUDY TWO: SCIATIC NERVE TRANSECTION WITH TISSUE RESECTION AND CNF CONDUIT LENGTH VARIATION	73
5.5 HISTOLOGICAL ANALYSIS	77
5.6 NON-HUMAN PRIMATE STUDY: CNF TOLERABILITY	80
5.7 CONCLUSION	82
CHAPTER SIX FINITE ELEMENT ANALYSIS OF DIFFUSION AND DISTRIBUTION OF OXYGEN AND GLUCOSE WITHIN CNF PERIPHERAL NERVE CONDUITS.....	84
6.1 INTRODUCTION:	84
6.2 COMSOL MULTIPHYSICS® FINITE ELEMENT ANALYSIS.....	86
6.3 OXYGEN DIFFUSION AND DISTRIBUTION	88
6.3.1 EFFECT OF CONDUIT DIAMETER ON OXYGEN CONCENTRATION AND DISTRIBUTION	90
6.3.2 EFFECT OF CONDUIT WALL PERMEABILITY ON OXYGEN CONCENTRATION AND DISTRIBUTION.....	94
6.3.3 EFFECT OF CONDUIT LENGTH EFFECT ON OXYGEN CONCENTRATION AND DISTRIBUTION.	100
6.4 GLUCOSE DIFFUSION AND DISTRIBUTION.....	104
6.4.1 EFFECT OF CONDUIT DIAMETER ON GLUCOSE CONCENTRATION AND DISTRIBUTION.....	106
6.4.2 EFFECT OF CONDUIT LENGTH ON GLUCOSE CONCENTRATION AND DISTRIBUTION	109
6.4.3 EFFECT OF CONDUIT WALL PERMEABILITY ON GLUCOSE CONCENTRATION AND DISTRIBUTION.....	114
6.5 CONCLUSIONS OF FINITE ELEMENT ANALYSIS MODELING OF OXYGEN AND GLUCOSE CONCENTRATIONS AND DISTRIBUTIONS WITHIN A CNF PERIPHERAL NERVE CONDUIT	117
CHAPTER SEVEN CONCLUSIONS.....	119
REFERENCES.....	125
APPENDIX	134
A1: CLEANROOM DESCRIPTION	134
A2: CLEANROOM BLUEPRINTS/DIAGRAMS.....	137
A3: GMP/GLP-BASED PROTOCOLS DOCUMENT	139
SCOPE AND APPLICABILITY	140
SUMMARY OF METHOD.....	141

CNF-SOP-01 CELLULOSE PULP STORAGE	142
CNF-SOP-02 GOWNING PROTOCOL	146
CNF-SOP-03 PULP SUSPENSION	150
CNF-SOP-04 CNF PRODUCTION	154
CNF-SOP-05 REFINER SYSTEM CLEANING	163
CNF-SOP-06 SLURRY FIBER ANALYSIS	167
CNF-SOP-07 CNF SHEET PRODUCTION	173
CNF-SOP-08 CNF CONDUIT PRODUCTION	177
CNF-SOP-09 GENERAL MAINTENANCE AND CLEANING	183
CNF-SOP-10 LABELING PROTOCOLS	187
CNF-SOP-11 STABILITY STUDIES	194
CNF-SOP-12 PRODUCT PACKAGING	198
A4: GLUCOSE DIFFUSION COEFFICIENT	202
A5: STATISTICAL ANALYSES FOR COMPARISONS	203
STATISTICAL ANALYSIS FOR COMPARISONS OF TENSILE STRENGTH	203
STATISTICAL ANALYSIS FOR COMPARISONS OF SURFACE ROUGHNESS	204
A6: VARIOUS CNF CONDUIT DESIGNS AND CNF RELATED DEVICES	207
A7: MURINE STUDIES AVERAGE DATA	210
MURINE STUDY 1 – AVERAGE GRIP STRENGTH DATA	210
MURINE STUDY 2 – GROUP 1 AVERAGE GRIP STRENGTH DATA	211
MURINE STUDY 2 – GROUP 1 AVERAGE GRIP STRENGTH DATA (CONT.)	212
MURINE STUDY 2 – GROUP 2 AVERAGE GRIP STRENGTH DATA	213
MURINE STUDY 2 – GROUP 2 AVERAGE GRIP STRENGTH DATA (CONT.)	214
MURINE STUDY 2 – GROUP 3 AVERAGE GRIP STRENGTH DATA	215
MURINE STUDY 2 – GROUP 3 AVERAGE GRIP STRENGTH DATA (CONT.)	216
MURINE STUDY 2 – GROUP 4 AVERAGE GRIP STRENGTH DATA	217
MURINE STUDY 2 – GROUP 4 AVERAGE GRIP STRENGTH DATA (CONT.)	218
MURINE STUDY 2 – GROUP 5 AVERAGE GRIP STRENGTH DATA	219
MURINE STUDY 2 – GROUP 5 AVERAGE GRIP STRENGTH DATA (CONT.)	220
MURINE STUDY 2 – WEIGHT TRENDS	221
BIOGRAPHY OF THE AUTHOR	222

TABLE OF FIGURES

Figure 1: Peripheral Nerve Structure	2
Figure 2: Action Potential Propagation.....	3
Figure 3: Saltatory Conduction of Action Potentials.....	4
Figure 4: Wallerian Degeneration and Axonal Regeneration	6
Figure 5: Methods of Neurorrhaphy.....	11
Figure 6: Method of Entubulation	13
Figure 7: Supermasscolloider Refining System	27
Figure 8: Supermasscolloider Refining System Components	29
Figure 9: Viscosity Characteristics of CNF Production by Percent Fines.....	31
Figure 10: MorFi Fiber Characteristic Analysis.....	33
Figure 11: Correlation of Energy and Fines.....	34
Figure 12: Glucose Diffusion Experiment.....	38
Figure 13: Glucose Hexokinase Assay Standard Curve	39
Figure 14: Mechanical Interlock Design.....	42
Figure 15: Zone Analysis of Tissue Sections.....	49
Figure 16: Tensile strength testing of CNF sheets	54
Figure 17: Surface Roughness Measurement Results.....	55
Figure 18: CNF Sheet Transparency	56
Figure 19: Mercury Porosimetry Results	57
Figure 20: MOCON Oxygen Permeability Results	58
Figure 21: Third Conduit Stability Study Results at 24 hours.....	65
Figure 22: Cellular Attachment Modification Study	69
Figure 23: First Murine Study Grip Strength Results	72

Figure 24: Second Murine Study Group Characteristics	74
Figure 25: Second Murine Study Grip Strength Results.....	76
Figure 26: Hematoxylin and Eosin Stain of Conduit Containing Tissue Section	77
Figure 27: Calcofluor White Stain of Conduit Containing Tissue Section	78
Figure 28: Luxol Fast Blue Stain of Peripheral Nerve Section	79
Figure 29: Histology of Non-Human Primate (Subject #2) Neural Tissue and Suture Material.....	81
Figure 30: COMSOL Nerve and Conduit Model	87
Figure 31: COMSOL Modeling Locational Analysis	87
Figure 32: Extrapolation of Oxygen Permeability from MOCON Analyses	89
Figure 33: Oxygen concentration profiles for lowest and highest nerve to conduit diameter ratios	91
Figure 34: Oxygen Modeling with Variable Nerve to Conduit Diameter Ratio.....	92
Figure 35: Oxygen Concentration with Varied Nerve to Conduit Diameter Ratio.....	94
Figure 36: Oxygen Concentrations with Variation of Measured Conduit Permeability	96
Figure 37: Oxygen Concentration with Variation of ISF-Based Conduit Permeability.....	97
Figure 38: Oxygen Modeling with Variable Conduit Length	101
Figure 39: Oxygen Concentration Plateau Profiles	103
Figure 40: Glucose Concentration Profiles of a 16 mm Length Conduit.....	107
Figure 41: Glucose Concentration Profiles of a 12mm Length Conduit.....	110
Figure 42: Glucose Concentration Profiles of a 0.70:1.00 Nerve-Conduit Diameter Ratio Conduit.....	112
Figure 43: Glucose Concentration Profiles of a 1.00:1.00 Nerve-Conduit Diameter Ratio Conduit.....	113
Figure 44: Glucose Concentration Profiles of a Conduit with Varied Conduit Permeability	116

TABLE OF TABLES

Table 1: Nerve Injury Classifications	10
Table 2: FDA Approved Peripheral Nerve Repair Devices	20
Table 3: Sample of Pre-Clinical Studies Using Neural Conduits	24
Table 4: Hematoxylin and Eosin Staining Procedure	50
Table 5: Sheet Thickness Analysis	52
Table 6: First Conduit Stability Study Results at 24 Hours	61
Table 7: First Conduit Stability Study Results at 14 and 46 Days	62
Table 8: Second Conduit Stability Study Results at 24 Hours	63
Table 9: Second Conduit Stability Study Results at 18 Days	64
Table 10: Physical Parameters of Nerve-Conduit Model	86
Table 11: Oxygen Diffusion Related Parameters	90
Table 12: Summary of the Dominant Diffusion Regimes	99
Table 13: Glucose Diffusion Related Parameters	104

TABLE OF EQUATIONS

Equation 1: Fick's First Law Adaptation	37
-----------------------------------------------	----

CHAPTER ONE

PERIPHERAL NERVOUS SYSTEM ANATOMY, PHYSIOLOGY AND NATIVE REPAIR MECHANISMS

1.1 PERIPHERAL NERVOUS SYSTEM

The human nervous system comprises two elements: the central and the peripheral nervous systems. The central nervous system (CNS) consists of the brain and the spinal cord, while the nerves branching from the CNS are defined to be components of the peripheral nervous system (PNS) [1, 2]. Differences exist in the regenerative abilities of the CNS and PNS, due largely to the presence of Schwann cells in the PNS [3, 4]. Injuries to the CNS can be life threatening, or lead to paralysis, as the CNS lacks the ability to regenerate [5, 6]. In contrast, injuries to the PNS can often be repaired either through native recovery, largely led by Schwann cells, or through surgical intervention [7]. The focus of the current work is to improve the efficacy and distance over which peripheral nerve injuries may be repaired through surgical intervention and via leveraging of the native ability of the PNS to regenerate.

1.2 PERIPHERAL NERVE ANATOMY

The structure of a peripheral nerve may be viewed as a bundle of bundles arrangement in which each bundle is encapsulated in a sheath that separates it from its surroundings, see Figure 1 [8]. The smallest fiber in a peripheral nerve is the axon (the functional unit of the nerve) which is encapsulated by the endoneurium [9, 10]. A bundle of several axons, each encapsulated by endoneurium, constitutes a fascicle [10]. The fascicle is encapsulated by the perineurium. A bundle of fascicles comprises the nerve as a whole which is wrapped by the epineurium [10].

As stated above, the smallest functional unit of a nerve is the axon [9]. Axons conduct electrical signals known as action potentials and are typically surrounded by an insulating layer of myelin which comprises a mixture of proteins and phospholipids. Myelin is deposited around the axons via Schwann cells in relatively short, repeating segments. Gaps between the myelin segments are known as nodes of Ranvier [9]. Interestingly, the myelin sheath of a given axon is deposited by a singular Schwann cell [11]. Efficient transfer of action potentials through an axon is dependent on the presence of both the myelin sheath and the Nodes of Ranvier and occurs via the phenomenon of saltatory conduction [12].

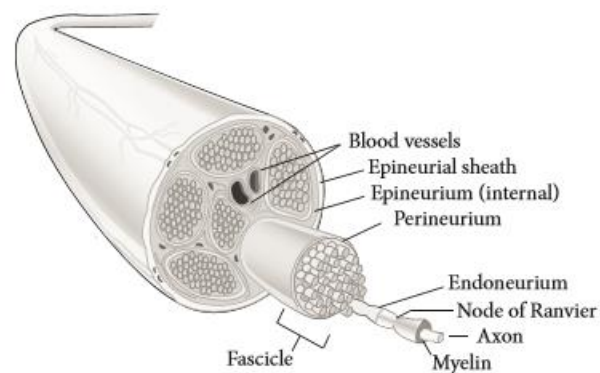


*Figure 1: Peripheral Nerve Structure
Adapted from Grinsell et al [104]*

1.3 ACTION POTENTIALS AND PROPAGATION

Action potentials are electrical signals that are produced by the CNS and PNS to communicate and to coordinate anatomical functions [13]. All cells possess a resting membrane potential that is maintained through the action of ion channels resident in the plasma membrane [14]. Propagation of an action potential occurs due to depolarization and repolarization of a membrane as a result of a stimulus that alters the membrane potential to a value that exceeds a threshold depolarization value. There are several key stages in action potential development and propagation that are summarized below and depicted in Figure 2 [11].

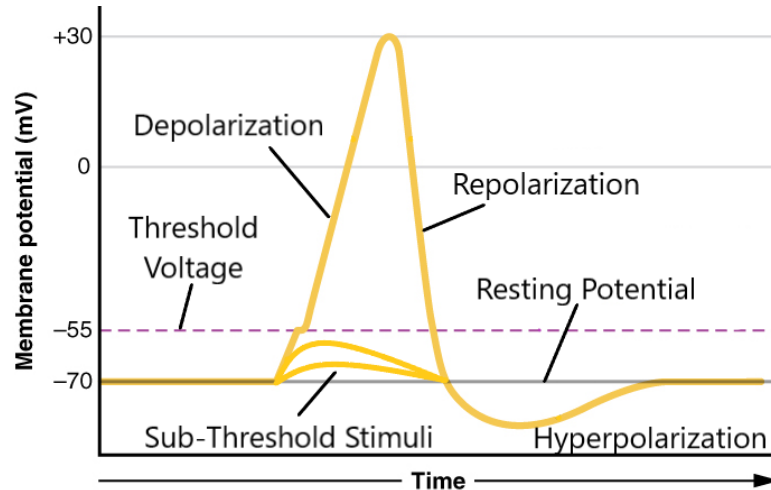


Figure 2: Action Potential Propagation
 Stages of an action potential, adapted from [105]

When the threshold voltage is exceeded due to action of the stimulus, a depolarization cascade ensues that drastically increases the membrane voltage (often resulting in membrane voltage changes from of the order of negative 70 mV to positive values of the order of 30 mV). Depolarization occurs due to an influx of sodium ions into the cell and the concomitant loss of potassium ions from the cell. The shift towards a positive membrane potential during depolarization is due to the differential rate of transport of sodium and potassium ions. Specifically, the diffusion rate of sodium exceeds that of potassium and as such sodium ions enter the cell at a much higher rate than potassium ions leave, resulting in an increasingly positive membrane potential. At the peak of the action potential (greatest membrane potential), the repolarization phase is initiated via closing of the sodium ion channels and the opening of potassium ion channels. Potassium ions are expelled from the cell and the membrane potential returns to a negative, polarized, potential. Indeed, during repolarization, potassium ions may leave the cell so rapidly that the membrane becomes hyperpolarized, that is temporarily assumes a potential below that of the resting membrane potential. The resting membrane potential is however, gradually restored [11, 14].

In the time period after an action potential and during the hyperpolarization phase, the plasma membrane has decreased sensitivity to stimuli, a phase referred to as the refractory period. The refractory period may be broken into two stages. The first stage is termed the absolute refractory period and is characterized by a complete lack of sensitivity to changes in the cellular membrane potential; no additional action potentials may be initiated during this stage [14, 15]. The second stage is termed the relative refractory period and is characterized by the fact that a second action potential may be activated, but the threshold is greatly increased relative to that pre-action potential. Successive action potentials are delivered through nerves via saltatory conduction.

1.4 SALTATORY CONDUCTION

Action potentials are propagated along both myelinated and unmyelinated nerve fibers of axons [16]. The potentials are transferred without any decrease in magnitude. Each action potential stimulates an adjacent area of the axon membrane to produce a new action potential. Therefore, each action potential causes the production of additional action potentials sequentially along the nerve fiber, that is,

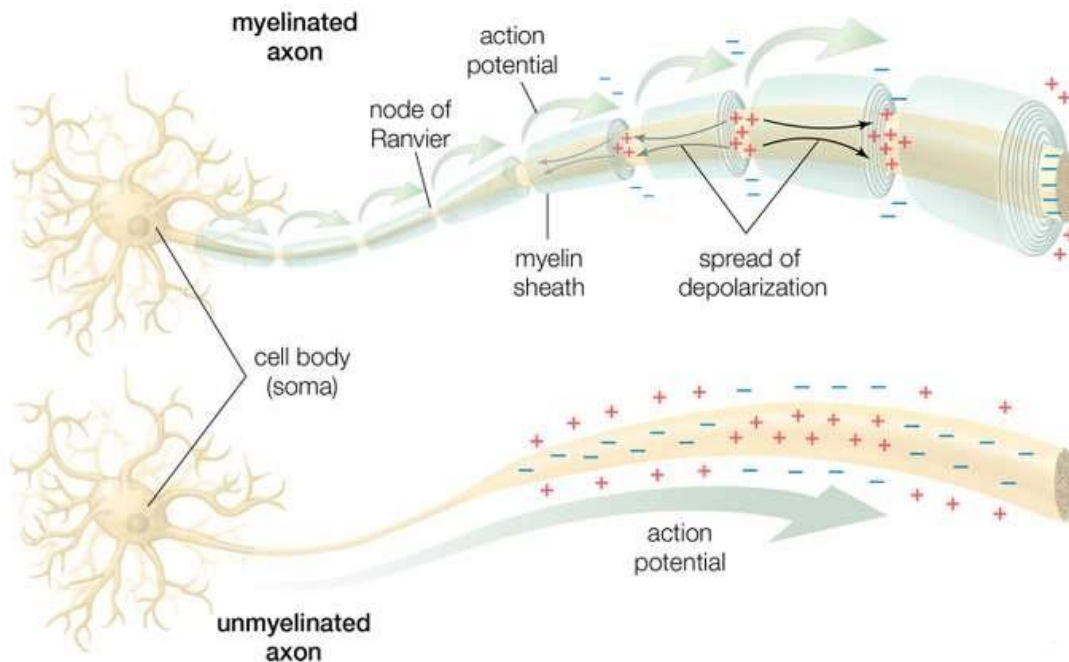


*Figure 3: Saltatory Conduction of Action Potentials
Comparison of myelinated and unmyelinated axons [106]*

the action potential is propagated serially by making 'copies' of itself. Propagation of action potentials along nerve fibers consequently differs from the flow of an electrical current through a wire, see Figure 3.

In unmyelinated axons, secondary (generated) action potentials are located immediately adjacent to the initial action potentials. In myelinated axon nerve fibers however, the action potential generated at one node of Ranvier may propagate rapidly or 'jump' (note the Latin word saltare – to leap) across the myelinated nerve segment to the next node of Ranvier [11, 12]. Myelinated axons propagate action potentials more efficiently than unmyelinated axons as fewer action potentials are required to span the length of a given axon. Efficient propagation of action potentials is possible due to the insulation provided by the proteins and phospholipids of the myelin sheath. In addition, it is noted that the nodes of Ranvier contain a high concentration of sodium ion channels which aid in propagation through efficient recreation of the action potential at each junction [16]. The speed of action potential propagation is dependent upon the extent of myelination and on axon diameter. Specifically, thicker and more abundant myelination as well as greater axon diameter result in increased rates of action potential propagation [16].

1.5 WALLERIAN DEGENERATION

Peripheral nerve repair following an injury occurs via a complex pathway that may be broken down into degeneration of the affected neural tissue (known as Wallerian degeneration), followed by various phases of axonal regeneration, see Figure 4. Wallerian degeneration is the first major phase of peripheral nerve repair and entails degeneration and removal of the damaged neural tissue to create an environment amenable to nerve regeneration [17].

Interestingly, Schwann cells, which are responsible for generation of the myelin sheath of peripheral nerves, and whose presence differentiates the regeneratable PNS from the non-

regeneratable CNS, are also crucial in the early stages of the repair process of peripheral nerve injuries [18]. When subjected to physical trauma, peripheral nerves fragment and release a variety of cell types, growth factors, and debris in the afflicted area. The segment of the axon distal to the injury site commences disintegration/degeneration within a 24-36 hour period post injury, degeneration occurs until the nearest node of Ranvier is reached [12]. During this time period, factors pertaining to myelination are downregulated, while factors attributed to nerve cell adhesion and support are upregulated. An immune response cascade is initiated at the distal stump by Schwann cells through upregulation of a variety of cytokines [19, 20].

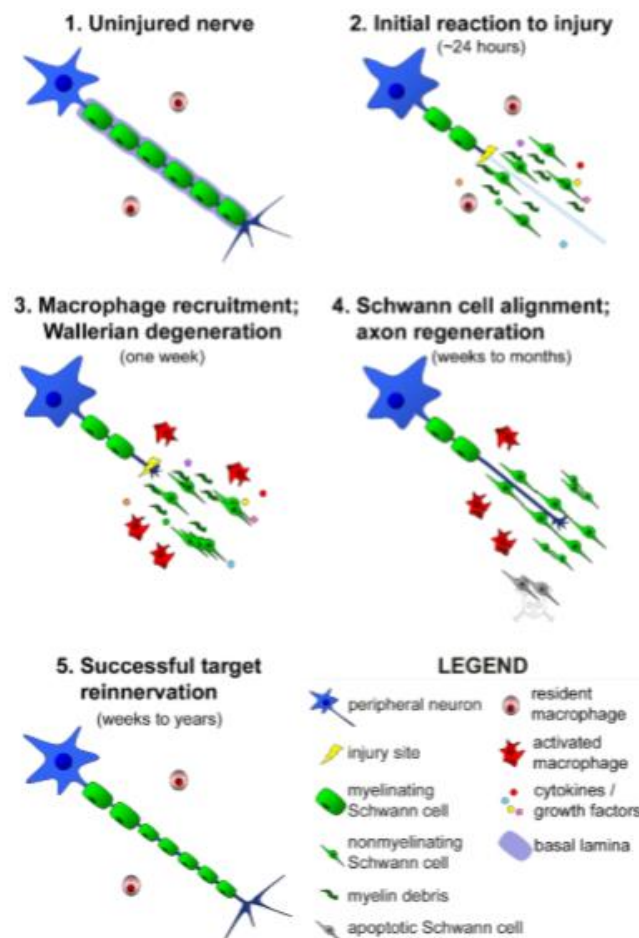


Figure 4: Wallerian Degeneration and Axonal Regeneration
Stages of reinnervation following a peripheral nerve injury [107]

Removal of degenerated neural tissue, myelin in particular, is key to repair as myelin is inhibitory for the regeneration of axons [21]. Macrophages clear the debris via phagocytosis, whilst

simultaneously excreting factors that aid in Schwann cell migration to the site of the injury [22]. During the initial phases of Wallerian degeneration Schwann cells aid in removal of debris. Wallerian degeneration acts to remodel the surrounding tissues and provide an environment conducive to nerve regeneration across the neural gap. The process is critical for neural repair as the distal stump is prepared for reconnection to the proximal stump, and inhibitory debris is removed. Four factors have been identified that dictate the efficacy of Wallerian degeneration: 1) the successful recruitment of Schwann cells, 2) secretion of neurotrophic factors, 3) existence of the basal lamina (specialized extracellular matrix), and 4) preservation of the distal nerve [23]. As the process of Wallerian degeneration nears completion, axonal regeneration is initiated.

1.6 AXONAL REGENERATION

Whilst debris is cleared, primarily by phagocytosis via Schwann cells and macrophages, a population of Schwann cells migrate to the distal end of the injury site, undergo a cell type transition to a non-myelinating form, proliferate, and begin to form bands of Bungner [19, 24]. Bands of Bungner, comprising longitudinally aligned Schwann cells, form inside each basal lamina tube which previously held myelinated axons, thereby creating a columnar pathway that directs axonal growth to achieve regeneration [22, 25]. Axonal growth cones in the form of filopodia, sprout from the proximal nerve stump and extend towards the bands of Bungner, which provide support for the regenerating nerve [26, 27]. Axonal elongation is promoted through upregulation of both neural and vascular growth factors. It is noted that successful regeneration may be impeded by an excessive distance required to bridge the neural gap, and if the microenvironment is not amenable to regrowth. The regenerated nerve is re-myelinated by Schwann cells, however distinct differences exist between the original nerve and the regenerated one in terms of the thickness of the myelin sheath, and the length of nerve covered by each myelin segment (i.e. the distance to the node of Ranvier) [17].

1.7 LIMITATIONS OF NATIVE PERIPHERAL NERVE REGENERATION

As outlined above, peripheral nerves have the innate ability to self-repair, however several factors dictate the extent to which regeneration is successful, and determine if surgical intervention is necessary [28]. The response of the proximal stump to injury is dependent upon the location of the transection/crush; if the damage is in the proximity of the neuronal body, then apoptosis may occur, otherwise the stump will sprout growth cones and extend toward the residual distal stump. Ideally, the response of the distal stump to injury follows the process of Wallerian degeneration leading to neural tissue degeneration back to the nearest node of Ranvier, phagocytosis of cellular debris, and the formation of bands of Bungner [12, 18].

Optimal recovery occurs for injuries that result in short axonal disruptions and limited damage to the surrounding tissue. Compression and blunt-transection injuries however disrupt the endoneurial tubing and create scar tissue which makes it difficult for bands of Bungner to form, leading to disorganized tissue growth and poor recovery [12]. Full remyelination of axons may not occur after regeneration due to poor stimulation of growth factors and hence limited activity by Schwann cells [29]. The length of the neural injury is negatively correlated with successful regeneration, that is, the greater the length of neural transection/crush the poorer the prognosis for functional recovery. Unfortunately, reinnervation and complete functional recovery are not synonymous. For example, even if neural reconnection is successful, for large injuries the time required for repair may be too great and the targeted, denervated muscle, may have atrophied beyond recovery [8, 30]. It is noted that muscle atrophy may occur in as little as 3 weeks, however structural integrity of the muscle may be maintained for up to a year. Fortunately, sensory end organs may maintain their integrity for two to three years without enervation, potentially allowing sensory recovery even after functional muscle has been lost.

It may be appreciated therefore that native nerve regeneration is possible, but for optimal results is limited to specific injury types and extents, and requires the careful orchestration of a range of degeneration and regeneration processes [18, 21]. It should not be surprising then that a range of surgical interventions have been developed to aid in restructuring the injury site. For example, neural transplants are a common approach, as are implants such as conduits that are employed to encase the site, isolating it from the surrounding tissue, and concentrating necessary cell types/factors within the neural gap [31, 32]. The various surgical methodologies for peripheral nerve repair, and their advantages and disadvantages, are presented in the following chapter.

CHAPTER TWO

SURGICAL INTERVENTIONS TO PROMOTE PERIPHERAL NERVE REPAIR

2.1 FREQUENCY AND SEVERITY OF PERIPHERAL NERVE INJURIES

Approximately 200,000 surgical procedures are performed each year in the United States to address peripheral nerve injuries [33]. Less than 50% of such interventions result in full functional recovery, and account for \$150 billion of health-care expenditures annually [8, 34]. Most peripheral nerve injuries occur in the upper limbs of young men (from 16-38 years old) and are the result of traumatic events such as automobile accidents, sport injuries, or occupation-related accidents [35]. Common nerves that are affected by these traumas are the brachial plexus, ulnar, median and peroneal nerves [35]. Peripheral nerve injuries are commonly graded using the Seddon-Sunderland classification system which differentiates injuries via the severity of damage to the nerve (scale of I-V with V being the most severe), see Table 1 [9].

*Table 1: Nerve Injury Classifications
Summary of Seddon-Sunderland nerve gradations [8, 9, 36]*

Grade	Classification	Description
I	Neurapraxia	Internal neural compression, no Wallerian degeneration, address via physical therapy
II	Axonotmesis	Axonal disruption, surroundings intact. Surgery generally not necessary. Observe, recovery anticipated in months.
III		Compression injuries, endoneurium disruption. Wallerian degeneration expected. Observe for up to 6 months and if poor recovery, surgery will be necessary.
IV		Blunt transection injury. Epineurium is only structure intact. Delay repair to assess neural damage. Surgical exploration and reconstruction typically necessary.
V	Neurotmesis	Lacerating injury, whole nerve is transected. Immediate repair required

Investigation of Table 1 reveals that severe peripheral nerve injuries occur via two means; blunt trauma (crush) and laceration. Traumatic crush injuries are classified as grade IV in the Seddon-

Sunderland system and typically result in only the epineurium remaining intact. Frequently there is a need to surgically intervene and debride the injury site to remove necrotic tissue and debris in order to promote repair [28]. Lacerated nerve injuries (grade V in the Seddon-Sunderland system) are characterized by complete neural discontinuity and require immediate surgical intervention, including at a minimum debriding the injury site [36].

2.2 CURRENT APPROACHES TO PERIPHERAL NERVE REPAIR

2.2.1 NEURORRHAPHY

Neurorrhaphy, also known as end-to-end, or direct, repair is a surgical technique employed when there is no loss of neural tissue and the two severed nerve stumps can be sutured together without inducing excessive tension on the nerves [28, 36]. It is a common and generally successful surgical method with several variants which are dependent upon the specifics of the neural injury as presented in Figure 5 [37].

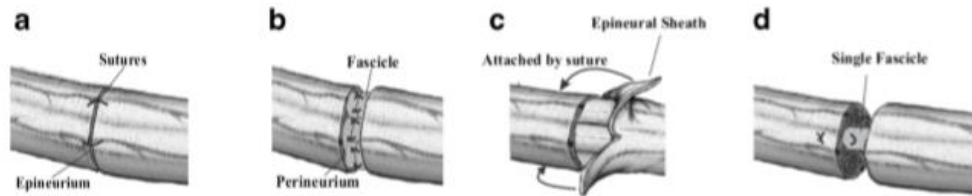


Figure 5: Methods of Neurorrhaphy

a) epineural repair, b) fascicular repair, c) Epineurial sheath repair, d) single fascicle repair [108]

Figure 5a depicts epineural repair in which the epineurium of the severed nerve is reconnected via sutures. Figure 5b presents fascicular repair in which the epineurium is retracted, and individual fascicles are sutured together. Epineurial sheath repair (Figure 5c) extends the intact epineurial sheath of one neural stump over the other stump, where it is sutured in place. In order to accomplish the overlap of sheaths, a portion of neural tissue of the receiving stump must be resected. Lastly, Figure 5d depicts single fascicle repair, a technique in which a single donor fascicle is sutured between the proximal and distal nerve stumps. It is noted that all four of the surgical methods presented in Figure 5 require a great deal of intricate suturing and have the potential to cause further damage to the injury site [9, 36].

2.2.2 GRAFTS

For peripheral nerve injuries in which the neural gap is sufficiently large that the nerve stumps cannot be reconnected without imposing significant tension, neural grafts are commonly utilized. Neural graft repairs generally have very good regenerative outcomes, and have been termed the 'gold standard' in peripheral nerve repair [38, 39]. The graft tissue may be sourced from the patient themselves (autograft), from another individual (allograft), or be a modified natural material. For an autograft, the donated nerve is sourced from a location of the patient deemed less important than the injury site [33], and is often the sural nerve, which renders the relevant region of the leg sensationless but not functionless [40]. Allografts are sourced from an individual other than the patient and as such require a regimen of immunosuppressant treatment to reduce the likelihood of rejection of the transplanted nerve [41]. Modified natural material grafts, such as AxoGen's Avance Nerve Graft, are produced from human peripheral nerve allografts processed to create an acellular extra cellular matrix derived scaffold [28, 42]. Prior to implantation the grafts are sterilized via gamma irradiation to reduce the likelihood of immunogenic responses, however such treatment has been shown to reduce the efficacy of regeneration [41].

2.2.3 CONDUITS

Neural conduits are an alternative option for repair of severe injuries, and are typically employed for neural gaps of 20 mm and less [41]. Conduits are advantageous in relation to nerve grafts in that a second surgical site is not required, and immunosuppressant regimens are generally not needed. Neural conduits are typically hollow cylinders into which the proximal and distal neural stumps are inserted, as illustrated in Figure 6. Conduits are sutured in place to ensure that the nerve stumps remain within the conduit throughout the regeneration process. The surgical methodology of employing a conduit for peripheral nerve repair is referred to as entubulation [36].

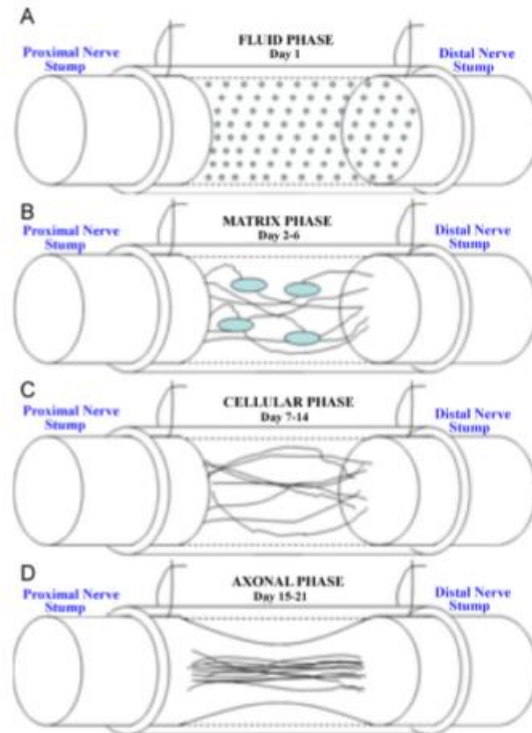


Figure 6: Method of Entubulation
Phases for peripheral nerve repair using conduit assisted repair [109]

The process of entubulation and the various phases of neural regeneration are depicted in Figure 6 [41]. The first phase, known as the fluid phase, occurs on the day of surgical implantation and is characterized by the presence of neurotrophic factors in the fluid filling the void within the conduit. During the following week, a scaffold of extracellular matrix forms between the proximal and distal stumps in preparation of cellular migration, a process known as the matrix phase. During the second week post implantation various cell types are recruited into the luminal space, perhaps most notably Schwann cells which accumulate at the distal stump, in what is known as the cellular phase, in preparation of bands of Bungers formation and axonal regeneration. The final phase, referred to as the axonal phase, is characterized by axonal sprouts occurring at the terminus of the proximal stump which extend via the bands of Bungers to the distal end to effect neuronal repair.

When designing a neural conduit, the objective is to create a microenvironment surrounding the injury site that is conducive to native regeneration, as outlined above. That is, to create an environment

that promotes isolation and containment of specific growth factors and cells critical to the regeneration process, whilst preventing an influx of inflammatory species [31]. Consequently, characteristics of conduits that should be considered include selective permeability, biocompatibility, biodegradability, structural stability and flexibility. In addition, the conduit should comprise a material amenable to sterilization [28]. The neural conduits employed in early studies were typically comprised of silicon (1982) [43] or Gore-tex (ePTFE, 1988) [44]. In the decades since these pioneering studies the number of materials used in the production of neural conduits has increased dramatically, as summarized below in the context of commercially available products:

a) Neurotube

Neurotube comprises polyglycolic acid (PGA), a highly crystalline and rigid polymer with low solubility in organic solvents [45]. PGA is resorbable and has beneficial mechanical properties for neural regeneration. Of the various FDA approved neural conduits, Neurotube has the greatest amount of clinical data available [41]. Neurotube has been highly successful in terms of clinical outcomes, surpassing neural grafts in certain studies, and has been employed for the repair of neural defects in the range of 2-40 mm, with a few studies performed on defects as large as 65 mm [46, 47].

b) NeuraGen, Neuroflex, NeuroMatrix, Neuromend and Neurawrap

NeuraGen, and associated conduits, are comprised of type 1 collagen, which is one of the few naturally occurring materials employed in neural conduit production [41]. Collagen is the most abundant protein in mammals, is easily isolated and purified, and presents a minimal risk for immunogenic responses [41, 48]. NeuraGen and associated conduits have performed well clinically, with outcomes that have been comparable to those obtained from neural grafts for defects up to 20 mm [49, 50, 51].

c) *AxoGuard/Surgisis Nerve Cuff*

AxoGuard/ Surgisis nerve cuffs comprise porcine small intestine submucosa (SIS) which is a strong, yet pliable, collagen matrix. Submucosa grafts are cell free and therefore minimally immunogenic [52]. SIS has been observed to assist in local tissue remodeling, and to induce a systemic response to resist infection [53]. Comparatively little data has been published regarding the efficacy of SIS in neural repair, however evidence of enhanced neural regrowth has been reported [54].

d) *Neurolac*

Neurolac conduits comprise poly D,L lactide-co- ϵ -caprolactone (PCL), which is a hydrophobic semi-crystalline polymer that is both straightforward and inexpensive to produce [41, 55]. It is noted that Neurolac conduits are the only FDA approved transparent products available, and are biodegradable, with non-toxic degradation products [55, 56]. Extensive pre-clinical data suggests that PCL conduits approach the efficiencies of grafts in the repair of neural defects up to 20 mm in length [41, 57, 58, 59, 60]. Clinical data of Neurolac conduit entubulation has been reported for defects in the 5-20 mm range with positive results observed [46, 61].

e) *Salutunnel and Salubridge (PVA)*

Salutunnel and Salubridge conduits comprise a non-biodegradable material, Salubria, which is a synthetic polyvinyl alcohol hydrogel (PVA). The hydrogel mimics the water content of human tissue, yet is readily sterilized and is mechanically stable [41, 62]. No data have been published regarding pre-clinical nor clinical studies employing Salutunnel or Salubridge [41].

2.3 LIMITATIONS OF CURRENT METHODS OF PERIPHERAL NERVE REPAIR

As seen above, peripheral nerve repair requires the orchestration of multiple processes to efficiently regenerate a nerve [21]. Natural regeneration of peripheral nerves is effective for minor

injuries and for those occurring on short length scales, an injury that exceeds the capabilities of the native regenerative processes however requires surgical intervention [9]. As would be expected, each of the surgical repair methods outlined in the preceding section have limitations and associated complications, which are reviewed below.

2.3.1 NEURORRHAPHY

Epineural sutures are employed when the damaged nerve has little or no tissue that has been, or needs to be, removed. Such injuries often arise from a clean sever of the nerve [32, 37]. Direct repair via epineural suturing is generally employed for neural gaps of less than 20 mm, and in scenarios where the two neural stumps can be aligned end-to-end without the introduction of excessive tension [9]. The process of epineural suturing can however subject the neural stumps to excessive handling and induce greater damage than caused by the original injury [8, 9]. Though direct end-to-end repair via epineural suturing is a common technique for the repair of minor nerve gaps, the success of the operation is heavily reliant on the skill of the surgeon in correctly aligning the nerve stumps and executing effective and minimally invasive sutures [9, 32]. Interestingly, some studies have demonstrated that implantation of a conduit over a small neural gap had better regenerative results than direct repair via epineural sutures, suggesting that conduit implantation may in the future become the preferred surgical repair methodology for such injuries. [37]

2.3.2 GRAFTS

Neural grafts are often considered the preferred means of peripheral nerve repair, although they are not without significant limitations [38, 41]. As stated above, there are two primary methods of neural graft repair, autograft and allograft. Autografts are the generally preferred choice as the neural tissue is donated by the patient that is receiving the graft and as such tissue rejection and immune system responses are rare [42]. However, a significant issue with autografts is that they require an additional surgical site and concomitant loss of sensation in the region of donation. If large numbers of

grafts are necessary the stocks of lesser-important nerves are diminished and one must resort to more impactful donor nerves, or employ alternate methodologies [42]. Conversely, allografts are neural grafts donated by an individual other than the patient who is receiving the nerve [41]. Allografts require an intense regimen of immunosuppressant medication for a period of approximately 18 months, a process which renders the patient susceptible to numerous opportunistic infections, or in some cases, tumor formation [41, 63]. Modified natural material grafts are an alternative that may be used to avoid the issues associated with donor donation sites and immunosuppressant side effects [42]. Synthetic grafts are donated tissues that have been processed to remove cells and hence decrease their immunogenicity, such as the product Avance. Limitations that have been observed in the use of acellular grafts include increased scarring and fibrosis attributed to host cell rejection, and reduced performance as a result of degradation during neural processing and sterilization [41]. As such it may be appreciated that while the degree of neural regeneration that can be achieved via grafts may be superior to other surgical interventions, they are not without limitations, including those related to availability, immunogenic responses, and potential performance issues due to degradation.

2.3.3 CONDUITS

Neural conduits are a viable alternative to neural grafts, particularly for neural gaps of 20 mm or less. However, the performance of conduits decreases rapidly at larger neural gaps, a major limitation of the technology, and one investigated in the present work [41]. Since conduits are a non-native construct, the material of choice can be a major determinant of clinical success, or failure. As noted above, conduits can be constructed employing natural or synthetic materials, and further, can be designed to be biodegradable. Commercially available conduits and their specific limitations are outlined below:

a) *Silicon/Teflon*

Conduits comprising silicon and polytetrafluoroethylene (ePTFE) were employed in the formative investigations of neural conduit entubulation. Performance of the conduits were deemed acceptable for neural gaps of below 15 mm for silicon and 6 mm for ePTFE conduits [43, 44]. Although both materials are considered biocompatible, neither biodegrade *in vivo*, and as such a second surgery was required to remove the conduit post-regeneration. Removal of the conduits was necessary as they were observed to restrict and compress the regenerating nerve, creating a poor environment for full recovery [41].

b) *Neurotube*

Neurotube conduits, as stated above, comprise the synthetic polymer polyglycolic acid (PGA). The mechanical properties of PGA conduits are favorable for regeneration in terms of structural stability and the conduits biodegrade comparatively quickly, obviating the need for a second surgery to remove the conduit post-regeneration. However, the degradation of PGA produces acidic byproducts that are harmful to the surrounding tissues in the body [41, 46]. Consequently, while it has been observed that Neurotube conduits aid in the regeneration of peripheral nerve injuries with neural gaps in the range of 10-30 mm, the surrounding tissue is irritated and damaged upon conduit degradation thereby requiring conduit removal despite its biodegradable nature [46, 64, 65].

c) *NeuraGen, Neuroflex, NeuroMatrix, Neuromend and Neurawrap*

The NeuraGen and associated conduits comprise collagen, which is a natural and abundant protein [41]. Collagen is both biocompatible and biodegradable, making it a logical and compelling choice for conduit production [48, 49]. The time scale for conduit degradation is specific to the various associated conduits. NeuraGen for example has been found to remain intact for up to 4 years *in vivo*, leading to unfavorable nerve compression comparable to

that seen in silicon/ePTFE conduits. Other conduits comprising collagen have been found to degrade in as few as 8 months [41, 51]. It should also be noted that instances of collagen conduits eliciting an immune response, which have required the implementation of an immunosuppressant regimen, have been observed [50].

d) *AxoGuard/Surgisis Nerve Cuff*

AxoGuard/Surgisis nerve cuffs comprise porcine small intestine submucosa (SIS) which have been processed to create an acellular matrix comprising primarily collagen [53]. A major limitation of SIS conduits is the incidence of immune responses (despite the removal of the native cellular species), interestingly the responses appear to be dependent on the species from which the material was harvested [41, 53]. The production process of SIS conduits is lengthy and relatively expensive. In addition, the resultant conduits have large variability in a range of physical/chemical properties, and indeed have a finite risk of infectious disease transmission. There are minimal pre-clinical and clinical data for use of SIS conduits, so assessments of efficacy are not currently possible [52].

e) *Neurolac*

Neurolac conduits comprise the polymer poly D,L lactide-co- ϵ -caprolactone (PCL) and, as stated above, are the only FDA approved conduits that are transparent, an attribute that aids in visualization of the surgical field during entubulation [41, 57]. PCL is however a very rigid material, a fact that has resulted in difficulties in implantation including the inability of surgeons to penetrate the conduit walls with needles during suturing, and associated disturbances of the injury site [41, 66]. As such, surgeons often use larger needles and sutures when implanting Neurolac vs other conduits, which has been observed to result in tearing of the neural tissue during implantation or afterwards if the neural stumps are under tension. Other issues that have been reported in association with Neurolac conduit

implantation include severe swelling, fragmentation of the conduit, and conduit collapse [58].

f) *Salutunnel and Salubridge*

Salutunnel/Salubridge conduits comprise a synthetic polyvinyl alcohol hydrogel called Salubria which is intended to mimic the high water content of human tissue [62, 67]. Though mechanically stable, Salubria is non-biodegradable and has been shown to lead to neural compression and potential tension of the suture attachment sites, further damaging neural tissue. To date there have been no clinical studies published on Salutunnel/Salubridge conduits making it difficult to gauge its efficacy in neural regeneration [41].

*Table 2: FDA Approved Peripheral Nerve Repair Devices
Summary of positive attributes and limitations of device materials*

Material	Tradename	Positive Attributes	Limitations
Acellular Graft	<i>Avance</i>	Readily available No donor site morbidity Reduced surgical times	Increased scarring/fibrosis Chance of host rejection Requires immunosuppression
PGA- Polyglycolic Acid	<i>Neurotube</i>	Excellent degradability Very good mechanical properties High cell viability Comparable to grafts (20 mm) Good efficacy up to 30 mm	High rate of degradation Degradation products are acidic Low solubility
Type I Collagen	<i>Neuragen</i> <i>Neuraflex</i> <i>Neurawrap</i> <i>Neuramatrix</i> <i>Neuramend</i>	Abundant and easily isolated Biocompatible Supports cell adhesion Supports tissue regeneration Comparable to grafts (20 mm) Good efficacy up to 40 mm	Slow degradation time may lead to compression (Neuragen only) Most degenerate in 8 months Undesirable immune response
Porcine	<i>Surgisis</i> <i>AxoGuard</i>	Physically supportive Supports tissue regeneration	Immune response can vary Very high cost Risk of infectious disease transmission

Table 2 Continued

PCL- Polylactide- co- caprolactone	<i>Neurolac</i>	Only FDA-approved transparent conduit Comparable to grafts (20 mm)	High rigidity, difficult to implant Requires large needles/sutures Greater chance of neural damage and foreign body reactions
PVA-Polyvinyl Alcohol	<i>Salubridge</i> <i>Salutunnel</i>	Tissue-like water content Mechanically stable Easily sterilized	Non-resorbable, may cause tension/compression No published studies on efficacy of material

2.4 DESIRED PROPERTIES OF NEURAL CONDUITS

It is evident that the conduits currently used for entubulation vary greatly in their positive attributes and in their limitations. Further, it may be seen that many of the positive aspects and the limitations stem from the physical properties of the materials used to create the conduits [41]. In order for entubulation to match and/or surpass the regenerative outcomes achieved via neural grafts, conduits must be created that have been optimized in terms of their mechanical, biodegradation and biocompatible/non-immunogenic properties. The relevant properties of currently available conduits, and the areas yet to be fully optimized are addressed below.

The ability of a conduit to biodegrade *in vivo* in a manner that is safe, occurs on the relevant timescale and that enables the maintenance of favorable mechanical properties during neural regeneration is critical. Of the current FDA approved conduits, none meet all of these degradation requirements. For example, Salubridge/Salutunnel conduits are non-resorbable and as such cause compression of the nerve in the end-stages of regeneration leading to neural degeneration. Other conduits, including those comprising PLC, collagen, and PGA do undergo degradation *in vivo*, but do so in non-ideal processes, or on timescales that are incompatible with the regeneration process. For example, Neurolac, composed of PLC, is biodegradable but is so rigid that the conduit is difficult to

implant, and may fragment during degradation. Collagen conduits have a range of degradation times; Neuragen, for example, degrades so slowly (4 years) that it essentially behaves as a non-degradable conduit and engenders compression of the regenerating nerve. Neurotube, composed of PGA, degrades on a favorable time scale and maintains excellent mechanical stability over the desired time period, however the products of the degradation process are acidic, and are detrimental to surrounding tissue. Therefore, a material has yet to be identified that has the required mechanical properties, undergoes degradation in a timeframe comparable to that of neural regeneration, and whose degradation products are benign.

Material selection for conduit construction must consider its biocompatibility/immunogenicity and likely response of the body to its presence. Synthetic materials, such as polylactide-co-caprolactone and polyglycolic acid have been observed to promote a foreign body response, and /or to produce tissue inflammation upon degradation, as such use of man-made materials is often avoided. Conversely, natural materials, such as collagen, which is a native protein in humans, may in fact elicit an immune response and require an immunosuppression regimen which may have unintended consequences. Attempts have been made to decrease the immunogenicity of naturally derived neural conduits by making acellular variants, for example Avance (acellular nerve allograft) and Surgisis (acellular porcine small intestine submucosa). The decellularization process employed to create the Avance grafts has been shown to decrease the performance of the graft and to result in scarring and fibrosis, characteristic of rejection. Surgisis is marketed as a non-immunogenic implant derived from porcine small intestine submucosa; however, patient responses to entubulation have been shown to be dependent upon the species of pig the conduit was harvested from. In addition, such implants have the potential to transmit infectious diseases.

2.5 TESTING OF THE EFFICACY OF CONDUIT ENTUBULATION FOR PERIPHERAL NERVE REPAIR

Many animal studies have been performed to investigate the efficacy of conduit entubulation in promoting peripheral nerve repair. Such studies have employed a wide range of animal models, and an equally wide range of nerve types distributed throughout animals under investigation. To gauge the effectiveness of nerve regeneration several forms of analysis have been employed, including grip strength, gait analysis, tissue microscopy and histology. The wide variety of animal model, nerve type and analytical methodology employed has made inter-experimental comparisons challenging, a fact commonly acknowledged in the literature. Broad consensus has been reached, however, that several specific conduits have been shown to perform as well as grafts up to a given injury length, and that epineural suturing has been determined to be inferior to conduit implantation for small neural gap injuries. Beyond these two broad conclusions however, little consensus has been reached. Indeed, several sources have stated that there is a dire need for a large-scale experiment to be performed in which all conduits available are tested, alongside grafts and neurorrhaphy, in the same animal trial to ensure consistency in analytical methods and injury models to provide translational results for inter-experimental comparisons [23, 33, 41]. Such a large-scale experiment could also provide a standard for future conduit development such that new products could be tested in the same manner to create a consistent database of products and techniques.

Table 3 provides a summary of several pre-clinical studies that have been performed to determine the efficacy of specific neural conduits in the regeneration of peripheral nerve injuries. Investigation of Table 3 highlights the fact that direct comparison of studies using the same animal model, conduit, nerve type and analysis methodology is currently infeasible.

Table 3: Sample of Pre-Clinical Studies Using Neural Conduits
 MAP-Muscle Action Potential, SAP-Sensory Action Potential, EMG-Electromyography; adapted from Kehoe et al [41]

Author	Animal Model	Conduit Used	Nerve Used	Analysis Techniques
Tyner (2007)	Rat	Neuragen	Sural, peroneal, tibial	Histology and autonomy scoring
Archibald (1995)	Nonhuman primate	Neuragen	Median and ulnar	MAP, SAP, histomorphology
Archibald (1991)	Rat and primate	Neuragen	Sciatic and median	MAP and SAP
Waitayawinyu (2007)	Rat	Neuragen Neurotube	Sciatic	Isometric contraction, muscle weight, histology
Dellon (1988)	Monkey	Neurotube	Ulnar	Morphometric analysis and electrophysiology
Meek (2009)	Rat	Neurolac	Sciatic	Functional analysis and light microscopy
Meek (2009)	Rat	Neurolac	Sciatic	Microscopy
Meek (2001)	Rat	Neurolac	Sciatic	EMG and video gait analysis
Meek (1996)	Rat	Neurolac	Sciatic	Walking track analysis and electrostimulation

2.6 THE POTENTIAL OF CELLULOSE NANOFIBER FOR NEURAL CONDUIT PRODUCTION

It is evident from the preceding sections that an opportunity and a need exists for the development of a neural conduit that minimizes immunogenicity whilst maximizing the characteristics of biocompatibility, biodegradability and mechanical stability. Further, such development work should employ a common animal model, a readily accessible nerve type, and standardized analysis methodologies. Given that the materials employed to construct current neural conduits have all been found to be deficient in one or more aspects, an alternate material, one not yet employed for conduit production, should be evaluated.

Cellulose nanofibrils (CNF) are an emerging natural material which is being evaluated for an exponentially increasing number of applications in a large variety of fields. In the biomedical realm it has been shown that CNF is relatively bio-inert [68], has excellent mechanical properties [69], degrades over time *in vivo* [70], and is flexible [71]. CNF consists of cellulose fibrils of the order tens to hundreds of nanometers in diameter, and hundreds of nanometers to many μm in length. The Process Development Center (PDC) of the University of Maine has become one of the top suppliers of cellulose nanomaterials in the world and is the only facility in the United States with 1 ton per day production capability [72]. CNF may be produced via a range of methodologies from a vast array of cellulosic and lignocellulosic feedstock materials. At the University of Maine, CNF is generally produced from a Kraft bleached softwood pulp with fiber diameters of tens of μm and is refined through means of mechanical defibrillation in an aqueous slurry to attain fibril diameters on the nanoscale.

Preliminary work by the author demonstrated that CNF can be readily employed in slurry form to produce thin sheets without additional treatment or functionalization, as presented in Section 4.1. The sheets had sufficient pliability to enable the ready formation of a tube, or conduit. It is evident therefore that CNF has the potential to be a viable material for neural conduit production, and that such conduits may address many of the deficiencies of current conduits. The following chapters present the work performed to develop, produce and characterize CNF neural conduits, to assess their efficacy in neural regeneration in a common animal model using standardized testing methods, and to model their facilitation of the diffusion of pro-regenerative species into the luminal space to shed light on the results of the regenerative studies.

CHAPTER THREE

EXPERIMENTAL METHODS

3.1 PULP PREPARATION

Wood pulp is the primary feedstock employed to produce CNF via mechanical defibrillation and segmentation of cellulose fibers. Bleached softwood Kraft pulp was acquired through the University of Maine Process Development Center from Resolute Forest Products. Oven-dried pulp (280 grams) was cut into pieces approximately 15.2 cm x 15.2 cm and placed in an 18.9 L bucket containing 13.72kg of DI water (17.4 M Ω -cm) and left overnight. The sheets of pulp were subsequently broken apart manually to release fibers and fiber aggregates. The resulting aggregates were less than 1 cm in diameter.

3.2 CONFIGURATION OF CONTINUOUS REFINEMENT VIA A SUPERMASSCOLLOIDER

A supermasscolloider was purchased from Masuko Sangyo Co., Ltd (model MKCA6-2J). The system was a benchtop model designed for batch refinement in which the lower of two stones (rotor) is rotated by an electric motor, and the feed material is pumped into the space between the rotating stone and a parallel, static, upper stone (stator). Coarse deep ditch stones (MKE6-46) of 15.2 cm diameter were employed to refine CNF from the pulp slurry prepared as described above. It is noted that the stones are generally used commercially to create pastes from fruits, vegetables, seeds, beans, rice etc. and are constructed of a combination of silicon carbide and aluminum oxide.

In typical operation, the supermasscolloider (SMC) was designed for batch refining in which the slurry makes a single pass through the system. If the desired slurry consistency was not achieved with a single pass, additional passes of the slurry through the system would be implemented manually. The refining of cellulose pulp to cellulose nanofiber however requires many passes through the SMC, as such modifications were made to the supermasscolloider to enable continuous refinement. Specifically, an extended hopper was added to increase the volume of feed material to the colloider, a recirculating

pump and reservoir (14 L) system were installed, and an overflow line connecting the hopper to the pump reservoir was implemented. The system was designed and built to contain a total slurry volume of 14 L between the overflow and the pump reservoir.

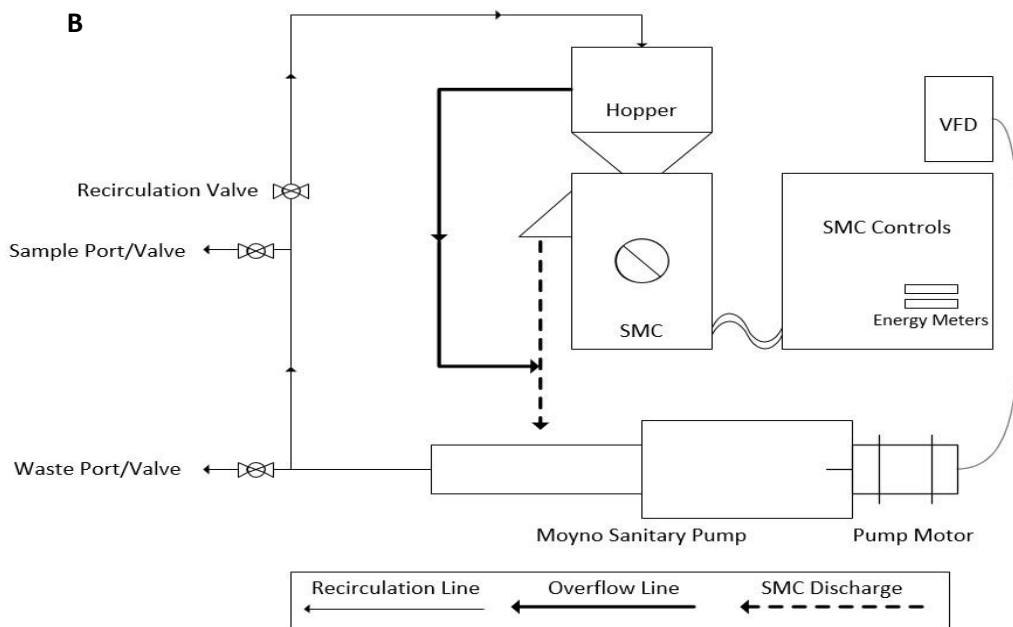
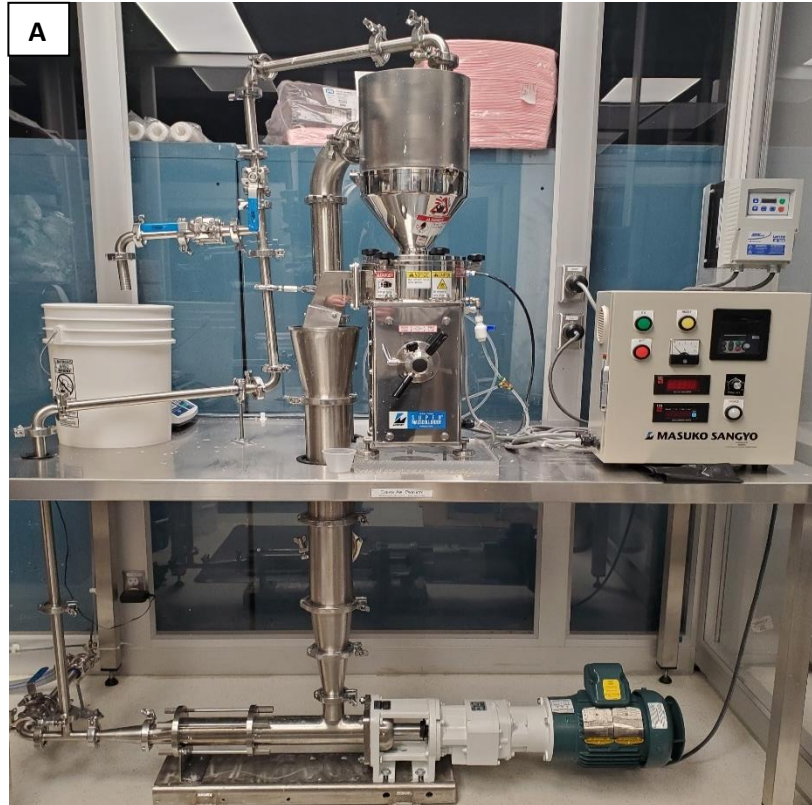


Figure 7: Supermasscolloider Refining System
(a) SMC refining system and (b) schematic view

As shown in Figure 7, cellulose pulp slurry was gravity fed into the hopper at the highest point of the SMC. The feed was directed into the gap between the rotor and stator stones where fibers were defibrillated, prior to passing out of the discharge port of the SMC. The gap between the rotor and stator was controlled via a manual adjustment with units of μm . The rotor was driven by an electric motor (Masuko, 208V 1.5kW) with rotational speed of 800-3000 rpm set via a digital control system. Cumulative electrical energy consumed by the motor driving the rotor for a given refining run was monitored via both a cumulative and instantaneous wattmeter (Load Controls Inc, KWH-3 cumulative meter and DM-100 instantaneous meter). The slurry discharged from the SMC was fed vertically into the reservoir of a positive displacement pump (Moyno Sanitary Pump FB1D-SSF-SAA, Baldor General Severe Duty 2HP/3-phase Gearmotor), the speed of which was controlled via a SMVector variable frequency drive (Lenze AC Tech, ESV152N04TXC). Slurry exiting the pump was subsequently fed into a recirculation line that led back to the feed hopper, thus completing a single refining cycle. Valves were incorporated into the recirculation line at two separate locations to facilitate removal of slurry from the system. Specifically, at the lowest point of the recirculation line a waste port and valve were installed to enable complete drainage of the system prior to cleaning. A sampling port and valve were installed approximately halfway up the recirculation line and were used to remove aliquots of the slurry as desired. As the flow rate of the pump was greater than the observed flow rate of slurry through the SMC, an overflow line was installed to direct excess slurry from the feed hopper to the pump reservoir. All piping, valves and fittings were 316 stainless steel and approved for food grade applications. The SMC was equipped with a water jacket for removal of excess heat generated during refining; cold municipal water was fed through the jacket at a rate of 5.1 L/minute. An image and a process flow diagram of the supermasscolloider configured for continuous refining may be seen in Figures 7a and 7b, respectively. Figure 8 presents detailed images of specific components of the system.

In order to provide a consistent and clean environment for CNF production, the SMC system was constructed within a temperature-controlled ISO 7 class cleanroom which included four HEPA filters and a custom recirculation chamber, see Appendix A1. The cleanroom was divided into a gowning area and a working area, with designated zones for each stage of the CNF and conduit production process, see Appendix A2. All procedures used in CNF production and neural conduit construction were developed, implemented and documented employing Good Manufacturing/Laboratory Practices (GMP/GLP) [73]. Appendix A3 provides Standard Operating Procedures (SOP) for all facets of CNF and conduit production.

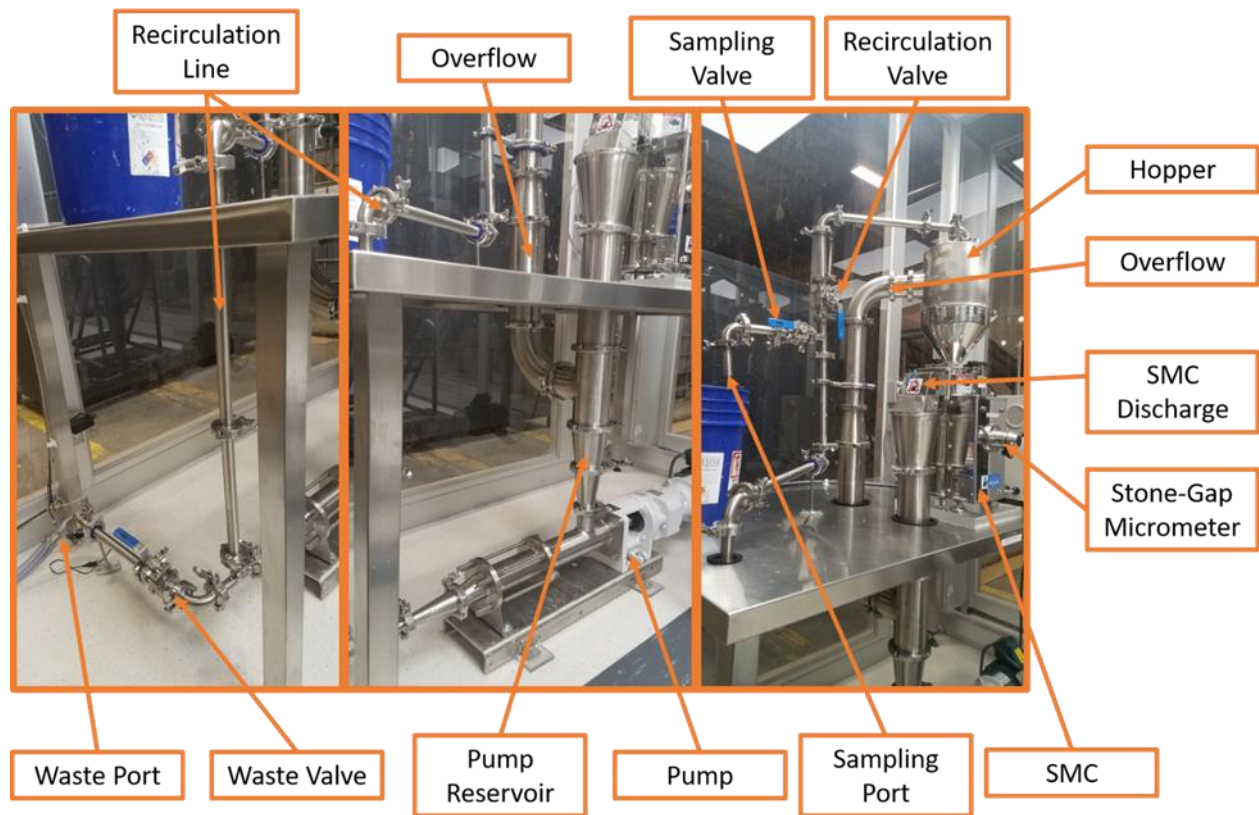


Figure 8: Supermasscolloider Refining System Components

3.3 SMC OPERATION

SMC operation was initiated by opening the gap between the refining stones (via the clearance adjustment) prior to turning on the drive motor; failure to separate the stones prior to engaging the drive motor could result in damaging them and/or the motor. The rotational speed of the stones was

initially set at 2,000 rpm, once this was achieved the gap between the stones was gradually decreased until there was a tonal change in the system characteristic of grazing stone contact. The inter-stone distance was set to zero under this condition via locking the gauging sleeve, and was used thereafter as a reference point, termed the zero point. Once the zero point had been determined and set, the inter-stone gap was opened to positive 50 μm in preparation for introduction of the pulp suspension to the system via the feed hopper. Feeding the system with an open but restricted gap ensured that all of the pulp that passed into the system experienced a preliminary refining period and that all fiber aggregates were subsequently broken down to dimensions less than the 50 μm inter-stone gap. When sufficient pulp suspension had been fed to the system to fill the intake line of the pump (14 L), circulation of the suspension was commenced via energizing the pump (set to 14.4 L/min). The system was filled to its 14 L capacity, at which point the slurry in the hopper continuously passed into the overflow passage for recirculation. Once the system was full and recirculation had commenced, a slurry sample, referred to as a zero-time sample, was taken from the recirculation line entering the hopper, via filling a 100 mL container; the inter-stone gap was subsequently reduced to negative 100 μm . There is intentional flexibility in the positioning of the stones such that when they are adjusted to a negative distance setting, the fluid between the stones will keep them flexed outward preventing harmful contact of the stones whilst providing pressure for grinding.

At each 15-minute time interval beyond the zero-time of the run, a 100 ml sample was removed from the system (with care taken to ensure that the total volume removed for the run did not exceed 1 L). When sampling from the SMC system, the gap was opened for one minute to positive 100 μm to allow the slurry to circulate freely throughout the system and to mix with the contents of the pump reservoir. The gap was subsequently returned to negative 100 μm , the cumulative electrical energy consumption of the run was recorded from the power meter, and the 100 ml sample was taken for off-site morphological analysis. It is noted that the SMC was typically run to a targeted cumulative energy

consumption value, which was demonstrated to correlate with reproducible CNF fiber morphology, see Section 3.5. A final sample was collected before removing the CNF from the system by opening of the waste valve on the recirculation line to allow the pump to force the slurry out of the system versus into the hopper. The pump was shut off prior to its inlet line being emptied (which would have risked damage to the pump). The system was subsequently cleaned by running a copious amount of DI water through it; the system was deemed clean when no fibers were visible in the waste stream.

3.4 CNF SLURRY CHARACTERIZATION

During the refining process, the viscosity of the pulp slurry increases dramatically as the percentage of fines (fibers less than 200 μm) increases, see Figure 9. The increase in viscosity is attributed to the progressively greater fiber/fibril entanglements that occur as the pulp fibers are increasingly segmented and defibrillated. The dramatic increase in viscosity (several orders of magnitude) makes refining a challenge as it becomes increasingly difficult to pump the slurry. Fortunately, however the CNF slurry is shear thinning, a fact that does enable processing if great care is

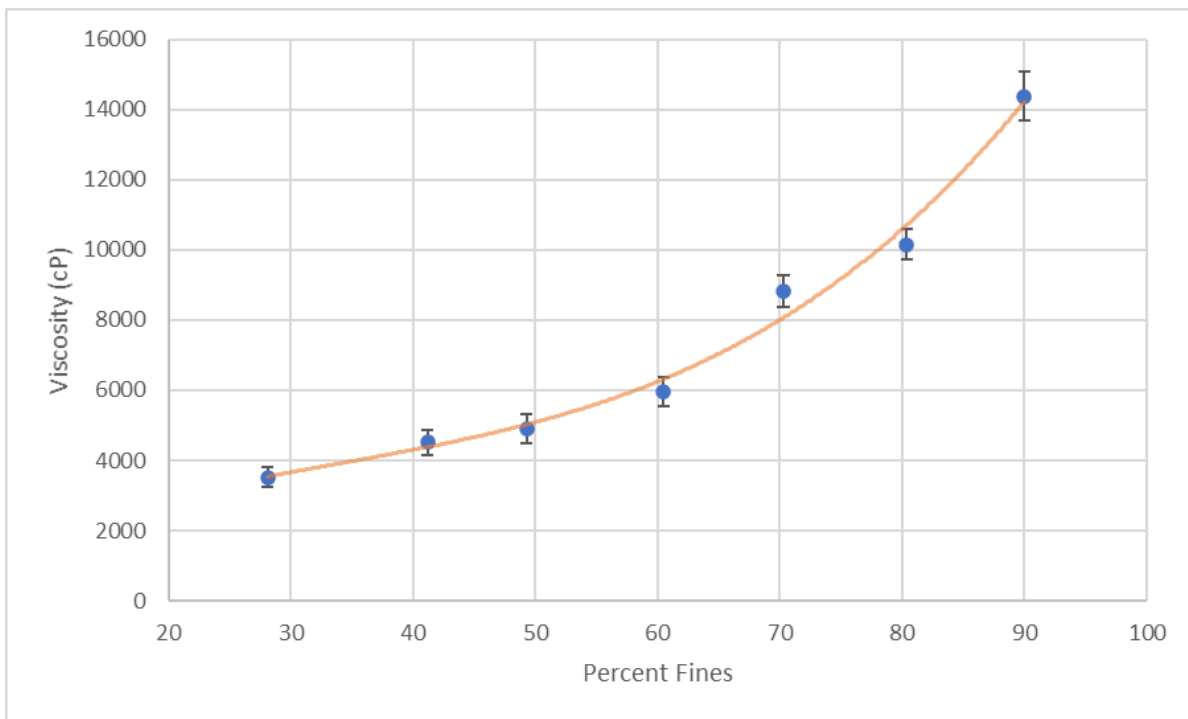


Figure 9: Viscosity Characteristics of CNF Production by Percent Fines
Viscosity of refined cellulose nanofiber slurries, at ~2% solids by weight, over a range of percent fines

taken in system design and operation. It is noted that the high viscosity of the CNF slurry also impedes mixing, care must therefore be taken to avoid inconsistencies throughout CNF slurry production, and other downstream processes. The viscosity of a CNF slurry is also heavily dependent upon the solids content. Care must therefore be taken to ensure CNF slurry production is performed at a solids content that enables appropriate fluid flow (typically 3wt% CNF or less).

3.5 CNF MORPHOLOGICAL DETERMINATION/DEVELOPMENT OF CALIBRATION CURVES

The MorFi Fiber and Shiv Analyzer (Techpap MorFi Compact) is the standard device employed in the pulp and paper industry to measure fiber size, fiber diameter, distribution of these values, kink angle, etc. The MorFi Fiber and Shiv Analyzer, referred to hereafter as the MorFi, housed in the Pilot Plant of the UMaine Process Development Center was employed throughout the present work for CNF fiber analysis. Specifically, a 25 g sample of CNF slurry produced by the supermasscolloider was diluted via addition of DI water bringing the solution up to 1 L, followed by a subsequent 1:100 dilution with deionized water to produce a 50 mg/L CNF slurry. The diluted suspension was circulated through the MorFi where several images of the fibers were taken. The MorFi performed several calculations on the images of the fibers in the diluted suspension and determined arithmetic means, distributions etc. of fiber physical parameters. Fibers that were greater than 200 μm in length may be measured by the MorFi; fibers of smaller dimensions that are not able to be measured are termed 'fines' and are reported as such. Consequently, a CNF slurry that had been measured by the MorFi as containing 90% fines comprised particulates, 90% of which had lengths less than 200 μm .

MorFi analysis was employed to track the progress of the refining of cellulose pulp to cellulose nanofiber through progressive segmentation and defibrillation, see Figure 10. It is important to note that the feedstock softwood pulp has a significant native percentage of fines (23%), prior to refinement in the SMC. Development of a consistent method to produce CNF resulted in the adoption of a 90% fines

slurry at a solids content of 2 wt% as the standard material for production of CNF sheets and hence conduits.

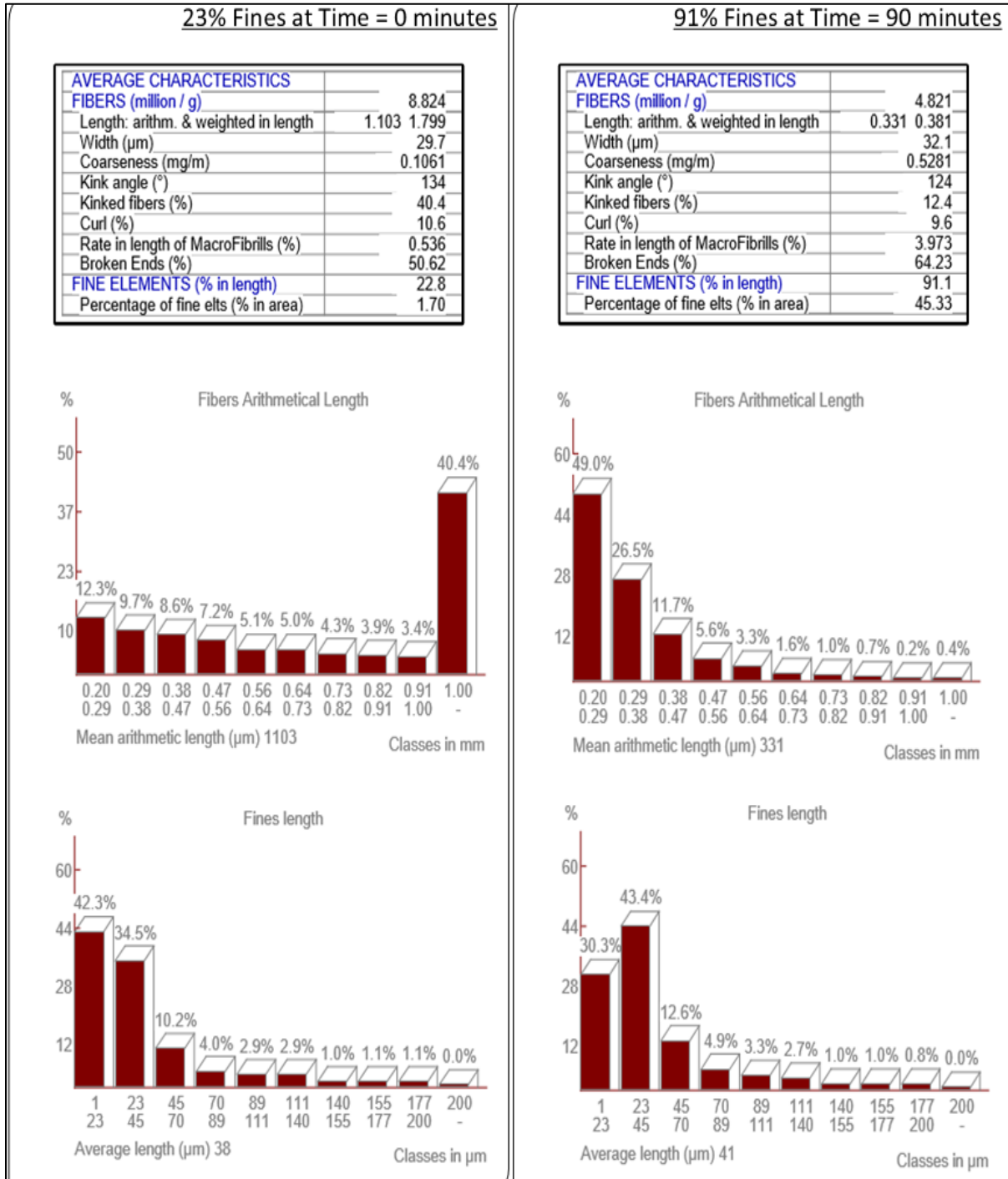


Figure 10: MorFi Fiber Characteristic Analysis
MorFi fiber analysis of the transition of fiber into fines through refinement of wood pulp (left) into cellulose nanofibers (right)

Cumulative energy consumption of the drive motor for the rotor of the SMC system (i.e. not including the recirculating pump energy consumption) was shown to be strongly correlated with the resultant cellulose fiber size, and the fiber distribution. As such, desired fiber distribution values were achieved through establishment of calibration curves, in triplicate, between fiber size/distribution and cumulative energy consumption values, see Figure 11.

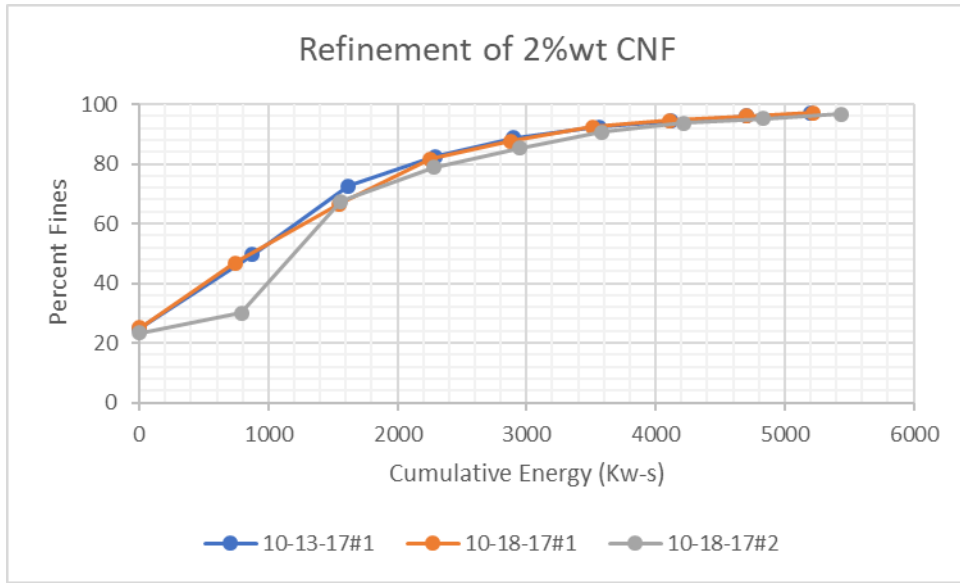


Figure 11: Correlation of Energy and Fines
Calibration of improved refining system to correlate fines with energy input for three trials

3.6 SHEET FORMATION

CNF was employed at 2 wt% solids and 90% fines to create sheets by spreading onto stainless steel plates. A casting knife film applicator was used to spread CNF into a wet sheet of 75 thousandths of an inch (~1.9 mm) thickness. The sheets were left to dry overnight on the stainless-steel plates under ambient conditions. The dried sheets were removed using razor blades to gently trim the sheets' edge from the plate followed by lifting the sheets from the top to the bottom as the edges were trimmed. After sheet removal, the sheets were left to adjust to standard temperature and humidity (23°C and 50%RH) in the Process Development Center (PDC's) TAPPI room.

3.7 CNF SHEET THICKNESS MEASUREMENTS

The thickness (caliper) of dried CNF sheets was measured employing a benchtop digital micrometer (TMI, 49-85) housed in the TAPPI room of the Pulp and Paper Process Development Center. Prior to making thickness measurements, CNF sheets were allowed to acclimatize for a 24-hour period in the 23 °C, 50% relative humidity conditions of the TAPPI room. Individual sheets were measured in twelve locations in a 3 row by 4 column configuration in the landscape orientation, with measurements evenly spaced. A mean and standard deviation were calculated from the twelve measurements of each sheet.

3.8 TENSILE STRENGTH MEASUREMENTS

The tensile strength of CNF sheets was measured employing a combination of TAPPI standard methods 220 (pulp handsheets) and 494 (paper and paperboard). Specifically, the sample size was as defined in TAPPI standard method 220 (10 cm in length by 1.5 cm in width), and the rate of elongation remained constant as per TAPPI standard method 494 (25 mm/min). CNF sheets were acclimatized to the temperature and relative humidity of the TAPPI room for 24 hours prior to measurements being made. An Instron model 5564 running the Instron Bluehill software package was employed to perform tensile strength measurements. Samples were cut to the specified dimensions and clamped within the upper and lower grips of the Instron machine, extension and load were recorded until the sample broke. It is noted that when casting the CNF sheets the action of the draw knife spreading the slurry potentially creates a 'machine direction'; as such samples for tensile testing were cut both parallel to, and perpendicular to, the machine direction.

To calculate the Young's modulus of each sample, load and extension were converted to stress and strain, respectively. Stress was found through dividing load by the cross-sectional area of the test strip. Strain was calculated as the ratio of the deformed length to the original length of the test strip. Stress was plotted on the y-axis as a function of strain on the x-axis. Young's modulus is defined as the

initial, linear, slope of the stress-strain curve and was determined by maximization of the R-squared value of the fitted trend line for each sample [74].

3.9 AIR PERMEABILITY MEASUREMENTS

Air permeability of CNF sheets was measured employing a Gurley 4340N Automatic Densometer and Smoothness Tester equipped with an air filter and desiccator to ensure the input air was clean and had a low moisture content. The Densometer was housed in the TAPPI room of the Process Development Center; all CNF sheets were acclimated in the TAPPI room for 24 hours prior to measurements being undertaken. The Densometer measured the amount of time required to pass 100 cubic centimeters of air through the material being tested, with data reported in Gurley Seconds. The greater the number of Gurley Seconds measured for a given sample, the less permeable it was. The measurement was performed by placing a CNF sheet into the Densometer where it was clamped in place over a charged cylinder that released air onto one surface of the sheet. Air that passed through the sheet flowed through an exit chamber equipped with a flow meter. The results from each test were recorded manually from the instruments display.

3.10 OXYGEN PERMEABILITY MEASUREMENTS

The oxygen permeability of CNF sheets was determined employing a MOCON OX-TRAN 2/22 OTR analyzer. CNF sheets were cut and double masked with aluminum foil to an area of 5 cm² and adhered to the lightly greased sample cell of the analyzer. The two halves of the sample cell were brought together on the respective sides of the sample to hold it in place and were pneumatically sealed during testing. Sample cells were subsequently loaded into the analyzer and 8 oxygen transmission rate tests were performed at four relative humidity values (duplicate measurements were performed at each relative humidity value). The temperature of the sample was maintained at 37°C and the permeant concentration of oxygen was set to 100%. The relative humidity was altered by modification of the test and carrier gas humidities permeating the sheet. The relative humidities

employed in the present work were 0%, 50%, 80%, and 90%. The duration of the measurement varied as the test was performed until a transmission rate was converged upon. Measurements were terminated when five consecutive transmission rates differed by less than 1%. The final value of transmission rate was converted into a permeation rate via normalization by the thickness of the CNF sheet. The resulting data at the four relative humidities were plotted and a value for the permeation rate of the CNF sheet at 100% was obtained via extrapolation. Oxygen permeability was measured by Dr. Mehdi Tajvidi of the University of Maine on CNF sheets provided by the author.

3.11 DIFFUSION COEFFICIENT OF GLUCOSE IN A CELLULOSE NANOFIBER SHEET

The diffusion coefficient of glucose in the cellulose nanofiber conduit wall was determined experimentally in the present work. Specifically, a series of tanks were designed and constructed that were equipartitioned via a cellulose nanofiber sheet comparable to those employed to create the conduits (~ 50 μm in thickness (dry)). One chamber per tank was filled with a phosphate buffered saline (PBS) solution of known glucose concentration (referred to as the donor chamber), the other chamber was filled with a PBS solution of zero glucose concentration (referred to as the receiver chamber). Due to the concentration gradient, glucose diffused across the CNF sheet from the donor to the receiver chamber; glucose concentrations in the receiver container were monitored as a function of time to enable calculation of a diffusion coefficient. Specifically, the diffusion coefficient was calculated via a method adapted from that of Suhaimi et al. [27], represented by Equation 1:

Equation 1: Fick's First Law Adaptation

$$\frac{\partial C_d}{\partial t} = -D_e A \cdot \frac{C_d - C_r}{l \cdot V_d} \rightarrow \frac{1}{A \cdot \frac{C_d - C_r}{l \cdot V}} \cdot \frac{\partial C_r}{\partial t} = D_e$$

where C_d and C_r are the initial glucose concentrations of the donor and receiver chambers, respectively, in mol/m^3 . l is the thickness of the CNF sheet in meters, A corresponds to the area of the CNF sheet in m^2 , V represents the volume of the donor/receiver chambers (which were equivalent) in m^3 , ∂C_r is the

difference in glucose concentration measured in the receiver chamber in mol/m^3 for a given time interval of ∂t in seconds. Finally, D_e is the effective diffusion coefficient of CNF to glucose in m^2/s . It is noted that all parameters in Equation 1 are known from the experimental design, or may be measured, to yield a diffusion coefficient.

The bi-chambered tanks, see Figure 12, were constructed from 3.175 mm thick polycarbonate with internal dimensions of 50 mm H x 50 mm W x 80 mm L; an acrylic plastic cement adhesive (SciGrip 16) was employed to glue and seal all joints. A central divider was implemented to separate the tanks into two equal sized chambers. The divider was constructed of two 50 mm x 50 mm pieces of polycarbonate from which approximately a 40 mm x 42.5 mm rectangle of polycarbonate had been removed from the center. A 50 mm x 50 mm sheet of CNF was placed between the two polycarbonate divider components and sandwiched in place employing SciGrip 16 adhesive. The divider was subsequently glued in place, again employing SciGrip 16 adhesive. After all the joints had cured (24

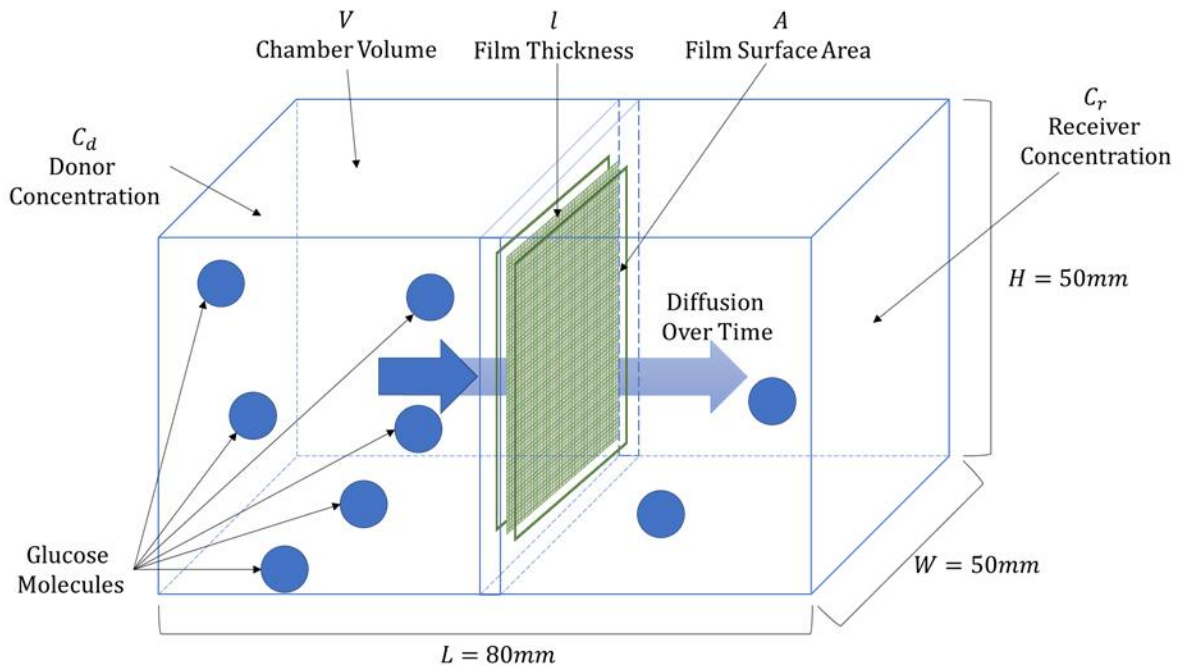
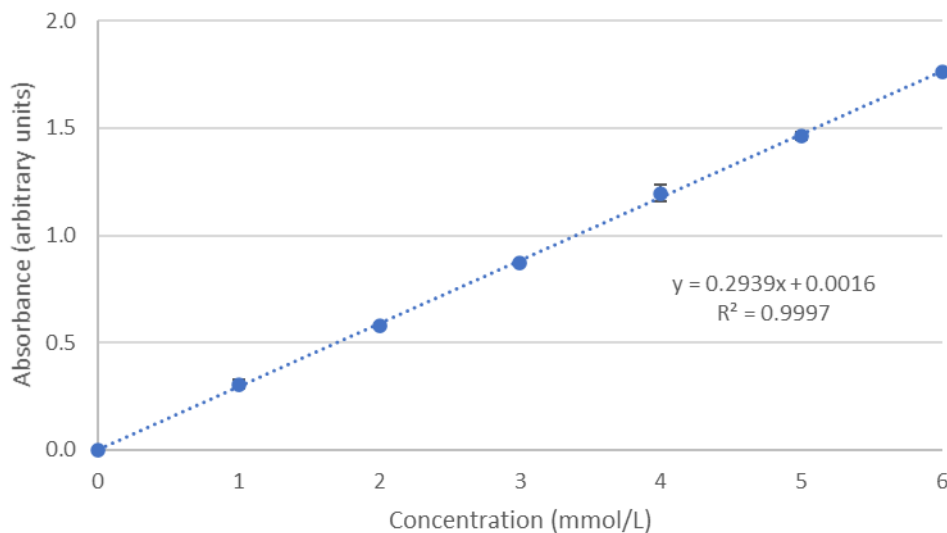


Figure 12: Glucose Diffusion Experiment
Glucose diffusion tank experimental setup for elucidation of the glucose diffusion coefficient of CNF sheets

hours), the chambers of a given device were filled with PBS solutions containing, or not, a defined concentration of glucose and subsequently sealed from the atmosphere employing Parafilm®.

Glucose concentration was measured in the receiving chamber employing a glucose hexokinase assay kit (Sigma Aldrich GAHK20). The assay kit operates via a two-step enzymatic reaction. Specifically, glucose and ATP are enzymatically phosphorylated to glucose-6-phosphate and ADP by hexokinase. Subsequently, glucose-6-phosphate dehydrogenase converts glucose-6-phosphate and NAD into 6-phosphocluconate and NADH. Each reaction is equimolar and consequently the concentration of NADH (which may be measured spectroscopically at 340nm) is directly proportional to the amount of glucose present in the original sample.



*Figure 13: Glucose Hexokinase Assay Standard Curve
Standard Curve for known glucose concentrations using a glucose hexokinase assay kit, error bars included using one standard deviation*

A calibration curve for NADH absorbance at 340 nm vs glucose concentration was developed employing the assay kit and standard solutions prepared with known glucose concentrations in 1x PBS. Glucose concentrations spanned the biologically relevant range of 0 – 6 mmol/L in increments of 1mmol/L. The measured NADH absorbance at 0 mmol/L was invariant from the reference and was hence determined a single time. The remaining 6 standards were tested in triplicate. A linear calibration curve resulted from the measured absorbance values with an r-squared value of 0.9997, see

Figure 13. Four bi-chambered diffusion tanks were created, resulting in a total of 12 absorbance values (and hence glucose concentrations) spanning a measured time range of 3 hrs to 96 hrs, see Appendix A4.

All parameters in Equation 1 were either defined by the experimental design, or readily measured, with the exception of CNF sheet thickness. The dry thickness of the sheet was readily determined using a digital caliper as $50 \pm 2 \mu\text{m}$. However, the relevant sheet thickness is that in the hydrated state. As such wet sheet thickness was measured via a digital caliper as approximately $70 \mu\text{m}$, indicating significant swelling, an observation confirmed via determination of the mass of water uptake. A sheet thickness of $70 \mu\text{m}$ was consequently used when employing Equation 1. Employing the data gathered from the bi-chambered diffusion experiments the glucose diffusion coefficient in CNF sheets was determined to be $1.7 \pm 0.9 \times 10^{-11} \text{ m}^2/\text{s}$, a value employed in subsequent COMSOL modeling.

3.12 CNF SHEET POROSITY

The porosity of CNF sheets was determined via the technique of mercury porosimetry employing a Micromeritics Autopore IV porosimeter. Specifically, the mass of a sample of a CNF sheet of approximately 0.02-0.03 g was measured to four decimal places and the sample mounted in the penetrometer. The penetrometer was subsequently sealed and inserted into the pressure chamber of the porosimeter. The pressure exerted on a reservoir of mercury in contact with the sample was progressively increased, thereby altering the characteristic contact angle of the mercury and forcing it into progressively smaller pores within the sample. The inverse relationship between pore size and applied pressure enabled calculation of pore size, pore size distributions, cumulative volume etc. The resulting data was exported in both numerical and graphical form. Mercury porosimetry measurements were performed by Dr. Lisa Weeks of the University of Maine on CNF sheets provided by the author.

3.13 CNF SHEET TOPOGRAPHY

The topography of CNF sheets was measured employing a Tencor Alphastep 500 mechanical profilometer. Specifically, CNF sheets were cut into strips approximately 38 mm long by 6 mm wide. Samples were cut in both the machine and cross-machine directions to check for variability. Each sample strip was fixed to a glass slide using double-sided tape. Samples were attached with either the side that dried in contact with the stainless-steel plate during sheet formation up, or the side that dried exposed to air up. Individual samples were loaded into the profilometer such that the stylus could scan from left to right, parallel to the length of the sample and centered on the width of the sample. The stylus position was set to zero at approximately $\frac{1}{4}$ of the sample length from the left edge. The profilometer was set to scan a 2 mm length and record the average surface roughness. The measurement was repeated for a total of three measurements per sample. It is noted that samples were taken from sheets cast on two different plates. Each combination of plate used for casting, machine or non-machine direction, and exposed surface during drying were tested 6 times.

3.14 CONDUIT FORMATION

In early work, conduits were made by employing a simple rectangular pattern of CNF sheet to roll cylinders comprising 2 to 7 layers; 2 layers became the standard over time based on feedback from surgeons regarding rigidity and transparency. Typically, conduit patterns were cut with dimensions of 1.5 x 2.5 cm. The pattern was rolled around a mandrel with a diameter of 1.65 mm to produce a 2-layered conduit that was 2.5 cm in length. Initially, conduits were sealed on the final wrap using water to leverage the native hydrogen bonding properties of cellulose. It was discovered however that as the diameter of the conduits increased 2 to 3-fold, the water seal was insufficient, and conduits had a tendency to delaminate and completely unroll. Improvements were made to the conduit design by employing CNF slurry instead of water to seal the final wrap. The slurry seal proved to be a dramatic improvement for smaller diameter conduits, however inconsistent results were obtained at the largest diameters.

To address the inconsistency of seal effectiveness at large diameters, i.e. 3-fold and larger, a mechanical interlock was developed for the outer layer. The interlocks consisted of tabs and corresponding slits. The interlocks proved so effective that they were adopted for all diameter conduits, and in later work interlocks were applied to the interior layer as well, see Figure 14. CNF slurry was applied to the exterior tabs after they had passed through the exterior slits in order to adhere the tabs to the conduit wall.

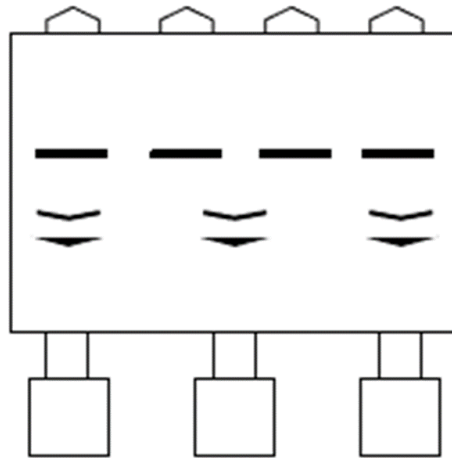


*Figure 14: Mechanical Interlock Design
Conduit design with exterior and interior interlocks to aid in retention of structural stability*

An additional coating of CNF was applied postproduction to improve the structural integrity of the conduits. Specifically, after the slurry seal of the conduit and its tabs had dried, and before removal of the conduit from the mandrel, an outer coating of 2 wt% CNF was applied to the conduit by submerging it in an aliquot of slurry. The coating was allowed to dry overnight whilst undergoing constant rotation, thereby creating a seamless final layer on the conduit.

3.15 PACKAGING

Completed conduits were packaged in polypropylene bags in preparation for shipping. Fully dried conduits were removed from the mandrels and inspected for any visible defects. It was common that residual CNF coating had to be removed from the ends of the conduit in order to provide a perfectly smooth and regular conduit. Conduits that passed visual inspection were bagged and sealed using an

impulse sealer under ambient conditions (ULINE H-161). Each polypropylene bag was labeled with the following information: conduit interior diameter, conduit length, description of conduit pattern, initials of producer, date produced, as well as a customized identification code. The identification code allowed tracking of production parameters such as pulp changes, slurry changes, which sheet the conduits were cut from, as well as additional notes as necessary. After each conduit had been packaged, they were sent to an off-site sterilization center where the conduits were subjected to ethylene oxide sterilization.

3.16 ETHYLENE OXIDE STERILIZATION

Conduits were sterilized using ethylene oxide gas (Anprolene, model number AN74i). Heat-sealed packages containing individual conduits were opened and each wrapped in a non-woven fabric sheet (Dynarex, CSR wrap) and placed in a resealable plastic bag. Each pouch was equipped with an Andersen package closure indicator strip to verify sufficient exposure to ethylene oxide gas upon treatment. Progressive exposure to ethylene oxide resulted in migration of a blue indicator bar from the left side of the strip toward the right side. Correct exposure to ethylene oxide had been achieved when the indicator bar reached a triangular mark on the strip. The resealable pouches, complete with indicator strips were left open, packed in a single liner bag and placed into the sterilization chamber. Care was taken to ensure that as the pouches were loaded into the liner bags, all pouches remained opened and if stacked they were not stacked on the opening of another. An additional indicator strip was inserted into approximately the center of the liner bag. One ampoule of ethylene oxide, in a gas-release bag, was inserted into the top of the liner bag followed by the purge probe. The opening of the liner bag was then sealed around the neck of the probe with a Velcro strap. With the door of the chamber open, the liner bag was purged for 1.5 minutes, removing some but not all air from the liner bag. The ampoule at the top of the liner bag was then carefully broken manually and the sterilization cabinet door was quickly closed and locked. The ethylene oxide gas released then filled the liner bag as well as the individual resealable pouches. The sterilization cycle proceeded for a 24-hour period; upon

completion, a two-hour air purge process was undertaken. All indicator strips were examined to confirm sufficient ethylene oxide exposure. Subsequently the chamber was unloaded and the resealable pouches were sealed while in the liner bag prior to disconnecting the purge probe from the liner bag. The sealed pouches containing the sterilized conduits were removed from the liner bag and set aside for future implantations. Ethylene oxide sterilization was performed by Dr. Paul Sweetnam of Redux Therapeutics on CNF conduits provided by the author.

3.17 CELL CULTURE AND CELL GROWTH STUDIES

Three cell types were employed to assess their ability to grow on CNF sheets. Motor neurons, Schwann cells, and macrophages were individually cultured to be seeded on polystyrene cell culture dishes, and separately, cellulose sheets. Schwann cells (ScienCell Research Laboratories, 1700) were purchased and cultured according to supplier specifications using Schwann cell medium (ScienCell Research Laboratories, 1701). Macrophages (ATCC, RAW 264.7 TIB-71) were purchased and cultured according to supplier instruction in Dulbecco's modified eagle's medium (ATCC, 30-2002). Motor neurons were differentiated from human embryonic stem cells (Harvard University, HuES-3 HB9::GFP) in mTeSR1 (STEMCELL Technologies, 85850) media [75]. All cells were incubated at 37°C in a 5% CO₂ environment.

Three substrates were employed in the cell growth study: standard polystyrene cell culture plastic, untreated CNF sheets, and laminin-infused CNF sheets. Prior to seeding cells on the plastic substrate, the surface was coated with Matrigel (VWR, 47743-706). CNF sheets were used without surface modifications. Laminin infused CNF sheets were formed via the addition of 1 mg of laminin, from a 1.19 mg/mL solution (Gibco, 23017015), to 20 mL of CNF slurry prior to sheet formation; no surface modifications were employed. Cells were seeded individually on each of the substrates and the respective growth media added. Cells were grown for 7 days before staining with Calcein AM (ThermoFisher, C1430) and fluorescently imaged. Calcein AM is a cell-permanent dye that is only

fluorescent in viable cells. Living cells cleave acetoxymethyl groups by intracellular esterases that converts the dye to a green fluorophore. Live cells of all 3 types on each of the substrates were imaged employing a fluorescence microscope at a wavelength of 520 nm. Cell culture studies were performed by Dr. Paul Sweetnam of Redux Therapeutics using CNF sheets provided by the author.

3.18 CONDUIT IMPLANTATION

Two murine studies were performed, in addition to a single non-human primate study, in the course of the present work. Murine studies were performed by the Eggan Laboratory at Harvard University. The non-human primate study was performed at the Southwest National Primate Research Center of the Texas Biomedical Research Institute. All experimental protocols and procedures were approved by the Animal Care and Use Review Office (ACURO) and the local Institute of Animal Care and Use Committee (IACUC).

For murine studies, the subjects were anesthetized with either a 1.25% (w/v) injection of tribromoethanol-tert-amyl alcohol in DI water (0.5 mL/25 g mouse) or 1-2% (v/v) isoflurane in an oxygen flow. The site of implantation was shaved and disinfected with a combination of betadine swabs and alcohol. The subjects also received a preemptive dose of buprenorphine, 0.05-0.1 mg/kg, to relieve pain. For the surgeries, only the left hindlimb was operated on and the right leg of each subject was left unaffected as a control leg. The hindlimbs were secured making a right angle at the knee joint relative to the body. An incision was made across the midline of the disinfected area, the skin was gently cut and folded back revealing the underlying musculature. The sciatic nerve was revealed in the left hindlimb through opening the plane between the gluteus maximus and the anterior head of the biceps femoris. Removal of the surrounding fascia allowed for clear access to the nerve to begin excision and implantation of the conduit.

The procedure for conduit implantation began with placement of two polypropylene sutures through the nerve at approximately 6 mm apart centered between the sciatic notch and the distal

bifurcation, as observed under a light microscope. The neural conduit was subsequently placed over the uncut sciatic nerve and the two suture ends at one terminus of the conduit were run axially through the interior of the conduit and out of the opposite terminus. Once conduit placement was confirmed and the suture ends appropriately positioned, the nerve was transected, creating a neural gap. The conduit was subsequently gently worked into the gap and over the nerve stumps by moistening the surgical area with sterile saline and inserting the neural stumps into the conduit. Upon successful placement of the nerve stumps within the conduit, the sutures were tied together on the outside of the implant. The suturing technique allowed for the conduit to remain centered over the neural gap, whilst also ensuring that the neural stumps could not be removed from the interior of the conduit. The musculature was subsequently sewn together with absorbable sutures, and clips were used to close the external wound. The wound clips were removed 7 days post-surgery.

Due to different objectives (discussed in Chapter 5), the two murine studies varied in several surgical details. The first study comprised two separate groups. The first group consisted of mice for which the sciatic nerve was transected, but no tissue was deliberately removed from the resulting nerve stumps, a conduit was implanted as described above. The second group consisted of mice for which the same sciatic nerve transection was performed, but with nerve stumps bridged by a single polypropylene suture to maintain neural alignment in the absence of a conduit. The second murine study comprised neural gaps created by deliberate excision of 1 mm or 3 mm segments of neural tissue, achieved by transection of both neural stumps. Additionally, the second study employed several minor variants of repair techniques that were necessitated via the experimental design, the specifics are detailed in Section 5.4.

The non-human primate study employed a radial nerve versus a sciatic nerve model due to the accessibility of the radial nerve and anticipated observations of digit mobility as an indicator. Comparable surgical methodologies to those employed for the murine study were adopted for the non-

human primate study. Three subjects were included in the study. Subjects 1 and 3 received conduits over a severed nerve, with no tissue removed. Subjects 1 and 2 received sutures at the site of injury to assist in alignment of the neural stumps. The results of this study are detailed in Section 5.6. Conduit implantation was performed by Dr. Joanie Mok and Dr. Maura Charlton of Harvard University using conduits provided by the author.

3.19 GRIP STRENGTH ANALYSIS OF MICE

The grip strength of the hindlimbs of mice was measured using a Bioseb grip strength testing device (Bio-GS3). The device was equipped with a T-handle bar attachment. Mice were positioned with the hind limb of interest over the bar, which they instinctively gripped. The mice were subsequently pulled backwards in the horizontal plane with respect to the device, until they released the bar. The peak tensile force recorded by the device was considered the maximum grip strength of the limb. Measurements were made in triplicate, and for both limbs, allowing normalization of the data from the limb that had been operated on by the control limb. Grip strength analysis was performed by Dr. Joanie Mok and Dr. Maura Charlton of Harvard University.

3.20 END OF LIFE ANALYSIS

At the completion of the murine studies (approximately 40 weeks for study one, and 20 weeks for study two), the mice were prepared for end of life analysis. Each mouse was weighed, a video taken to observe hindlimb locomotion, and the grip strength of the hindlimb, with and without the implant, measured. Grip strength was measured in triplicate as described above. Humane euthanasia was performed using 100% (v) isoflurane followed by transcardial perfusion with 4% (w/v) paraformaldehyde in phosphate buffered saline (PBS) to prepare for dissection and tissue removal. The hindlimbs were dissected to reveal the sciatic nerve in the control limb as well as the conduit and nerve in the opposing limb. An image was taken of the surrounding tissues prior to resection to allow for qualitative assessment of the surgical site. Both the control nerve and the conduit-repaired neural segment were

resected from the respective hindlimbs for tissue processing. As the neural segments were removed, each received a suture on the proximal end of the segment to ensure consistent alignment and orientation during tissue embedding.

Neural segments were immersed in 4% (w/v) paraformaldehyde in PBS for 24 hours before undergoing several saline wash cycles. Pairs of control and conduit-repaired segments from each animal were blotted dry and set into HistoGel (ThermoFisher, 22-110-678) with care taken to ensure proximal end correlation, and parallel alignment. The HistoGel-embedded neural segments were placed in a biopsy cassette (Globe Scientific, 1090W) to facilitate the paraffin-embedding process. Specifically, the samples were subjected to multiple alcohol washes of increasing concentration in order to progressively dehydrate the tissues. The samples were subsequently washed with xylene three times (with the residence time of each wash progressively increasing from 30 to 60 minutes), and finally washed twice with paraffin with a residence time of one hour per wash.

Embedding of the tissues in paraffin allowed for the neural segments to be sectioned employing a microtome (Leica RM2255). Each tissue block was assigned three zones, labeled A - C as indicated in Figure 15, to denote the proximal stump, the conduit region, and the distal stump, respectively. Cross-sectional samples were collected by floating 4 μm thick sections in triplicate on the water surface in a heated water bath and then collecting the sections on a slide submerged at an angle into the water bath. Five slides were collected serially per 100 μm of tissue to be analyzed using a variety of histological techniques. Excess tissue sections per 100 μm regions were either mounted for test-staining or disposed of appropriately. End of life analysis was performed by Dr. Joanie Mok and Dr. Maura Charlton of Harvard University.

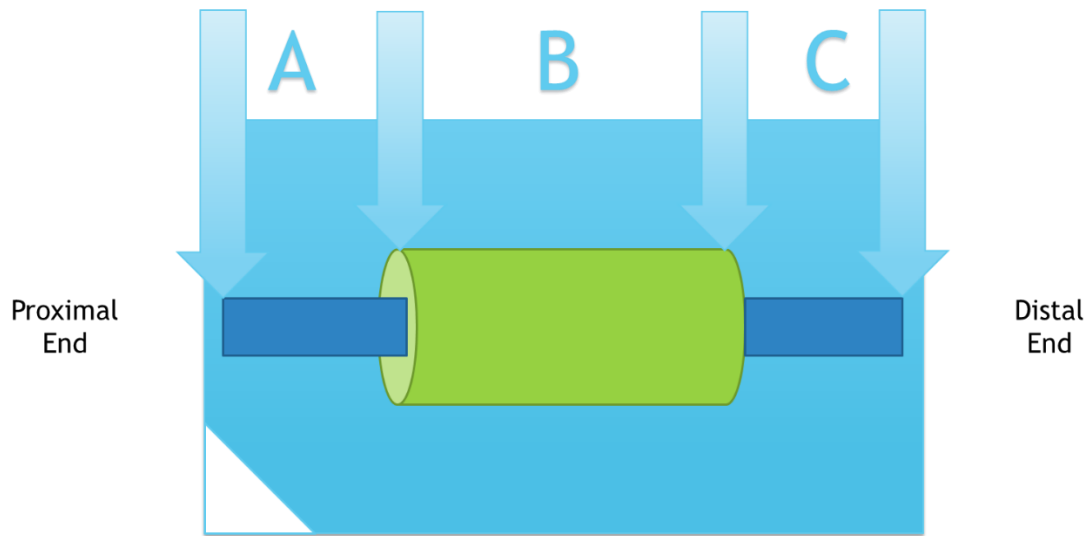


Figure 15: Zone Analysis of Tissue Sections
 Division of zones for tissue sectioning to separate the proximal stump (A), the conduit and regeneration zone in the neural gap (B), and the distal stump (C)

3.21 SLIDE PREPARATION AND STAINING

Once sectioned and mounted on slides, the paraffin wax in which the tissues were embedded had to be moved, and the samples rehydrated, to facilitate staining. HistoClear II (VWR, 64111-04) was employed to remove paraffin from the tissue sections. Specifically, slides were washed two times with HistoClear for 5 minutes each wash. Samples were subsequently washed with alcohol solutions of decreasing concentration to gradually rehydrate the tissues. After two 1-minute washes, in each of the three descending alcohol concentrations (100%, 95%, 70%), the slides were washed in DI water for 2 minutes to fully rehydrate the neural sections. The hydrated tissues were subsequently stained for histological analysis.

Three histological staining systems were employed on the neuronal tissue sections; Hematoxylin and Eosin (H&E) for visualization of cellular structure and cell types (Sigma-Aldrich, HHS128 and HT1101128), Luxol Fast Blue for identification of myelin (VWR, KT022), and Calcofluor White for localization of cellulose (Sigma-Aldrich, 18909). The H&E staining procedure was performed as follows: first, hematoxylin was applied to the tissues to stain the nuclei of cells a red-purple color. An acid wash was subsequently employed to remove excess hematoxylin from surrounding tissues. Scotts bluing

agent was then applied to darken the hematoxylin stain. Lastly, eosin was employed as a counter stain to color non-nuclear elements of the tissue with various shades of red/pink which were viewed via brightfield microscopy. The staining procedure for H&E required significant optimization in order to maximize contrast, see Table 4.

*Table 4: Hematoxylin and Eosin Staining Procedure
Adaptations performed on general Hematoxylin and Eosin procedures to increase contrast*

<i>Alterations in timing to improve staining</i>			
<i>Stain/Step</i>	Test #1	Test #2	Test #3
<i>Hematoxylin</i>	3 min	4 min	4 min
<i>Water</i>	2 min	2 min	2 min
<i>Acid Alcohol</i>	2 quick dips	1 quick dip	1 quick dip
<i>Water</i>	1 min	1 min	1 min
<i>Scott's Blue</i>	3 min	3 min	3 min
<i>Water</i>	1 min	1 min	1 min
<i>Eosin</i>	1 min	2 min	3 min
<i>95% EtOH</i>	1 min x2	1 min x2	1 min x2
<i>100% EtOH</i>	1 min x3	1 min x3	1 min x3
<i>Histoclear</i>	1 min x3	1 min x3	1 min x3

The presence and distribution of myelin in the tissue samples was determined via application of the myelin-specific stain Luxol Fast Blue. First, a coplin staining jar was filled with approximately 55 ml of Luxol Fast Blue, the container was subsequently placed in an oven that had been pre-heated to 60 °C. Once the stain had reached the target temperature, the dewaxed slides were immersed in the solution, where they remained for a period of 4 hours at 60 °C. The slides were subsequently removed from the Luxol Fast Blue solution and rinsed with copious amounts of DI water to remove excess stain. The tissues were subsequently differentiated using a dropper to apply lithium carbonate to the tissue section for 30 seconds. Finally, the slides were rinsed again with DI water to remove residual lithium carbonate and then placed in clean container for storage. Stained slides were viewed via brightfield microscopy. It is noted that a counterstain procedure was not performed, as such myelin in the tissue samples was stained deep blue.

Calcofluor White is a non-specific fluorochrome that binds to cellulose and chitin in cell walls and is typically used for detection of yeast and pathogenic fungi. In the present work Calcofluor White was employed for identification of cellulose nanofiber comprising the neural conduits. Calcofluor White was deposited directly onto the dewaxed tissue sections via a dropper, covering the surface of the tissue section. The stain was allowed to equilibrate for 60 seconds before excess was removed from the slide by wicking into an absorbent material from the edge of the slide. After removal of excess stain, the slides were immediately imaged via fluorescence microscopy. Preliminary histology was performed by the author, in addition to Dr. Joanie Mok, and Dr. Maura Charlton of Harvard University.

CHAPTER FOUR

CELLULOSE NANOFIBER SHEET CHARACTERIZATION AND NEURAL CONDUIT DEVELOPMENT

4.1 CNF SHEET CHARACTERIZATION

CNF sheets were created by casting 100mL of 2 wt% CNF slurry directly onto stainless steel plates, as per the methodology detailed in Section 3.6. It should be noted that in the development phase of CNF sheet production, a variety of materials were trialed as casting plates with mixed results. Specifically, plastic and plastic-coated metal plates created deformed and inconsistent sheets, aluminum plates resulted in metal particulate contaminants in the sheet upon removal, and glass plates bound the CNF sheets to the extent that they could not be removed intact. CNF sheets were successfully cast on stainless steel plates and characterized in a variety of manners as detailed in the following sections.

4.1.1 SHEET THICKNESS

A series of 12 CNF sheets were created, 6 each on two different stainless steel plates. The thickness of each sheet was measured in order to assess the consistency of sheet formation. Thickness

Table 5: Sheet Thickness Analysis

Sheet thickness consistency of 12 CNF sheets cast on two separate stainless steel plates, all values reported in μm .

1st Stainless Steel Plate						2nd Stainless Steel Plate						
Sheet A	Sheet B	Sheet C	Sheet D	Sheet E	Sheet F*	Sheet A	Sheet B	Sheet C	Sheet D	Sheet E*	Sheet F**	
1/2/2018	1/3/2018	1/4/2018	1/8/2018	1/9/2018	1/10/2018	1/3/2018	1/4/2018	1/8/2018	1/9/2018	1/10/2018'	1/11/2018	
54	53	54	52.5	52.5	55	54	54	53.5	56.5	55.5	59	
55	54	53	52.5	56.5	56.5	55.5	54	57	58	56	60	
57.5	56	55	51.5	53.5	60.5	51.5	55	51	57.5	60.5	58.5	
58.5	58.5	55.5	56.5	57	60.5	53	56.5	57.5	55	57	58	
55	55.5	58.5	54	57.5	53.5	57.5	55	56	58.5	57	61	
58.5	57	53	52.5	57.5	56.5	55	51	53.5	57	59.5	60.5	
54.5	57.5	56.5	54.5	56.5	63	58.5	54	57	54	57.5	57	
55.5	56.5	57	55.5	58.5	56	57.5	57	56.5	58.5	58	58.5	
57.5	54.5	55	55.5	55.5	53.5	56	53	55	57.5	59	58	
59.5	56.5	57.5	57.5	54.5	57	56.5	52	53.5	57	58	59	
58.5	57.5	57	56.5	57	59.5	56	54.5	56.5	56.5	59.5	60	
59	55.5	56	56	55.5	55.5	55.5	54	56	57.5	56.5	56	
Per Sheet												
Avg.	55.5	54.2	55.3	57.0	57.8	58.8	56.9	56.0	55.7	54.6	56.0	57.3
StDev.	1.9	1.6	1.9	1.3	1.5	1.4	1.9	1.5	1.7	1.9	1.7	2.9

*Humidity was 34% these days versus 25% in the first day

**Humidity was 23% these days versus 25% in the first day

Overall Avg. 56.2 μm
StDev. 1.3 μm

measurements were made employing a benchtop digital caliper as per the methodology described in Section 3.7. The 12 sheets were measured to have an average thickness of 56.2 μm with a standard deviation of less than 1.5 μm (less than 3% of the sheet thickness), see Table 5. It should be noted that sheet thickness was found to be readily adjustable through variation of the solids content of the CNF slurry employed to cast the sheet.

4.1.2 TENSILE STRENGTH TESTING

Tensile strength testing was performed on the CNF sheets in order to ascertain the Young's modulus, or the modulus of elasticity under tension – defined as the ratio of the stress acting on a material to the strain produced. Tensile testing was performed as described in Section 3.8 and the Young's modulus was taken as the gradient of the linear portion of each stress vs strain curve, as may be seen in Figure 16. Tensile data were recorded for CNF sheets oriented parallel to the machine (blade) direction, with Young's modulus values observed to range from 4.99-5.71 GPa. Tensile data recorded for CNF sheets oriented perpendicular to the machine direction (cross machine direction) resulted in Young's modulus values in the range of 4.62-5.10 GPa. Statistical analysis via Minitab (two sample t-test, $P < 0.001$, see Appendix A5) revealed that the average Young's modulus of samples taken in the parallel direction was statistically greater than the average of samples taken in the perpendicular direction.

4.1.3 SURFACE PROFILOMETRY MEASUREMENTS

Due to the casting method employed to create the CNF sheets, as described in Section 3.6, the resultant sheets possessed two markedly different surfaces. Specifically, the face that dried in contact with the stainless steel plate was smoother and had a greater sheen relative to that which dried exposed to air, as evidenced by both visual and tactile investigation. To quantify the surface roughness of the sheets, sample strips were collected from sheets cast on two different stainless-steel plates (designated P1 and P2). Strips were cut in both the machine (blade) and cross-machine direction, (designated M and C, respectively). The surface roughness of all strips was measured employing a Tencor Alphastep 500



Figure 16: Tensile strength testing of CNF sheets
Samples taken in the machine and cross-machine directions

mechanical profilometer, as described in Section 3.13. The surface roughness of both sides of each sheet was tested with the side that was dried in contact with the steel plate designated S, and the side that was dried exposed to air designated A. For each combination of parameters, two individual CNF strips were cut and analyzed (a and b), each individual measurement was performed in triplicate. Figure 17 presents the surface roughness data obtained. It is evident from examination of Figure 17 that neither

the direction that the CNF strip was cut relative to the casting process, nor the individual stainless steel plate employed for casting, had any significant effect on the surface roughness of the sheets. However, the air-exposed, and stainless steel plate contacting, surfaces were consistently statistically different (see Appendix A5, 2 sample t-test with $p < 0.001$). Indeed, the surface dried exposed to air had an average surface roughness across all sheets of $3.17 \mu\text{m}$, while the surface dried in contact with the stainless steel plate had an average surface roughness across all sheets of $0.70 \mu\text{m}$.

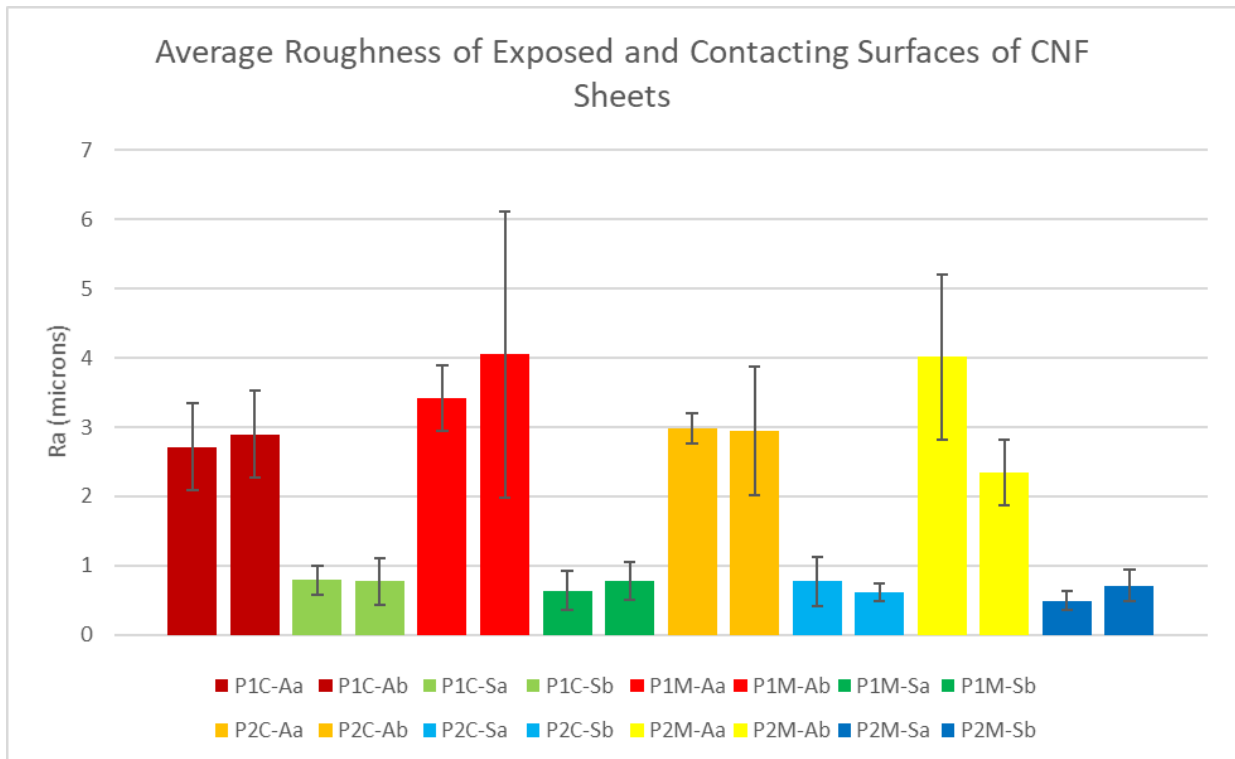


Figure 17: Surface Roughness Measurement Results
Average surface roughness (Ra) of two distinct sheet sides. P1-plate 1, P2-plate 2, C-cross machine direction, M-machine direction, A-air exposed, S-steel contacting, a-sample one, and b-sample 2

4.1.4 CNF SHEET TRANSPARENCY

CNF sheets, and hence neural conduits constructed from CNF sheets, inherently possess a degree of transparency; a significant attribute that aids surgeons visualize the surgical field. In order to ascertain the extent to which CNF sheet transparency could be controlled, sheets of varying thickness were created via modification of the solids content of the slurry cast on the stainless steel plates, and by variation of the height of the casting knife applicator. The resulting dried sheets were conditioned in a

temperature and humidity-controlled environment, in compliance with TAPPI standards, prior to measurement of their thicknesses. All sheets were made in duplicate. One of each duplicate CNF sheet was hot calendared in the UMaine Process Development Center via two passes through the nip of two heated steel rollers. Figure 18 presents the solids content of the slurry employed, the thickness of the sheets resulting from variation of the height of the casting knife applicator, and images depicting the transparency of the calendared and non-calendared sheets. Investigation of Figure 18 reveals that the thinner the initial CNF sheet the greater the transparency, and that the transparency is significantly increased via calendaring.

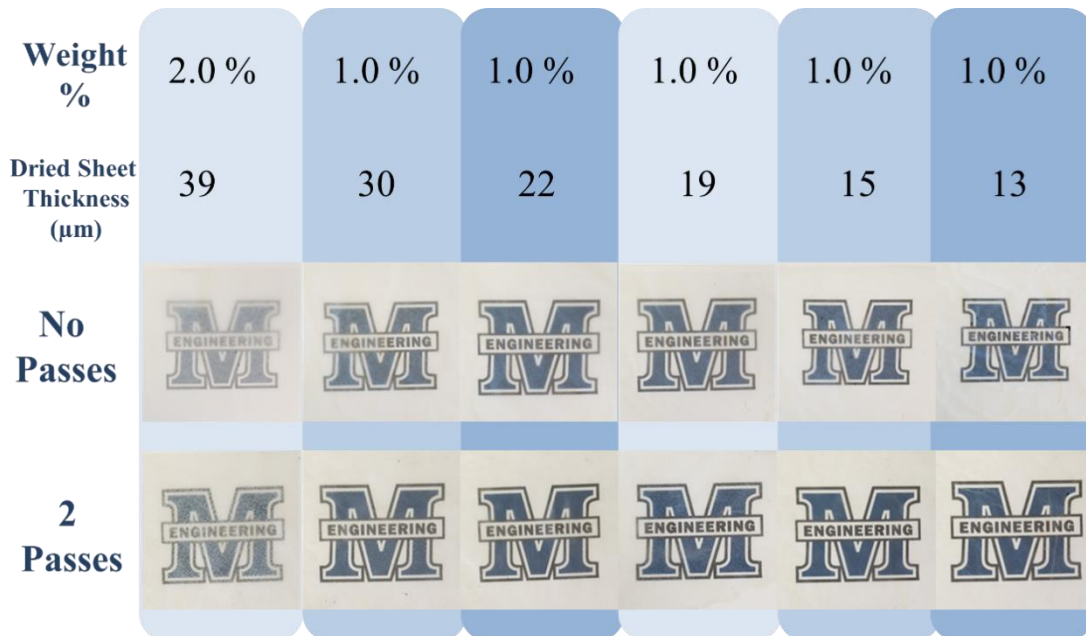


Figure 18: CNF Sheet Transparency
The effect of varying sheet thickness and calendaring on transparency.

4.1.5 AIR PERMEABILITY OF CNF SHEETS

The air permeability of CNF sheets was determined employing a Gurley 4340N Automatic Densometer and Smoothness Tester via the methodology described in Section 3.9. The densometer measures the amount of time required to pass 100 cm³ of air through a sample and reports in units of Gurley Seconds over a range of 0-50,000. Testing of CNF sheets consistently resulted in an output of

“Too dense to read”, implying that the sheets were highly impermeable to air and required in excess of 50,000 seconds for the passage of 100 cm³ of air.

4.1.6 MERCURY POROSIMETRY OF CNF SHEETS

The porosity of CNF sheets was determined employing a mercury porosimeter, as described in Section 3.11. A representative plot of cumulative pore volume vs pore diameter is presented in Figure 19. Investigation of Figure 19 reveals that the CNF sheet possess no pores with diameters between 0.01 and 10 μm. It is noted that a spurious data point occurs at a pore diameter of ~10 μm which is attributed to a mechanical switch in pressure made by the operator to increase the pressure in the sample chamber. At extremely small pore diameters, Figure 19 possesses an anomalous peak (in the 0.01-0.03 μm range). Measurements in this pore diameter regime are known to be affected by the surface roughness of the sheet. As evidenced by the profilometer measurements, presented earlier in this section, the surface of the CNF sheet that was dried in contact with air was statistically rougher than the surface that was dried in contact with the stainless steel plate, likely giving rise to the inconsistent

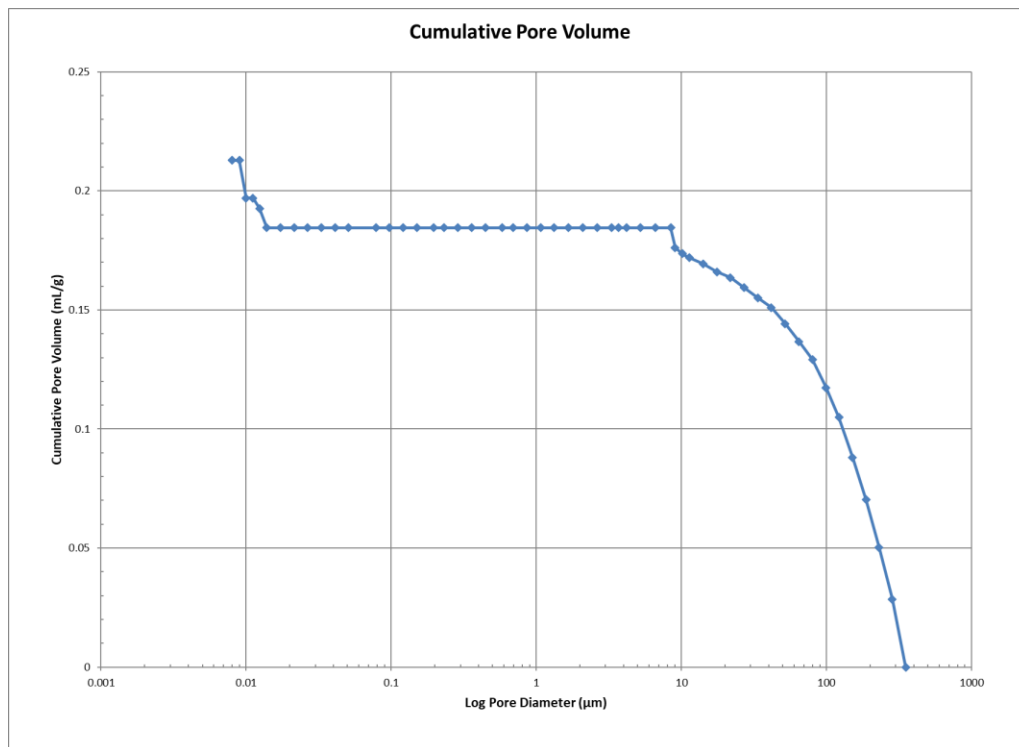


Figure 19: Mercury Porosimetry Results
Pore volume analysis of a CNF sheet

mercury porosimetry data at very low pore diameters. Taken in combination, the mercury porosimetry and the air permeability data suggest that the CNF sheets do not have any pores that completely traverse the thickness of the sheet, only small surface vacancies resulting from surface roughness.

4.1.7 OXYGEN PERMEABILITY OF CNF SHEETS

The oxygen permeability of CNF sheets was determined employing a MOCON OX-TRAN analyzer at relative humidity values of 0, 50, 80, and 90% via the methodology described in Section 3.10. Two CNF sheet samples were tested at each humidity, the resultant plot of oxygen permeation rate as a function of relative humidity is presented in Figure 20. It is evident from investigation of Figure 20 that the CNF sheets are permeable to oxygen and that the permeation rate increases in an exponential manner as the relative humidity increases above a value of 50%. Indeed at a relative humidity value of 90% the oxygen transmission rate of the CNF sheets was measured to be $\sim 181 \text{ cc}/(\text{m}^2\text{day})$, not dissimilar to the literature value for polyvinyl chloride of $150 \text{ cc}/(\text{m}^2\text{day})$ [76]. It is noted that polyvinyl chloride is widely used as a food wrap due to its semi-permeability to oxygen.

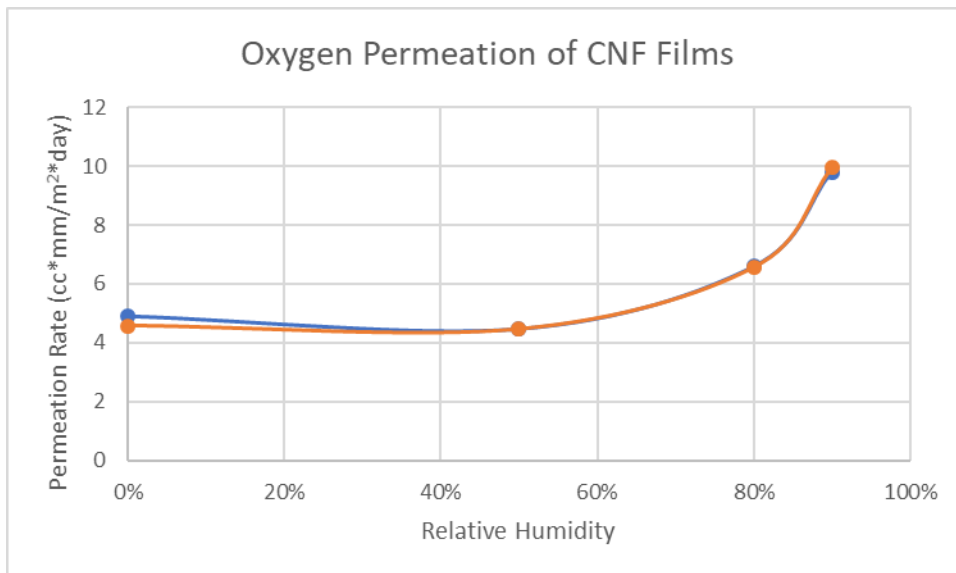


Figure 20: MOCON Oxygen Permeability Results
CNF sheet oxygen permeability measurements made on a MOCON Ox-Tran from 50-90% relative humidity. Initial measurements (blue) and duplicate measurements (orange)

4.2 CNF CONDUIT DEVELOPMENT

Various options were considered for initial development of CNF conduits, including casting methods such as drying the slurry in between an inner and an outer cylinder. However, due to the large amount of water that is removed upon drying (~98% of the slurry's wet weight), and the concomitant shrinkage, few methods were deemed viable. Indeed, the simplest, most robust method was determined to be rolling multi-layer tubes from sheets of dried CNF. Such a method enabled the shrinkage resulting from drying to occur in the sheet formation process, giving rise to changes in sheet thickness that could be controlled by the solids content, and the thickness of the slurry spread by the casting knife applicator. Once a CNF sheet of suitable thickness had been cast and dried, it was a straightforward process to cut the sheet into a rectangular form and roll it into a multilayer conduit employing a mandrel.

It was determined that in order to seal the outer flap of the CNF sheet to the wall of the conduit, and thereby produce a self-supporting, robust implant, a method should be developed that avoided the use of an adhesive. The decision to avoid the use of an adhesive was made based on the desire not to introduce an additional material into the CNF conduit construct that might require regulatory approval. As such a range of methods of sealing the outer flap of the CNF sheet to the conduit were evaluated. Numerous additional CNF conduit geometries and CNF devices are presented in Appendix A6.

4.3 CONDUIT SEAL EMPLOYING NON-MECHANICAL MEANS

The simplest method to seal the outer flap of the CNF sheet was to wet the inner face of the sheet with water and press it onto the conduit wall, thereby using the well-known hydrogen bonding nature of CNF to seal the conduit layers together [77]. Initial inspection and qualitative testing of the water sealed conduits suggested however, that they were not as stable when exposed to an aqueous environment (such as that found *in vivo*) as was hoped for. An alternative method of sealing the outer flap of the conduit was therefore evaluated. Specifically, rather than applying solely water to the inner

surface of the flap, 2 wt% CNF slurry was applied thereby enhancing the hydrogen bonding capabilities of the seal by including suspended cellulose nanofiber. A final methodology developed to aid in sealing the CNF conduit layers was to coat the entire construct in CNF (post construction, with the outer flap sealed with CNF slurry) by submerging it in 2 wt% CNF slurry and allowing it to air dry. The coating was intended to provide a seamless final layer which would function to prevent delamination of the external layer of the conduit.

4.4 EVALUATION OF CONDUIT SEAL INTEGRITY

In order to assess the integrity of the outer seal of the conduits made via water, CNF slurry, and CNF slurry coupled with an external CNF coating, a static immersion test was developed. Specifically, conduits were immersed in vials containing aqueous solutions of biological relevance, namely water, saline solution (9 g NaCl in 1 L water), ringer's solution (7.2 g NaCl, 0.37 g KCl, and 0.17 g CaCl₂ in 1 L water), and PBS buffer (1X concentration) and their structural integrity assessed as a function of time. In order to determine if the number of CNF sheet wraps employed to construct the conduits factored into the stability of the outer seal, conduits employing 1, 2 and 3 wraps were evaluated. Two conduits were employed for each of the nine conditions (1 wrap water seal, 2 wraps water seal, 3 wraps water seal, 1 wrap CNF seal, 2 wraps CNF seal, 3 wraps CNF seal, 1 wrap CNF seal-dip coated, 2 wraps CNF seal-dip coated, 3 wraps CNF sealed dip-coated) in each of the four solutions, resulting in a total of 72 conduits. Once the pairs of conduits were placed in the relevant vials, they were left undisturbed for the duration of the test.

The structural integrity of each conduit was assessed at three time points: 24 hours (1 day), 2 weeks (14 days), and 1.5 months (46 days). Conduits that were observed to have delamination of the outer layer were assigned a score of 0. A score of 1 was given to conduits that were intact and stable. The results for each conduit at the 24-hour time point are presented in Table 6. Investigation of Table 6 reveals that conduits sealed with water performed poorly with only 25% of the conduits remaining

intact. The CNF sealed, and CNF sealed and CNF coated, conduits performed significantly better with 62.5% and 75% remaining intact, respectively. It was concluded therefore that the water seal was inferior to the CNF seal. No clear trend with regard to the stability of the conduits as a function of the number of wraps was evident at the 24-hour time point.

*Table 6: First Conduit Stability Study Results at 24 Hours
Analysis of conduits composed of varying number of layers and seal techniques after 24 hours in various solutions
Scoring of 1 means the conduit passed inspection, 0 indicates structural failure*

		CONDUITS									Sum / Soln.
		Water Seal			CNF Seal			Dipped			
		1-Wrap	2-Wrap	3-Wrap	1-Wrap	2-Wrap	3-Wrap	1-Wrap	2-Wrap	3-Wrap	
Solutions	Water	0	0	0	1	1	0	1	1	1	7
		0	0	0	1	0	0	0	1	0	
	Ringer's	0	1	1	0	0	0	0	1	1	9
		0	1	0	1	1	0	0	1	1	
PBS	1	0	1	1	1	1	0	1	1	14	
	0	0	1	1	1	1	1	1	1		
Saline	0	0	0	1	1	0	1	1	0	9	
	0	0	0	1	1	0	1	1	1		
Sums / Seal / #Wrap		1	2	3	7	6	2	4	8	6	
Sums / Seal		6			15			18			

Table 7 presents data for conduit stability at the 14 day and 1.5-month time points. Investigation of Table 7 reveals that only 8% of the water sealed conduits remained intact after 46 days: not a surprising result given the 24 hour and two-week data. As at the earlier time points, the CNF sealed conduits performed better than the water sealed conduits, although only 25% remained intact after 1.5 months. The CNF sealed and CNF coated conduits performed significantly better than the other variants at the 1.5-month time point with ~46% of conduits remaining intact. The data of Table 7 indicate that the stability of the conduits is not a strong function of the number of wraps of CNF sheet employed in their construction, although 2-wrap conduits were consistently either the most stable, or equal most stable, versus 1 and 3-wrap conduits.

Table 7: First Conduit Stability Study Results at 14 and 46 Days
 Analysis of conduits composed of varying number of layers and seal techniques after 14 and 46 days in various solutions
 Scoring of 1 means the conduit passed inspection, 0 indicates structural failure

Solutions	CONDUITS									Sum / Soln.																				
	Water Seal			CNF Seal			Dipped																							
	1-Wrap	2-Wrap	3-Wrap	1-Wrap	2-Wrap	3-Wrap	1-Wrap	2-Wrap	3-Wrap																					
Water	0	0	0	0	1	0	1	1	0	3																				
	0	0	0	0	0	0	0	0	0																					
Ringer's	0	1	0	0	0	0	0	1	1	3																				
	0	0	0	0	0	0	0	0	0																					
PBS	1	0	0	0	1	1	0	0	1	8																				
	0	0	0	1	1	0	1	1	0																					
Saline	0	0	0	1	0	0	1	1	0	5																				
	0	0	0	0	0	0	1	0	1																					
<table border="1" style="width: 100%; border-collapse: collapse;"> <tr> <td style="width: 15%;">Sums / Seal / #Wrap</td> <td style="width: 10%;">1</td> <td style="width: 10%;">1</td> <td style="width: 10%;">0</td> <td style="width: 10%;">2</td> <td style="width: 10%;">3</td> <td style="width: 10%;">1</td> <td style="width: 10%;">4</td> <td style="width: 10%;">4</td> <td style="width: 10%;">3</td> </tr> <tr> <td>Sums / Seal</td> <td colspan="3">2</td> <td colspan="3">6</td> <td colspan="3">11</td> </tr> </table>											Sums / Seal / #Wrap	1	1	0	2	3	1	4	4	3	Sums / Seal	2			6			11		
Sums / Seal / #Wrap	1	1	0	2	3	1	4	4	3																					
Sums / Seal	2			6			11																							
<div style="background-color: #fce4d6; padding: 2px; display: inline-block;">Conduit Failed After 1.5 Month Period</div> <div style="background-color: #fff9c4; padding: 2px; display: inline-block;">Conduit Failed After 2 Week Period</div>																														

4.5 EVALUATION OF THE EFFECT OF CNF SHEET THICKNESS ON CONDUIT INTEGRITY

A potentially important parameter in the stability of CNF conduits is the effect of the thickness of the sheet employed in their construction. CNF sheet thickness was considered to be potentially important as the stiffness of the sheet increases with thickness, and the flexibility and pliability decrease accordingly. As such a study was performed to determine the effect of CNF sheet thickness on the stability of conduits. Employing the findings from the conduit seal investigation, 2 wrap conduits were constructed employing the CNF seal and CNF coating method. Sheets of four different thicknesses, 52, 59, 76, and 86 μm were employed to create pairs of conduits which were subsequently placed in vials containing the same aqueous solutions employed in the seal integrity study. The stability of the conduits was assessed at time points of 24 hours and 18 days, with the binary scoring system of 0 for a delaminated conduit and 1 for an intact conduit applied.

Table 8: Second Conduit Stability Study Results at 24 Hours
 Analysis of conduits composed of varying sheet thicknesses after 24 hours in various solutions
 Scoring of 1 means the conduit passed inspection, 0 indicates structural failure

CONDUITS						
	Sealing Method	Two-Wrap & Dipped				Sum / Soln.
	Sheet Thickness	52um	59um	76um	86um	
Solutions	Water	1	1	0	0	4
		1	0	1	0	
	Ringer's	0	1	1	1	5
		1	1	0	0	
	PBS	1	1	0	0	5
		1	1	0	1	
	Saline	1	1	0	0	4
		1	0	1	0	
Sums / Sheet Thickness		7	6	3	2	

Table 8 presents data for conduit stability as a function of CNF sheet thickness at the 24-hour time point. Investigation of Table 8 reveals that conduit stability decreased monotonically with increasing sheet thickness, with conduits constructed from 52 and 59 μm CNF sheets remaining largely intact while conduits constructed of 76 and 86 μm CNF sheets largely failing. Little if any effect of variation of the aqueous solution on conduit stability was observed. Table 9 presents data for conduit stability as a function of CNF sheet thickness at the 18-day time point. Comparison of the data of Table 9 with those of Table 8 reveals very little change. Specifically, the number of structurally intact conduits constructed from the two thinnest CNF sheets remained unchanged, while one additional conduit constructed from each of the thicker CNF sheets failed. It was concluded from the study that conduits are most stable when constructed of thinner CNF sheets, preferably in the $\sim 50 \mu\text{m}$ range. It is noted that it is challenging to reproducibly create defect free CNF sheets with thicknesses less than 50 μm , hence the lower limit of the study.

Table 9: Second Conduit Stability Study Results at 18 Days
 Analysis of conduits composed of varying sheet thicknesses after 18 days in various solutions
 Scoring of 1 means the conduit passed inspection, 0 indicates structural failure

CONDUITS						
	Sealing Method	Two-Wrap & Dipped				Sum / Soln.
	Sheet Thickness	52um	59um	76um	86um	
Solutions	Water	1	1	0	0	3
		1	0	0	0	
	Ringer's	0	1	1	1	5
		1	1	0	0	
	PBS	1	1	0	0	4
		1	1	0	0	
	Saline	1	1	0	0	4
		1	0	1	0	
Sums / Sheet Thickness		7	6	2	1	

4.6 MECHANICAL INTERLOCKING CNF CONDUITS

The investigations of the effect of CNF seal methodology and sheet thickness on conduit stability were highly informative, however it is noted that even the optimized conduit designs had a portion of the samples that failed. It was determined therefore that an alternate method of conduit construction should be developed, while adhering to the premise that no additional materials should be introduced to the design. To achieve this objective, a series of mechanically interlocking closure devices were implemented to physically prevent delamination of both the inner and outer CNF layers.

Specifically, the previously rectangular CNF form was modified to contain tabs on both the top and bottom edges, with corresponding slits in the body of the sheet, see Section 3.14, Figure 14. When the CNF sheet was rolled around the mandrel to form a cylinder, the tabs were passed through the slits to provide a mechanical interlock, thereby preventing unravelling. The interior interlocks were held in place by the tension imparted by the rolling of the conduit. The exterior tabs were folded to pass through the slits and then unfurled to provide a profile broader than the slit and hence a mechanical

interlock. The tabs were subsequently adhered to the exterior surface of the conduit with CNF slurry, and the entire conduit coated in CNF to form a continuous, seamless outer surface.

4.7 EVALUATION OF THE STABILITY OF MECHANICALLY INTERLOCKED CNF CONDUITS

In order to evaluate the stability of the mechanically interlocked CNF conduits relative to their non-mechanically interlocked predecessors, and to do so in a relatively short time frame, a more intensive stability assay was developed. Specifically, conduits were immersed in DI water within 50 mL plastic centrifuge tubes and placed horizontally on an orbital shaker table (Innova 2000). The table was set to an agitation speed of 140 rpm and run for a 24-hour period. At the completion of the agitation cycle each conduit was evaluated with regard to mechanical stability/integrity.

The newly developed agitation assay was employed to perform a study of the effectiveness of the mechanical interlock in maintaining the structural integrity of the CNF conduit. Specifically, three types of conduits were assessed: mechanical interlock with a CNF coating, mechanical interlock without a CNF coating, and a non-mechanically interlock CNF sealed conduit with a CNF coating. Three conduits were constructed for each condition. Figure 21 presents an image of the nine conduits within their respective centrifuge tubes upon completion of the 24-hour agitation cycle. Investigation of Figure 21 reveals that the conduits created employing a mechanical interlock and a CNF coating (A-C) maintained

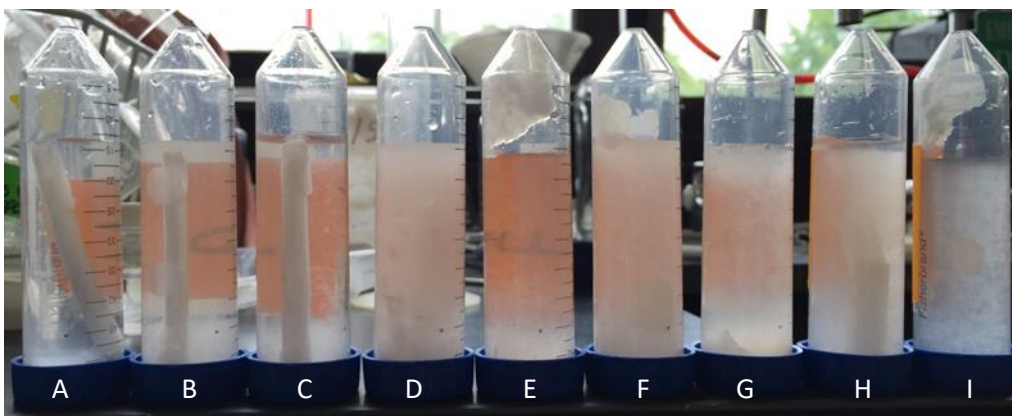


Figure 21: Third Conduit Stability Study Results at 24 hours
Third conduit stability study 24-hour analysis of three groups: mechanical interlock with CNF coating (A-C), mechanical interlock without CNF coating (D-F), and non-mechanical interlock with CNF coating (G-I) that were graded by retention of structure

their mechanical stability and experienced only occasional lifting of the external tabs. The conduits created employing a mechanical interlock but without a CNF coating (D-F) universally lost their mechanical integrity, as did the non-mechanical interlock conduits created with a CNF seal and CNF coating (G-I). It is evident therefore that conduits created employing a mechanical interlock and a CNF coating are remarkably stable, even under extreme conditions.

4.8 CONCLUSION

Neural conduits comprising CNF were successfully created from sheets of CNF. To create well defined and consistent conduits the precursor CNF sheets were thoroughly characterized. Specifically, sheets were cast on stainless steel plates and were determined to have a dried thickness of 56.2 ± 1.3 μm . A mechanical profilometer was employed to determine that the two sides of the CNF sheets had very different surface roughnesses; the side dried with exposure to air had an average roughness of 3.17 μm , while the side dried in contact with the stainless steel plate had an average roughness of 0.70 μm . The sheets were determined to be non-porous via both Gurley densometer and mercury porosimetry measurements. The CNF sheets were found to be semi-permeable to oxygen, with permeability increasing with relative humidity. The tensile strength of the CNF sheets was comparatively high with a Young's modulus average of approximately 5.3 GPa in the machine direction and 4.9 GPa in the cross-machine direction. It was determined that the transparency of the CNF sheets increased with decreasing sheet thickness, and increased with the application of hot calendaring.

Conduits were created from the CNF sheets by wrapping a CNF form around a mandrel. Various means of closing the outer flap of the conduit were evaluated and tested. Adhering the outer flap to the conduit via wetting with water was found to result in loss of conduit structural integrity in aqueous solutions. Adhering the outer flap with CNF slurry gave improved results, but still led to a large proportion of conduit failures. Adding a coating of CNF to CNF sealed conduits further improved conduit stability, however with extended immersion times conduit failures were still observed. It was

determined that a CNF sheet of approximately 50 μm thickness was optimal for conduit stability. Conduits closed with internal and external mechanical interlocks were developed to promote structural integrity. It was determined that conduits created with the interlocking tabs adhered with CNF slurry, and the entire conduit coated in CNF were extremely stable, even under testing conditions far more rigorous than found *in vivo*.

CHAPTER FIVE

CELLULAR COMPATIBILITY WITH CELLULOSE NANOFIBER AND *IN VIVO* STUDIES

5.1 CELLULAR PROLIFERATION ON, AND COMPATIBILITY WITH, CELLULOSE NANOFIBER SHEETS

In order to determine if CNF is in fact a viable material from which to construct neural conduits, a study was performed to evaluate the ability of various relevant cell types to be cultured on CNF. In addition, CNF sheets were modified via the inclusion of the extracellular matrix protein laminin to ascertain whether cellular interaction with the sheet could be tailored/enhanced. Three cell types were investigated: macrophages, Schwann cells and motor neurons. Macrophages were selected as they are one of critical cell types associated with a foreign body/inflammatory response and their interaction with CNF could be an indicator of the potential of CNF to induce a negative *in vivo* reaction. Schwann cells were investigated since they are the primary non-neural cell type associated with peripheral nerve regeneration and their interaction with CNF could potentially be predictive of the likelihood of CNF to directly support Schwann cell proliferation. Motor neurons were studied to determine if CNF could directly support neural regeneration.

CNF sheets were prepared via the procedures outlined in Section 3.6. Laminin containing CNF sheets were prepared by adding 1 mg of murine-derived laminin (Gibco, 23017015) to 20 mL of CNF slurry at 2 wt% solids and proceeding with sheet formation as per the standard procedure. Cell culture was performed via the methodologies presented in Section 3.17. As quantified in Section 4.1.3, the CNF sheets produced in the present work were distinctly 'sided'; cell culture was performed on the side dried with exposure to air given its comparatively high surface roughness (RMS average $\sim 3.17 \mu\text{m}$) and hence greatest likelihood of cellular attachment. Cellular number, distribution and morphology were

determined in a qualitative fashion employing fluorescent image analysis. Images were collected on a fluorescence microscope after cells were fluorescently labeled employing Calcein AM via methodologies presented in Section 3.16. Each cell type was cultured directly on standard cell culture plastic (polystyrene coated with Matrigel), on an untreated CNF sheet, and on a laminin-infused CNF sheet. Representative images of each condition are presented in Figure 22.

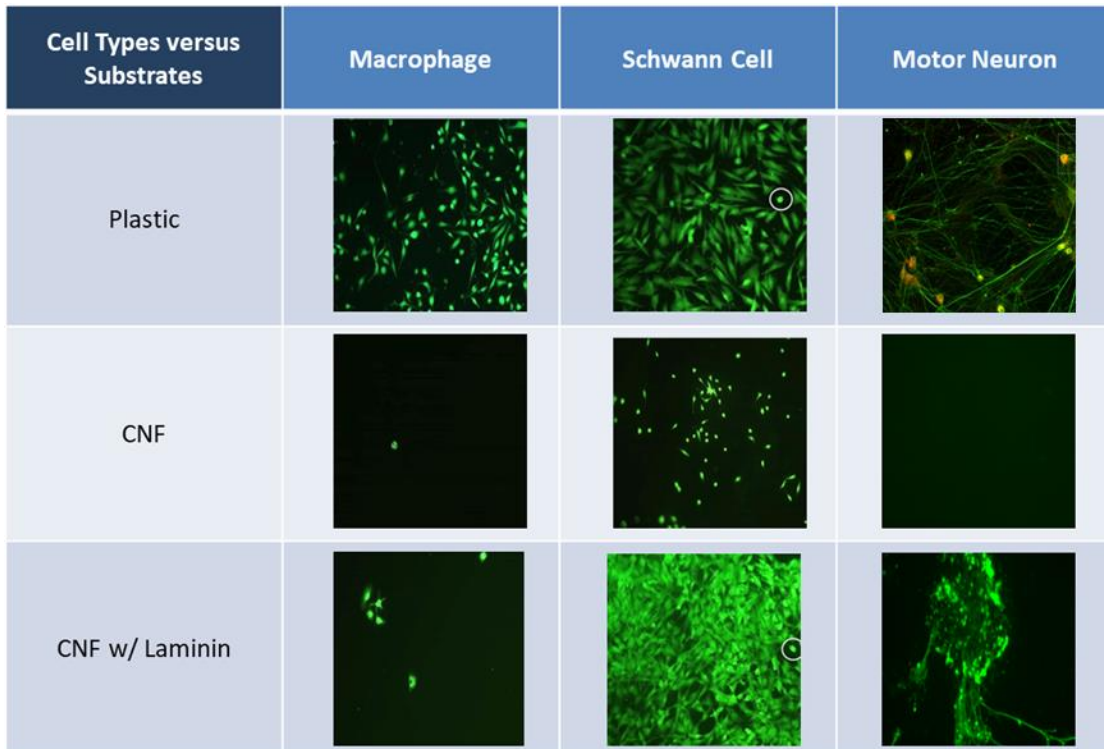


*Figure 22: Cellular Attachment Modification Study
Analysis of cellular attachment of Schwann cells, macrophages, and motor neurons on a plastic substrate, a CNF sheet, and a Laminin-infused CNF sheet. Motor neuron on plastic adapted from Moakley et al. [113]*

Investigation of Figure 22 reveals that macrophage growth was greatest on the plastic substrate, and further, that the cellular morphology was elongated/non-spherical indicating activation. Macrophage growth on the CNF sheet was negligible, with a single cell in the field of view. It is interesting to note that the single cell is comparatively spherical, indicating a non-activated state. The addition of laminin to the CNF sheet resulted in greater macrophage growth relative to the neat CNF sheet, although the numbers were comparatively low; a non-spherical morphology indicated a degree of activation. It is evident from Figure 22 that Schwann cell proliferation on the plastic substrate was

significant and that the cellular morphology was elongated indicating activation. Schwann cells had a comparable proliferation on the CNF sheet as on the plastic substrate, however their morphology was largely spherical suggesting an inactive state. The proliferation of Schwann cells on the laminin infused CNF substrate was extensive and the morphology was elongated. Motor neurons of the same cell line were cultured on the plastic substrate by Moakley et al. As may be seen in Figure 22, the cell culture plastic did support modest motor neuron growth and neurite extension. Unmodified CNF did not support motor neuron growth as may be seen from their absence in Figure 22. However, infusing a CNF sheet with laminin did lead to the growth and neurite extension of motor neurons, as evidenced by the lower right panel of Figure 22.

It may be concluded from the cellular proliferation and compatibility study that the plastic cell culture substrate led to macrophage proliferation and activation, an undesirable result. The plastic substrate did however promote Schwann cell proliferation and extension, in addition to modest motor neuron growth and neurite extension. CNF sheets were shown to be non-supportive of macrophage proliferation and extension-likely meaning that CNF would not elicit a significant foreign body/inflammatory response *in vivo*, a very important and positive finding. Schwann cells and motor neurons were largely not effective in proliferation and extension on CNF sheets, suggesting that CNF will likely not play an active role in neural regeneration, but rather may be present as an inert material construct. Interestingly, laminin infused CNF was largely non-supportive of macrophages, suggesting it may elicit only a weak foreign body/inflammatory response, but was highly successful in promoting Schwann cell and motor neuron proliferation and extension. The latter findings are extremely interesting and provide a path forward if in fact a conduit is desired that actively promotes and participates in neural regeneration.

5.2 INTRODUCTION TO *IN VIVO* STUDIES

With confidence that macrophages have very little if any interaction with CNF, and were certainly not activated by the material, and further, that Schwann cells and motor neurons experienced limited interactions with CNF, it was determined that *in vivo* studies of conduit implantation were viable. Two murine studies were performed to determine the efficacy of CNF neural conduits in promoting regeneration of peripheral nerves. A single, preliminary, non-human primate study was performed to determine the tolerance of the animal to CNF conduits. The murine studies were performed in collaboration with the Eggan Laboratory of Harvard University, while the non-human primate study was performed in collaboration with the Southwest National Primate Research Center of the Texas Biomedical Research Institute. All experimental protocols and procedures were approved by ACURO and local IACUC.

5.3 MURINE STUDY ONE: SCIATIC NERVE TRANSECTION WITH NO TISSUE RESECTION

The first murine study was aimed at determining the efficacy of implantation of CNF conduits over a severed sciatic nerve when no neural tissue was resected. Twenty, 8-week old female mice were employed. Female mice were used as age-related decline in motor nerve conduction has been shown to be less than that of male mice [78]. The cohort was broken into two groups, the first group comprised five animals which underwent surgery to have the sciatic nerve in the left leg severed and the nerve stumps sutured to surrounding tissues to keep them in place; no conduits were implanted in these animals. The second group comprised fifteen animals which underwent surgery to have the sciatic nerve in the left leg severed and a conduit sutured over the neural gap as per the methodology detailed in Section 3.18. The conduits used were 1 mm in diameter, 2 mm in length, approximately 100 μm in thickness, and sealed with water. In both groups, the sciatic nerve was severed in the left leg, therefore the right leg was used as a control to provide initial/maximum grip strength data. Over the course of 40 weeks the grip strength of the left and the right leg of each animal (both groups) were measured at 4-

week intervals employing the methodology described in Section 3.19, see Figure 23. Grip strength data are presented in Appendix A7.

Investigation of Figure 23 reveals that sciatic nerve regeneration within an implanted CNF conduit was far superior to regeneration when a conduit was not employed (sham surgeries). The grip strength of the conduit implanted legs increased monotonically to a maximum value at approximately 30 weeks and was of the order of six times the grip strength of legs that underwent the sham surgeries at the same time point. Indeed, comparison of the strength of the left leg with the right leg (control) enabled calculation of the percent recovery for each group. The conduit-implanted group obtained approximately 66% of the initial grip strength, while the sham surgery group obtained approximately 11% of the initial grip strength.

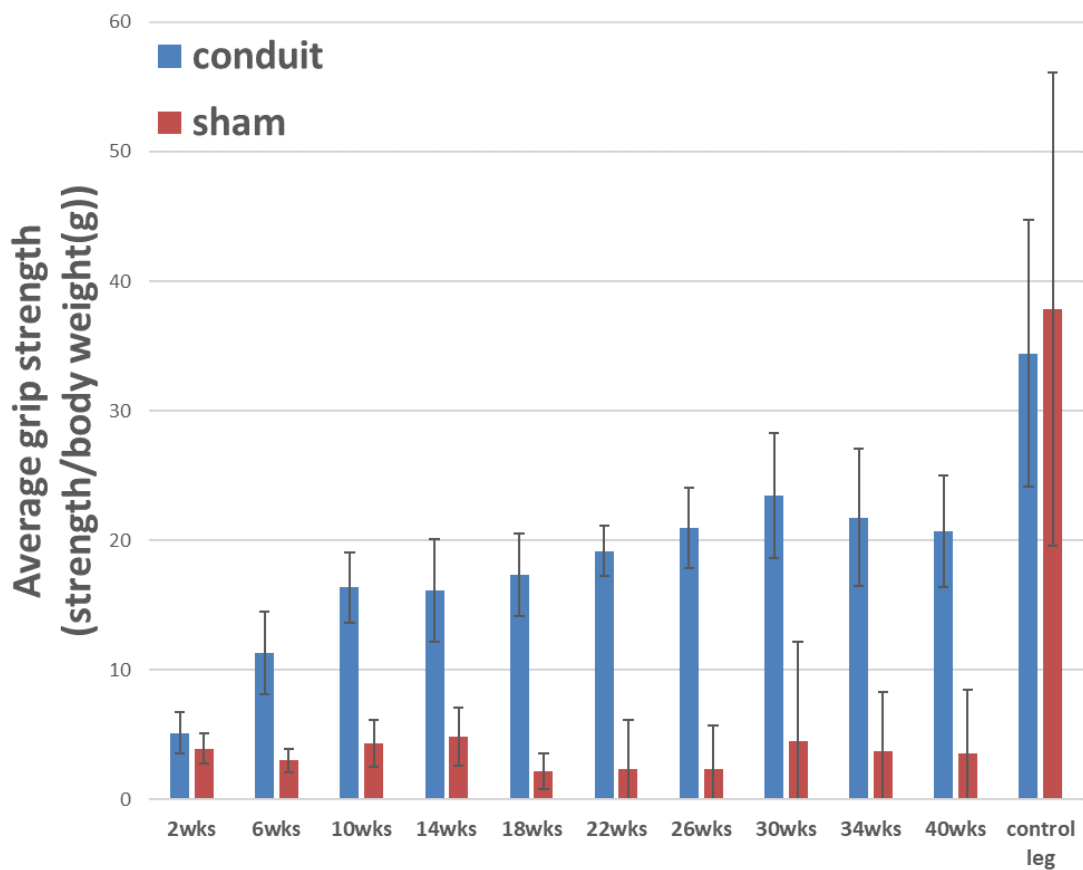


Figure 23: First Murine Study Grip Strength Results
Grip Strength measurements for first murine study over 40 weeks. Weeks 2-40 were measured from the left hindlimb whereas the control leg measurements were taken from the right hindlimb for both conduit and sham groups

The study was concluded at the 40-week time point when it became clear that grip strength recovery had plateaued for mice that had received a CNF conduit implant. It may be concluded from the data of the study that CNF does serve as a viable material from which to construct peripheral nerve conduits, and that such implants are highly effective in promoting neural regeneration. It should be noted however that in some respects the first murine study was, by design, limited. First, the number of animals employed was low, a decision made for ethical reasons given the uncertainty associated with implantation of a new material. Second, no neural tissue was resected; the nerves were transected and then the stumps abutted resulting in minimal neural gap. Third, no variation in the dimensions (length in particular) of the conduit was investigated. As such, and with the knowledge that CNF conduit implantation does indeed promote neural regeneration, a second murine study was undertaken to address these observations.

5.4 MURINE STUDY TWO: SCIATIC NERVE TRANSECTION WITH TISSUE RESECTION AND CNF CONDUIT LENGTH VARIATION

The second murine study was conducted to determine the efficacy of CNF conduits in promoting peripheral nerve repair when various amounts of neural tissue were resected. In addition, the study aimed to determine the effect of varying the conduit length on neural repair. One hundred and ten, 8-week old female mice were employed and were broken into five groups of twenty mice and one group of ten mice. The latter group served as a control in which the animals underwent no surgery. As per the first murine study, a sciatic nerve model was employed with mice in groups 1 through 5 having surgeries performed on the left leg, with the right leg serving as a control. Neural tissue of 1mm or 3 mm length was excised, and conduits were either not employed, or were employed in lengths of 3 or 5 mm. The specifics of the surgeries performed on each group were as follows: 3mm excision of neural tissue without a conduit or suture (Group 1), 3 mm excision of neural tissue without a conduit and with a suture connection (Group 2), 3 mm excision of neural tissue with a 5 mm conduit (Group 3), 1 mm excision of neural tissue with a 5 mm conduit (Group 4), and a 1 mm excision of neural tissue with a 3

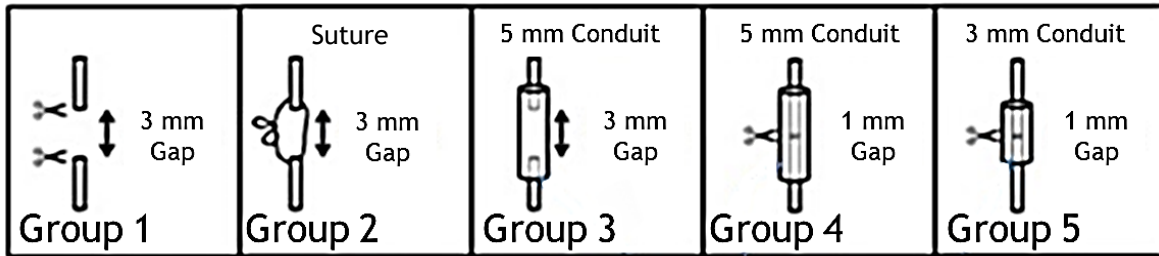


Figure 24: Second Murine Study Group Characteristics
Groupings for second study picturing variation in repair techniques, neural gap size, and conduit length for five groups

mm conduit (Group 5). Figure 24 provides a graphical depiction of the surgeries performed on each group.

The surgical configurations of Groups 1 and 2 were selected to provide baseline data for neural regeneration with significant tissue resection (3 mm) versus that employed in the first study (no resection). Specifically, Group 1 investigated regeneration in the absence of any intervention, while Group 2 investigated regeneration when a suture was employed to stabilize the relative positions of the neural stumps. The surgical configuration of Group 3 was selected to investigate the effect of employing a 5 mm long conduit over the same 3 mm neural gap employed in Groups 1 and 2. The surgical configuration of Group 4 was selected to study neural regeneration using a fixed conduit length (5 mm) but a shorter neural gap (1 mm) by comparison with Group 3. The configuration of the surgery performed on Group 5 was selected to approximate that of the first murine study, that is use of a 3 mm conduit and a minimal neural gap (nominally zero in the first study and 1 mm in the second study). Group 5 therefore provided some continuity between the two studies. In addition, the configuration of the surgery performed on Group 5 enabled study of the effect on neural regeneration of shortening the conduit employed over a fixed neural gap (1 mm) by comparison to Group 4.

The grip strength of the left and right leg of each mouse was measured every two weeks for the 20-week duration of the study and is presented in Figure 25 in the same manner as the data from the first murine study. It is noted that the second murine study was half the length of the first murine study,

a fact dictated by the more rapid obtainment of a maxima/plateau in the data of the second study. Investigation of Figure 25 reveals that the neural regeneration of mice in Group 1 was lowest, not a surprising result given the large tissue excision (3 mm) and the lack of any surgical intervention. Indeed, the magnitude of the grip strength approximates that observed for mice undergoing the sham surgeries of the first murine study. The addition of a suture bridging the 3 mm gap between the two neural stumps resulted in a modest increase in the average grip strength of mice in Group 2 vs those in Group 1, indicating that even a minor surgical intervention fixing the position of the neural stumps has regenerative advantages. Comparison of the grip strength for mice in Group 3 with those in Groups 1 and 2 indicates that the implantation of a 5 mm long CNF conduit over a 3 mm neural gap does indeed promote greater neural regeneration than either no surgical intervention (Group 1), or a suture bridging the nerve gap (Group 2). The observation that implantation of a CNF conduit supports neural regeneration is consistent with the findings of the first murine study, but importantly extends the work to large neural gaps. Indeed, application of allometric scaling laws indicates that a 3 mm neural gap in a mouse is equivalent to approximately a 9 cm gap in a human, a fact that emphasizes the importance of the data of Figure 25. It is noted that the grip strength data of Group 3 has an apparent plateauing trend in the 12 to 20-week time period, potentially indicating the maximum extent of regeneration possible with the surgical configuration employed.

The grip strength data of mice in Group 4 (1 mm nerve gap and 5 mm conduit) approximated those of mice in group 3 (3 mm nerve gap and 5 mm conduit), a somewhat surprising result that appears to indicate that the extent of neural regeneration within a conduit is independent of the extent of tissue excision, at least at the length scales employed in the present study. Investigation of the grip strength data of Group 5 (1 mm nerve gap and 3 mm conduit) reveals that a maximum value of approximately 10g was reached at the 16-week time point, the greatest value observed in the entire study. Given the uncertainty in the data it is unclear if the maximum value was maintained for the remainder of the time

course of the study, or if a minor decrease occurred. Interestingly, comparison of the data for Groups 4 and 5 indicates that for a fixed nerve gap (1 mm) decreasing the length of the conduit from 5 to 3 mm, respectively, increases the maximum extent of neural regeneration. Comparison of the data of Group 5 of the second murine study with the approximately 20 week data of the first murine study reveals that the average grip strength of mice that underwent a 1 mm nerve resection was considerably less than those without a recession when both received a 3 mm long conduit implant. Analysis of the weight of each mouse indicated that each group (1-5) gained weight over the course of the study. Available grip strength and weight data are presented in Appendix A7.

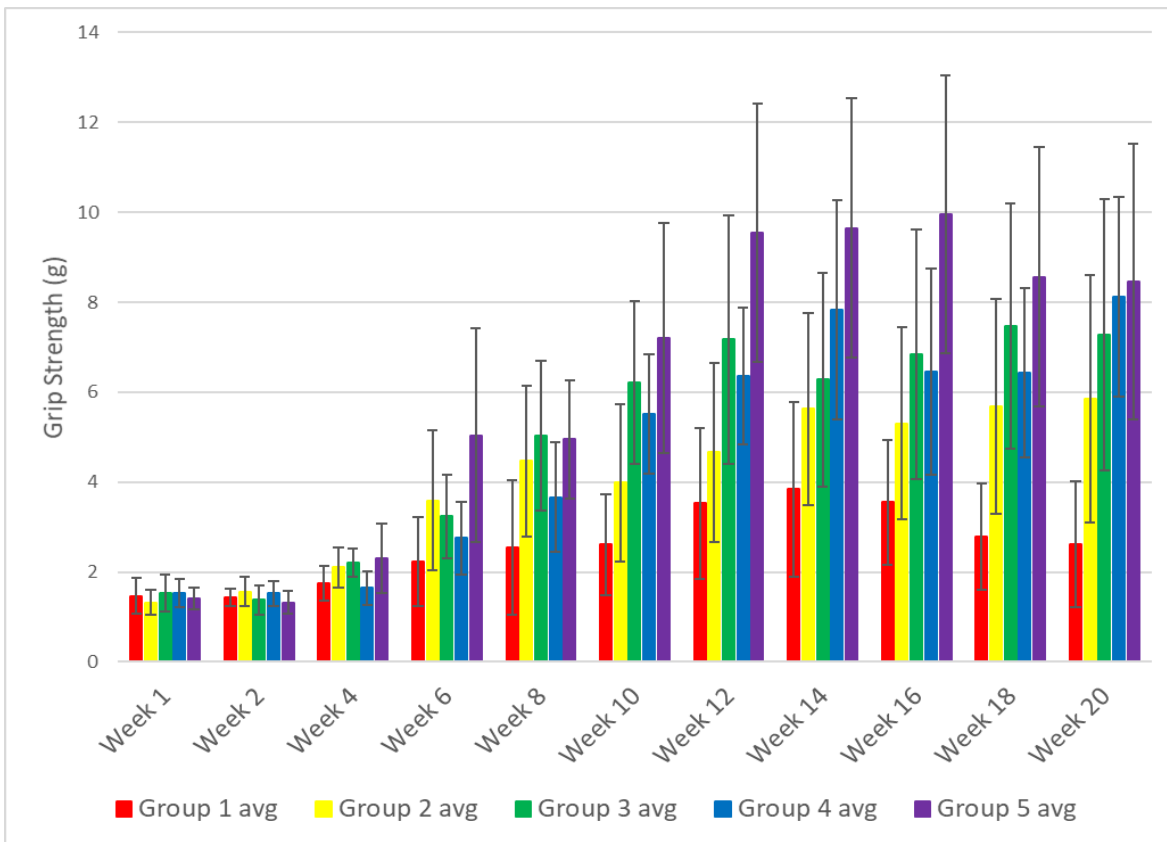


Figure 25: Second Murine Study Grip Strength Results
 Grip strength measurements for five groups in the second murine study over 20 weeks, error bars are standard deviation

Two major conclusions may be drawn from the second murine study. First, CNF conduits promote neural regeneration and do so over gaps that scale to very large injuries in humans. Second, the extent of neural regeneration is dependent upon the length of the conduit employed and appears to

be greatest for shorter conduits. The cause for the greater neural regeneration engendered by shorter conduits is not known, but it may be hypothesized that it could relate to the rates of diffusion in and out of the conduit of pro and anti-regenerative species, a possibility that is investigated in silico in Chapter 6.

5.5 HISTOLOGICAL ANALYSIS

A preliminary histological analysis was performed on select tissue samples from the second murine study. The aim of the work was to optimize the staining methods to facilitate investigation of neural tissues, and to determine cell types and distribution within the conduit. Hematoxylin and Eosin (H&E) stains were employed for visualization of cellular structure and to aid in identification of cell types, Luxol Fast Blue was used for identification of myelin, and Calcofluor White was employed to facilitate localization of cellulose. The tissue sectioning, mounting and staining methods employed are detailed in Section 3.21. Images of cross sections of conduits/tissues were taken in quadrants to enable assembly of the images and hence construction of a complete image of the full cross section. Images were overlaid manually by identification and alignment of distinct features within the tissue/conduit.

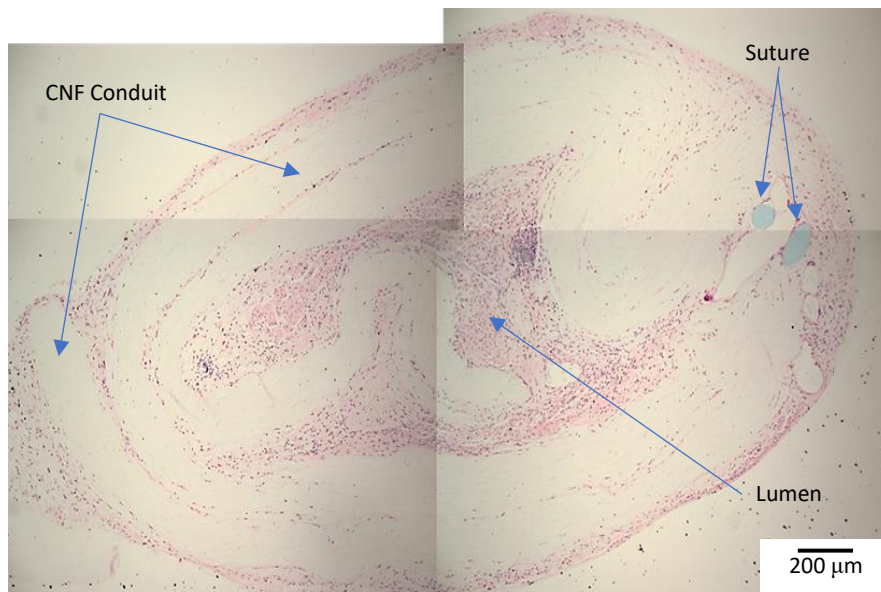


Figure 26: Hematoxylin and Eosin Stain of Conduit Containing Tissue Section

A representative image of an H&E stained cross section is presented in Figure 26, the cross section was located 600 μm into zone B from the proximal side. It is evident from investigation of Figure

26 that there are extensive tissues within the lumen of the conduit, as may be seen from the large number of cellular nuclei that were stained purple by the Hematoxylin stain, each surrounded by the non-nuclear cellular material stained pink by the Eosin stain. Interestingly the non-stained, light regions of the image are identified as the CNF sheet comprising the conduit. The two-layer wrap structure of the conduit is evident, as are some minor cellular populations in between the CNF layers themselves, and on the outside of the conduit. On the left side of the image the outer flap of the conduit may be seen, and in the center of the lumen it appears that the inner flap may have delaminated, a possibility that will be investigated more fully with the Calcofluor White stain. The light blue anomaly observed in upper right of the image is the suture employed for implantation. The sutures ran through the length of the conduit in sets of two in opposite directions such that 2-4 sutures were commonly identified in each tissue section. Suture segments were observed to be subject to shifting within the tissue section during microtoming, an unfortunate phenomenon that left gouges in the tissue section and clear vacancies.

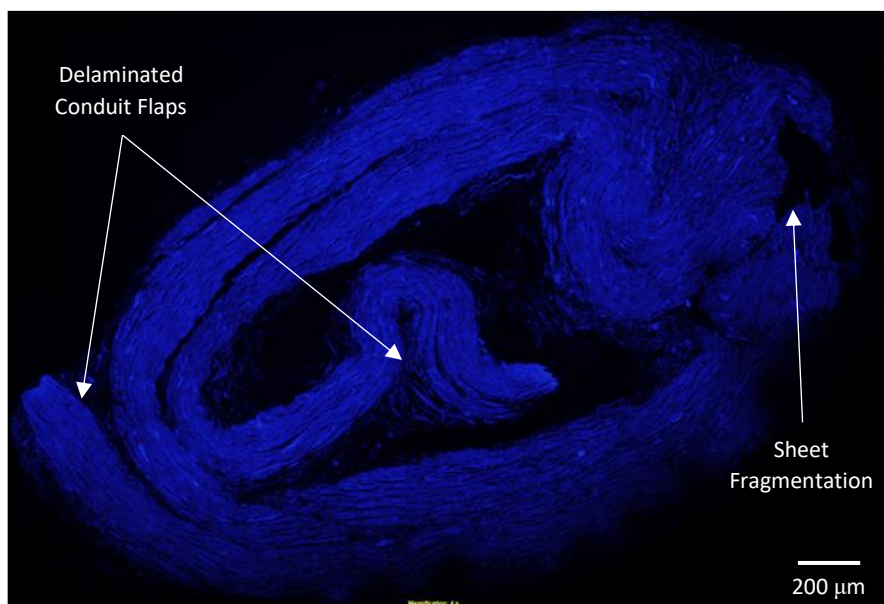


Figure 27: Calcofluor White Stain of Conduit Containing Tissue Section

In order to clearly identify and characterize the condition of the CNF conduit, Calcofluor White staining was performed, see the representative image of Figure 27. Investigation of Figure 27 confirms the impressions gained from analysis of Figure 26, that is, that the conduit had largely retained its

tubular conformation, however the outer flap had commenced delamination, and the inner flap was extensively detached. It should be noted that the conduits used in the second murine study were non-mechanically interlocked and used solely CNF on the outer flap, followed by coating the full conduit in CNF. Detailed investigation of Figure 27, particularly at the edges of the CNF sheets, reveals a loss of integrity of the sheets themselves, that is, the onset of an apparent fraying/degrading process. Given that the intent of the CNF conduit is to promote neural regeneration and then to degrade *in vivo*, thereby obviating the need for a second surgery to remove the conduit, the apparent CNF degradation at the 20-week time point is highly encouraging.

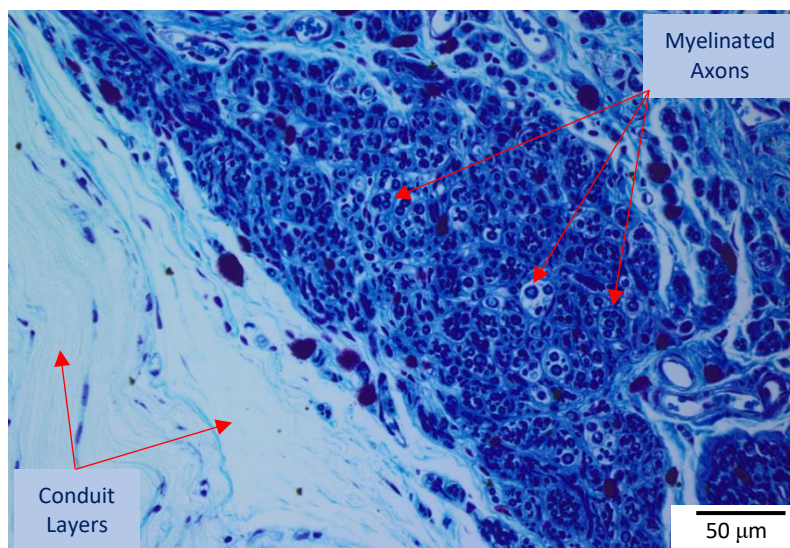


Figure 28: Luxol Fast Blue Stain of Peripheral Nerve Section

In order to determine if Luxol fast blue was a suitable stain for the myelin sheath surrounding nerve fibers of axons, a preliminary test was performed on a tissue section from the first murine study. The tissue section was taken approximately one-third of the conduit length from the proximal end in order to ensure the presence of myelinated nerves. Figure 28 presents an image of the resultant stained tissue. Investigation of Figure 28 reveals the presence of a large number of dark blue annuli that represent the cross sections of the myelin coatings of healthy nerves. Also evident in Figure 28 is the non-stained wall of the CNF conduit in the lower left of the image. It is concluded therefore that Luxol

fast blue is indeed an appropriate stain for the myelin sheath of the nerve fibers of axons and could be employed in future studies to elucidate the presence and distribution of nerves.

5.6 NON-HUMAN PRIMATE STUDY: CNF TOLERABILITY

The non-human primate (baboon) study was conducted to assess the ability of the animal to tolerate the CNF implant and to thereby determine the extent of biocompatibility of the CNF conduits in an animal closely related to humans. The study and all protocols were approved by ACURO and the local IACUC. In order to minimize the invasiveness of the surgery, the radial motor nerve in the forearm was transected versus the sciatic nerve in the hind limb as was done in the murine studies. The initial study employed a single animal. The radial nerve was severed and a 1.5 cm long mechanical interlocked CNF conduit of ~3.2 mm diameter was implanted employing a comparable methodology to that employed in the murine studies, see Section 3.18. It should be noted that the sutures used to implant the conduit were non-resorbable polypropylene Surgipro sutures, as were employed in the previous murine studies. Vicryl 2-0 sutures, commonly used in nonhuman primate surgeries, were used to close the exterior wound.

Observation of the baboon in the days and weeks post-surgery indicated that there was no significant difference in the motor function of the arm/wrist/fingers relative to that prior to the procedure. It was concluded therefore that transection of the radial nerve resulted in a decrease in sensory function rather than motor function. In addition, it was noted that the wound site was inflamed, a fact that could potentially be attributed to poor hygiene, self-mutilation, a response to the suture and/or the conduit, or a combination of these factors. As such, the animal was taken down for histopathological analysis. Histological analysis revealed elevated levels of neutrophils localized around the Surgipro sutures. Additionally, giant cells were found to be present, and to contain an unidentified foreign material, again indicative of an inflammatory/foreign body response.

Based upon the available data, it was determined that the baboon had likely experienced a foreign body response to the Surgipro sutures used to implant the CNF conduit. To test this hypothesis a two animal, follow-on study was performed to identify the source of inflammation. Specifically, subjects 2 and 3 had the same radial nerve severed as the initial animal (subject 1), however alternate repair techniques were employed. For subject 2 a Surgipro suture was employed to bridge the neural gap between the nerve stumps. For subject 3 a 1.5 cm long, ~2.4 mm diameter mechanical interlock CNF conduit was placed over the nerve gap, however it was not sutured into place. Vicryl 2-0 sutures were employed to close the external wound of both animals.

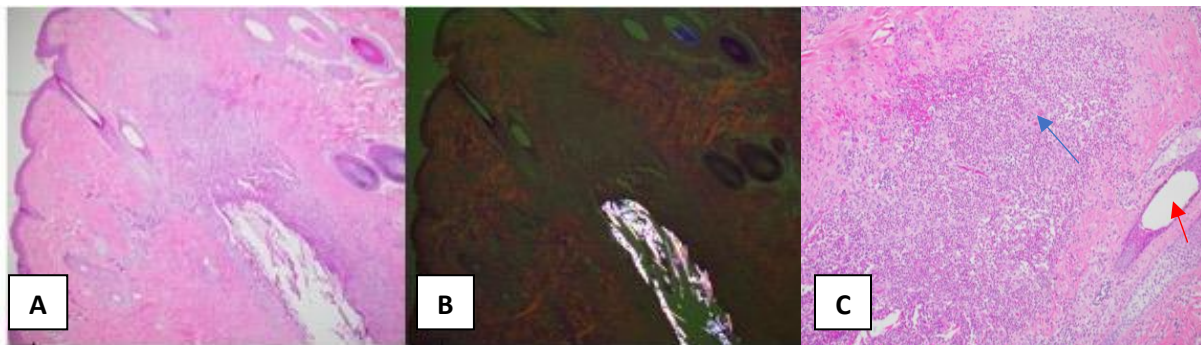


*Figure 29: Histology of Non-Human Primate (Subject #2) Neural Tissue and Suture Material
A) Hematoxylin and Eosin stain showing suture material and surrounding neutrophils and Giant cells. B) Polarized light demonstrating foreign material (suture). C) Closer look of extreme neutrophil invasion (blue arrow) at site of active inflammation surrounding suture (Red arrow)*

Subjects 2 and 3 were monitored for four weeks post-surgery before being taken down for evaluation. No changes in behavior were observed post-surgery in the subjects. Histological analysis of the tissues of subject 2 revealed extensive neutrophil and Giant cell infiltration at the site of the Surgipro suture, see Figure 29, an observation consistent with that of the first study. Analysis of the tissues of subject 3, revealed no evidence of neutrophil or Giant cell infiltration in the region of the conduit. It was concluded therefore that the inflammation observed in initial non-human primate study arose from the suture employed to implant the CNF conduit, and was not attributable to the conduit itself. Indeed, the second study demonstrated that the CNF conduit was well tolerated and elicited no foreign body/inflammatory response.

5.7 CONCLUSION

In order to determine if cellulose nanofiber is a viable material from which to construct neural conduits, an ex vivo cellular proliferation and compatibility study was performed in cell culture. It was determined that macrophages had very little interaction with CNF, a fact that likely means implants comprising CNF will not elicit a strong foreign body/inflammatory response. In addition, it was shown the neither Schwann cells nor motor neurons proliferate well on CNF, suggesting that a CNF conduit would likely be a non-participatory material in a neural conduit. Importantly, CNF infused with the extracellular matrix protein laminin had a significantly stronger macrophage response, but also was highly supportive of both Schwann cell and motor neuron attachment and proliferation - thereby potentially providing a ready means of modifying the behavior of a CNF conduit from non-participatory to strongly participating in neural regeneration.

Two murine studies and one non-human primate study were performed to determine the efficacy of CNF conduits in peripheral nerve repair. The first murine study employed a sciatic nerve model where the nerve was transected, but no tissue was excised. The nerve ends were abutted and entubulated within a CNF conduit; the conduit was subsequently sutured in place. Neural regeneration was assessed via functional recovery of grip strength of the hind limb. Conduit implant results were compared to those of sham surgeries where the nerve was transected, but no conduit was implanted. It was found that at 30 weeks the grip strength of the hind limb with the implanted conduit was 6 times greater than that of the limb that underwent the sham surgeries, representing an approximately 66% recovery of initial grip strength and indicating that CNF conduits were very effective in promoting peripheral nerve regeneration.

The second murine study was undertaken to determine the efficacy of CNF conduits in promoting peripheral nerve repair when various amounts of neural tissue were resected. In addition, the study aimed to determine the effect of varying the conduit length on neural repair. A comparable

experimental approach to that of the first murine study was employed with additional controls implemented. It was concluded from the study that CNF conduits promote neural regeneration and do so over gaps that scale to very large injuries in humans. In addition, and somewhat surprisingly, it was shown that the extent of neural regeneration is dependent upon the length of the conduit employed and appears to be greatest for shorter conduits. Histological analysis revealed the presence of significant tissue in the luminal space of the conduit. Treatment with a cellulose specific stain revealed that the CNF conduit largely retained its tubular geometry, although delamination of the inner and outer flaps was evident, suggesting the need for a mechanical interlock design rather than solely a CNF slurry seal and coating. The cellulose specific staining also revealed the onset of CNF conduit degradation at the 20 week time point, an important observation consistent with the desire to create a biodegradable conduit that would obviate the need for a second surgery to remove it post neural regeneration.

The non-human primate study was undertaken to determine the ability of an animal species known to be very sensitive to foreign bodies to tolerate the CNF conduit. It was determined that conduits comprising CNF were very well tolerated and histological examination showed no evidence of a foreign body/inflammatory response, a finding consistent with the cell culture study. The suture employed in both the murine and the non-human primate surgeries to implant the conduit, however, engendered a strong foreign body/inflammatory response. It is recommended that future *in vivo* studies in non-human primates employ an alternate suture.

CHAPTER SIX

FINITE ELEMENT ANALYSIS OF DIFFUSION AND DISTRIBUTION OF OXYGEN AND GLUCOSE WITHIN CNF PERIPHERAL NERVE CONDUITS

6.1 INTRODUCTION

Functional recovery data from the second murine study revealed that implantation of a 3 mm long conduit over a 1 mm neural gap was more efficacious in promoting regeneration than implantation of a 5 mm conduit (see Section 5.4). It was hypothesized that the increased conduit length may have altered the diffusive path of molecules known to be beneficial, and conversely detrimental, to peripheral nerve regeneration; for example oxygen, calcium, glucose, and carbon dioxide [24, 31]. Indeed, it is known that a critical aspect of conduit performance is facilitation of diffusion of pro-regenerative molecules into the interior of the conduit, and promotion of diffusion of waste materials out of the conduit [31]. In addition to length, other conduit parameters considered likely to be relevant to molecular diffusion include wall permeability and nerve to conduit diameter ratio.

One of the primary molecules of interest in the present work was oxygen, arguably the most critical chemical species required for homeostasis. In addition, it is noted that while necessary for successful nerve regeneration, the detailed role of oxygen in nerve regeneration is unclear [79, 80]. For example, Cho et al. found that intermittent hypoxia may be beneficial to nerve regrowth as the lack of oxygen triggers the activation of Hypoxia-Inducible Factor (HIF) [81]. When activated, this transcriptional mediator recruits co-activators and modifies the chromatin structure of the injured nerve, which controls gene expression for the transcriptional response. It was discovered that the absence of HIF resulted in impaired nerve regeneration, suggesting that hypoxia may potentially enhance nerve regeneration [81]. In addition, Yao et al. have shown that hypoxic conditions indirectly improve neural regeneration by enhancing cell migration to the injury, particularly Schwann cells [82].

Conversely, other studies have indicated that hyperbaric oxygen (HBO) therapy (inducing hyperoxygenation) may be an effective treatment for nerve injuries [83, 84]. Indeed, HBO studies employing a murine sciatic nerve model demonstrated greater nerve regeneration with less evidence of edema, coupled with enhanced conservation of cytostructural features versus controls [85]. HBO is a method of treatment that has been employed for more than 30 years and promotes regeneration through hyperoxygenation as well as several secondary mechanisms [85]. For example, increased oxygen concentration is known to be correlated with increased ATP and GTP levels. HBO is also known to reduce the inflammatory response and aids in the conservation of healthy tissue by reducing oxidative stress and preventing apoptosis [85]. Interestingly, Lim et al. have demonstrated that the regenerating proximal nerve consumes approximately twice as much oxygen as a healthy nerve, supporting the concept that elevated concentrations of oxygen may be beneficial [86]. Clearly such findings are, however, contrary to those indicating that hypoxic conditions support repair, and highlight the need for a greater understanding of the role of oxygen in nerve regeneration.

Perhaps equally important as oxygen for the regeneration of peripheral nerves is the concentration and distribution of glucose, the primary energy source for neural function [87, 88]. Indeed, it has been estimated that at homeostasis, 60-70% of the energy derived from glucose is used for maintenance of the membrane potential required for neural signal propagation (see Section 1.3) [89]. Under conditions of nerve regeneration, however, glucose consumption is expected to be far greater and may potentially be rate limiting [90]. It is important to ensure that glucose concentrations are maintained above $\sim 4 \text{ mol/m}^3$, as concentrations lower than this value are considered hypoglycemic and are associated with deleterious effects on tissues [91]. As such, knowledge of the concentration and distribution of both oxygen and glucose within a peripheral nerve conduit during regeneration is critical to the design of effective and efficient neural conduits. Consequently, COMSOL Multiphysics®, a finite element analysis software package, was employed to model the diffusive behavior of oxygen, and

separately, glucose within a peripheral nerve conduit system as a function of conduit length, the nerve to conduit diameter ratio, and the permeability of the conduit wall.

6.2 COMSOL MULTIPHYSICS® FINITE ELEMENT ANALYSIS

COMSOL Multiphysics® is a powerful finite element analysis programming suite which employs various supplemental physics packages to study phenomena such as heat transfer, fluid flow, acoustics, etc. The specific package employed in the present work was *Transport of Diluted Species*. A model of a CNF conduit implanted over a peripheral nerve injury was constructed in COMSOL to replicate select conditions of the second murine study. Specifically, the larger of the two nerve gaps employed in the *in vivo* study (3 mm), was chosen in order to maximize the concentration gradients. The nerve diameter was set to be 3 mm and conduit diameters were ranged from 3 mm to 4.28 mm. The conduit wall thickness was selected to be twice the thickness of the CNF sheet employed to construct the physical conduits since two layers of CNF sheet were used in creation of the conduits. The conduit length and conduit diameter were varied during the analyses as presented in Table 10. It is noted that the conduit diameter was varied to give progressive, specific, values of the ratio of the diameter of the nerve to the diameter of the conduit. The ratio ranged from 1.00:1.00 to 0.75:1.00 and was referred to as the nerve to conduit diameter ratio. It is noted that at a nerve to conduit diameter ratio of 1.00:1.00 the nerve and conduit were the same diameter and no luminal space existed between them. At a nerve to conduit diameter ratio of 0.75:1.00 however the nerve had a smaller diameter than the conduit and significant

*Table 10: Physical Parameters of Nerve-Conduit Model
Dimensions of neural tissue, conduit, and interstitial space in COMSOL model*

Component	Parameter	Value	Units
Conduit	Length	12, 13, 14, 15, 16	mm
	Diameter	3.00, 3.16, 3.34, 3.52, 3.76, 4.00, 4.28	mm
	Thickness	0.1	mm
Neural Tissue	Diameter	3	mm
	Distal Length	19	mm
	Proximal Length	18	mm
	Proximal Tip Length	1	mm
Interstitial Fluid	Neural Gap Length	3	mm
	Conduit to Nerve Radial Gap	Conduit Diameter – Nerve Diameter	mm

luminal space existed between the outer surface of the nerve and the inner wall of the conduit. Such space, and the space existing between the nerve ends, was modeled to be filled with interstitial fluid.

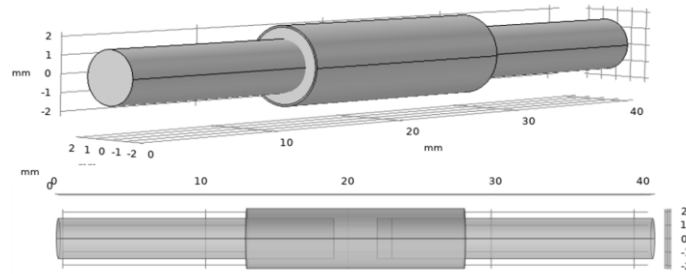


Figure 30: COMSOL Nerve and Conduit Model
Model view of neural stumps and conduit. Solid angled view (top) and transparent side view (bottom)

The nerve-conduit system was modeled to comprise 3 components; the nerve stumps were modeled as two cylinders spaced by the neural gap, while the conduit was considered a hollow cylinder centered over the neural gap, see Figure 30. COMSOL Multiphysics was employed to determine the concentration of oxygen, and separately glucose, at three locations within the conduit; at the center of the distal stump (Location 1), the center of the gap between the nerve stumps (Location 2), and at the center of the proximal stump at the intersection of the regenerating tip (a 1 mm long segment at the end of the stump) and baseline sections (Location 3), see Figure 31. Location 1 was chosen as a representation of a region with normal, baseline oxygen and glucose consumption by a nerve. Location 2 was chosen to be the center of the nerve gap, and the center of the conduit. At Location 2 there was no direct oxygen or glucose consumption by the nerves (due to their absence), however oxygen and glucose could potentially be depleted from this region due to consumption by the two neighboring nerve stumps. Location 3 was selected because initial testing indicated that the interface between the

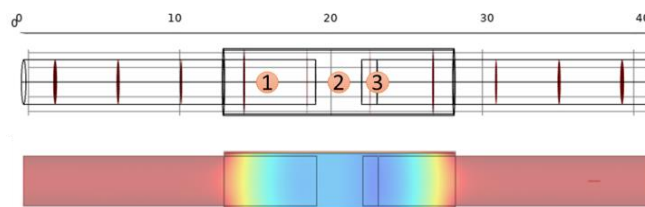


Figure 31: COMSOL Modeling Locational Analysis
Three locations observed during modeling (top) and sample concentration profile (bottom)

regenerating nerve and the baseline proximal stump consistently had the lowest oxygen concentration in the system. Analysis of the oxygen and glucose concentration at each location as a function of time provided insight into how these species diffused into the luminal space, and how variation of system parameters altered concentration profiles.

6.3 OXYGEN DIFFUSION AND DISTRIBUTION

In order to model the concentration of oxygen at the three locations within the nerve-conduit system as a function of time, a series of parameters required quantification. In addition to the physical dimensions of the neural stumps and conduits derived from the murine studies and defined in Table 10, values for initial concentrations of oxygen at the three locations, the diffusion coefficient of oxygen through the conduit wall, neural tissue and interstitial fluid, and the rates of oxygen consumption at the three locations required definition. Appropriate values were derived from literature, calculated, or determined experimentally as described below.

The baseline oxygen concentration in the ISF was taken to be that of the average partial pressure of oxygen in arterioles ($PO_2 = 26.4\text{mmHg}$) [92] and was assumed to be constant since the vasculature continuously replenishes it. The oxygen diffusion coefficient for ISF was estimated to be equivalent to that for water and was obtained by extrapolating data of oxygen diffusion coefficient vs. temperature reported by Han et al. [93] to physiologic temperature. The oxygen diffusion coefficient through mouse peripheral nerve tissue was assumed to be equivalent to that through rat peripheral nerve tissue as reported by Lagerlund et al. [94]. Oxygen consumption rates were based on the premise that the only entities consuming oxygen in the system were the nerve stumps, and that consumption was through both normal metabolic processes [93], and through active repair mechanisms [86]. Two studies ([86] and [93]) provided values for baseline metabolic consumption that were almost identical (within a few percent), the higher value was adopted for use in the present work.

A critical parameter that was determined experimentally in the present work was the diffusion coefficient of oxygen through the conduit wall. Since the *in vivo* experiments involved implantation of the conduits in an aqueous environment, the diffusion coefficient of oxygen under comparable conditions had to be determined. As described in Section 4.1.7, a MOCON OX-TRAN Model 22/2 (L) instrument was employed to measure the oxygen permeability of CNF sheets at a series of relative humidity (RH) values over the range of 50-90% and a value for the oxygen permeability of CNF at 100 %RH obtained via extrapolation. Specifically, two oxygen permeability values were obtained at 50, 80 and 90 %RH and plotted versus relative humidity, see Figure 32. A linear extrapolation to 100%RH was performed by plotting the inverse of the permeability values on the y-axis versus the relative humidity on the x-axis. A trendline with an R^2 value of 0.969 was fit to the data points which, when extrapolated to 100 %RH, resulted in a permeability of $1.41 \times 10^{-13} \text{ m}^2/\text{s}$. When the data were replotted with the inclusion of the value obtained from the extrapolation however it was evident that the projected value was a low estimate. A secondary extrapolation of the data was therefore performed using only the data points from the 80 and 90 %RH permeability measurements; a value of $2.22 \times 10^{-13} \text{ m}^2/\text{s}$ was obtained at 100 %RH via a trendline with an R^2 value of 1.00. The latter value was considered a high estimate for the

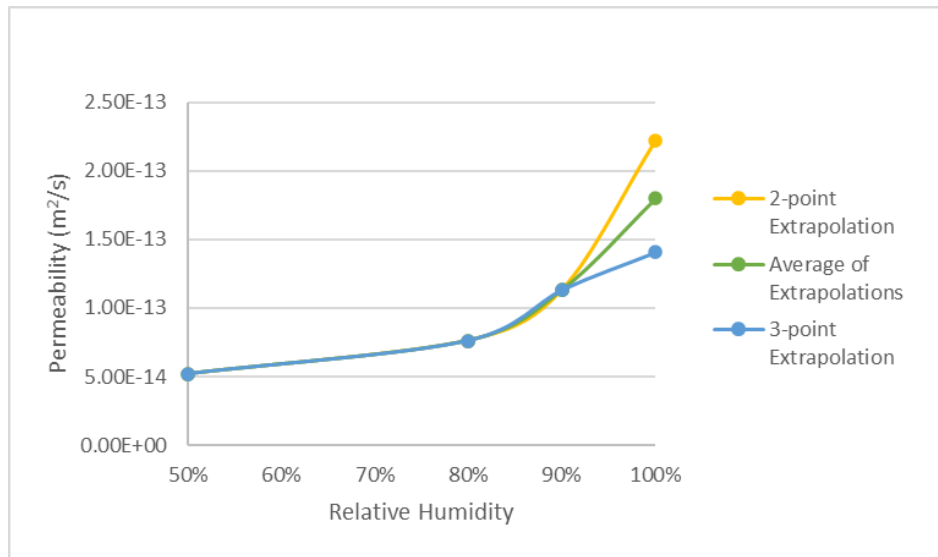


Figure 32: Extrapolation of Oxygen Permeability from MOCON Analyses
Extrapolated data from oxygen permeability through CNF sheets

value of the permeability of the CNF sheet at 100 %RH, as such the average value of the two extrapolated numbers was employed, namely $1.8 \times 10^{-13} \text{ m}^2/\text{s}$. Table 11 presents a summary of the oxygen diffusion coefficient, concentration and consumption values employed in the modeling work.

*Table 11: Oxygen Diffusion Related Parameters
Initial oxygen concentration, diffusion coefficient and consumption rate for the conduit neural tissue and interstitial fluid*

Component	Parameter	Value	Units	
Conduit	Initial Concentration	0	mol/m ³	
	Diffusion Coefficient	1.8×10^{-13}	m ² /s	
	Consumption	0	mol/ (m ³ · s)	
Neural Tissue	Initial Concentration	1.4	mol/m ³	
	Diffusion Coefficient	1.7×10^{-9}	m ² /s	
	Consumption	Baseline	9.2×10^{-4}	mol/ (m ³ · s)
		Regeneration	1.84×10^{-3}	mol/ (m ³ · s)
Interstitial Fluid	Initial Concentration	1.4	mol/m ³	
	Diffusion Coefficient	2.73×10^{-9}	m ² /s	
	Consumption	0	mol/ (m ³ · s)	

The COMSOL model was run for a simulated time range of 1500 minutes by which time oxygen concentrations throughout the conduit had either plateaued or reached a value of 0. The mesh that was employed for the COMSOL analyses was ‘*extra fine*’ to ensure accurate iterative calculations.

6.3.1 EFFECT OF CONDUIT DIAMETER ON OXYGEN CONCENTRATION AND DISTRIBUTION

One of the major variables of interest was the effect of nerve to conduit diameter ratio on oxygen concentration profiles. In order to evaluate the effects, the COMSOL Multiphysics® model was run at the six different nerve to conduit diameter ratio values over the time period required to reach equilibrium, or until oxygen concentrations at Location 1 reached the minimum possible value of 0 mol/m³. Figure 33 presents the final oxygen concentration profile of the model run for the lowest and highest nerve to conduit diameter ratios and is presented as an axial-cut plane on a continuous color scale of blue (0 mol/m³) to maroon (1.4 mol/m³).

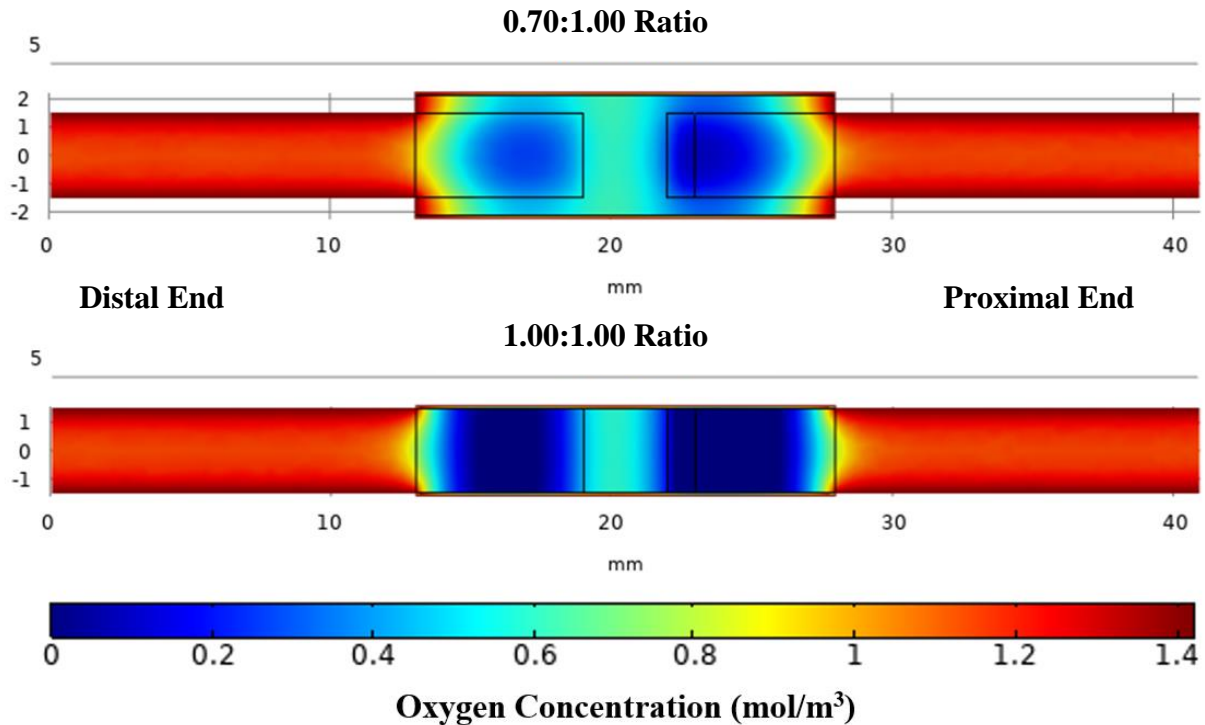


Figure 33: Oxygen concentration profiles for lowest and highest nerve to conduit diameter ratios
 The conduit was 15 mm long and the model was run for 30 minutes and 50 minutes respectively

It may be seen from investigation of Figure 33 that the regions of lowest oxygen concentration were located toward the end of the nerve stumps within the conduit, and that the lowest overall concentration was at the interface of the regenerating region and the baseline region of the proximal stump where oxygen consumption is twice that of baseline nerve consumption. It is further evident from Figure 33 that varying the ratio of the nerve to conduit diameter does not change the general oxygen distribution profile, however the actual oxygen concentration at given points is affected. Specifically, lower oxygen concentrations are observed within the conduit for higher nerve to conduit diameter ratios (that is, when the conduit diameter approaches that of the nerve diameter), a fact likely attributable to decreased axial diffusion due to the reduced volume of luminal interstitial fluid (ISF). The oxygen concentration in the center of the nerve gap is greater than toward the ends of the nerve stumps, an observation which is consistent with the lack of consumption. At the ends of the conduit where the nerve stumps transition from being enclosed to non-enclosed, the oxygen concentration is

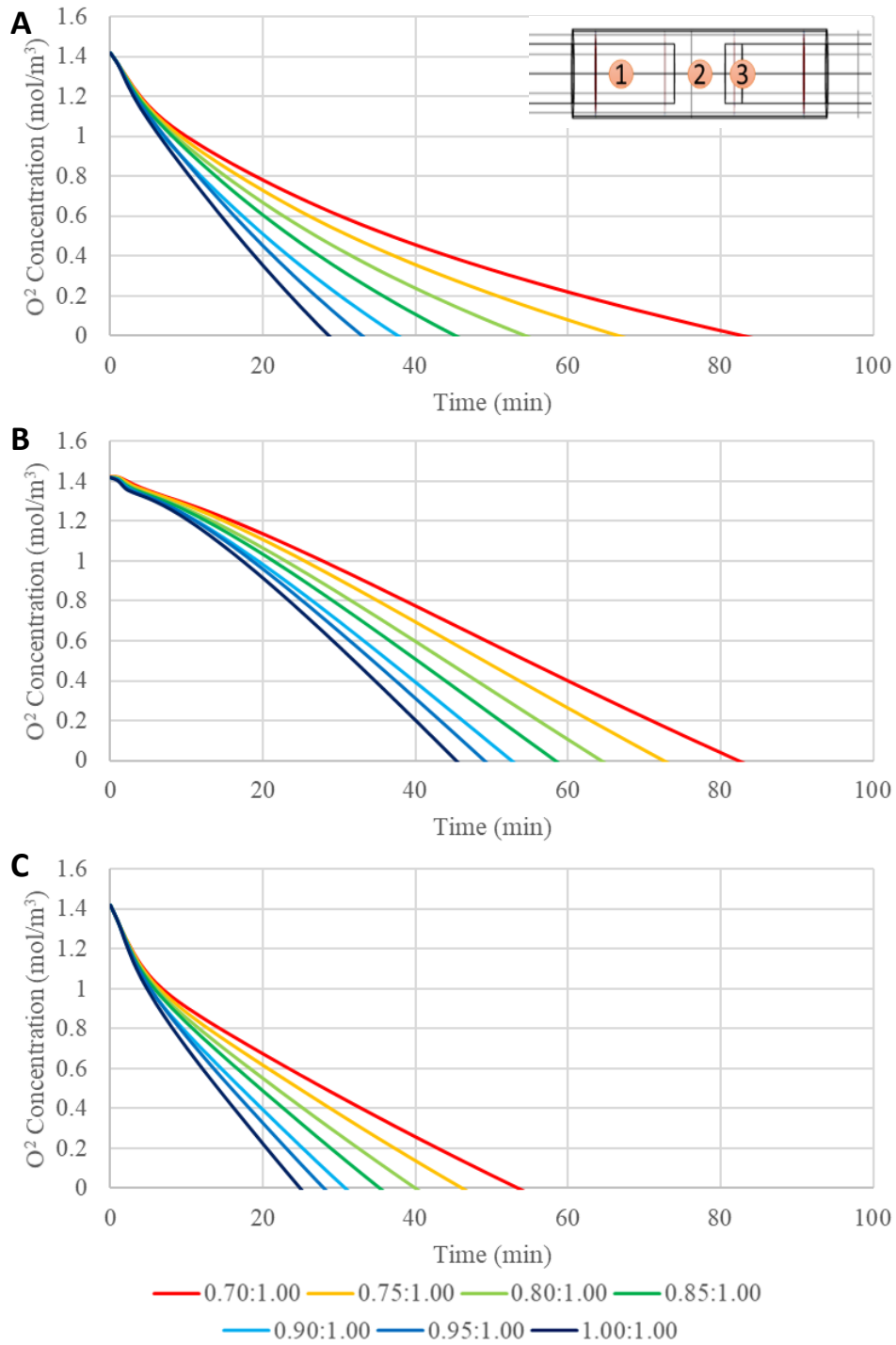


Figure 34: Oxygen Modeling with Variable Nerve to Conduit Diameter Ratio
 Oxygen concentration profiles of a 16 mm length conduit with variable nerve to conduit diameter ratio at (A) Location 1, (B) Location 2, and (C) Location 3

observed to rapidly increase to that of the exterior oxygen concentration present in the ISF. The qualitative representation of the oxygen concentration data of Figure 33 may be presented in a

quantitative manner employing the three locations described above and plotting oxygen concentration vs time at each, see Figure 34.

Investigation of the graphs of Figure 34 reveals several interesting attributes of the model and its relationship to conduit oxygen permeability. First, it is noted that at Location 3 the oxygen concentration for all nerve to conduit diameter ratios reached a concentration of 0 mol/m³ in the shortest time period of the three locations (under 60 minutes for all nerve to conduit diameter ratios), a finding that is consistent with the observation from the qualitative data of Figure 33 that the oxygen concentration at Location 3 was lower than at locations 1 and 2. Additionally, analysis of the concentration vs time curves of Figure 34 (A), (B) and (C) indicates that the curves for locations 1 and 3 are of similar shape, although of different scale, with a rapid, near linear, initial decline followed by a transition to a more gradual decay. Conversely the curves for Location 2 have a shallower initial decline followed by a transition to a slightly more rapid decay. For each location a clear trend in the oxygen concentration at a given time as a function of the nerve to conduit diameter ratio is evident, with concentration decreasing at all locations as nerve to conduit diameter increases. Figure 35 presents a plot of oxygen concentration vs nerve to conduit diameter ratio at an arbitrary time point of 25 minutes.

From investigation of Figure 35 it is evident that there is a relatively linear relationship between decreasing oxygen concentration and increasing nerve to conduit diameter ratio at all locations. Location 2 has the highest overall oxygen concentration, a fact attributable to the lack of oxygen consumption in the region between the two nerve stumps. Location 3, conversely, has the lowest overall oxygen concentration, an observation that is consistent with the proximal stump terminating with a region that consumes twice the oxygen of a non-regenerating nerve. The observed relationship of decreasing oxygen concentration within the conduit with increasing nerve to conduit diameter ratio may be understood via consideration of the resultant decrease in luminal ISF volume that results from a more closely matched nerve and conduit diameter (i.e. greater nerve to conduit diameter ratio).

Specifically, as the nerve to conduit diameter ratio increases, the distance between the nerve and the conduit inner wall (filled with ISF) decreases and hence the cross sectional area through which oxygen within the ISF can diffuse axially into the conduit decreases, leading to lower oxygen concentrations at locations within the conduit. The high linearity of the relationship between oxygen concentration and nerve to conduit diameter ratio suggests that there is very little influence of radial diffusion of oxygen through the walls of the conduit (or that it is invariant with nerve to conduit diameter ratio).

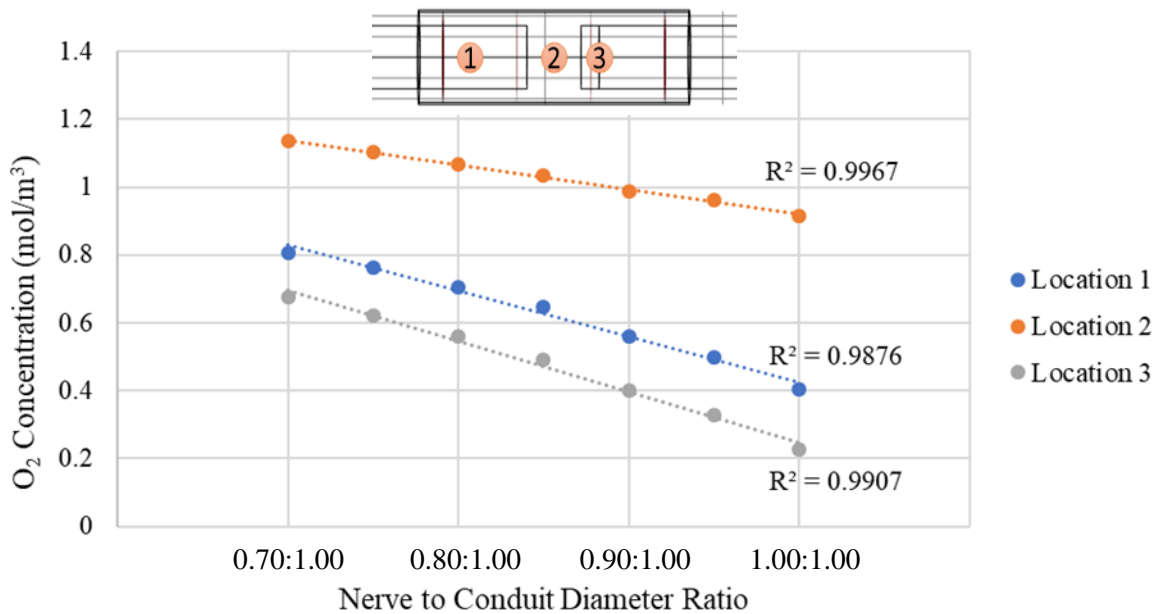


Figure 35: Oxygen Concentration with Varied Nerve to Conduit Diameter Ratio
Nerve to conduit diameter ratio at $t=25$ min for all 3 Locations

6.3.2 EFFECT OF CONDUIT WALL PERMEABILITY ON OXYGEN CONCENTRATION AND DISTRIBUTION

To determine the sensitivity of the model predictions to the permeability of the conduit walls to oxygen, simulations were run employing CNF permeabilities one order of magnitude above and one order of magnitude below the value listed in Table 11. The results of this analysis are presented in Figure 36 as plots of oxygen concentration vs time at the three locations within the conduit employing CNF permeabilities spanning two orders of magnitude.

Investigation of Figure 36 reveals that varying the oxygen permeability of the CNF conduit walls by two orders of magnitude has only a minimal effect on the oxygen concentration within the conduit. As such, it is concluded that the value employed for the oxygen permeability of CNF in the present work is likely sufficiently accurate to give the COMSOL Multiphysics® model reliable predictive power. It is noted however that the majority of the model predictions trend to zero oxygen concentration within the conduit in a timeframe that is very short (typically hours) relative to the implant durations (weeks-months), a continuously hypoxic scenario that is likely not favorable for nerve regeneration *in vivo*. It was therefore determined that simulations should be run with significantly greater conduit wall permeability in order to verify the veracity of the model itself, and to provide insight into how radial diffusion pathways affect the resultant oxygen concentration profile when employing conduits with greater wall oxygen permeability.

In order to determine an appropriate range for testing the effect of the oxygen permeability of the conduit wall on oxygen concentrations within the conduit, the permeability of materials currently used for conduit construction were reviewed, and related to the limiting case of a conduit wall with the permeability of the surrounding media, i.e. interstitial fluid (ISF). Specifically, the oxygen permeability of a material commonly employed for peripheral nerve conduit fabrication, collagen, is of the order of 10^{-10} m²/s [95]. By comparison, the oxygen permeability of interstitial fluid is reported to be 2.7269×10^{-9} m²/s [93], approximately an order of magnitude higher than that of collagen. It is noted that the oxygen permeability of CNF is approximately an order of magnitude lower than that of collagen. As such, a range of oxygen permeabilities was selected from 10 times lower than ISF (1 order of magnitude \equiv collagen) to 100 times lower (two orders of magnitude \equiv CNF). Specifically, the oxygen permeability of the conduit wall was modeled employing values of 10x, 20x, 50x, and 100x less than that of ISF. The resultant oxygen concentration vs time graphs for each conduit permeability (not shown) were very

similar to those presented in Figure 34, however it is noted that as the conduit became progressively less permeable, the curves took longer to plateau and plateaued at significantly lower oxygen concentrations. Figure 37 presents the plateau values for oxygen concentration as a function of nerve to

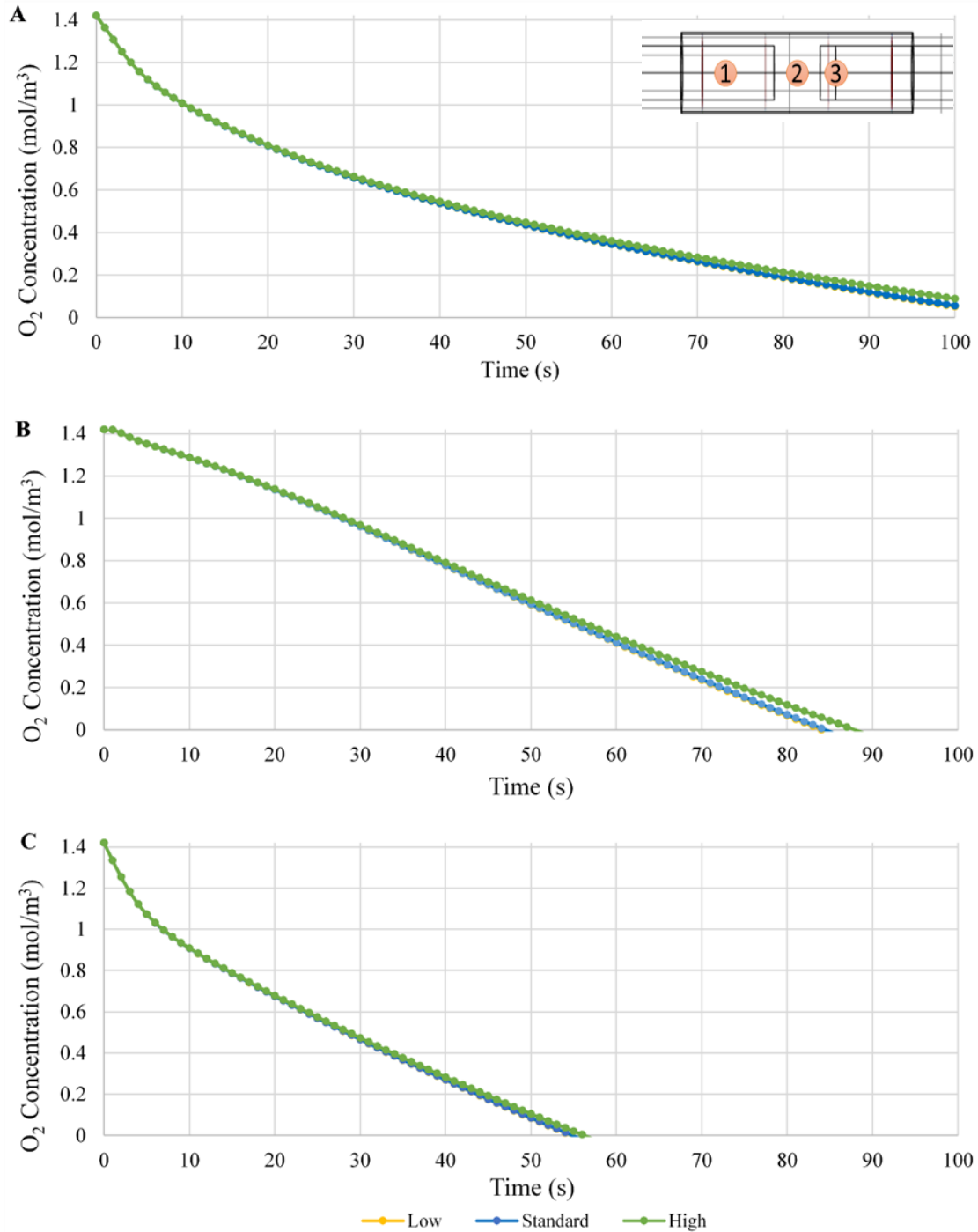


Figure 36: Oxygen Concentrations with Variation of Measured Conduit Permeability
Employing a CNF oxygen permeability value as per Table 11 (standard), a permeability on order of magnitude lower (low), and a permeability one order of magnitude higher (high). Shown for (A) Location 1, (B) Location 2, and (C) Location 3 from $t=0$ min to $t=100$ min

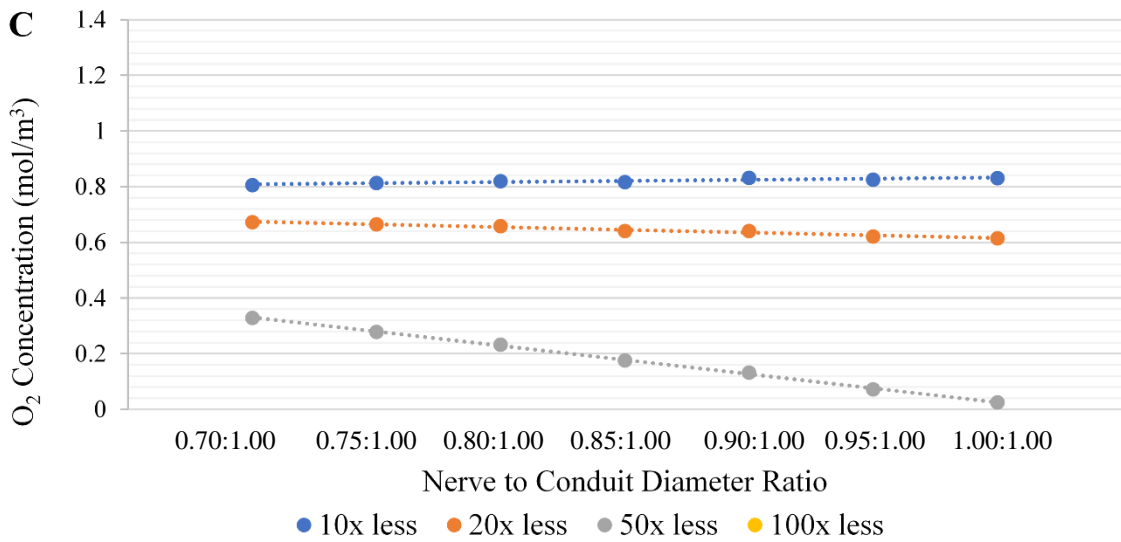
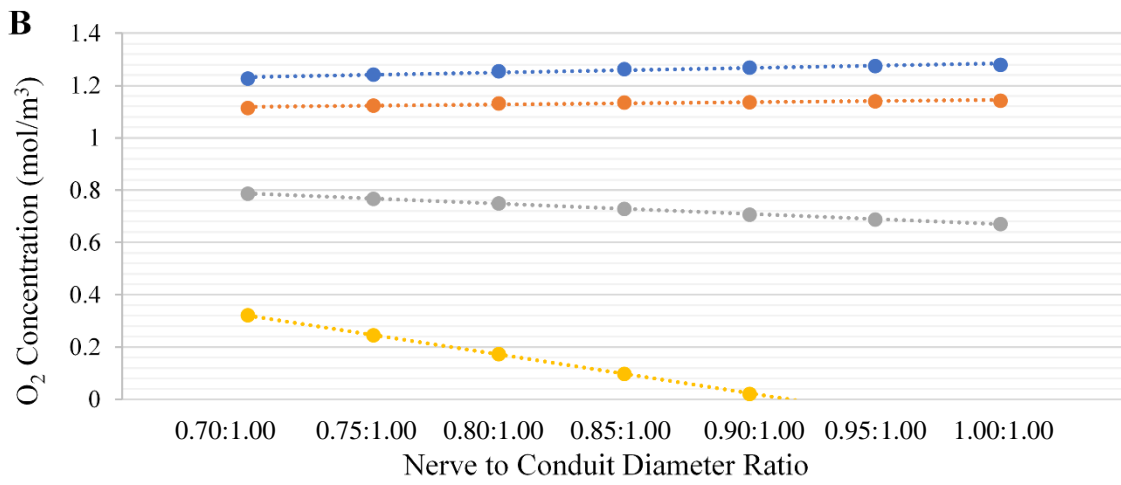
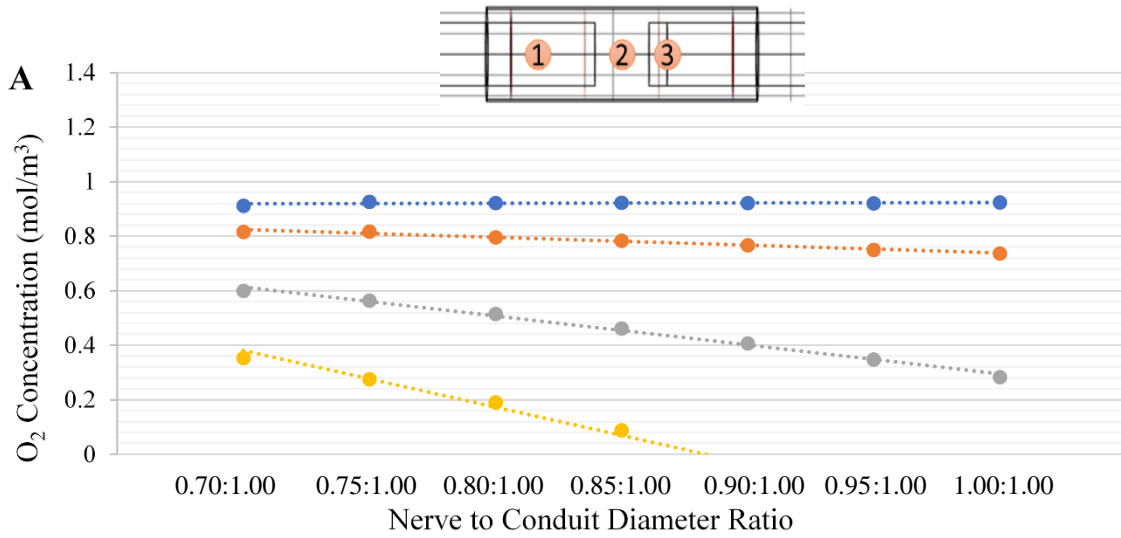


Figure 37: Oxygen Concentration with Variation of ISF-Based Conduit Permeability
 Nerve to conduit diameter ratio at Locations 1 (A), 2 (B) and 3 (C) for varying conduit wall oxygen permeabilities of 10 (blue), 20 (orange), 50 (grey) and 100 (yellow) times less than ISF

conduit diameter ratio for the 10, 20, 50 and 100 times less than ISF wall permeability values at locations 1, 2 and 3. Figure 37 was generated in a manner comparable to that employed to create Figure 35.

It is evident from investigation of Figure 37 that the 10, 20, and 50 times less permeable than ISF wall variants maintained oxygen concentrations greater than zero at all nerve to conduit diameter ratios, at all three locations. Further, it is noted that the oxygen concentrations were consistently lower at all locations at comparable nerve to conduit diameter ratios with progressively decreasing wall permeability. Taken together these two findings suggesting that oxygen diffusion radially across the wall of the conduit does indeed impact concentrations within the conduit and is modulated by the permeability of the wall. The data for the 100 times less than ISF wall permeability variants have oxygen concentrations that trend to 0 mol/m³ as the nerve to conduit diameter ratio approaches 1, an observation made at all three locations. As such, for the 100 times less permeable than ISF wall variants, the interior of the conduit is completely hypoxic at all nerve to conduit diameter ratios once the oxygen concentration plateaus, a finding consistent with the CNF modeling results.

It may also be seen from investigation of Figure 37 that for the 10 times less permeable than ISF wall variants there is little to no effect on the oxygen concentration at a given location as the nerve to conduit diameter ratio increases, suggesting that the wall is so permeable to oxygen that radial diffusion dominates over axial diffusion irrespective of the volume of ISF between the inner wall of the conduit and the nerve stumps. It is noted however that the baseline oxygen concentrations at the three locations do follow the expected trend of highest at Location 2 where there is no consumption, lowest at Location 3 where there is twice the baseline oxygen consumption, and intermediate at Location 1. As the wall permeability is decreased to 20 times less permeable than ISF, the oxygen concentration vs the nerve to conduit diameter curves at Locations 1 and 3 (where there is oxygen consumption) trend negatively, indicating that radial diffusion of oxygen across the conduit wall is less dominant, and that

axial diffusion in the ISF filled space between the nerve and the inner wall of the conduit becomes progressively more important. Interestingly at Location 2 the oxygen concentration remains invariant with nerve to conduit diameter ratio at the 20 times less permeable than ISF wall permeability, an observation potentially attributable to the fact that there is no oxygen consumption at this location making it less susceptible to restricted supply and that radial diffusion remains dominant. A further decrease in wall permeability to 50 times less permeable than ISF results in negative trends in the oxygen concentration vs nerve to conduit diameter ratio curves at all locations, indicating dominance of axial diffusion over radial diffusion, driven by the restricted oxygen diffusion across the conduit wall. It is noted however that radial diffusion of oxygen does occur at this wall permeability value and is critical to maintaining an oxygenated environment within the conduit; a finding exemplified by the hypoxic environment at all locations observed at the 100 time less permeable than ISF wall variants. A summary of the findings derived from Figure 37 is presented in Table 12. Specifically, the conduit wall permeability and location in the model are paired in order to provide an overview of the mode of diffusion that is dominant.

*Table 12: Summary of the Dominant Diffusion Regimes
Observed for paired conduit wall permeabilities (relative to ISF) and locations within the conduit. All combinations apply to conduits of any length in the tested range of 12-16mm.*

	10x	20x	50x	100x
Location 1	Radial Wall Diffusion	Axial Gap Diffusion	Axial Gap Diffusion	Axial Gap Diffusion
Location 2	Radial Wall Diffusion	Radial Wall Diffusion	Axial Gap Diffusion	Axial Gap Diffusion
Location 3	Radial Wall Diffusion	Axial Gap Diffusion	Axial Gap Diffusion	Axial Gap Diffusion

6.3.3 EFFECT OF CONDUIT LENGTH EFFECT ON OXYGEN CONCENTRATION AND DISTRIBUTION

Due to the data from the second murine study indicating that for a fixed nerve gap the length of the conduit employed has a significant effect on peripheral nerve regeneration (see Section 5.4), modeling was performed to explore the effect of conduit length on oxygen concentration and distribution. Five different conduit lengths were tested, ranging from 12 mm to 16 mm in 1 mm increments. The base CNF permeability of Table 11 was employed, and the model was run until the oxygen concentration reached 0 mol/m^3 . Figure 38 presents the resultant oxygen concentration vs time data as a function of conduit length for a nominal nerve to conduit diameter ratio of 0.70:1.00.

Investigation of Figure 38 indicates that as the conduit length increases the time required for the oxygen concentration to reach 0 mol/m^3 progressively decreases, a trend observed at all three locations and attributable to impaired axial diffusion due to enhanced luminal distances. The data at Location 1 show greater dependence of the gradient of the curves at varying conduit lengths relative to those at Locations 2 and 3, a fact attributable to the shorter axial diffusion distance for Location 1 vs that at either Location 2 or 3 and hence a greater sensitivity of oxygen concentration to conduit length. It is noted that these observations are specific to conditions promoting dominance of axial diffusion over radial diffusion (low nerve to conduit diameter ratio, and low conduit wall permeability). Finally, comparison of the data for the 16 mm conduit (dark blue line) of Figure 38 with the comparable data of Figure 34 (red line) reveals complete agreement, implying internal consistency of the model.

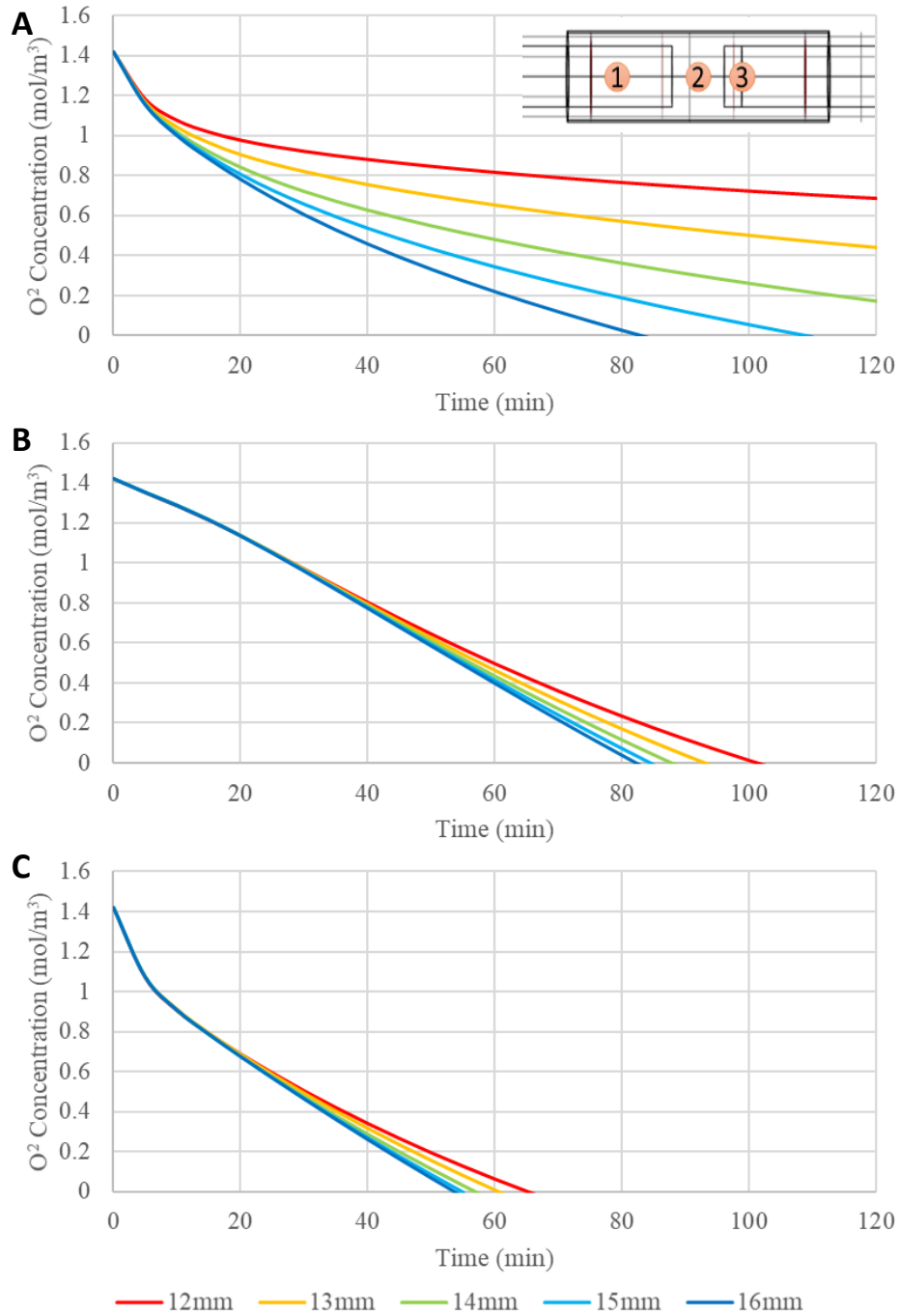


Figure 38: Oxygen Modeling with Variable Conduit Length
 Oxygen concentration profiles of a conduit with a 0.70:1.00 nerve to conduit diameter ratio and variable conduit length at (A) Location 1, (B) Location 2, and (C) Location 3

One significant point of interest under conditions such as those above in which axial diffusion is dominant over radial diffusion, is that the trends observed in oxygen concentrations with varying nerve to conduit diameter ratios were typically comparatively linear (or biphasic linear). The observed linearity

is somewhat surprising given that the cross section of the model is cylindrical, and as such changes in the radius of the conduit relative to the nerve results in changes in the cross-sectional area of the ISF filled gap by πr^2 . As such one would predict that the relationship between oxygen concentration and nerve to conduit diameter ratios should have an r^2 dependence in axial diffusion dominant regimes. One potential reason that the observed data did not exhibit a strong r^2 dependence is that the difference between the oxygen diffusion coefficients in ISF and in the nerve itself is very small (see Table 11). In order to test this hypothesis, the conduit wall oxygen permeability was set at zero (to force the system into an axial diffusion dominant regime), and an artificially large difference in oxygen diffusion coefficients for ISF and the nerve were implemented. Specifically, the diffusion coefficient of oxygen through the ISF was increased by a factor of 100, and the nerve diffusivity was maintained at its base value. Setting the parameters as indicated essentially made changes in conduit radii and hence the cross-sectional area of ISF, the sole variable impacting oxygen concentration within the conduit. Figure 39 presents an analysis of oxygen concentration at Locations 1, 2, and 3 as a function of nerve to conduit diameter ratio, in both a qualitative and quantitative manner.

Investigation of Figure 39 (a) indicates that when there is a substantial cross-sectional area of ISF through which oxygen can readily diffuse (0.70:1.00 nerve to conduit diameter ratio) there is significant oxygen concentration throughout the interior of the conduit. Conversely, when the nerve diameter and the conduit diameter are equal and no cross-sectional area of ISF exists (Figure 39 (b)), oxygen can only diffuse through the nerve tissue and as a result virtually the entire interior of the conduit is hypoxic with essentially zero oxygen concentration. Figure 39 (c, d, e) present the plateau oxygen concentration values as a function of nerve to conduit diameter ratios for Locations 1, 2 and 3 respectively. It is evident that at all locations there is only a slight dependence of oxygen concentration on nerve to conduit diameter ratio until a value of approximately 0.90:1.00, at which point a reverse logarithmic decay trend is observed. It is noted that the final data points of Figure 39 (c, d, e) are plotted as negative oxygen

concentrations, which hold no physical meaning - however they are included to illustrate that indeed the model does predict a strong non-linear dependence of oxygen concentration on nerve to conduit diameter ratio under axial diffusion dominant conditions.

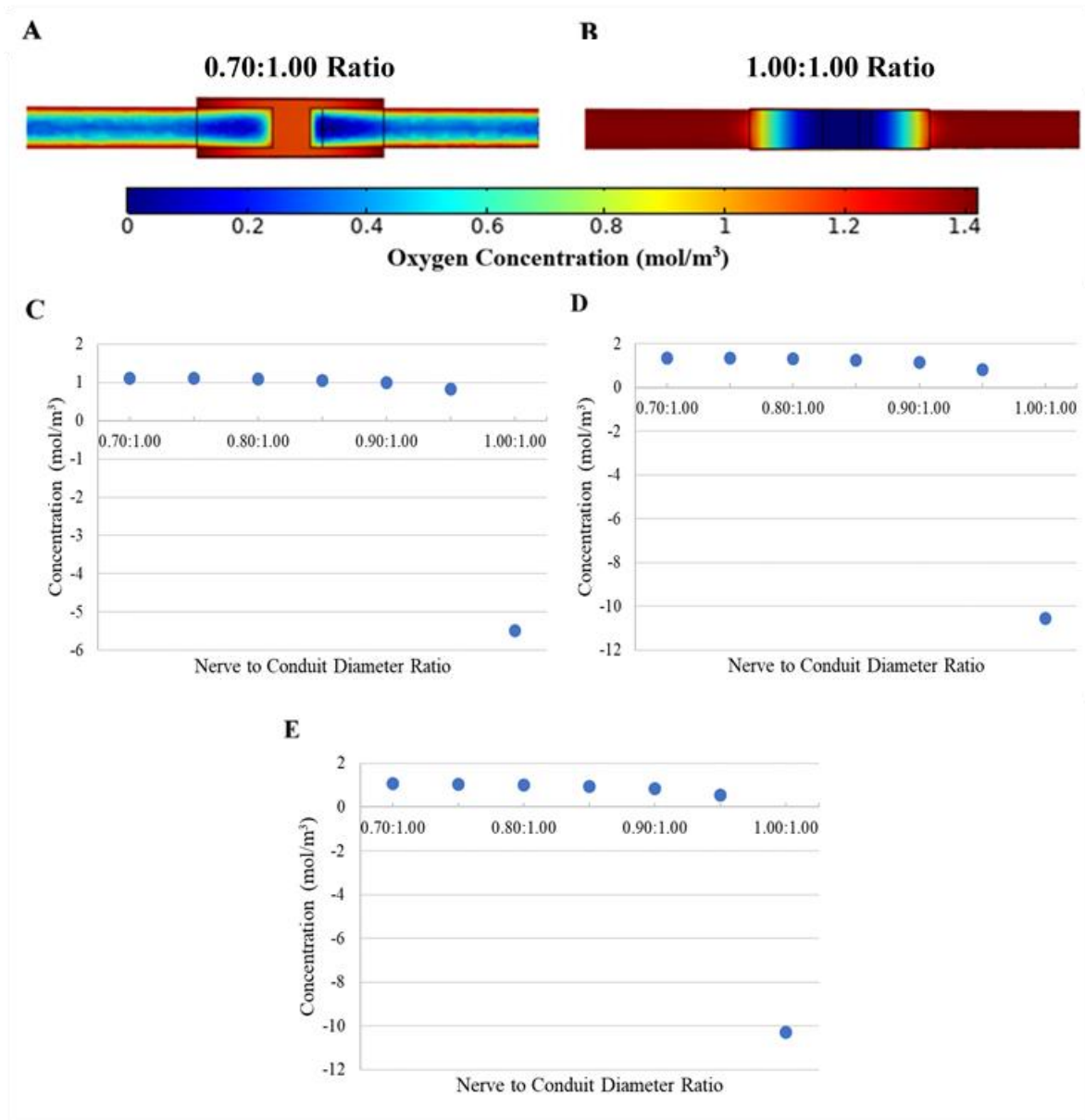


Figure 39: Oxygen Concentration Plateau Profiles
Nerve to conduit diameter ratios (A) 0.70:1.00 ratio and (B) 1.00:1.00 ratio. Oxygen concentration vs nerve to conduit diameter ratio for (C) Location 1 (D) Location 2 and (E) Location 3. Note that the conduit wall oxygen permeability was set to zero and the ISF oxygen diffusion coefficient was increased to 100 times its baseline value. Negative oxygen concentration values clearly have no physical meaning but are included to highlight the r^2 dependence of the data.

6.4 GLUCOSE DIFFUSION AND DISTRIBUTION

In order to model the concentration and distribution of glucose, the primary energy source for neural regeneration, within the CNF conduit, a series of parameters required definition. The physical dimensions of the nerve and conduit remained the same as were employed for the oxygen modeling study and are summarized in Table 11. Additional parameters that required definition included the initial concentration of glucose within the conduit, the neural tissue and the ISF, the diffusion coefficient of glucose through the conduit wall, within the neural tissue and through the ISF, and finally the consumption rate of glucose by the conduit, the neural tissue and the ISF. Each of these parameters were derived from literature, or experimentally determined as described below, and are summarized in Table 13.

*Table 13: Glucose Diffusion Related Parameters
Initial glucose concentration, diffusion coefficient and consumption rate for the conduit
neural tissue and interstitial fluid*

Component	Parameter	Value	Units	
Conduit	Initial Concentration	0	mol/m ³	
	Diffusion Coefficient	1.7 x 10 ⁻¹¹	m ² /s	
	Consumption	0	mol/ (m ³ · s)	
Neural Tissue	Initial Concentration	6	mol/m ³	
	Diffusion Coefficient	2.64 x 10 ⁻¹⁰	m ² /s	
	Consumption	Baseline	1.673 x 10 ⁻⁴	mol/ (m ³ · s)
		Regeneration	3.345 x 10 ⁻⁴	mol/ (m ³ · s)
Interstitial Fluid	Initial Concentration	6	mol/m ³	
	Diffusion Coefficient	5.7 x 10 ⁻¹⁰	m ² /s	
	Consumption	0	mol/ (m ³ · s)	

Blood glucose levels of healthy individuals are known to be in the range of 4.2 to 8.3 mmol/L [91], with most individuals having a blood glucose level of greater than 5 mmol/L [96]. In addition, it has been shown that interstitial fluid glucose concentration is comparable to that of blood plasma, with no measurable lag time [97]. As such a nominal value of 6 mmol/L was selected as the initial interstitial fluid glucose concentration. The neural tissue was assumed to have equilibrated with the large glucose reservoir of the body's interstitial fluid and was therefore assigned an initial concentration of 6 mmol/L. The CNF conduit was assigned an initial glucose concentration within the wall of 0 mmol/L.

A literature value for the rate of consumption of glucose by peripheral neural tissue was unavailable, as such a range was determined via known values for consumption of glucose by brain tissue, and via application of a known relationship between neural oxygen consumption (which is well established) and the rate of glucose consumption. First, Mergenthaler reported a value of 5.6 mg of glucose consumed per 100 mg of human brain tissue per minute [88]. Employing average values for brain volume [98] and weight [99], coupled with the molecular mass of glucose, enabled calculation of a glucose consumption rate of $5.828 \times 10^{-3} \text{ mol}/(\text{m}^3 \cdot \text{s})$. It is known that the brain consumes glucose at a greater rate than peripheral neural tissue [100], although the precise proportionality is unknown, as such this value should be considered a high (likely maximum) value. Second, Mergenthaler [88], and separately Lim et al. [90], have reported that there is a direct relationship between the rate of oxygen consumption by neural tissue and the rate of glucose consumption by the same tissue. Specifically, the rate of glucose consumption is 5.5-5.8 times lower than that of oxygen consumption. Oxygen consumption in a regenerating nerve has been found Lim et al, [90] to be approximately twice that of a healthy nerve. Given the known linear relationship between neural oxygen and glucose consumption rates [88, 101], it follows that the glucose consumption rate in a regenerating nerve should be double the baseline value. Applying this scaling factor to known oxygen consumption rates of peripheral neural tissue at baseline metabolic conditions and under active repair conditions (as reported by Lim et al. [86, 90] and Han et al. [93]) results in estimated values for glucose consumption rates of 1.673 and $3.345 \times 10^{-4} \text{ mol}/(\text{m}^3 \cdot \text{s})$, respectively. It is noted that these values are approximately an order of magnitude lower than those obtained employing the known glucose consumption rate of brain tissue (which are certainly an over estimation for peripheral neural tissue) and are adopted here for the non-regenerating regions of the nerve stumps, and the regenerating tip of the proximal nerve, respectively.

The permeability of the neural tissue was approximated via a value for the glucose diffusion coefficient reported by Khalil et al. for epithelial tissue and dura mater as $2.64 \times 10^{-10} \text{ m}^2/\text{s}$ [102]. It is

noted however that the ends of the proximal and distal nerves not within the conduit were modeled as impermeable to glucose since *in vivo* they would extend significant distances within the body and would not be subject to glucose flux axially from an open end. The diffusion coefficient of interstitial fluid was approximated via a value reported by Suhaimi et al. for glucose diffusivity in cell culture medium as $5.67 \times 10^{-10} \text{ m}^2/\text{s}$ [103]. Lastly, the diffusion coefficient of glucose in the cellulose nanofiber conduit wall was determined experimentally in the present work to be $1.7 \times 10^{-11} \pm 0.9 \times 10^{-11} \text{ m}^2/\text{s}$ see Section 3.11.

COMSOL Multiphysics® simulations were run for a duration of 1000 minutes, by which time glucose concentrations had generally either plateaued, or had decreased below the hypoglycemic threshold value of $4 \text{ mol}/\text{m}^3$ [91].

6.4.1 EFFECT OF CONDUIT DIAMETER ON GLUCOSE CONCENTRATION AND DISTRIBUTION

An investigation into the effect of variation of the nerve to conduit diameter ratio on the glucose concentration profile and distribution was performed for a 16mm conduit over a range of 0.70:1.00 to 1.00:1.00 in increments of 0.05, see Figure 40. It is evident that at all three locations within the conduit the glucose concentration progressively decreases as the nerve to conduit diameter ratio increases, that is, as the nerve and conduit diameters tend toward the same value. It is also noted that glucose concentrations plateaued in the range of $\sim 5\text{-}5.75 \text{ mol}/\text{m}^3$, i.e. above the upper limit of hypoglycemia of $4 \text{ mol}/\text{m}^3$ [91]. The sensitivity of glucose concentration to nerve to conduit diameter ratio at the three locations may be understood in terms of length of the diffusion path axially within the conduit, the length of the radial diffusion pathway from the inner conduit wall to the nerve, and on the relative glucose consumption rates at the given locations. Notably, at Location 1 the axial diffusion path for glucose is the shortest of the three locations and hence axial diffusion is a significant contributor to the instantaneous glucose concentration. The effect of nerve to conduit diameter ratio is greatest at Location 1 (greatest range of plateau concentration values), a fact that may be attributed to the decrease in volume of interstitial fluid between the inner conduit wall and the nerve as the conduit

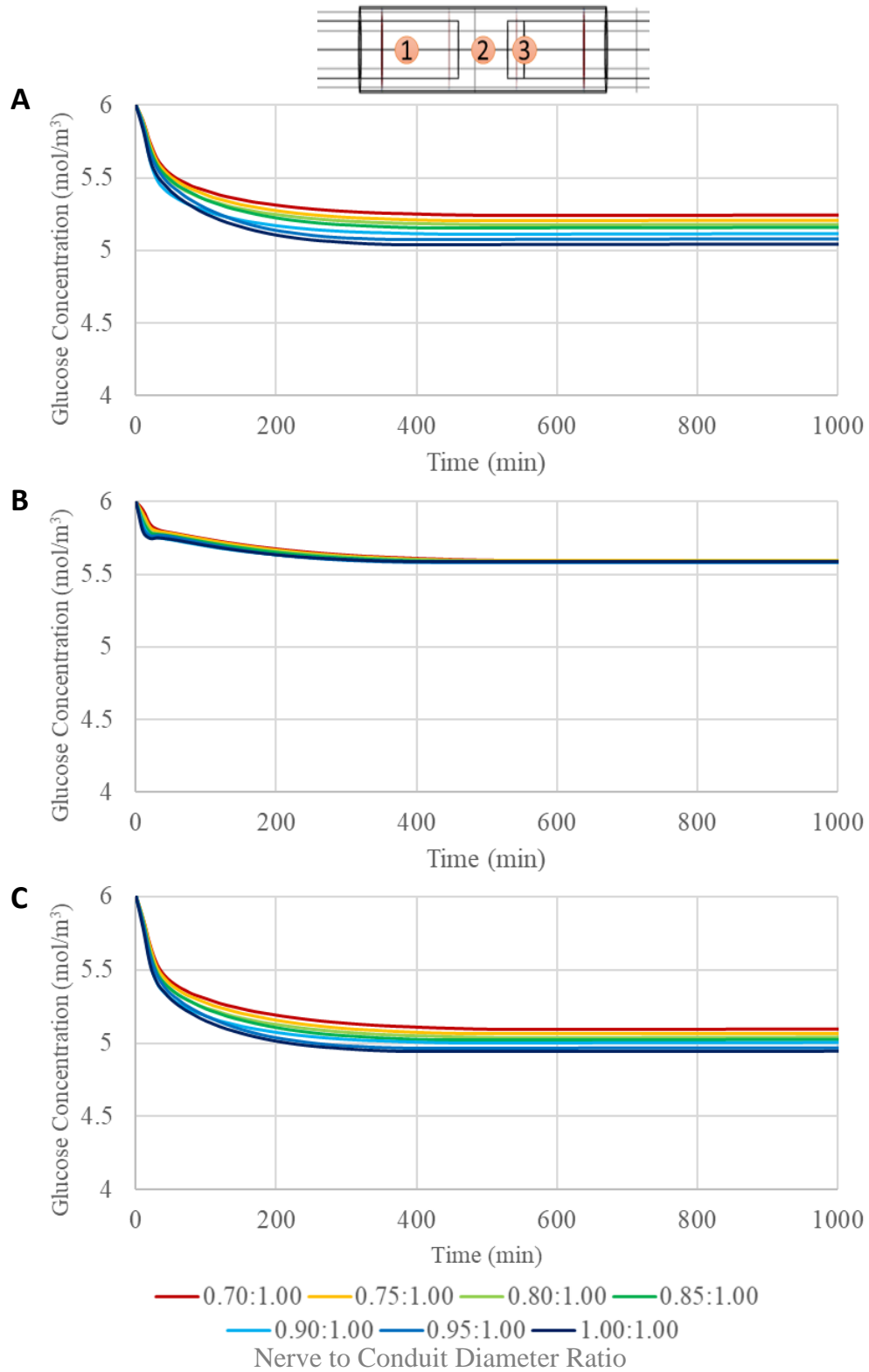


Figure 40: Glucose Concentration Profiles of a 16 mm Length Conduit Variable nerve to conduit diameters at (A) Location 1, (B) Location 2, and (C) Location 3

diameter approaches that of the nerve. The diffusion coefficient of glucose in interstitial fluid is approximately twice that of neural tissue, and more than an order of magnitude greater than in the CNF conduit wall, as such the effect of reduction of ISF volume is significant in regimes that have a dependence on axial diffusion. It is expected that radial diffusion of glucose does contribute to the instantaneous concentration at Location 1, although changes in nerve to conduit diameter are not expected to result in large changes in glucose concentrations resulting from radial diffusion since the change in diffusion distance from the inner conduit wall to the nerve is minor when compared to typical axial diffusion paths. It is noted that the plateau glucose concentrations at Location 1 are intermediate between those of Locations 2 and 3, a fact attributed to baseline neural glucose consumption, versus no consumption at Location 2 and twice baseline consumption at Location 3. At Location 2 the axial diffusion distance for glucose is the greatest of the three locations, as such it is expected that axial diffusion will play a minor role in the instantaneous glucose concentration, and that radial diffusion will dominate. The glucose concentration at Location 2 plateaued to the same value irrespective of the nerve to conduit diameter, an observation attesting to the dominance of radial diffusion over axial diffusion. As observed above, the instantaneous glucose concentrations at Location 2 are the highest of the three locations, a fact attributed to the lack of neural consumption in the gap between the nerve stumps. Location 3 resides at an axial distance from the end of the conduit that is intermediate between that of Locations 1 and 2 and as such likely has instantaneous glucose concentrations that are influenced by both axial and radial diffusion. Indeed, a similar but less strong dependence on nerve to conduit diameter ratio is observed at Location 3 versus that at Location 1, suggesting not quite as strong an axial diffusion dependence, and a greater radial diffusion dependence. It is noted that the glucose consumption rate is twice that which occurs at Location 1, a fact reflected in the glucose concentrations at Location 3 being the lowest of the three locations.

6.4.2 EFFECT OF CONDUIT LENGTH ON GLUCOSE CONCENTRATION AND DISTRIBUTION

To assess the impact of the potentially confounding effect of changing conduit length on the trends observed in glucose concentrations as a function of nerve to conduit diameter ratio, a similar analysis to that performed in Figure 40 on the longest (16mm) conduit was performed on the shortest (12mm) conduit, see Figure 41. It is evident from comparison of Figures 41 and 42 that the shorter conduit resulted in higher glucose concentrations at Location 1, but invariant concentrations at Locations 2 and 3. The findings suggest that axial diffusion is a significant contributor to the instantaneous glucose concentration at Location 1. However, at Locations 2 and 3 radial diffusion dominates over axial diffusion as evidenced by the negligible effect a significant reduction of the axial diffusion distance had on the instantaneous glucose concentrations.

A comprehensive analysis of the effect of conduit length on glucose concentration profiles and distributions was performed at a nerve to conduit diameter ratio of 0.70:1.00 over the full conduit length range of 12 to 16mm in 1mm increments, see Figure 42. Investigation of Figure 42 reveals that at all locations within the conduit the glucose concentration plateaus to a positive value, above 4 mol/m^3 , for all conduit lengths. It is noted that the plateau concentrations follow the same trend as observed in sensitivity to nerve to conduit diameter ratio as a result of axial diffusion path length, radial diffusion path length, and rate of glucose consumption, namely highest at Location 2, intermediate at Location 1 and lowest at Location 3. Further, at each location the glucose concentration progressively decreases with incremental increases in conduit length, a fact attributed to the increasing axial diffusion path length for glucose to reach each of the three locations within the conduit.

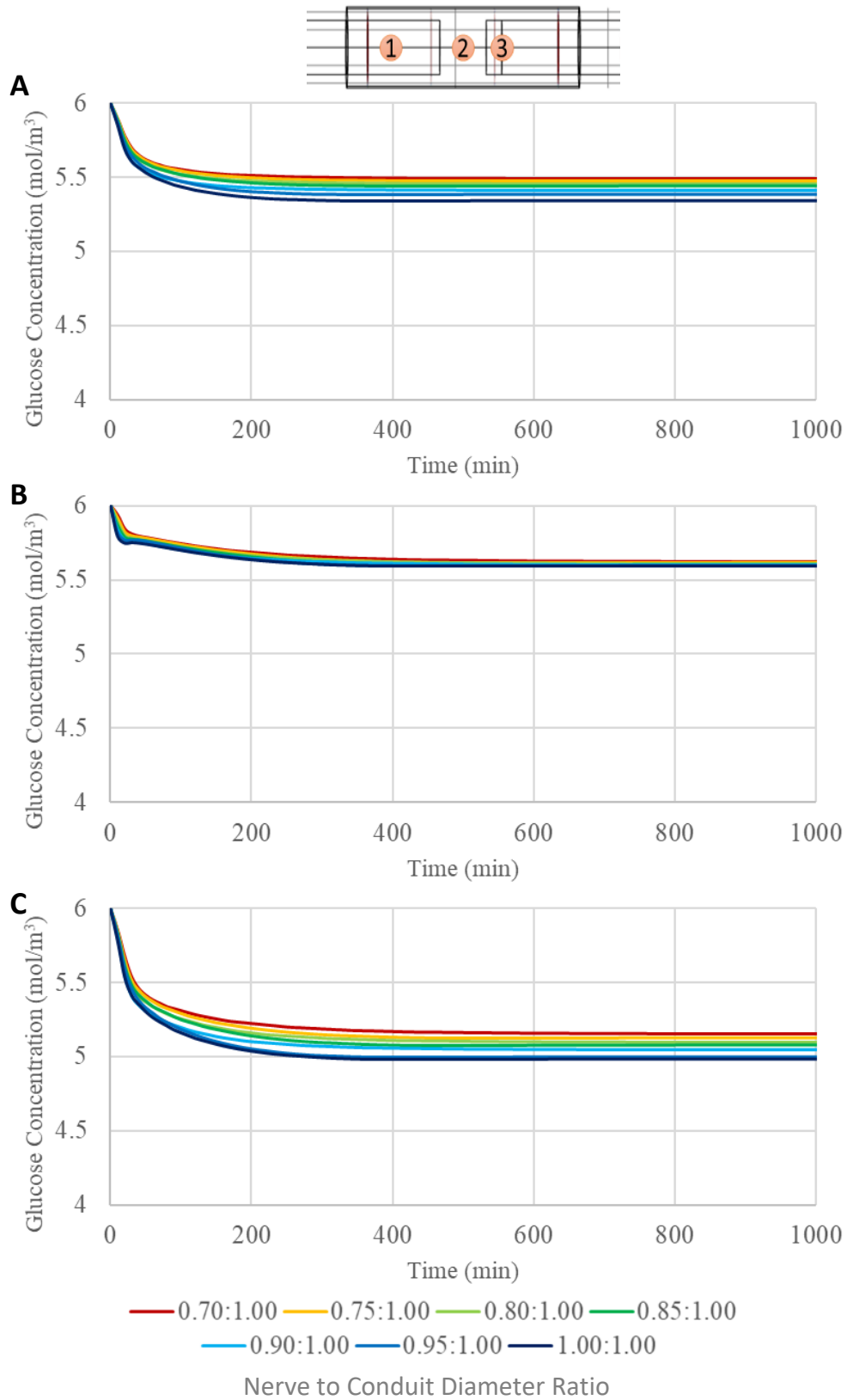


Figure 41: Glucose Concentration Profiles of a 12mm Length Conduit Variable nerve to conduit diameter ratio at (A) Location 1, (B) Location 2, and (C) Location 3

In order to test the dependence of the glucose concentration profiles on conduit length when the luminal volume of interstitial fluid was minimized, simulations were run for conduit lengths varying from 12 to 16mm in 1mm increments at a nerve to conduit diameter ratio of 1.00:1.00, see Figure 43. Comparison of Figures 43 and 44 reveals that increasing the nerve to conduit diameter ratio from 0.70:1.00 to 1.00:1.00 decreases the glucose concentrations at all three locations and for all conduit lengths, although the decreases are comparatively minor, particularly at Locations 2 and 3. The glucose concentration at Location 1 decreased by approximately 0.3 mol/m^3 upon increasing the nerve to conduit diameter ratio. At Locations 2 and 3 minor decreases in glucose concentrations were observed upon increasing the nerve to conduit diameter ratio, and the effect on glucose concentration of modification of the length of the conduit was suppressed. The observed differences revealed that the glucose concentration profiles at Location 1 were most sensitive to changes in conduit length and diameter due to its comparatively short axial diffusion path and baseline consumption rate, however the sensitivities at Locations 2 and 3 were far less pronounced, showing very minor, if any, shifts in concentration. These data demonstrate the importance of axial diffusion of glucose through the interstitial fluid resident in the gap between the nerve and the inner conduit wall, particularly at Location 1. Specifically, if the gap and hence the interstitial fluid, are removed by employing a conduit with the same diameter as the nerve, glucose concentrations are decreased as the only modes of potentially active diffusion are axially through the nerve itself, and radially across the conduit wall. The findings suggest that the minor decreases in glucose concentrations seen by both increasing the length of the conduit and increasing the nerve to conduit diameter ratio are due to reduction of axial diffusion. It is noted that glucose concentrations remain well above hypoglycemic conditions with axial diffusion pathway reductions suggesting that diffusivity of glucose radially through the CNF conduit wall and/or axially along the neural tissue itself is sufficient for maintaining healthy glucose levels.

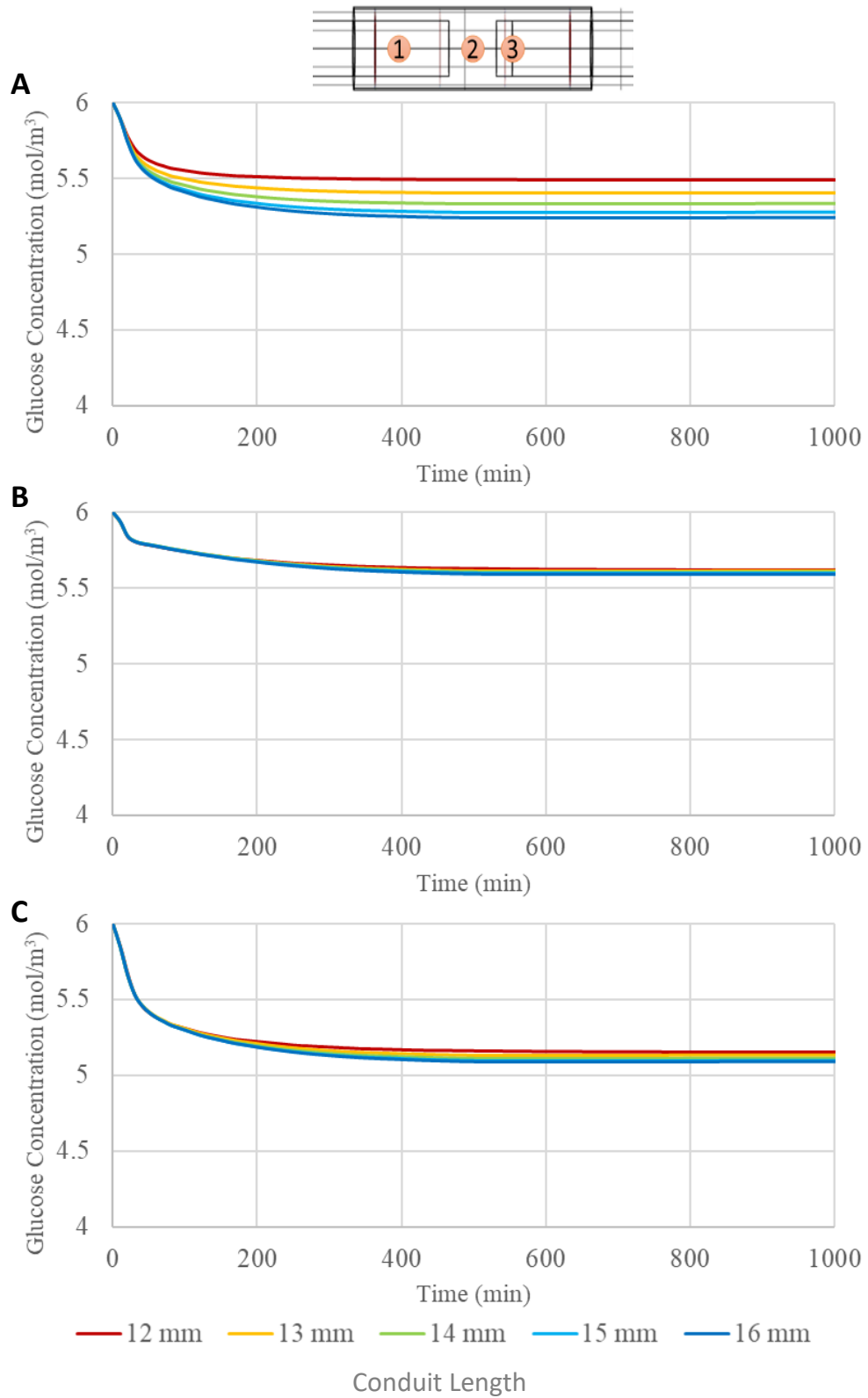


Figure 42: Glucose Concentration Profiles of a 0.70:1.00 Nerve-Conduit Diameter Ratio Conduit Variable conduit length at (A) Location 1, (B) Location 2, and (C) Location 3

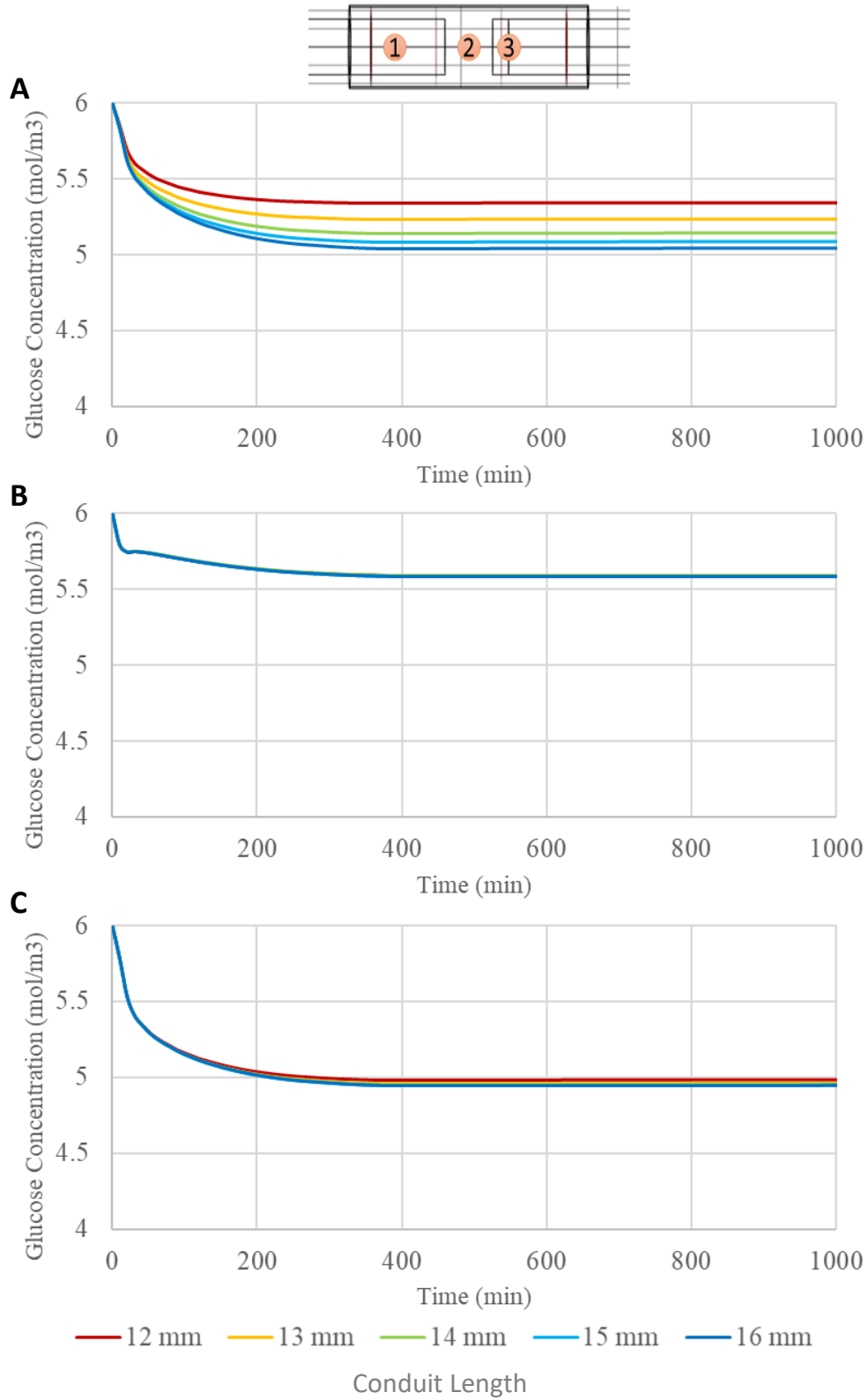


Figure 43: Glucose Concentration Profiles of a 1.00:1.00 Nerve-Conduit Diameter Ratio Conduit Variable conduit length at (A) Location 1, (B) Location 2, and (C) Location 3

6.4.3 EFFECT OF CONDUIT WALL PERMEABILITY ON GLUCOSE CONCENTRATION AND DISTRIBUTION

Clearly, limiting the axial diffusion of glucose through the interstitial fluid resident in the luminal space between the nerve and the inner conduit wall via reduction of the conduit diameter has only a minor effect on the glucose concentration and distribution within the conduit. Radial diffusion across the CNF conduit wall, and/or axially through the neural tissue appear to be the dominant diffusion modalities. As such an investigation of the effect of varying the permeability of the conduit wall to glucose was performed to determine if a reduction in radial diffusion into the luminal space may lead to hypoglycemic levels. Conduit parameters for the investigation were set at a nerve to conduit diameter ratio of 0.70:1.00 and a conduit length of 16 mm. The baseline conduit diffusion coefficient employed in the work to date has been $1.7 \times 10^{-11} \text{ m}^2/\text{s}$, a value based on the experimental measurement of glucose diffusion through a cellulose nanofiber sheet. It is of interest to explore the effect of varying the conduit wall permeability over a practical range. The highest obtainable conduit wall permeability would arise from a wall material with a glucose diffusion coefficient equivalent to that of interstitial fluid, i.e. $5.7 \times 10^{-10} \text{ m}^2/\text{s}$, this value was therefore selected as the upper boundary of the glucose diffusion coefficient. Two additional diffusion coefficient values were selected based on the application of one standard deviation above and below the measured experimental value yielding values of 2.6×10^{-11} and $8.0 \times 10^{-12} \text{ m}^2/\text{s}$, respectively. Finally, a lower boundary value of $1 \times 10^{-12} \text{ m}^2/\text{s}$ was selected given that it represents the lowest value in the order of magnitude in which the experimental value minus one standard deviation fell. Figure 44 presents the instantaneous glucose concentrations plotted as a function of time at the three locations within the conduit employing the five selected conduit wall diffusion coefficients. It may be seen from investigation of Figure 44 that employing a conduit wall diffusion coefficient equivalent to that of interstitial fluid ($5.7 \times 10^{-10} \text{ m}^2/\text{s}$) results in glucose concentrations at all locations that are only slightly lower than the baseline interstitial fluid concentration, a fact arising from the absence of a barrier for radial diffusion across the conduit wall and therefore dominance of the radial

diffusion mode over the axial diffusion mode. It is noted however that at the locations where glucose consumption occurs (1 and 3), the plateau concentrations are lower than at Location 2. Decreasing the diffusion coefficient of the conduit wall progressively to the experimental value plus one standard deviation, the experimental value, and the experimental value minus one standard deviation is observed to result in monotonic reductions in the plateau values of the glucose concentrations at all three locations within the conduit, with the relative concentrations following the previously observed trend of highest at Location 2, intermediate at Location 1, and lowest at Location 3. Reducing the diffusion coefficient to the lower boundary value of $1 \times 10^{-12} \text{ m}^2/\text{s}$ resulted in a dramatic decrease in the instantaneous glucose concentrations and the lack of attainment of a plateau concentration in the timescale investigated at all 3 locations. Running the simulation for a longer period of time indicated that at Location 1, a plateau value of $3.8 \text{ mol}/\text{m}^3$ was eventually reached (at ~ 3000 minutes). It is noted that a concentration of $3.8 \text{ mol}/\text{m}^3$ is below the threshold of hypoglycemia. At Locations 2 and 3, the application of the lower boundary value of the diffusion coefficient resulted in a glucose concentration profile that entered the hypoglycemic regime at 800 and 700 minutes, respectively. The data of Figure 44, coupled with the experimentally measured glucose diffusion coefficient for cellulose nanofiber sheets, implies that under the conditions of the present study radial diffusion through the conduit wall is the dominant pathway for glucose to enter the luminal space, and that axial diffusion, while present, appears to have only marginal significance, primarily at Location 1.

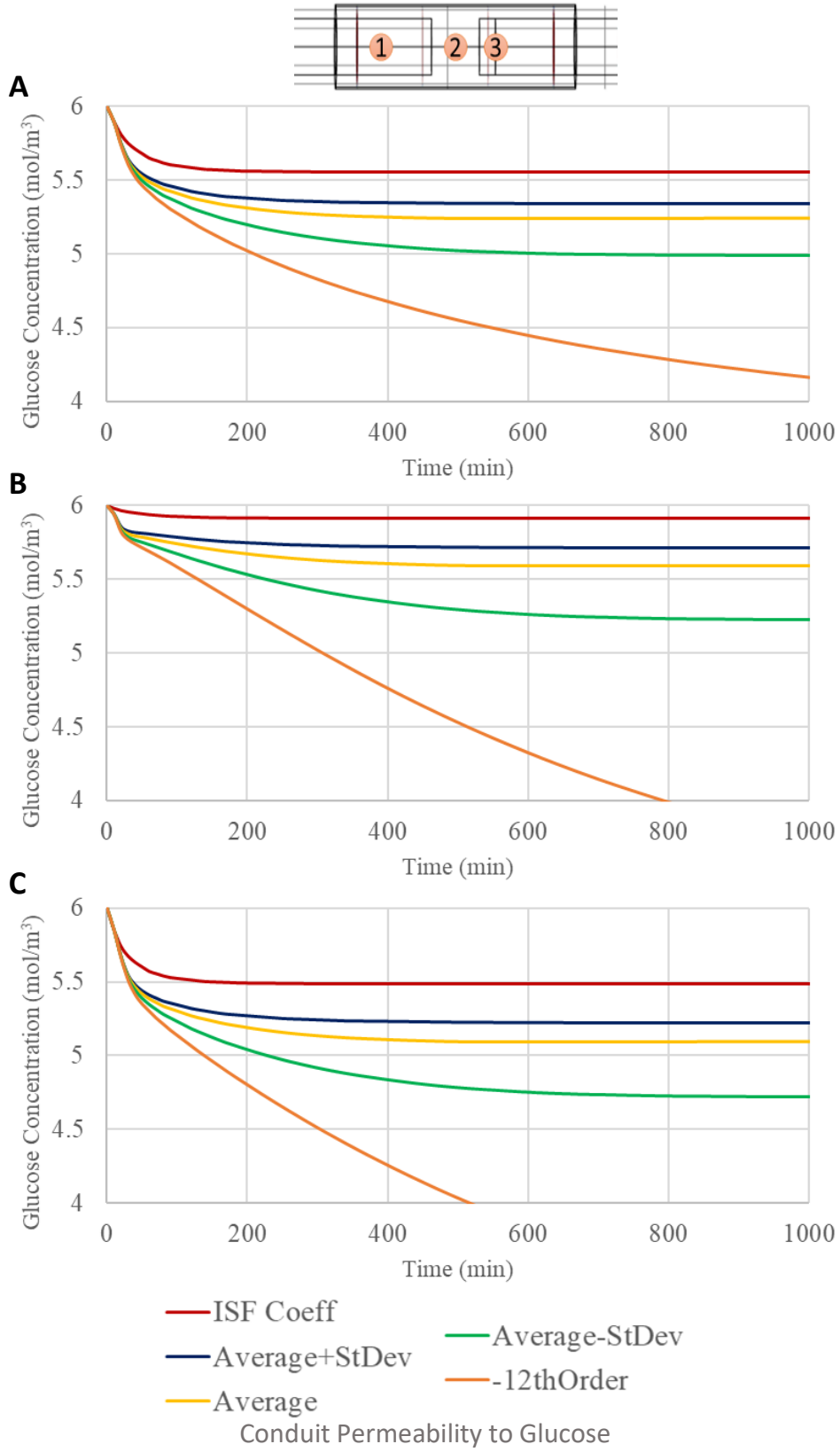


Figure 44: Glucose Concentration Profiles of a Conduit with Varied Conduit Permeability 0.70:1.00 nerve to conduit diameter ratio and conduit length of 16 mm with variable conduit permeability at (A) Location 1, (B) Location 2, and (C) Location 3

6.5 CONCLUSIONS OF FINITE ELEMENT ANALYSIS MODELING OF OXYGEN AND GLUCOSE CONCENTRATIONS AND DISTRIBUTIONS WITHIN A CNF PERIPHERAL NERVE CONDUIT

In order to provide insight into the concentration and distribution of oxygen and glucose within a peripheral nerve conduit, a COMSOL Multiphysics® model of a peripheral nerve injury comprising a 3 mm gap between the proximal and distal stumps was created. The injury site was enclosed within a cellulose nanofiber conduit. The end of the regenerating proximal stump was modeled to consume twice the oxygen and glucose per unit time vs baseline nerve consumption (as per literature). The concentration and distribution of oxygen and glucose at three locations within the conduit were analyzed as a function of the nerve to conduit diameter ratio, the permeability of the conduit wall to oxygen and glucose, and the length of the conduit.

It was found that the lowest oxygen concentration within the conduit occurred at the end of the proximal stump where regeneration was occurring. The end of the distal stump had the second lowest oxygen concentration (with baseline oxygen consumption), with the gap in between the stumps having the highest concentration (where no oxygen consumption occurs). Increasing the nerve to conduit diameter ratio (effectively decreasing the ISF filled gap between the nerve and the inner wall of the conduit) led to progressively lower oxygen concentrations for all conduit lengths and locations tested and for conduit wall oxygen permeabilities in accordance with those used in *in vivo* studies. The findings were attributed to the dominance of axial diffusion over radial diffusion of oxygen and the decreased ISF filled axial volume as the nerve and conduit diameters approach each other. Increasing the oxygen permeability of the conduit walls to values 10 times less than that of ISF (vs the baseline case of 100 times less permeable than ISF) resulted in the oxygen concentration at all locations within the conduit being invariant with the nerve to conduit diameter ratio, implying that radial diffusion of oxygen across the conduit wall is the dominant mechanism of oxygen migration for highly permeable conduits. Progressively decreasing the conduit wall permeability led to reversion to the axial diffusion regime at all locations. Increasing the length of the conduit employing the baseline wall permeability resulted in a

consistent decrease in oxygen concentration at all locations within the conduit as the axial distance required for oxygen diffusion increased. The model was shown to be internally consistent, and to follow expected trends with regard to the effect of changes of conduit radii and concomitant change of the ISF filled axial volume on oxygen concentration in an axial diffusion-controlled regime.

It was found that as the nerve to conduit diameter ratio increased, the glucose concentration at all locations decreased, a finding consistent with decreased axial diffusion. It was noted however that the small changes in glucose concentration that resulted suggest that axial diffusion was not the dominant diffusion mode. Investigation of the effect of variation in conduit length revealed similar trends. As conduit length increased, glucose concentrations progressively decreased, although again the effects were comparatively minor in the nerve gap and proximal nerve, suggesting that radial diffusion is the dominant regime at these locations. Lastly, the effect of variation of the glucose diffusion coefficient of the cellulose nanofiber conduit wall was investigated. Progressively decreasing the glucose diffusion coefficient of the CNF conduit wall consistently reduced the instantaneous glucose concentrations at all locations. At a diffusion coefficient of $1 \times 10^{-12} \text{ m}^2/\text{s}$, more than an order of magnitude below the experimentally determined value, the glucose concentrations at all locations were reduced below the hypoglycemic threshold of $4 \text{ mol}/\text{m}^3$, a finding attributed to inhibited radial diffusion of glucose. It is concluded therefore, that under the experimental conditions employed, radial diffusion of glucose into the luminal space of the conduit is the dominant diffusion modality at all locations, with axial diffusion only contributing to a minor extent in the distal nerve stump due to the shorter axial distance from the end of the conduit to the monitoring location.

CHAPTER SEVEN

CONCLUSIONS

The present work developed conduits comprising cellulose nanofiber (CNF) which showed great efficacy in promotion of peripheral nerve repair. CNF was produced from bleached softwood pulp via mechanical segmentation and defibrillation. A recirculating flow supermasscolloider was constructed within a temperature-controlled cleanroom at the University of Maine Technology Research Center. A series of GMP/GLP based protocols were developed to ensure production of verifiable quality CNF. Importantly, a cumulative energy meter was installed on the supermasscolloider to track the total energy applied to the cellulose slurry, which was shown to correlate well with the resulting fines content of the CNF.

Cylindrical neural conduits were created by rolling two layers of a sheet of CNF around a plastic mandrel, followed by sealing of the outer flap. As such, it was critical that CNF sheets be reproducibly created from the CNF slurry derived from the defibrillation process. It was found that dried CNF sheet thickness was proportional to the percent solids content of the CNF slurry employed to cast the sheet, as well as the thickness of the wet sheet spread by the casting knife film applicator. The CNF sheet production process was optimized to produce sheets with a thickness of $56.2 \pm 1.3 \mu\text{m}$. Physical characterization of the sheets was performed to determine strength, surface roughness, porosity/permeability and transparency. Tensile strength testing revealed that the Young's modulus of the CNF sheets was of the order of 4.6 to 5.7 GPa. Due to the fact that the CNF sheets were cast on a stainless steel plate and hence had two surfaces that dried in contact with different media (stainless steel and air), the surface roughness of the two sides were considerably different. Specifically, the side of the CNF sheet that dried in contact with the stainless steel plate was comparatively smooth with an

average roughness, as determined by mechanical profilometry, of 0.5-1.0 μm , while the side that dried in contact with air was comparatively rough with an average roughness of 2.5-4.0 μm .

Sheet porosity and permeability were characterized in order to understand the likely extent of passage of pro and anti-regenerative species through the CNF walls of the neural conduits. Measurement of air passage through the CNF sheets was unsuccessful, indicating that they were non-permeable, at least in the dry state. Mercury porosimetry measurements of CNF sheets confirmed the findings of the air permeability analysis; no evidence for sheet porosity was found down to the limit of the technique of 10 nm. Sheet transparency was shown to increase with decreased sheet thickness, and to increase with hot calendaring. Oxygen diffusion across the CNF sheets was measured as a function of relative humidity in the range of 50-90 %RH. The data enabled extrapolation to a diffusion coefficient of $1.8 \times 10^{-13} \text{ m}^2/\text{s}$ at the physiologically relevant condition of 100% relative humidity. The diffusion coefficient of glucose through the CNF was experimentally determined to be $1.7 \pm 0.9 \times 10^{-11} \text{ m}^2/\text{s}$, approximately two orders of magnitude greater than that of oxygen. It was noted CNF sheets swell significantly in aqueous solutions, expanding to approximately 70 μm thickness in the wet state from an initial dry thickness of approximately 50 μm .

A significant amount of work was performed to develop an effective means of sealing the internal and external flaps of the multi-layer CNF conduits, and to determine the optimal CNF sheet properties. The efficacy of various sealing methods, CNF sheet thickness, and number of CNF sheet layers were determined by evaluating the mechanical stability of conduits in a range of aqueous solutions under both static and dynamic conditions. In terms of mechanical stability, it was determined that the optimal number of CNF sheet layers was two and that sheets of approximately 52 μm thickness were most effective. Three different sealing methods were investigated. Applying an aqueous layer beneath the flap was found to be ineffective for extended periods of time. Applying CNF slurry beneath

the flap and coating the finished conduit in CNF slurry was found to produce a product with very good stability for up to approximately 6 weeks. The final and most stable method developed for sealing the conduit flaps was to employ mechanical interlocks on the inner and outer CNF layers; such conduits maintained their integrity even under dynamic conditions far more extreme than would be experienced *in vivo*.

CNF conduits were implanted in two murine sciatic nerve animal studies, and one non-human primate tolerability study. The first murine trial demonstrated that the conduits were well tolerated by the animals and were highly effective in promoting peripheral nerve regeneration when the sciatic nerve was transected, and no tissue excised. Indeed grip strength measurements of the hindlimbs of the test subjects 30 weeks post-surgery demonstrated approximately six times greater grip strength (~66% functional recovery) in animals that received a CNF conduit vs animals that had the sciatic nerve transected but did not receive a conduit. The second murine study investigated the efficacy of repair of the sciatic nerve employing five different repair techniques. Specifically, Group 1 used a 3mm nerve gap and no assistive repair intervention, Group 2 employed a suture to connect the nerve stumps across a 3mm nerve gap, Group 3 employed a 5mm conduit over a 3mm nerve gap, Group 4 employed a 5mm conduit over a 1mm nerve gap, and Group 5 employed a 3mm conduit over a 1mm nerve gap. It was concluded from the study that CNF conduits promote neural regeneration and do so over gaps that scale to very large injuries in humans. In addition, and somewhat surprisingly, it was shown that the extent of neural regeneration is dependent upon the length of the conduit employed and appears to be greatest for shorter conduits. Histological analysis revealed the presence of significant tissue in the luminal space of the conduit. Treatment with a cellulose specific stain revealed that the CNF conduit largely retained its tubular geometry, although delamination of the inner and outer flaps was evident, suggesting the need for a mechanical interlock design rather than solely a CNF slurry seal and coating. The non-human primate study was undertaken to determine the ability of an animal species known to be very sensitive

to foreign bodies to tolerate the CNF conduit. It was determined that conduits comprising CNF were very well tolerated and histological examination showed no evidence of a foreign body/inflammatory response, a finding consistent with a cell culture study. The suture employed in both the murine and the non-human primate surgeries to implant the conduit, however, engendered a strong foreign body/inflammatory response in the baboons.

The observation in the second murine study that the physical dimensions of the CNF conduit employed directly impacted the extent of neural regeneration led to the development of a finite element analysis model of the peripheral nerve-conduit system. Specifically, COMSOL Multiphysics® was employed to model the peripheral nerve-conduit system, and to predict the concentration and distribution of species likely to be important for neural regeneration as a function of the physical dimensions of the conduit, and the permeability of its walls. Indeed the time-dependent concentrations of oxygen, and separately, glucose were modeled throughout the nerve-conduit system as a function of conduit length, the nerve to conduit diameter ratio, and the permeability of the CNF conduit wall to the species of interest. It was found that all three parameters influenced the concentration and distribution of oxygen and separately, glucose, throughout the nerve/conduit system. Oxygen concentrations within the conduit were found to be heavily influenced by the conduit dimensions and to be dominated by axial diffusion through the ISF filled luminal space between the nerve and the inner conduit wall; little dependence on radial diffusion across the CNF wall of the conduit was found, a fact attributed to the relative impermeability of CNF to oxygen. Conversely, glucose concentrations within the conduit were found to be heavily influenced by radial diffusion across the CNF conduit wall, a fact attributed to the high permeability of CNF to glucose; axial diffusion of glucose through the ISF filled luminal space between the nerve and the inner conduit wall was found to be far less significant. The outcomes of the COMSOL Multiphysics® modeling study are significant in that they demonstrate that oxygen concentration within a CNF conduit *in vivo* may be modulated by the physical dimensions of the implant

relative to the nerve; and further that glucose concentration within the conduit is mostly controlled by the diffusion coefficient of glucose across the conduit wall. The *in vivo* murine studies revealed that neural regeneration was greatest when a shorter conduit was implanted over a fixed neural gap, a condition that the COMSOL model predicts would result in greater oxygen concentrations within the conduit, and glucose concentrations well above the hypoglycemic threshold. It is concluded therefore that the COMSOL model was predictive and explanatory of the *in vivo* results. Extension of the model to determine the concentration and distribution of the primary waste product of metabolism, carbon dioxide, would be an interesting future effort.

In addition to modeling the impact of conduit properties on carbon dioxide concentration, other aspects of the CNF conduit that could modulate neural regeneration should be explored in future studies to target an optimal regenerative environment. Indeed, although the first and second murine studies demonstrated that conduit implantation resulted in greater neural regeneration than was achieved in their absence, it was observed that the degree of regeneration decreased as the neural gap increased. Research is therefore required to increase the extent of neural regeneration in CNF conduits over large neural gaps. To this end, preliminary work was undertaken by the author and collaborators to embed axial growth guidance cables in the inner wall of the CNF conduit that could potentially support and direct neural regeneration. Further, chemical and/or biological modifications of the conduit could be undertaken to convert the implant from an essentially inert construct into one which actively promotes cellular proliferation. Indeed, the author and collaborators demonstrated the potential of the extracellular matrix protein laminin to favorably modify CNF in such a manner. Such an approach could be utilized to spatially template growth tracks for the regenerating neurons along the inner wall of the conduit, and/or could be coupled with guidance cables to further enhance regeneration. In addition, pro-regenerative species such as growth factors that are necessary to initiate regeneration could be incorporated into the conduit to guarantee threshold concentrations are met. Finally, the ability of the

CNF slurry/hydrogel itself to support cellular growth should be evaluated. If shown to be viable, CNF conduits could be filled with CNF slurry comprising essential cells and growth factors prior to implantation. Such a CNF construct could provide not only a microenvironment conducive to neural regeneration, but also a reservoir of supportive cells and factors.

REFERENCES

- [1] C. E. Schmidt and J. B. Leach, "Neural Tissue Engineering: Strategies for Repair and Regeneration," *Annual Review of Biomedical Engineering*, vol. 5, pp. 293-347, 2003.
- [2] N. Kyritsis, C. Kizil and M. Brand, "Neuroinflammation and central nervous system regeneration in vertebrates," *Trends in Cell Biology*, vol. 24, no. 2, pp. 128-135, 2014.
- [3] I. Duncan and R. Hoffman, "Schwann cell invasion of the central nervous system of the," *Journal of Anatomy*, vol. 190, pp. 35-49, 1997.
- [4] T. Gordon and K. Gordon, "Nerve regeneration in the peripheral nervous system versus the central nervous system and the relevance to speech and hearing after nerve injuries," *Journal of Communication Disorders*, vol. 43, pp. 274-285, 2010.
- [5] A. B. Lutz and B. A. Barres, "Contrasting the Glial Response to Axon Injury in the Central and Peripheral Nervous Systems," *Developmental Cell*, vol. 28, pp. 7-17, 2014.
- [6] L. Illis, "Central nervous system regeneration does not occur," *Spinal Cord*, vol. 50, pp. 259-263, 2012.
- [7] P. J. Horner and F. H. Gage, "Regenerating the damaged central nervous system," *NATURE*, vol. 407, pp. 963-970, 2000.
- [8] D. Grinsell and C. P. Keating, "Peripheral Nerve Reconstruction after Injury: A Review of Clinical and Experimental Therapies," *BioMed Research International*, no. Article ID 698256, 2014.
- [9] M. J. Barton, J. W. Morley, M. A. Stoodley, A. Lauto and D. A. Mahns, "Nerve repair: toward a sutureless approach," *Neurosurgical Review*, vol. 37, pp. 585-595, 2014.
- [10] P. Tate, "Central and Peripheral Nervous Systems," in *Seeley's Principles of Anatomy and Physiology: Second Edition*, McGraw-Hill, 2012, pp. 299-342.
- [11] P. Tate, "Functional Organization of Nervous Tissue," in *Seeley's Principles of Anatomy and Physiology: Second Edition*, McGraw-Hill, 2012, pp. 267-298.
- [12] R. M. G. Menorca, T. S. Fussell and J. C. Elfar, "Peripheral Nerve Trauma: Mechanisms fo Injury and Recovery," *Hand Clinics*, vol. 29, pp. 317-330, 2013.
- [13] C. Webber and D. Zochodne, "The nerve regenerative microenvironment: Early behavior and partnership of axons and Schwann cells," *Experimental Neurology*, vol. 223, pp. 51-59, 2010.
- [14] M. W. Barnett and P. M. Larkman, "The action potential," *Practical Neurology*, vol. 7, pp. 192-197, 2007.

- [15] M. Raastad and G. M. Sheperd, "Single-axon action potentials in the rat hippocamal cortex," *The Journal of Physiology*, vol. 548, no. 3, pp. 745-752, 2003.
- [16] J. L. Salzer and B. Zalc, "Myelination," *Current Biology Magazine*, vol. 26, pp. 937-980, 2016.
- [17] A. D. Gaudet, P. G. Popovich and M. S. Ramer, "Wallerian degeneration: Gaining perspective on inflammatory events after peripheral nerve injury," *Journal of Neuroinflammation*, vol. 8, no. 110, 2011.
- [18] K. Christie and D. Zochodne, "Peripheral axon regrowth: New molecular approaches," *Neuroscience*, vol. 240, pp. 310-324, 2013.
- [19] K. R. Jessen and R. Mirsky, "The repair Schwann cell and its function in regenerating nerves," *The Journal of Physiology: Neuroscience*, vol. 594, no. 13, pp. 3521-3531, 2016.
- [20] F. Teixeira, M. M. Carvalho, N. Sousa and A. J. Salgado, "Mesenchymal stem cells secretome: a new paradigm for central nervous system regeneration?," *Cellular and Molecular Life Sciences*, vol. 70, pp. 3871-3882, 2013.
- [21] S. Rotshenker, "Wallerian degeneration: the innate-immune response to traumatic nerve injury," *Journal of Neuroinflammation*, vol. 8, no. 109, 2011.
- [22] J. Scheib and A. Hoke, "Advances in peripheral nerve regeneration," *Nature Reviews Neurology*, vol. 9, pp. 668-676, 2013.
- [23] S. Ichihara, Y. Inada and T. Nakamura, "Artificial nerve tubes and their application for repair of peripheral nerve injury: an update of current concepts," *Injury, International Journal of the Care of the Injured*, vol. 39S4, pp. 29-39, 2008.
- [24] S. Shim and G.-I. Ming, "Roles of channels and receptors in the growth cone during PNS axonal regeneration," *Experimental Neurology*, vol. 223, pp. 38-44, 2010.
- [25] M. A. Lopez-Verrilli, F. Picou and F. A. Court, "Schwann Cell-Derived Exosomes Enhance Axonal Regeneration in the Peripheral Nervous System," *GLIA*, vol. 61, no. 11, pp. 1795-1806, 2013.
- [26] E. Doron-Mandel, M. Fainzilber and M. Terenzio, "Growth control mechanisms in neuronal regeneration," *FEBS Letters*, vol. 589, pp. 1669-1672, 2015.
- [27] A. Muheremu and Q. Ao, "Past, Present, and Future of Nerve Conduits in the Treatment of Peripheral Nerve Injury," *BioMed Research International*, no. Article ID 237507, 2015.
- [28] R. Gaudin, C. Knipfer, A. Henningsen, R. Smeets, M. Heiland and T. Hadlock, "Approaches to Peripheral Nerve Repair: Generations of Biomaterial Conduits Yielding to Replacing Autologous Nerve Grafts in Craniomaxillofacial Surgery," *BioMed Research International*, no. Article ID 3856262, 2016.

- [29] B. W. Hughes, L. L. Kusner and H. J. Kaminski, "Molecular Architecture of the Neuromuscular Junction," *Muscle & Nerve*, vol. 33, pp. 445-461, 2006.
- [30] T. Gordon, "The physiology of neural injury and regeneration: The role of neurotrophic factors," *Journal of Communication Disorders*, vol. 43, pp. 265-273, 2010.
- [31] L. E. Kokai, Y.-C. Lin, N. M. Oyster and K. G. Marra, "Diffusion of soluble factors through degradable polymer nerve guides: Controlling manufacturing parameters," *Acta Biomaterialia*, vol. 5, pp. 2540-2550, 2009.
- [32] J. S. Taras, V. Nanavati and P. Steelman, "Nerve Conduits," *Journal of Hand Therapy*, vol. 18, pp. 191-197, 2005.
- [33] S. Mobini, B. S. Spearman, C. S. Lacko and C. E. Schmidt, "Recent advances in strategies for peripheral nerve tissue engineering," *Current Opinion in Biomedical Engineering*, vol. 4, pp. 134-142, 2017.
- [34] M. Georgiou, J. P. Golding, A. J. Loughlin, P. J. Kingham and J. B. Phillips, "Engineered neural tissue with aligned, differentiated adipose-derived stem cells promotes peripheral nerve regeneration across a critical sized defect in rat sciatic nerve," *Biomaterials*, vol. 37, pp. 242-251, 2015.
- [35] J. A. Kouyoumdjian, "Peripheral Nerve Injuries: A Retrospective Survey of 456 Cases," *Muscle & Nerve*, vol. 34, pp. 785-788, 2006.
- [36] L. B. Dahlin and M. Wiberg, "Nerve injuries of the upper extremity and hand," *Efort Open Reviews*, vol. 2, pp. 158-170, 2017.
- [37] P. Zhang, N. Han and T. Wang, "Biodegradable Conduit Small Gap Tubulization for Peripheral Nerve Mutilation: A Substitute for Traditional Epineurial Neuroorrhaphy," *International Journal of Medical Sciences*, vol. 10, no. 2, pp. 171-175, 2013.
- [38] B. D. Bushnell, A. D. McWilliams and G. B. Whitener, "Early Clinical Experience with Collagen Nerve Tubes in Digital Nerve Repair," *The Journal of Hand Surgery*, vol. 33, no. 7, pp. 1081-1087, 2008.
- [39] P. G. d. Summa, P. J. Kingham and C. C. Campisi, "Collagen (NeuraGen) nerve conduits and stem cells for peripheral nerve gap repair," *Neuroscience Letters*, vol. 572, pp. 26-31, 2014.
- [40] B. K. Moor, M. Haefeli, S. Bouaicha and L. Nagy, "Results after delayed axillary nerve reconstruction with interposition of sural nerve grafts," *Journal of Shoulder and Elbow Surgery*, vol. 19, pp. 461-466, 2010.
- [41] S. Kehoe, X. F. Zhang and D. Boyd, "FDA approved guidance conduits and wraps for peripheral nerve injury: A review of materials and efficacy," *International Journal of the Care of the Injured*, vol. 43, pp. 553-572, 2011.

- [42] D. Neubauer, J. B. Graham and D. Muir, "Chondroitinase treatment increases the effective length of acellular nerve grafts," *Experiment Neurology*, vol. 207, pp. 163-170, 2007.
- [43] L. Goran, L. B. Dahlin, N. Danielsen, R. H. Gelberamn, F. M. Longo, H. C. Powell and S. Varon, "Nerve Regeneration in Silicone Chambers: Influence of Gap Length and of Distal Stump Components," *Experimental Neurology*, vol. 76, pp. 361-375, 1982.
- [44] N. Danielsen, L. Williams, L. Dahlin, S. Varon and G. Lundborg, "Peripheral nerve regeneration in Gore-tex chambers," *Scandinavian Journal of Plastic and Reconstructive Surgery and Hand Surgery*, vol. 22, no. 3, pp. 207-210, 1988.
- [45] H. Tabesh, G. Amoabediny and N. S. Nik, "The role of biodegradable engineered scaffolds seeded with Schwann cells for spinal cord regeneration," *Neurochemistry International*, vol. 54, pp. 73-83, 2009.
- [46] B. Schlosshauer, L. Dreesmann and H.-E. Schaller, "Synthetic Nerve Guide Implants in Humans: A Comprehensive Survey," *Neurosurgery*, vol. 59, pp. 740-748, 2006.
- [47] R. Weber, W. Breidenbach, R. Brown, M. Jabaley and D. Mass, "A randomized prospective study of polyglycolic acid for digital nerve reconstruction in humans," *Plastic and Reconstructive Surgery*, vol. 106, no. 5, pp. 1036-1045, 2000.
- [48] L. S. Nair and C. T. Laurencin, "Biodegradable polymers as biomaterials," *Progress in Polymer Science*, vol. 32, pp. 762-798, 2007.
- [49] R. Midha, M. Shoicet and P. Dalton, "Tissue Engineered Alternatives to Nerve Transplantation for Repair of Peripheral Nervous System Injuries," *Transplantation Proceedings*, vol. 33, pp. 612-615, 2001.
- [50] F. Stang, H. Fansa and G. Wolf, "Structural parameters of collagen nerve grafts influence peripheral nerve regeneration," *Biomaterials*, vol. 26, pp. 3083-3091, 2005.
- [51] A. Farole and B. T. Jamal, "A Bioabsorbable Collagen Nerve Cuff (NeuraGen) for Repair of Lingual and Inferior Alveolar Nerve Injuries: A Case Series," *Journal of Oral and Maxillofacial Surgery*, vol. 66, pp. 2058-2062, 2008.
- [52] T. W. Jernigan, M. A. Croce and C. Cagiannos, "Small Intestinal Submucosa for Vascular Reconstruction in the Presence of Gastrointestinal Contamination," *Annals of Surgery*, vol. 239, no. 5, pp. 733-740, 2004.
- [53] Y. Su, B.-F. Zeng and C.-Q. Zhang, "Study of biocompatibility of small intestinal submucosa (SIS) with Schwann cells in vitro," *Brain Research*, vol. 1145, pp. 41-47, 2007.
- [54] R. M. Smith, C. Wiedl and P. Chubb, "Tolerance of Small Intestine Submucosa (SIS) as a Nerve Conduit: Preliminary Report," *Journal of Investigative Surgery*, vol. 17, pp. 339-344, 2004.

- [55] M. A. Woodruff and D. W. Hutmacher, "The return of a forgotten polymer - Polycaprolactone in the 21st century," *Progress in Polymer Science*, vol. 35, pp. 1217-1256, 2010.
- [56] J. G. Sanchez, A. Tsuchii and Y. Tokiwa, "Degradation of polycaprolactone at 50 °C by a thermotolerant *Aspergillus* sp.," *Biotechnology Letters*, vol. 22, pp. 849-853, 2000.
- [57] M. F. Meek and W. F. D. Dunnen, "Porosity of the wall of a Neurolac nerve conduit hampers nerve regeneration.," *Microsurgery*, vol. 29, no. 6, pp. 473-478, 2009.
- [58] M. F. Meek and K. Jansen, "Two years after in vivo implantation of poly(DL-lactide-ε-caprolactone) nerve guides: Has the material finally resorbed?," *Journal of Biomedical Materials Research Part A*, vol. 89, no. 3, pp. 734-738, 2009.
- [59] A. L. Luis, J. M. Rodrigues and S. Amado, "PLGA 90/10 AND CAPROLACTONE BIODEGRADABLE NERVE GUIDES FOR THE RECONSTRUCTION OF THE RAT SCIATIC NERVE," *Microsurgery*, vol. 27, no. 2, pp. 125-137, 2007.
- [60] R. Shin, P. Friedrich and B. Crum, "Treatment of a segmental nerve defect in the rat with use of bioabsorbable synthetic nerve conduits: a comparison of commercially available conduits," *Journal of Bone and Joint Surgery*, vol. 91, no. 9, pp. 2194-2204, 2009.
- [61] M. J. Bertleff, M. F. Meek and J.-P. A. Nicolai, "A prospective clinical evaluation of biodegradable neurolac nerve guides for sensory nerve repair in the hand.," *Journal of Hand Surgery*, vol. 30, no. 3, pp. 513-518, 2005.
- [62] D. N. Ku, "Poly(vinyl alcohol) hydrogel". US Patent US6231605B1, 9 November 1999.
- [63] D. Muir, "The potentiation of peripheral nerve sheaths in regeneration and repair," *Experimental Neurology*, vol. 223, pp. 102-111, 2010.
- [64] T. Waitayawinyu, D. Parisi and B. Miller, "A comparison of polyglycolic acid versus type 1 collagen bioabsorbable nerve conduits in a rat model: an alternative to autografting," *Journal of Hand Surgery*, vol. 32, no. 10, pp. 1521-1529, 2007.
- [65] S. Mackinnon and A. Dellon, "Clinical nerve reconstruction with a bioabsorbable polyglycolic acid tube," *Plastic and Reconstructive Surgery*, vol. 85, no. 3, pp. 419-424, 1990.
- [66] A. Haug, "US Food and Drug Administration/Conformit Europe-approved absorbable nerve conduits for clinical repair of peripheral and cranial nerves," *Letters to the Editor - Annals of Plastic Surgery - Vol 62 Issue 6*, p. 710, June 2009.
- [67] B. Seal, T. Otero and A. Panitch, "Polymeric biomaterials for tissue and organ regeneration," *Materials Science and Engineering Reviews*, vol. 34, pp. 147-230, 2001.
- [68] S. Lohrasbi, E. Mirzaei and A. Karimizade, "Collagen/cellulose nanofiber hydrogel scaffold: physical, mechanical and cell biocompatibility properties," *Cellulose*, vol. 27, no. 2, pp. 927-940, 2020.

- [69] H. Takagi and A. Asano, "Effects of processing conditions on flexural properties of cellulose nanofiber reinforced "green" composites," *Composites Part A: Applied Science and Manufacturing*, vol. 39, no. 4, pp. 685-689, 2008.
- [70] Y. Xue, Z. Mou and H. Xiao, "Nanocellulose as a sustainable biomass material: Structure, properties, present status and future prospects in biomedical applications," *Nanoscale*, vol. 9, no. 39, pp. 14758-14781, 2017.
- [71] X. Niu, Y. Liu, G. Fang, C. Huang, O. J. Rojas and H. Pan, "Highly Transparent, Strong, and Flexible Films with Modified Cellulose Nanofiber Bearing UV Shielding Property," *Biomacromolecules*, vol. 19, no. 12, pp. 4565-4575, 2018.
- [72] C. Walker, "The Process Development Center," The University of Maine, [Online]. Available: <https://umaine.edu/pdc/>. [Accessed 21 April 2021].
- [73] World Health Organization, "WHO good practices for pharmaceutical quality control laboratories," WHO Technical Report Series, No. 957, 2010, Annex 1, 2010.
- [74] "Property Information - Young's Modulus and Specific Stiffness," University of Cambridge - Department of Engineering, 25 2 2002. [Online]. Available: <http://www-materials.eng.cam.ac.uk/mpsite/properties/non-IE/stiffness.html>. [Accessed 29 1 2020].
- [75] E. Kiskinis, J. Sandoe and L. A. Williams, "Pathways Disrupted in Human ALS Motor Neurons Identified through Genetic Correction of Mutant SOD1," *Cell Stem Cell*, vol. 14, pp. 1-15, 2014.
- [76] "Bottle Basics Plastics Comparison Chart," Alpha Packaging - Stock and Custom Plastic Packaging, [Online]. Available: <http://www.alphap.com/bottle-basics/plastics-comparison-chart.php>. [Accessed 4 September 2020].
- [77] A. C. Khazraji and S. Robert, "Interaction Effects between Cellulose and Water in Nanocrystalline and Amorphous Regions: A Novel Approach Using Molecular Modeling," *Journal of Nanomaterials*, vol. 2013, pp. 1-10, 2013.
- [78] M. E. Walsh, L. B. Sloane and K. E. Fischer, "Use of Nerve Conduction Velocity to Assess Peripheral Nerve Health in Aging Mice," *The Journals of Gerontology Series A: Biological Sciences and Medical Sciences*, vol. 70, no. 11, pp. 1312-1319, 2015.
- [79] A. Aydin, B. C. Ozden, S. Karamursel, S. Solakoglu, S. Aktas and M. Erer, "Effect of hyperbaric oxygen therapy on nerve regeneration in early diabetes," *Microsurgery*, vol. 24, no. 3, pp. 255-261, 2004.
- [80] B. Oroglu, T. Turker, S. Aktas, V. Olgac and M. Alp, "Effect of hyperbaric oxygen therapy on tense repair of the peripheral nerves," *Undersea & Hyperbaric Medicine*, vol. 38, no. 5, pp. 367-373, 2011.

- [81] Y. Cho, J. E. Shin, E. E. Ewan, Y. M. Oh, W. Pita-Thomas and V. Cavalli, "Activating Injury-Responsive Genes with Hypoxia Enhances Axon Regeneration through Neuronal HIF-1 α ," *Neuron*, vol. 88, no. 4, pp. 720-734, 2015.
- [82] C. Yao, X. Shi, Z. Zhang, S. Zhou, T. Qian, Y. Wang, F. Ding, X. Gu and B. Yu, "Hypoxia-Induced Upregulation of miR-132 Promotes Schwann Cell Migration After Sciatic Nerve Injury by Targeting PRKAG3," *Molecular Neurobiology*, vol. 53, no. 8, pp. 5129-5139, 2016.
- [83] T. Haapaniemi, G. Nylander, M. Kanje and L. Dahlin, "Hyperbaric Oxygen Treatment Enhances Regeneration of the Rat Sciatic Nerve," *Experimental Neurology*, vol. 149, no. 2, pp. 433-438, 1998.
- [84] Z. Shams, A. R. Khalatbary, H. Ahmadvand, Z. Zare and K. Kian, "Neuroprotective effects of hyperbaric oxygen (HBO) therapy on neuronal death induced by sciatic nerve transection in rat," *BMC Neurology*, vol. 17, no. 1, p. 220, 2017.
- [85] E. C. Sanchez, "Hyperbaric oxygenation in peripheral nerve repair and regeneration," *Neurological Research*, vol. 29, no. 2, pp. 184-198, 2007.
- [86] T. Lim, X. Shi and J. Johnson, "Peripheral Nerve Injury Induces Persistent Vascular Dysfunction and Endoneurial Hypoxia, Contributing to the Genesis of Neuropathic Pain," *J Neurosci*, vol. 35, no. 8, pp. 3346-59, 2015.
- [87] N. R. Sibson, A. Dhankar, G. F. Mason, D. L. Rothman, K. L. Behar and R. G. Shulman, "Stoichiometric coupling of brain glucose metabolism and glutamatergic neuronal activity," *PNAS*, vol. 95, no. 1, pp. 316-321, 1998.
- [88] P. Mergenthaler, "Sugar for the brain: the role of glucose in physiological and pathological brain function," *Trends Neurosci*, vol. 36, no. 10, pp. 587-97, 2014.
- [89] J. M. Berg, J. L. Tymoczko and L. Stryer, "Section 30.2 Each Organ Has a Unique Metabolic Profile," in *Biochemistry, Fifth Edition*, NCBI Bookshelf ID:NBK22436, W. H. Freeman and Company, 2002.
- [90] T. Lim, M. Rone and S. Lee, "Mitochondrial and Bioenergetic Dysfunction in Trauma-Induced Painful Peripheral Neuropathy," *Mol Pain*, vol. 11, no. 58, pp. 1-9, 2015.
- [91] M. Stecker and M. Stevenson, "Effect of glucose concentration on peripheral nerve and its response to anoxia," *Muscle and Nerve*, vol. 49, no. 3, pp. 370-7, 2014.
- [92] I. Torres Filho, Y. F. Leunig M and J. R. Intaglietta M, "Noninvasive measurement of microvascular and interstitial oxygen profiles in a human tumor in SCID mice," *Proc Natl Acad Sci USA*, vol. 91, no. 6, pp. 2081-5, 1994.
- [93] B. D. Han P, "Temperature Dependence of Oxygen Diffusion in H₂O and D₂O," *J Phys Chem*, vol. 100, pp. 5597-602, 1996.

- [94] T. Lagerlund and P. Low, "A mathematical simulation of oxygen delivery in rat peripheral nerve," *Microvasc Res*, vol. 34, no. 2, pp. 211-22, 1987.
- [95] U. Cheema, Z. Rong, O. Kirresh, A. J. MacRobert, P. Vadgama and R. A. Brown, "Oxygen diffusion through collagen scaffolds at defined densities: implications for cell survival in tissue models," *Journal of Tissue Engineering and Regenerative Medicine*, vol. 6, no. 1, pp. 77-84, 2012.
- [96] A. Tirosh, I. Shai and A. Rudich, "Normal Fasting Plasma Glucose Levels and Type 2 Diabetes in Young Men," *N Engl J Med*, vol. 354, no. 1, pp. 87-8, 2006.
- [97] S. Thennadil, J. Rennert and B. Wenzel, "Comparison of glucose concentration in interstitial fluid, and capillary and venous blood during rapid changes in blood glucose levels," *Diabetes Technol Ther*, vol. 3, no. 3, pp. 357-65, 2001.
- [98] J. Allen, H. Damasio and T. Grabowski, "Normal Neuroanatomical Variation in the Human Brain: An MRI-Volumetric Study," *Am J Phys Anthropol*, vol. 358, no. June 2001, pp. 341-58, 2002.
- [99] P. Harrison, N. Freemantle and J. Geddes, "Meta-analysis of brain weight in schizophrenia," *Schizophr Res*, vol. 64, no. 1, pp. 25-34, 2003.
- [100] V. Jensen, A. Molck and I. Bogh, "Effect of insulin-induced hypoglycaemia on the peripheral nervous system: Focus on adaptive mechanisms, pathogenesis and histopathological changes," *J Neuroendocrinol*, vol. 26, no. 8, pp. 482-96, 2014.
- [101] J. Towne, N. Carter and D. Neivandt, "COMSOL Multiphysics® Modelling of Oxygen Diffusion Through a Cellulose Nanofibril Conduit Employed for Peripheral Nerve Repair," *Under Review*, 2020.
- [102] E. Khalil, K. Krestos and G. Kasting, "Glucose partition coefficient and diffusivity in the lower skin layers," *Pharm Res*, vol. 23, no. 6, pp. 1227-34, 2006.
- [103] H. Suhaimi, S. Wang and D. Das, "Glucose diffusivity in cell culture medium," *Chem Eng J*, vol. 269, pp. 323-7, 2015.
- [104] D. Grinsell and C. P. Keating, *Peripheral Nerve Anatomy*, Adapted Image: Hindawi Publishing Corporation, 2014.
- [105] R. University, *Graph of Action Potential*, Adapted Image: Pressbooks, 2019.
- [106] K. Rogers, *Node of Ranvier*, Adapted Image: Encyclopedia Britannica, 2012.
- [107] A. D. Gaudet, P. G. Popovich and M. S. Ramer, *Progression of Wallerian degeneration and axon regeneration after peripheral nerve injury (PNI)*, Image: BioMed Central, 2011.
- [108] M. J. Barton, *Diagram of different nerve repair devices*, Adapted Image: Springer, 2014.
- [109] S. Kehoe, *Principle of nerve entubulization*, Image: Elsevier, 2012.

- [110] H. Suhaimi, S. Wang and T. Thornton, "On glucose diffusivity of tissue engineering membranes and scaffolds," *Chem Eng Sci*, vol. 126, pp. 244-56, 2015.
- [111] A. Lovatt and H. Shercliff, *Young's Modulus - Density (Image)*, University of Cambridge Department of Engineering, 2002.
- [112] C. A. d. Assis, M. C. Iglesias and M. Bilodeau, "Cellulose micro- and nanofibrils (CMNF) manufacturing - financial and risk assessment," *Biofuels, Bioprod. Bioref*, no. 12, pp. 251-264, 2018.
- [113] D. Moakley, J. Koh and J. D. Pereira, "Pharmacological Profiling of Purified Human Stem Cell-Derived and Primary Mouse Motor Neurons," *Nature Scientific Reports*, vol. 9, no. 10835, pp. 1-10, 2019.

APPENDIX

A1: CLEANROOM DESCRIPTION

A cleanroom was constructed off site at the Technology Research Center of the Forest Bioproduct Research Institute to house a refining center and laboratory space for conduit development from wood pulp feedstock. The overall cleanroom exterior dimensions of the cleanroom were 13' wide x 17' long x 12' tall. The interior ceiling height was 10 ft, creating a 2 ft tall air chamber in the ceiling of the entire cleanroom for air flow. Installed in the ceiling were four HEPA air filtration units as well as four flat panel LED lights. The two longest sides of the cleanroom were constructed with a double wall with approximately a 1-foot gap for air recirculation. The air flow in the room blew down from the ceiling and was separated into two streams; airflow into the recirculation chambers of the double walled sides and excess air pushed through a sweeper seal at the bottom of the entrances. The air flow created positive pressure in the room meaning a constant flow of air outward from the room preventing unwanted particles drifting into the room. A prefilter was installed in the roof of the cleanroom such that fresh, filtered air could be pulled into the air chamber, mixed with recirculated air, and cycled into the cleanroom. An 18,000 BTU air conditioner and heat pump (Home Depot, 309068909) was installed in the ceiling space to maintain temperature of the cleanroom space.

The interior space was divided into two separate rooms, a working area and a gowning area. Doors existed to partition the gowning area from the outside, and separately, the work area from the gowning area. Only one should be opened at any given time to ensure maintenance of the clean positive pressure environment. The gowning area, approximately 4' x 12', contained a storage shelf for personal protective equipment (PPE), a coat rack, a shoe rack, and a bench. All PPE was donned while in the gowning room with both doors closed. Once PPE was donned, an individual could enter the work area. The work area was 10' x 12' with two 6' x 3' stainless steel work benches delineating two distinct work areas (dry and wet). Dry work consisted of pulp preparation, sheet production, conduit production, and

other work in which water could potentially damage products. Wet work was performed on the second bench which housed the supermasscolloider.

The supermasscolloider (SMC) setup was the centerpiece of the cleanroom and was employed to refine bleached softwood kraft pulp into cellulose nanofiber. The SMC was configured to enable continuous refinement. A food grade positive displacement pump was employed, sized appropriately to move slurry prepared at 2% solids by weight. All contacting surfaces of the sanitary fittings were 316 stainless steel, joined with silicone gaskets, and were secured with quick lock fittings made of 304 stainless steel. The diameters of the fittings and lines ranged from 1" ID on the recirculation line, sampling port, and waste line on the output side of the pump, 2" for the input of the pump, 3" on the overflow, 4" on the pump reservoir and 6" for the SMC output receiver. The larger diameter on the pump input side were necessary for the gravity-fed flow of viscous CNF slurry.

The ability to operate the SMC as a continuous, recirculating system relied upon the ability for fluid flow to occur simultaneously in the pump and in the colloider. If either section of equipment were to possess stagnant slurry, damage to the equipment and potential contamination of the slurry could occur. It was critical to size each fitting volumetrically such that the entire volume of slurry in the system (14 liters) could be held in the pump reservoir, and that the recirculation line and hopper volume together were less than half of the system volume. Compliance with the volumetric restrictions meant that with a full recirculation line, hopper and overflow line, neither the pump nor colloider were in danger of dry operation. Optimizing the pump reservoir volume was key for consistent slurry production as it maximized mixing of the slurry. Operationally it should be noted that as the viscosity of the slurry increases with the extent of refining, the pump speed should be slowed to account for the decreased flow from the gravity fed overflow line.

Sample	8-29-17#1	8-29-17#2	9-18-17#1	10-13-17#1	10-18-17#1	10-18-17#2
SAMPLED ALIQUOT	95.40%*	92.90%*	95.40%	96.90%	97.10%	96.60%
AGGREGATE ALIQUOT	74.20%	73.60%	86.20%	97.20%	97.10%	96.60%
DIFFERENCE IN ALIQUOTS	21.20%	19.30%	9.20%	0.30%	0.00%	0.00%

*Time sampled at 105mins
 1. Adjusted Flow Rate
 2. Adjusted System Volume

*Figure 1: Optimization of Continuous SMC System
 Alterations were made to the pump speed and pump reservoir to increase the mixing capabilities of the system. Sample aliquots were taken from the hopper and aggregate aliquots were taken from the whole slurry after dispensing from the system.*

The SMC is an open system that was designed for continuous refining of wood pulp dispersed in water into a CNF slurry. Air quality was critical, hence the placement in a clean room. Similarly, water quality was controlled via use of purification system. To ensure consistent, high quality CNF production amenable to the creation of biomedical implants, Standard Operation Procedures and Protocols were developed for each stage of the process from pulp preparation to conduit packaging. All protocols were based on GMP and GLP protocols commonly used in the pharmaceutical industry. Quality Control Checklists were developed for different stages of the process to ensure consistency and the prevention of downstream complications. The Standard Operating Procedures and Quality Control Checklists may be found in the subsequent appendices.

A2: CLEANROOM BLUEPRINTS/DIAGRAMS

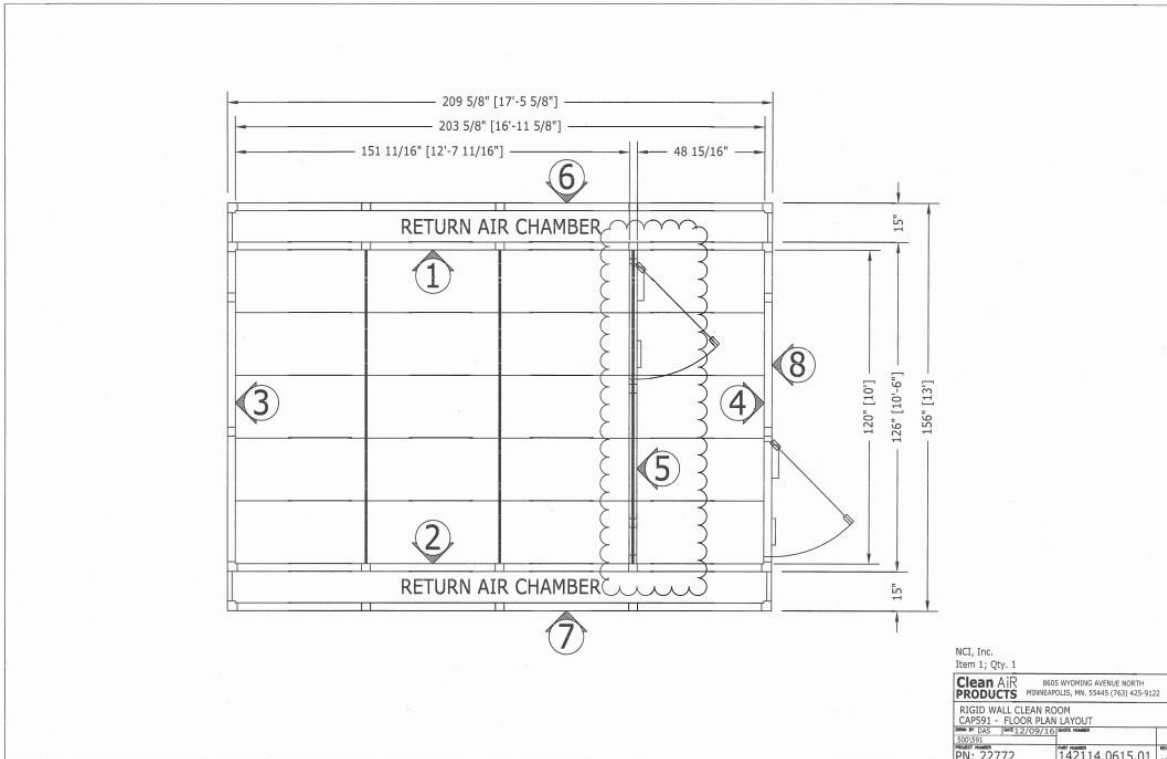


Figure 2: Technical Drawing of the Cleanroom



Figure 3: Image of the Constructed Cleanroom

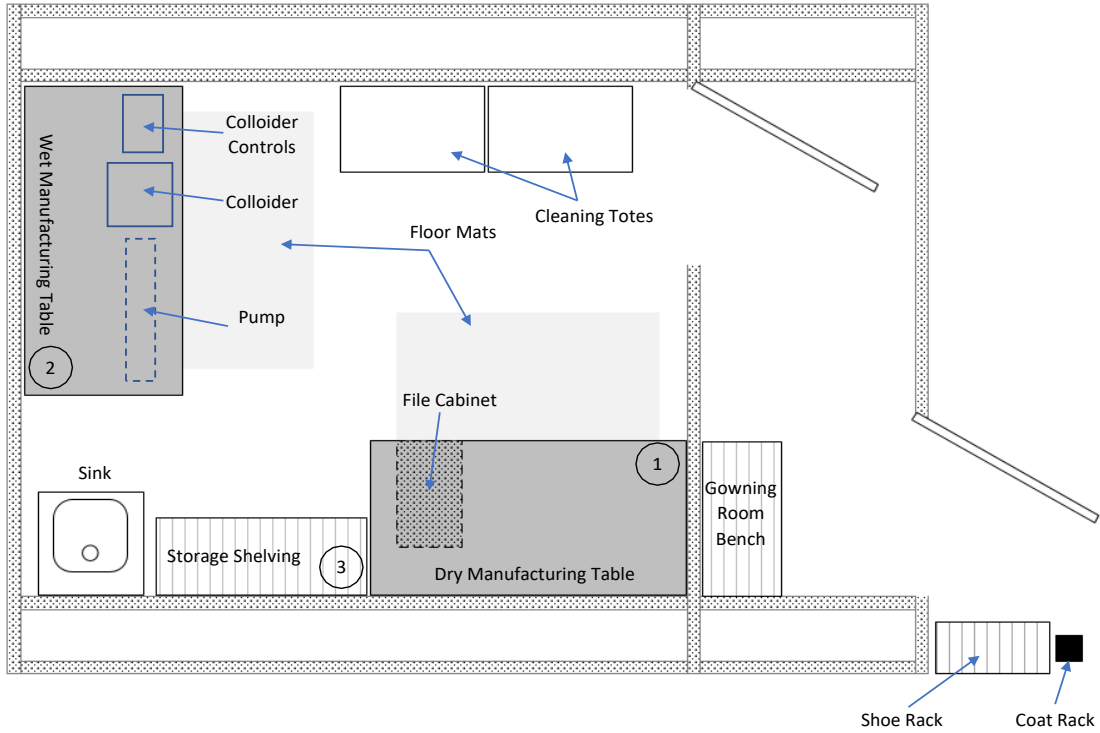


Figure 4: Equipment Layout of Cleanroom with Three Distinct Working Areas
 Dry Manufacturing of sheets and conduits (1), producing slurry (2), and sample storage (3)

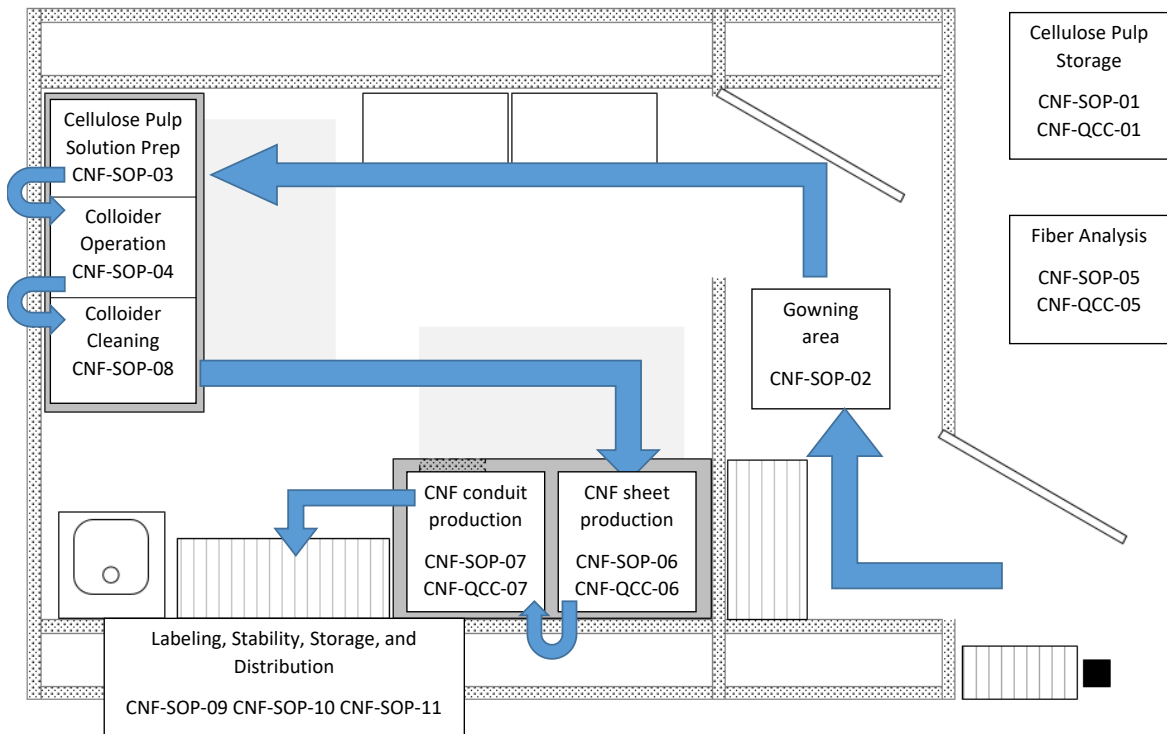


Figure 5: Workflow Diagram of Cleanroom Activities with Standard Operating Procedures and Quality Control Checks

A3: GMP/GLP-BASED PROTOCOLS DOCUMENT

**GOOD MANUFACTURING PRACTICES (GMP) COMPLIANT METHOD TO PRODUCE CELLULOSE
NANOFIBRIL NEURAL CONDUITS**



2/12/2018

Including All Standard Operating Procedures and Quality Control Checklists

(FOR RESEARCH PURPOSES ONLY)

Approved by:	Signature	Date
Originator	Nicklaus Carter and Mary Bourque	
Manager	David Neivandt	
Quality Assurance	David Neivandt and Caitlin Howell	

SCOPE AND APPLICABILITY

The purpose of the following documents is to establish a clean process with multiple levels of quality control and quality assurance to produce and distribute cellulose nanofibril (CNF) conduits. The methods described in the Standard Operating Procedures (SOPs) enclosed are used to produce a medical-grade CNF conduit from bleached cellulose pulp to be used for neural applications. The SOPs and Quality Control Checklists (QCCs) do not include tests for pathogens, microbial growths, or sterility beyond multiple visual inspections during production. The University of Maine has partnered with researchers in the Egan Laboratory at Harvard University, Nano Terra, and the Southwest National Primate Research Center (SNPRC) of the Texas Biomedical Research Institute in San Antonio, Texas to test the conduits for efficacy *in vivo*, and these teams have developed their own protocol to sterilize the conduits prior to implantation.

Two specialized environments are needed to produce CNF conduits: A humidity-controlled environment is required to store the cellulose pulp. A clean room with air filters and a gowning area prior to entry is required for pulp suspension production, CNF slurry production, conduit production, and stability studies (see Appendix A.1 and 2). The workflow plan for the cleanroom is presented in Appendix A.3. The TAPPI-certified room in the University of Maine's Process Development Center (PDC) stores the pulp (see Appendix B.1 for PDC and TAPPI room floor plans) and a clean room housed in the University of Maine's Technology Research Center (TRC) is employed for production (see Appendix C for TRC floor plan.) See Appendix D for further specifications and maintenance protocol of the clean room. The analysis of cellulose pulp moisture content and the measurement of fines and fibers using a MorFi Fiber Analyzer may take place in any laboratory environment. For the pilot operation described, separate laboratory spaces in the facilities of the University of Maine in Orono are used (see Appendix B.2, and 3 for floor plans).

All operations and facilities are designed to adhere to the following Good Manufacturing Practices (GMP): WHO GMP for active pharmaceutical ingredients stated as per Annex 2- WHO Technical Report Series (TRS), No. 957, 2010; GMP guide for Active Pharmaceutical Ingredients ICH Harmonised Tripartite Guideline stated as per ICH Q9; and GMP requirements as per Directives No. 2001/83/EC latest amended *vide* Directive 2011/62/EU). See Appendix E for the whole-facility self-appraisal based on these GMP guidelines. The whole-facility self-appraisal will be reevaluated on a yearly basis and all revisions made will be documented.

See next page for a listing of the operation's SOPs and QC checklists.

SUMMARY OF METHOD

Nicklaus Carter, a Ph.D. candidate at the University of Maine (2017), has worked laboriously with developing the process to product neural conduits. Therefore, Nicklaus was the originator of all SOPs and QCCs. Mary Bourque, pursuing a B.S. in Chemical Engineering at Columbia University (2018), was a participant of the NSF-funded Research Experience for Undergraduates (REU) in the Forest Bioproducts Research Institute (FBRI) at the University of Maine and worked closely with Nicklaus to complete the SOPs and QCCs. The SOPs and QCCs are numbered in the order they should be completed. The following is a summary of methods detailed in each SOP document:

1. **(CNF-SOP-01)** Cellulose pulp sample is obtained, properly stored in a humidity-controlled environment, and analyzed for moisture content, adhering to ISO 287 protocol.
2. **(CNF-SOP-02)** Personnel change into appropriate PPE prior to entering the clean room.
3. **(CNF-SOP-03)** Cellulose pulp is added to water and allowed to sit overnight. The pulp is agitated and broken down into smaller particulates.
4. **(CNF-SOP-04, CNF-SOP-05, CNF-SOP-06)** The pulp suspension is circulated through a super mass colloidier (SMC) where it is refined until 90% fines is achieved. A calibration curve relating the cumulative energy and fines content using a MorFi Fiber Analyzer is used to determine the level of refinement while running the SMC. The SMC is cleaned after each batch.
5. **(CNF-SOP-07)** The slurry collected from the SMC is used to form CNF sheets by using a film applicator and air drying.
6. **(CNF-SOP-08)** Dry sheets are measured for thickness before being rolled and employed as neural conduits.
7. **(CNF-SOP-09)** The clean room and all equipment are cleaned regularly for quality control measures.
8. **(CNF-SOP-10)** A detailed log of QCCs are kept to properly label each product. Example labels are included.
9. **(CNF-SOP-11)** Products are tested for stability in different environments and timescales.
10. **(CNF-SOP-12)** The supervisor approves distribution of products, ensuring all QCCs are complete.

Quality Control and Quality Assurance

The following quality control checklists have been developed for applicable steps of production to ensure consistent products as well as to create a traceable log of batch details and personnel responsibility:

1. **Cellulose Pulp (CNF-QCC-01)**
2. **Processed Fiber (CNF-QCC-06)**
3. **Sheet Production (CNF-QCC-07)**
4. **Conduit Production (CNF-QCC-08)**

CNF-SOP-01 CELLULOSE PULP STORAGE

Nanocellulose Conduit Production
Standard Operating Procedure #01
Cellulose Pulp Storage

Rev	Date	Description
1	1/19/2017	Draft Development Document-Nicklaus Carter
2	7/28/2017	Revision-Mary Bourque
3	8/1/2017	Revision-David Neivandt and Mary Bourque
4	8/14/17	Revision – Nicklaus Carter

Approved by:	Signature	Date
Originator	Nicklaus Carter	
Manager	David Neivandt	
Quality Assurance	David Neivandt and Caitlin Howell	

1.0 Purpose

- 1.1. To store cellulose pulp in a temperature and humidity-controlled environment such that the moisture content of an aliquot can be calculated.

2.0 Health and Safety Warnings

- 2.1. Take care when lifting or carrying large or heavy loads: Improper form or the inability to lift heavy loads can cause strains and sprains.
- 2.2. Use appropriate personal protective equipment PPE (laboratory coats, gloves, safety glasses when applicable) while working in the laboratory.
- 2.3. Work in a well-ventilated laboratory area.
- 2.4. PPE is worn only in laboratory areas and removed before entering non-laboratory areas.
- 2.5. Hazardous waste must be disposed in designated waste container.
- 2.6. Be familiar with the MSDS/SDS for all chemicals employed in the procedure.

3.0 Cautions

- 3.1. The sample of cellulose pulp used for the pulp suspension must be stored in a temperature and humidity-controlled environment in order for the calculated moisture content to be representative of the entire sample.
- 3.2. Do not process recovered, re-conciliated, or damaged materials or equipment. Visually inspect all materials, and make note of any damaged or lost material in the corresponding QC checklist as well as reporting the loss to Dr. Neivandt.
- 3.3. Ensure filters have been on and running for at least 24 hours. If the filters have not been on for at least 24 hours, turn the filters on and wait until a full 24 hours has passed before entry to prevent contamination due to airborne particles.
- 3.4. If the clean room pressure is not twice that of the gowning room, do not enter the clean room, for this may indicate end of the filter life.

4.0 Interferences

- 4.1. Improper storage of the pulp sample (malfunctioning temperature and moisture control, improperly sealed bags, storage of the pulp sample in an open environment, etc.) will yield inaccurate calculations of the weight percent solids of the pulp suspension.

5.0 Personnel Responsibilities and Qualifications

5.1. Supervisor:

- Ensure operators are trained on this procedure.
- Ensure operators conduct procedures as instructed.

5.2. The Operator:

- Must be trained on all equipment and procedures prior to operation.
- Complete this procedure as instructed.
- Report any deviations to this procedure to Dr. Neivandt.
- Follow Safety and Environmental Management (SEM) lock-out tag-out procedure for equipment that needs repair. Remove broken equipment from the room.
- Must be able to lift up to 50 pounds.

6.0 Equipment and Materials

6.1. Equipment

- 6.1.1. Laboratory scale (Fisher Scientific, 01-920-120)
- 6.1.2. Heating/drying oven (Fisher Scientific, 15-10-0508)

6.2. Materials (as listed or equivalent)

- 6.2.1. Bleached cellulose pulp (Vendor, Cat #XXXXXX)

7.0 Quality Control and Quality Assurance

7.1. Complete the quality control checklist CNF-QCC-01 (Cellulose Pulp) for the pulp sample to be stored in the TAPPI room. Remove a sample of approximately five sheets of pulp from the lot and store in a temperature and humidity-controlled environment for a minimum of 24 hours prior to analysis of moisture content. Calculate the moisture content using the ISO 287 standard procedure using an aliquot of the sample. The moisture content calculated will be representative of the entire sample removed from the lot and stored in a temperature and humidity-controlled environment. Moisture content need only be recalculated if storage conditions of the sample change or a new sample from the lot has been stored in the TAPPI room to be used. While performing this SOP, record in the accompanying quality control checklist CNF-QCC-01, Cellulose Pulp:

- 7.1.1. Storage conditions in the TAPPI room
- 7.1.2. Mass of sample
- 7.1.3. Moisture content (%) of aliquot
- 7.1.4. Visual inspection
- 7.1.5. Notes
- 7.1.6. Initials and date

8.0 References

- 8.1. CNF-QCC-01 (Cellulose Pulp Quality Control Checklist)
- 8.2. ISO 287 (Paper and board – Determination of moisture content of a lot – Oven-drying method)

8.3. CNF-SOP-09 (General Maintenance and Cleaning Protocol)

8.4. CNF-SOP-10 (Labeling Procedure for Stocks, Samples, and Products)

9.0 Procedures

9.1. Calculation of Moisture Content (as outlined in ISO 287)

9.1.1. Remove a pulp sample (five sheets) from the lot and store in the TAPPI room for a minimum of 24 hours prior to analysis of moisture content

9.1.2. Transfer an aliquot of pulp (100g) from the sample to a dry container and obtain the mass

9.1.3. Dehydrate the aliquot of pulp in a drying oven at a temperature of $105^{\circ}\text{C} \pm 2^{\circ}\text{C}$

9.1.4. Reweigh the pulp aliquot. Repeat drying and weighing until there is no change in mass

9.1.5. Obtain a moisture content value of the aliquot. The aliquot's moisture content will be representative of the sample stored in the TAPPI room

9.2. Cleaning and Maintenance

9.2.1. Clean the station as outlined in CNF-SOP-09. Record all maintenance and cleaning performed in the maintenance and cleaning logs at the station.

CNF-SOP-02 GOWNING PROTOCOL

***Nanocellulose Conduit Production
Standard Operating Procedure #02
Gowning Prior to Clean Room Entry***

Rev	Date	Description
1	7/13/2017	Draft Development Document-Nicklaus Carter
2	7/28/2017	Revision-Mary Bourque
3	8/1/2017	Revision-David Neivandt and Mary Bourque
4	8/14/17	Revision – Nicklaus Carter

Approved by:	Signature	Date
Originator	Nicklaus Carter	
Manager	David Neivandt	
Quality Assurance	David Neivandt and Caitlin Howell	

1.0 Purpose

- 1.1. To ensure that the cleanroom is entered by all personnel in a clean and consistent manner

2.0 Health and Safety Warnings

- 2.1. Use appropriate personal protective equipment PPE (laboratory coats, gloves, safety glasses when applicable) while working in the laboratory.
- 2.2. Work in a well-ventilated laboratory area.
- 2.3. PPE is worn only in laboratory areas and removed before entering non-laboratory areas.
- 2.4. Hazardous waste must be disposed in designated waste container.
- 2.5. Be familiar with the MSDS/SDS for all chemicals employed in the procedure.

3.0 Cautions

- 3.1. Improper execution of the gowning procedure may contaminate all products within the room.
- 3.2. Ensure filters have been on and running for at least 24 hours. If the filters have not been on for at least 24 hours, turn the filters on and wait until a full 24 hours has passed before entry to prevent contamination due to airborne particles.
- 3.3. If the clean room pressure is not twice that of the gowning room, do not enter the clean room, for this may indicate end of the filter life.
- 3.4. Do not process recovered, re-conciliated, or damaged materials or equipment. Visually inspect all materials and make note of any damaged or lost material in the corresponding QC checklist as well as reporting the loss to Dr. Neivandt.

4.0 Personnel Responsibilities and Qualifications

4.1. Supervisor:

- Ensure operators are trained on this procedure.
- Ensure operators conduct procedures as instructed.

4.2. The Operator:

- Must be trained on all equipment and procedures prior to operation.
- Complete this procedure as instructed.
- Report any deviations to this procedure to Dr. Neivandt.
- Follow Safety and Environmental Management (SEM) lock-out tag-out procedure for equipment that needs repair. Remove broken equipment from the clean room.

5.0 Equipment and Materials

- 5.1. Materials (as listed or equivalent)

- 5.1.1. Bouffant (Fisher Scientific, 17-624-136)
- 5.1.2. Clean room specific shoes (Vendor, Cat #)
- 5.1.3. Shoe covers (Fisher Scientific, 17-624-136)
- 5.1.4. Frocks (Fisher Scientific, 19-162-628)
- 5.1.5. Gloves (Fisher Scientific, 19-169-069)
- 5.1.6. Beard cover (Fisher Scientific, 17-100-925)
- 5.1.7. Hand sanitizer (Fisher Scientific, 12-544-105)

6.0 Quality Control and Quality Assurance

- 6.1. Visually inspect all materials to be brought into the clean room. Be sure all containers are closed and sealed prior to entry.

7.0 Procedures

7.1. General Attire

- 7.1.1. Ensure that all personnel are NOT wearing open toed shoes, shorts, skirts, or dresses
- 7.1.2. Ensure that all personnel are following a regular schedule of hygiene

7.2. Before entering the gowning room

- 7.2.1. Remove bulky outerwear such as coats, scarves, sweatshirts, etc.
- 7.2.2. Remove shoes, hats, and any jewelry
- 7.2.3. Ensure that hair is tied back and that there are no dangling items of clothing or jewelry
- 7.2.4. Turn the lights on to the clean room
- 7.2.5. Ensure filters have been on and running for at least 24 hours. If the filters have not been on for at least 24 hours, ensure the filters are on and wait until a full 24 hours has passed
- 7.2.6. Record the status of the HEPA filters and clean room and gowning pressures on the clean room sign-in sheet. If the clean room pressure is not twice that of the gowning room, do not enter the clean room
- 7.2.7. Close and seal all containers to be brought into the clean room
- 7.2.8. Enter the gowning room and close the door to the surrounding facility

7.3. Before entering the clean room

- 7.3.1. Ensure that the air filtration system is operating
- 7.3.2. Ensure that there is a supply of clean room garments in the gowning room

- 7.3.3. Apply hand sanitizer
- 7.3.4. Put on clean room shoes stored in the gowning area and place shoe covers over them, one pair per individual should be stored in the gowning room
- 7.3.5. Put on frock, bouffant, and beard cover as necessary
- 7.3.6. Put on gloves and be sure that the glove cuffs overlap the cuffs of the frock
- 7.3.7. Perform a self-review to ensure the individual entering is wearing a bouffant, clean room shoes, shoe covers, frock, gloves, and beard cover (if applicable)
- 7.3.8. Make sure that the gowning room door is closed before entering the clean room

CNF-SOP-03 PULP SUSPENSION

***Nanocellulose Conduit Production
Standard Operating Procedure #03
Creation of Cellulose Pulp Suspension***

Rev	Date	Description
1	1/19/2017	Draft Development Document-Nicklaus Carter
2	3/23/2017	Revision-Mark Paradis
3	7/28/2017	Revision-Mary Bourque
4	8/1/2017	Revision-David Neivandt and Mary Bourque
5	8/14/17	Revision – Nicklaus Carter

Approved by:	Signature	Date
Originator	Nicklaus Carter	
Manager	David Neivandt	
Quality Assurance	David Neivandt and Caitlin Howell	

1.0 Purpose

- 1.1. To prepare a cellulose pulp suspension: An unrefined dispersion of hardwood, softwood or other cellulosic fibers in water

2.0 Definitions

- 2.1. CNF: Cellulose nanofibrils
- 2.2. DIW: Deionized distilled water (17.45-17.46 Megaohms-cm)

3.0 Health and Safety Warnings

- 3.1. Take care when lifting or carrying large or heavy loads: Improper form or the inability to lift heavy loads can cause strains and sprains.
- 3.2. Use appropriate personal protective equipment PPE (laboratory coats, gloves, safety glasses when applicable) while working in the laboratory.
- 3.3. Work in a well-ventilated laboratory area.
- 3.4. PPE is worn only in laboratory areas and removed before entering non-laboratory areas.
- 3.5. Hazardous waste must be disposed in designated waste container.
- 3.6. Be familiar with the MSDS/SDS for all chemicals employed in the procedure.

4.0 Cautions

- 4.1. The whole sample of cellulose pulp used for the pulp suspension must be stored in a temperature and humidity-controlled environment for the calculated moisture content of the aliquot to be representative of the entire sample.
- 4.2. Do not process recovered, re-conciliated, or damaged materials or equipment. Visually inspect all materials, and make note of any damaged or lost material in the corresponding QC checklist as well as reporting the loss to Dr. Neivandt.
- 4.3. Ensure filters have been on and running for at least 24 hours. If the filters have not been on for at least 24 hours, turn the filters on and wait until a full 24 hours has passed before entry to prevent contamination due to airborne particles.
- 4.4. If the clean room pressure is not twice that of the gowning room, do not enter the clean room, for this may indicate end of the filter life.

5.0 Interferences

- 5.1. Improper storage of the pulp sample (malfunctioning temperature and moisture control, improperly sealed bags, storage of the pulp sample in an open environment, etc.) will yield inaccurate calculations of the weight percent solids of the pulp suspension.

6.0 Personnel Responsibilities and Qualifications

- 6.1. Supervisor:

- Ensure operators are trained on this procedure.
- Ensure operators conduct procedures as instructed.

6.2. The Operator:

- Must be trained on all equipment and procedures prior to operation.
- Complete this procedure as instructed.
- Report any deviations to this procedure to Dr. Neivandt.
- Follow Safety and Environmental Management (SEM) lock-out tag-out procedure for equipment that needs repair. Remove broken equipment from the room.
- Must be able to lift up to 50 pounds.

7.0 Equipment and Materials

7.1. Equipment

- 7.1.1. 5-Gallon plastic pail (ULINE, S-7914W)
- 7.1.2. Gamma seal lid for plastic pail (ULINE, S17945W)
- 7.1.3. Laboratory scale (Global Industrial, 240878)
- 7.1.4. Heating/drying oven (Fisher Scientific, 15-103-0508)

7.2. Materials (as listed or equivalent)

- 7.2.1. 280 g bleached cellulose pulp (Vendor, Cat #XXXXX)
- 7.2.2. 13.72 kg sterile deionized-distilled water (17.45-17.46 Megaohms-cm)

8.0 Quality Control and Quality Assurance

- 8.1. Before commencing the procedure in this document, complete the quality control checklist CNF-QCC-01 (Cellulose Pulp) for the pulp sample to be used. Store the sample from the pulp lot in the temperature and humidity-controlled environment of the TAPPI room for a minimum of 24 hours prior to analysis of moisture content. Calculate the moisture content using the ISO 287 standard procedure for an aliquot of the sample. The moisture content calculated will be representative of the entire sample removed from the lot and stored in the TAPPI room.

9.0 References

- 9.1. CNF-QCC-01 (Cellulose Pulp Quality Control Checklist)
- 9.2. ISO 287 (Paper and board – Determination of moisture content of a lot – Oven-drying method)
- 9.3. CNF-SOP-09 (General Maintenance and Cleaning Protocol)
- 9.4. CNF-SOP-10 (Labeling Procedure for Stocks, Samples, and Products)

10.0 Procedures

10.1. Preparation of the Cellulose Pulp Mixture

- 10.1.1. Visually inspect all containers prior to use: If an individual container does not pass visual inspection, clean according to CNF-SOP-09, General Maintenance and Cleaning Protocol.
- 10.1.2. Add 13.720 kg of DIW to the 5-gallon pail
- 10.1.3. Obtain 280 g pulp on a dry basis (or humid equivalent after obtaining moisture content of the sample) to create a suspension of 2% solids by weight
- 10.1.4. Submerge the sample of cellulose pulp in the pail
- 10.1.5. Cover the mixture and allow the pulp to saturate for a minimum of 12 hours

10.2. Dispersing pulp in suspension

- 10.2.1. Agitate the saturated pulp
- 10.2.2. Repeat stirring/shearing until the suspension is a continuous dispersion
- 10.2.3. Break down any large particulates into particles smaller than 1" diameter to prevent plugging lines in the SMC

10.3. Cleaning and Maintenance

- 10.3.1. Clean the station as outlined in CNF-SOP-09. Record all maintenance and cleaning performed in the maintenance and cleaning logs at the station.

***Nanocellulose Conduit Production
Standard Operating Procedure #04
Production of CNF Using a Supermasscolloider***

Rev	Date	Description
1	1/19/2017	Draft Development Document-Nicklaus Carter
2	3/23/2017	Revision-Mark Paradis
3	7/28/2017	Revision-Mary Bourque
4	8/1/2017	Revision-David Neivandt and Mary Bourque
5	8/14/17	Revision – Nicklaus Carter

Approved by:	Signature	Date
Originator	Nicklaus Carter	
Manager	David Neivandt	
Quality Assurance	David Neivandt and Caitlin Howell	

1.0 Purpose

- 1.1. To operate a super mass colloidier (SMC) to refine a cellulose pulp suspension into a cellulose nanofibril (CNF) slurry

2.0 Definitions

- 2.1. CNF: Cellulose nanofibrils
- 2.2. DIW: Deionized distilled water (17.45-17.46 Megaohms-cm)
- 2.3. SMC: Super mass colloidier

3.0 Health and Safety Warnings

- 3.1. Do not put fingers or any other part of the body below the overflow inside the hopper, inside of the discharge, or near the grinding stones of the SMC when in operation. Doing so could cause personal injury.
- 3.2. Take care when lifting or carrying either large or heavy loads: Improper form or the inability to lift heavy loads can cause strains and sprains.
- 3.3. Use appropriate personal protective equipment PPE (laboratory coats, gloves, safety glasses when applicable) while working in the laboratory.
- 3.4. Work in a well-ventilated laboratory area.
- 3.5. PPE is worn only in laboratory areas and removed before entering non-laboratory areas.
- 3.6. Hazardous waste must be disposed in designated waste container.
- 3.7. Be familiar with the MSDS/SDS for all chemicals employed in the procedure.
- 3.8. Must be able to lift up to 50 pounds overhead.

4.0 Cautions

- 4.1. The Moyno pump used during this operation must not be turned on when there is no fluid in the holding tank. Operating the pump dry will cause damage to its internal components.
- 4.2. Do not operate the system with both the recirculation and sample port valves closed.
- 4.3. Do not process recovered, re-conciliated, or damaged materials or equipment. Visually inspect all materials, and make note of any damaged or lost material in the corresponding QC checklist as well as report the loss to Dr. Neivandt.
- 4.4. Ensure filters have been on and running for at least 24 hours. If the filters have not been on for at least 24 hours, turn the filters on and wait until a full 24 hours has passed before entry to prevent contamination due to airborne particles.
- 4.5. If the clean room pressure is not twice that of the gowning room, do not enter the clean room, for this may indicate end of the filter life.

5.0 Interferences

5.1. If the pulp solution does not recirculate properly through the system, the refinement and production of CNF will not be uniform.

6.0 Personnel Responsibilities and Qualifications

6.1. Supervisor:

- Ensure operators are trained on this procedure.
- Ensure operators conduct procedures as instructed.

6.2. The Operator:

- Must be trained on all equipment and procedures prior to operation.
- Complete this procedure as instructed.
- Report any deviations to this procedure to Dr. Neivandt.
- Follow Safety and Environmental Management (SEM) lock-out tag-out procedure for equipment that needs repair. Remove broken equipment from the room.
- Must be able to lift up to 50 pounds overhead.

7.0 Equipment and Materials

7.1. Equipment

- 7.1.1. Super mass colloidier (Masuko, MKCA6-2)
- 7.1.2. Energy Measuring Universal Power Cell (Load Controls, UPC-KWH)
- 7.1.3. Digital Energy Meter (Load Controls, KWH-3)
- 7.1.4. Digital Load Meter (Load Controls, DM-100)
- 7.1.5. Stainless steel piping system, various fittings (McMaster Carr. See Appendix 8.1)
- 7.1.6. Moyno sanitary positive displacement pump (Atlantic Pump and Engineering, MOFB1D-SSQ-SAA)
- 7.1.7. 4 oz. plastic portion cups with covers, (Uline, S-21201 and S21202)
- 7.1.8. 5-gallon pail (ULINE, S-7914W)

7.2. Materials (as listed or equivalent)

- 7.2.1. Cellulose pulp suspension (CNF-SOP-03, Creation of Cellulose Pulp Suspension)

8.0 Quality Control and Quality Assurance

8.1. Create a calibration curve of cumulative energy and total fines produced prior to running the SMC for a product of end use. To create the calibration curve, follow the procedure outlined in this SOP, collecting 50 mL samples of refined suspension from the SMC hopper with a 100-mL container-with-cover for analysis of fines and fibers (CNF-SOP-06, Analysis of

Fines and Fibers in CNF Slurry) every 15 minutes, noting the cumulative energy at each time of sampling.

8.2. After a calibration curve has been created, the SMC can be run to produce CNF. Samples should be collected every 15 minutes and analyzed for fines and fibers to validate the calibration curve and identify possible interferences in the process. If parts are replaced in the SMC, new materials are used, or other environmental changes occur, the calibration curve should be reproduced.

8.3. Record the following data in the accompanying quality control checklist, CNF-QCC-06, Processed Fiber:

8.3.1. Pulp sample used

8.3.2. Date produced

8.3.3. Cumulative Energy

8.3.4. Time elapsed during refinement

8.3.5. Final fines %

8.3.6. Weight percent of solids

8.3.7. Volume of slurry collected

8.3.8. Additional notes

8.3.9. Initial and Date

9.0 References

9.1. CNF-QCC-01 (Cellulose Pulp Quality Control Checklist)

9.2. CNF-SOP-03 (Creation of Cellulose Pulp Suspension)

9.3. CNF-SOP-05 (Protocol for Cleaning of the Colloider and Piping System)

9.4. CNF-QCC-06 (Processed Fiber Quality Control Checklist)

9.5. CNF-SOP-09 (General Maintenance and Cleaning Protocol)

9.6. CNF-SOP-10 (Labeling Procedure for Stocks, Samples, and Products)

10.0 Procedures

10.1. Calibration of the SMC grinding stones

10.1.1. Prior to operation of the SMC, the gap between the grinding stones needs to be calibrated and the SMC must be visually inspected for cleanliness. If equipment is not clean, follow the procedure outlined in CNF-SOP-05, Colloider Cleaning Procedure, and CNF-SOP-09, General Cleaning Procedure

- 10.1.2. Turn the stone-gap micrometer (see Appendix 11.2) counterclockwise a minimum of 5 full turns to open the gap, ensuring no contact between the stones occurs during start up
- 10.1.3. Turn on the SMC and set stone rotation to 2,000 RPM
- 10.1.4. Carefully turn the stone-gap micrometer clockwise until the stones just slightly touch while spinning. Contact is achieved when a slight clicking of the stones is heard
- 10.1.5. Mark position as the calibrated zero-point: Unlock the stone-gap micrometer handle when the stones make contact and adjust such that the micrometer shows zero when re-locked

10.2. Filling the SMC

- 10.2.1. Open the stone-gap to positive 5, relative to the zero point, while the SMC is running at 2000 RPM
- 10.2.2. Slowly pour the 14 L of pulp solution into the SMC such that the hopper is not overflowed into the overflow tube, ensuring all pulp uniformly passes through the stones prior to circulation through the system
- 10.2.3. **The Moyno pump used during this operation must not be turned on when there is no fluid in the pump reservoir. Operating the pump dry will cause damage to its internal components:** When the pump reservoir is full, turn on the pump. Once recirculation of the slurry is observed (i.e. slurry is pumping through all lines without becoming plugged), adjust the stone-gap to negative 10 for continued refining
- 10.2.4. Begin a timer to record the elapsed time of refinement

10.3. Sampling from the SMC

- 10.3.1. Every 15 minutes a sample of slurry will be removed to measure fines for quality control. Before removing the sample, open the stone-gap to plus 15 while the SMC is still running to completely drain the hopper into the pump reservoir, mixing the slurry contained in the SMC
- 10.3.2. Return the stone-gap to the zero point, refilling the hopper. Visually inspect to ensure a clean sampling container to remove a 50-mL sample from the hopper and record the cumulative energy at each time of sampling. Return the stone-gap to negative 10. Do not put fingers or any other part of the body near the grinding stones when the SMC is operating. Doing so could cause personal injury
- 10.3.3. Seal the sample for later measurement of fines content using a Techpap MorFi Fiber Analyzer, located in the Process Development Center (CNF-SOP-06)

10.4. Collection of Slurry

- 10.4.1. Run the SMC until the energy reading corresponds to a fines percentage of 90%, as determined by the calibration curve produced in Section 8.1

10.4.2. Place a clean (visually inspected) 5-gallon bucket underneath the sample port. Open the sample port valve and then close the recirculation line valve to begin pumping slurry into the bucket

10.4.3. **The Moyno pump used during this operation must not be turned on when there is no fluid in the holding tank. Operating the pump dry will cause damage to its internal components:** Take caution to turn off the pump before the reservoir empties and/or before the collection container becomes too full

10.4.4. Stop the timer and record the elapsed time of refinement and the cumulative energy

10.5. Determination of Weight Percent of Solids in CNF Slurry

10.5.1. Weigh the mass of a new, empty, 100 mL container

10.5.2. Fill the container with 100mL of newly refined slurry

10.5.3. Weigh the mass of the full container (full container mass minus the mass of the empty container is equivalent to mass of CNF collected)

10.5.4. Place the container in the oven just as in the evaluation of moisture content (CNF-SOP-01)

10.5.5. As the mass of the container of dry CNF plateaus, calculate the weight percent of solids as seen below (subtracting container mass renders the mass of dried CNF):

$$\frac{\text{Mass of Dry CNF}}{\text{Mass of CNF Collected}} \times 100 \sim 2\% \text{ (Desired Wt \% of Solids)}$$

10.6. Cleaning and Maintenance

10.6.1. Clean the station as outlined in CNF-SOP-09 and CNF-SOP-05. Record all maintenance and cleaning performed in the maintenance and cleaning logs at the station

10.7. Assembly/disassembly of the SMC (if necessary)

10.7.1. To disassemble the system, remove the sections, starting at the highest points in manageable portions: Start with the recirculation section, then the overflow section, and finally the pump reservoir section

10.7.2. Break down each section into the individual fittings by removal of all quick clamps and gaskets

10.7.3. Assemble the system in reversed order of disassembly

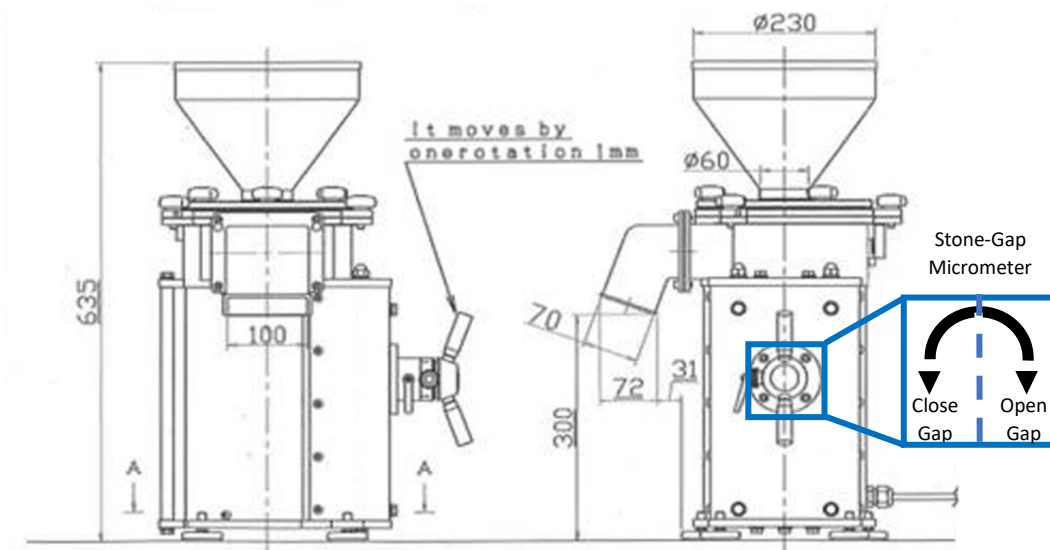
11.0 Appendices

11.1. McMaster Carr Fittings

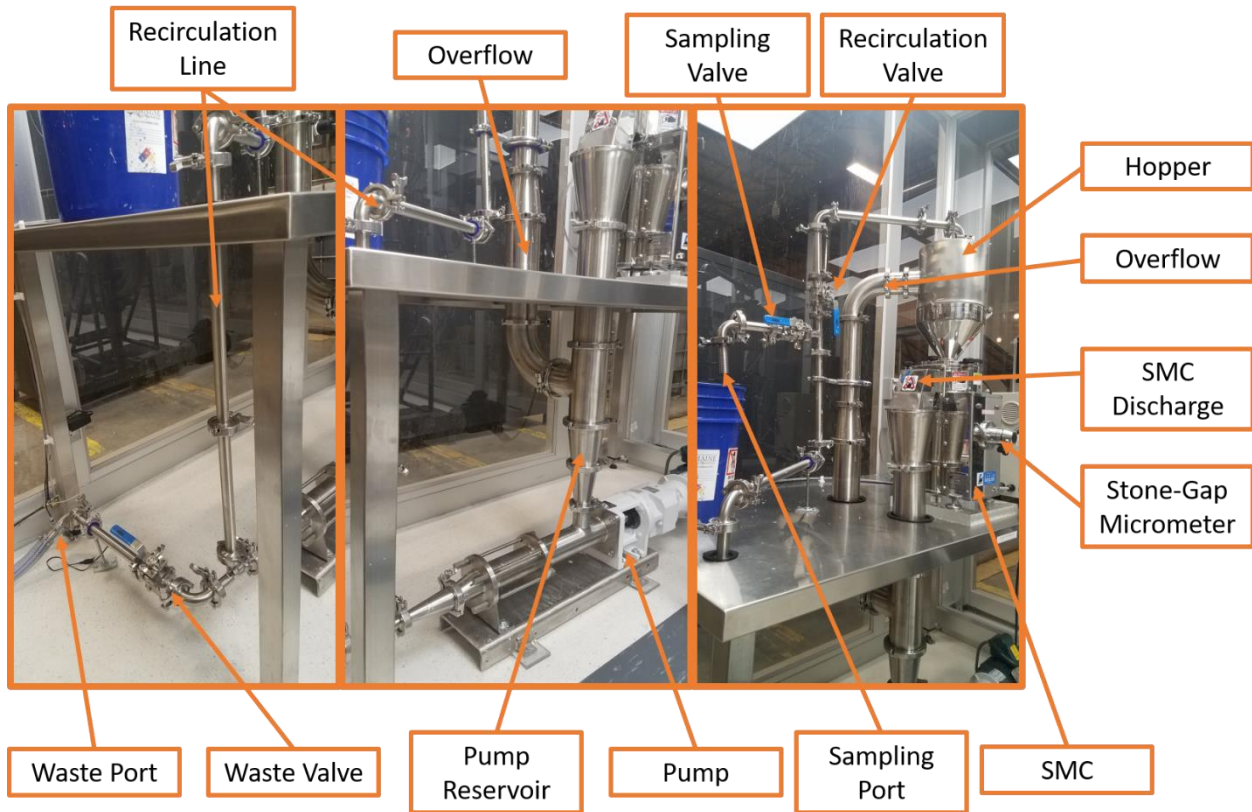
Quantity	Description	Item Code
4	High-Polish Quick-Clamp Sanitary Tube Fitting 316L Stainless Steel Straight Connector for 1" Tube OD, 4" Long	50485K73
1	High-Polish Quick-Clamp Sanitary Tube Fitting 316L Stainless Steel Straight Connector for 1" Tube OD, 6" Long	50485K73
4	High-Polish Quick-Clamp Sanitary Tube Fitting 316L Stainless Steel Straight Connector for 1" Tube OD, 12" Long	50485K73
2	High-Polish Quick-Clamp Sanitary Tube Fitting 316L Stainless Steel Straight Connector for 1" Tube OD, 18" Long	50485K73
7	High-Polish Quick-Clamp Sanitary Tube Fitting 316L Stainless Steel 90 Degree Elbow Connector for 1" Tube OD	50485K111
2	High-Polish Quick-Clamp Sanitary Tube Fitting 316L Stainless Steel Inline Tee Connector for 1" Tube OD	50485K141
2	High-Polish Quick-Clamp Sanitary Tube Fitting 316L Stainless Steel Adapter for 1" Tube OD x 1" Barbed Hose ID	50485K773
3	On/Off Valve for Food and Beverage Sanitary Quick-Clamp for 1" Tube OD	44755K113
1	High-Polish Quick-Clamp Sanitary Tube Fitting 316L Stainless Steel Adapter for 3" Tube x Butt-Weld, 1-13/16" Long	50485K185
1	High-Polish Quick-Clamp Sanitary Tube Fitting 316L Stainless Steel Straight Connector for 3" Tube OD, 4" Long	50485K39
1	High-Polish Quick-Clamp Sanitary Tube Fitting 316L Stainless Steel Straight Connector for 3" Tube OD, 12" Long	50485K39
1	High-Polish Quick-Clamp Sanitary Tube Fitting 316L Stainless Steel 90 Degree Elbow Connector for 3" Tube OD	50485K115
2	High-Polish Quick-Clamp Sanitary Tube Fitting 316L Stainless Steel Straight Connector for 4" Tube OD, 12" Long	50485K41
1	High-Polish Quick-Clamp Sanitary Tube Fitting, 316L Stainless Steel 90 Degree Elbow Connector for 4" Tube OD	50485K116
1	High-Polish Quick-Clamp Sanitary Tube Fitting, 316L Stainless Steel Inline Tee Connector for 4" Tube OD	50485K146

1	High-Polish Quick-Clamp Sanitary Tube Fitting 316L Stainless Steel Straight Reducer for 2" x 1" Tube OD	50485K232
1	High-Polish Quick-Clamp Sanitary Tube Fitting 316L Stainless Steel Straight Reducer for 3" x 2" Tube OD	50485K237
2	High-Polish Quick-Clamp Sanitary Tube Fitting 316L Stainless Steel Straight Reducer for 4" x 3" Tube OD	50485K239
1	High-Polish Quick-Clamp Sanitary Tube Fitting 316L Stainless Steel Straight Reducer for 6" x 4" Tube OD	50485K242
25	High-Polish Quick-Clamp Sanitary Tube Fitting 304 Stainless Steel Clamp with Wing Nut for 1" and 1-1/2" Tube OD	4322K152
2	High-Polish Quick-Clamp Sanitary Tube Fitting 304 Stainless Steel Clamp with Wing Nut for 2" Tube OD	4322K153
5	High-Polish Quick-Clamp Sanitary Tube Fitting 304 Stainless Steel Clamp with Wing Nut for 3" Tube OD	4322K155
6	High-Polish Quick-Clamp Sanitary Tube Fitting 304 Stainless Steel Clamp with Wing Nut for 4" Tube OD	4322K156
25	High-Temperature Silicone Gasket for Quick-Clamp Fittings, for 1" Tube OD	4520K43
2	High-Temperature Silicone Gasket for Quick-Clamp Fittings, for 2" Tube OD	4520K45
5	High-Temperature Silicone Gasket for Quick-Clamp Fittings, for 3" Tube OD	4520K47
6	High-Temperature Silicone Gasket for Quick-Clamp Fittings, for 4" Tube OD	4520K48
3	Washdown Threaded-Rod-Mount Clamping Hanger Vibration-Damping Silicone Rubber Cushion, 1" ID	8831T35
1	Washdown Threaded-Rod-Mount Clamping Hanger Vibration-Damping Silicone Rubber Cushion, 3" ID	8831T41

11.2. Colloider Diagram and Stone-Gap Micrometer Operation



11.3. Colloider Piping System



CNF-SOP-05 REFINER SYSTEM CLEANING

Nanocellulose Conduit Production
Standard Operating Procedure #05
Protocol for Cleaning of the Colloider and Piping System

Rev	Date	Description
1	1/19/2017	Draft Development Document-Nicklaus Carter
2	7/28/2017	Revision-Mary Bourque
3	8/1/2017	Revision-David Neivandt and Mary Bourque
4	8/14/17	Revision – Nicklaus Carter

Approved by:	Signature	Date
Originator	Nicklaus Carter	
Manager	David Neivandt	
Quality Assurance	David Neivandt and Caitlin Howell	

1. Purpose

1.1. To remove debris and sanitize the colloid system

2. Definitions

2.1. CNF: Cellulose nanofibrils

2.2. DIW: Deionized distilled water (17.45-17.46 Megaohms-cm)

2.3. Fines: Cellulose nanofibrils that are less than 200 μm in length

2.4. SMC: Super mass colloid

3. Health and Safety Warnings

3.1. Acidic cleaning solution can cause irritation to eyes and skin: Wear gloves.

3.2. Take care when lifting or carrying either large or heavy loads: Improper form or the inability to lift heavy loads can cause strains and sprains.

3.3. Use appropriate personal protective equipment PPE (laboratory coats, gloves, safety glasses when applicable) while working in the laboratory.

3.4. Work in a well-ventilated laboratory area.

3.5. PPE is worn only in laboratory areas and removed before entering non-laboratory areas.

3.6. Hazardous waste must be disposed in designated waste container.

3.7. Be familiar with the MSDS/SDS for all chemicals being employed in the procedure.

4. Cautions

4.1. Follow instructions for dilution of alkaline and acidic cleaners: Failing to do so may corrode or damage to equipment.

4.2. Do not process recovered, re-conciliated, or damaged materials or equipment. Visually inspect all materials and make note of any damaged or lost material in the corresponding QC checklist as well as reporting the loss to Dr. Neivandt.

4.3. Ensure filters have been on and running for at least 24 hours. If the filters have not been on for at least 24 hours, turn the filters on and wait until a full 24 hours has passed before entry to prevent contamination due to airborne particles.

4.4. If the clean room pressure is not twice that of the gowning room, do not enter the clean room, for this may indicate end of the filter life.

5. Interferences

5.1. Creating a cleaning solution that is too dilute may not clean and sanitize the equipment effectively.

6. Personnel Responsibilities and Qualifications

6.1. The Supervisor:

- Ensure operators are trained on this procedure.
- Ensure operators conduct procedures as instructed

6.2. The Operator:

- Must be trained on all equipment and procedures prior to operation.
- Complete this procedure as instructed.
- Report any deviations to this procedure to Dr. Neivandt.
- Follow Safety and Environmental Management (SEM) lock-out tag-out procedure for equipment that needs repair. Remove broken equipment from the clean room.
- Must be able to lift up to 50 pounds.

7. Equipment and Materials

7.1. Equipment

7.1.1. 2 - 116 Qt. storage tote (Home Depot, SKU #1000030696)

7.1.2. PBW-Alkali Cleaner (Northern Brewer Homebrew Supply, SKU#U005)

7.1.3. Star San (Northern Brewer Homebrew Supply, SKU#U001)

7.1.4. 1 - 32 oz. Spray Bottle (Home Depot, SKU#255852)

7.2. Materials (as listed or equivalent)

7.2.1. Deionized Water (17.45-17.46 Megaohms-cm)

8. Quality Control and Quality Assurance

8.1. Cleaning of the SMC should occur after every batch production of slurry. The system has been properly sanitized when it has demonstrated proper recirculation and there is no visible debris or particulates on the equipment.

9. References

9.1. CNF-SOP-04 (Production of CNF Using a Super Mass Colloider)

10. Procedures

10.1. Preparation of alkaline scrub solution – Tote mix

10.1.1. Fill the tote marked “alkaline” with 10 gallons of water

10.1.2. Weigh 10 ounces of PBW powder and mix into the water

10.2. Preparation of acidic sanitary solution – Tote mix

10.2.1. Fill the tote marked “acidic” with 10 gallons of water

10.2.2. Measure 2 ounces of Star San (Bettix bottle) and mix into the water

10.3. Cleaning the colloid system in place

10.3.1. Recirculate the PBW “alkaline” solution through the system in the same manner as refining a cellulose slurry, but with the stone gap opened by 3 turns

10.3.2. After 30 minutes of PBW recirculation, drain the PBW solution and circulate DIW through the system to rinse remaining PBW

10.3.3. Drain the DIW. Gently recirculate the Star San “acidic” solution (Turn off the colloid and ensure that the gap is open by 3 full turns

10.3.4. Circulate the solution for 5 minutes, drain the Star San solution, and rinse a final time with DIW

10.3.5. Allow the system to air dry for 12 hours

10.3.6. Record cleaning in the cleaning log at the wet table station

10.4. Cleaning stainless steel surfaces

10.4.1. Use the PBW solution to clean debris from surfaces.

10.4.2. Rinse surfaces with DIW and let dry

10.4.3. Apply the Star San via the 32 oz spray bottle solution

10.4.4. Let the Star San solution contact the surfaces for 2 minutes, then wipe dry

10.4.5. Apply a DIW rinse

10.4.6. Fill out the station’s cleaning log

CNF-SOP-06 SLURRY FIBER ANALYSIS

*Nanocellulose Conduit Production
Standard Operating Procedure #06
Analysis of Fines and Fibers in Slurry*

Rev	Date	Description
1	1/19/2017	Draft Development Document-Nicklaus Carter
2	3/23/2017	Revision-Mark Paradis
3	7/28/2017	Revision-Mary Bourque
4	8/14/17	Revision – Nicklaus Carter

Approved by:	Signature	Date
Originator	Nicklaus Carter	
Manager	David Neivandt	
Quality Assurance	David Neivandt and Caitlin Howell	

1.0 Purpose

- 1.1. To determine the level of refinement of cellulose nanofibrils (CNF) by analyzing the percentage of fines present in a sample of slurry

2.0 Definitions

- 2.1. CNF: Cellulose Nanofibrils
- 2.2. DIW: Deionized distilled water (17.45-17.46 Megaohms-cm)
- 2.3. Fines: Cellulose Nanofibrils that are less than 200 μm in length
- 2.4. SMC: Super mass colloidier

3.0 Health and Safety Warnings

- 3.1. Use appropriate personal protective equipment PPE (laboratory coats, gloves, safety glasses when applicable) while working in the laboratory.
- 3.2. Work in a well-ventilated laboratory area.
- 3.3. PPE is worn only in laboratory areas and removed before entering non-laboratory areas.
- 3.4. Hazardous waste must be disposed of in the designated waste container.
- 3.5. Be familiar with the MSDS/SDS for all chemicals being used in this procedure.

4.0 Cautions

- 4.1. Do not process recovered, re-conciliated, or damaged materials or equipment. Visually inspect all materials and make note of any damaged or lost material in the corresponding QC checklist as well as reporting the loss to Dr. Neivandt.
- 4.2. Visually inspect all equipment prior to operation: If equipment does not pass visual inspection, clean using protocol outlined in CNF-SOP-09, General Maintenance and Cleaning Protocol.
- 4.3. Ensure filters have been on and running for at least 24 hours. If the filters have not been on for at least 24 hours, turn the filters on and wait until a full 24 hours has passed before entry to prevent contamination due to airborne particles.
- 4.4. If the clean room pressure is not twice that of the gowning room, do not enter the clean room, for this may indicate end of the filter life.

5.0 Interferences

- 5.1. Ensure the DIW in the wash beaker is replaced after every run. The wash beaker has a designated position (position 6) on the MorFi Fiber Analyzer carousel and should not be moved.
- 5.2. Improper calculations during the two dilutions of slurry will yield inaccurate concentrations and percent total fines.

6.0 Personnel Responsibilities and Qualifications

6.1. Supervisor:

- Ensure operators are trained on this procedure.
- Ensure operators conduct procedures as instructed.

6.2. The Operator:

- Must be trained on all equipment and procedures prior to operation.
- Complete this procedure as instructed.
- Report any deviations to this procedure to Dr. Neivandt.
- Follow Safety and Environmental Management (SEM) lock-out tag-out procedure for equipment that needs repair. Remove broken equipment from the room.

7.0 Equipment and Materials

7.1. Equipment

- 7.1.1. 1 L Griffin Beakers, (Fisher Scientific, 14-379-019)
- 7.1.2. 100 mL sample containers with covers, (Uline, S-9934)
- 7.1.3. 1 L Graduated Cylinder, (Fisher Scientific, 14-379-140)
- 7.1.4. 100 mL Graduated Cylinder, (Fisher Scientific, 14-379-142)
- 7.1.5. Laboratory scale (Fisher Scientific, 01-920-120)
- 7.1.6. Laboratory spatula (Fisher Scientific, 14-357Q)
- 7.1.7. MorFi Fiber Analyzer (Techpap. MorFi Compact)

7.2. Materials (as listed or equivalent)

- 7.2.1. 100 mL samples of fully processed or partially processed CNF

8.0 Quality Control and Quality Assurance

8.1. Record the following data in the accompanying quality control checklist, Processed Fiber (CNF-QCC-06):

- 8.1.1. Pulp sample used
- 8.1.2. Date CNF was produced
- 8.1.3. Cumulative Energy
- 8.1.4. Time elapsed during refinement
- 8.1.5. Final fines %

- 8.1.6. Weight percent of solids
- 8.1.7. Volume of slurry collected
- 8.1.8. Additional notes
- 8.1.9. Initial and Date

9.0 References

- 9.1. CNF-SOP-04 (Production of CNF Using a Super Mass Colloider)
- 9.2. CNF-QCC-06 (Processed Fiber)
- 9.3. CNF-SOP-10 (Labeling Procedure for Stocks, Samples, and Products)

10.0 Procedures

10.1. Preparation of Sample

- 10.1.1. Measurement of the length and fines of the fibers requires a 50 mg/L solids content of the slurry
- 10.1.2. Calculate the mass of slurry necessary to generate the 50 mg/L solids content, from the 100 mL sample collected from SMC
 - 10.1.2.1. 50 mg/L is divided by sample concentration (% solids content, estimated from input of pulp mass/ water mass)
 - 10.1.2.2. This value is then multiplied by ten to account for a dilution step
 - 10.1.2.3. The final value, in grams, describes the mass of slurry from the sample that must be used in the first 1L dilution.

$$50 \frac{mg}{L} \times \frac{1}{\% \text{ solids}} \times \frac{1 g}{1000 mg} \times \frac{1000 mL}{100 mL} \times 1L$$

= Mass (g) required from slurry sample

10.1.3. Dilute Sample to 50 mg/L

- 10.1.3.1. Measure out calculated mass of sample from 100 mL slurry sample container into a small beaker using a spatula
- 10.1.3.2. Add sample to 1 L graduated cylinder, then fill to 1 L with DIW
- 10.1.3.3. Mix solution thoroughly between two 1L beakers and measure out 100 mL into the 100 mL graduated cylinder; discard remaining material and rinse out the empty containers
- 10.1.3.4. Add the 100 mL dilution to the 1 L graduated cylinder and fill to 1 L with DIW once more
- 10.1.3.5. Mix thoroughly and pour contents into a 1 L beaker. The 1L dilution will be used for fiber analysis

10.1.3.6. Discard the remaining solutions by diluting with water: the slurry is safe to discard down the floor drain

10.1.4. Loading samples on MorFi Fiber Analyzer carousel

10.1.4.1. The carousel has 6 positions correlating to 5 samples and 1 wash of DIW

10.1.4.2. The DIW in the wash beaker should be replaced each run

10.1.4.3. Up to 5 samples can be run at a time, and as few as one

10.1.4.4. The wash beaker has a designated position (position 6) and should not be moved

10.1.4.5. The samples can be placed in any other carousel position

10.2. Operation of the MorFi Fiber Analyzer

10.2.1. Turn on the computer and open the “MorFi” software

10.2.2. Click the “Carousel” button in the bottom bar of the screen to open sample menu

10.2.3. In the sample menu the following information must be provided:

10.2.3.1. Family: Select “HR - Fibers and Fines”, preset measuring protocol selection

10.2.3.2. Consistency: Enter “50 mg/L”, the concentration of the sample

10.2.3.3. ID: Enter “Operator’s Initials and day/month/year”, the filename for the saved file (i.e. NRC-8-14-17)

10.2.3.4. Coarseness: Enter “Material-timepoint of sample refinement”, additional file differentiation (i.e. cotton-90mins)

10.2.3.5. Number: Enter “#”, correlates to the position of sample on the carousel

10.2.4. When all information is entered into the window, the measurement can be initiated in one of two ways:

10.2.4.1. “Start with List Open”: Select this option if there are more samples to measure. It will start measuring the first in line and keep the menu open to add additional samples to the queue.

10.2.4.2. “Start and Close List”: Select this option if the info just entered is the only sample or the last sample being analyzed.

10.2.5. The device will measure each sample, with a rinse in between, and save the data according to the user provided ID and coarseness

10.2.6. Reports can be printed at the end of the measurement during a time delay between samples or can be accessed from the saved files. All reports are to be printed and stored in the clean room

10.2.7. After all measurements are complete discard solutions and clean all containers for future samples

CNF-SOP-07 CNF SHEET PRODUCTION

***Nanocellulose Conduit Production
Standard Operating Procedure #07
Cellulose Nanofiber Sheet Fabrication***

Rev	Date	Description
1	1/19/2017	Draft Development Document-Nicklaus Carter
2	7/28/2017	Revision-Mary Bourque
3	8/14/17	Revision – Nicklaus Carter

Approved by:	Signature	Date
Originator	Nicklaus Carter	
Manager	David Neivandt	
Quality Assurance	David Neivandt and Caitlin Howell	

1.0 Purpose

- 1.1. To spread CNF slurry to form a CNF sheet that is 50 μm thick

2.0 Definitions

- 2.1. CNF: Cellulose Nanofibrils
- 2.2. DIW: Deionized distilled water (17.45-17.46 Megaohms-cm)

3.0 Health and Safety Warnings

- 3.1. Blades are sharp and can cause cuts: Use caution when using razor blades.
- 3.2. Use appropriate personal protective equipment PPE (laboratory coats, gloves, safety glasses when applicable) while working in the laboratory.
- 3.3. Work in a well-ventilated laboratory area.
- 3.4. PPE is worn only in laboratory areas and removed before entering non-laboratory areas.
- 3.5. Hazardous waste must be disposed of in the designated waste container.
- 3.6. Be familiar with the MSDS/SDS for all chemicals being used in this procedure.

4.0 Cautions

- 4.1. Visually inspect all equipment prior to use: If equipment does not pass visual inspection, clean using protocol outlined in CNF-SOP-09, General Maintenance and Cleaning Protocol.
- 4.2. Do not process recovered, re-conciliated, or damaged materials or equipment. Visually inspect all materials, and make note of any damaged or lost material in the corresponding QC checklist as well as reporting the loss to Dr. Neivandt.
- 4.3. Ensure filters have been on and running for at least 24 hours. If the filters have not been on for at least 24 hours, turn the filters on and wait until a full 24 hours has passed before entry to prevent contamination due to airborne particles.
- 4.4. If the clean room pressure is not twice that of the gowning room, do not enter the clean room, for this may indicate end of the filter life.

5.0 Interferences

- 5.1. Overloading the film applicator may create an uneven spread of slurry.

6.0 Personnel Responsibilities and Qualifications

- 6.1. Supervisor:
 - Ensure operators are trained on this procedure.
 - Ensure operators conduct procedures as instructed.
- 6.2. The Operator:

- Must be trained on all equipment and procedures prior to operation.
- Complete this procedure as instructed.
- Report any deviations to this procedure to Dr. Neivandt.
- Follow Safety and Environmental Management (SEM) lock-out tag-out procedure for equipment that needs repair. Remove broken equipment from the room.

7.0 Equipment and Materials

7.1. Equipment

7.1.1. Casting Knife Film Applicator, 8" wide, (Elcometer, K0003580M007)

7.1.2. Stainless Steel Plate, 12" x 18" x $\frac{3}{8}$ " thick, (McMaster Carr, 8983K252)

7.1.3. Single Edge Razor Blades, (Harbor Freight, 39748)

7.1.4. Benchtop Digital Micrometer, (Testing Machines Inc., 49-85)

7.1.5. 150 mL Griffin Beakers, (Fisher Scientific, 14-379-022)

7.2. Materials (as listed or equivalent)

7.2.1. CNF slurry (CNF-SOP-04, Production of CNF Using a Super Mass Colloider)

8.0 Quality Control and Quality Assurance

8.1. Record the following data in the accompanying quality control checklist, Processed Sheet (CNF-QCC-07):

8.1.1. Slurry used

8.1.2. Date/Time spread

8.1.3. Date/Time lifted

8.1.4. Volume of slurry used

8.1.5. Casting thickness

8.1.6. Dried thickness

8.1.7. End use

8.1.8. Additional notes

8.1.9. Initial and Date

8.2. The final sheet thickness must be within $\pm 5\%$ of the accepted dried sheet thickness

9.0 References

9.1. CNF-SOP-04 (Production of CNF Using a Super Mass Colloider)

- 9.2. CNF-QCC-07 (Processed Sheet Quality Control Checklist)
- 9.3. CNF-SOP-09 (General Maintenance and Cleaning Protocol)
- 9.4. CNF-SOP-10 (Labeling Procedure for Stocks, Samples, and Products)

10.0 Procedures

10.1. Spreading the CNF slurry

- 10.1.1. Measure 100 mL of the CNF slurry in a griffin beaker
- 10.1.2. Pour the slurry onto a stainless steel plate in a line such that the length doesn't exceed the width of the film applicator (8")
- 10.1.3. Set the height of the applicator blade to 0.075 inches (1.9 mm)
- 10.1.4. Drag the applicator down the plate to start spreading the slurry into a sheet with a vertical chopping action
- 10.1.5. Use a smooth second pass of the film applicator to even out the ridges left from chopping
- 10.1.6. Trim and discard irregular edges of the sheet with a new single edged razor blade (razor blades are discarded daily in the sharps container)
- 10.1.7. Move the stainless steel plate to a secluded area on the dry table and leave to dry for 24 hours (be sure it is away from items that may fall into the wet sheet)

10.2. Measuring CNF sheet thickness

- 10.2.1. Lift the dried sheet from the plate using a single edged razor blade: Slide the blade approximately $\frac{1}{4}$ " under the sheet around the entire perimeter
- 10.2.2. Remove the sheet from the plate and transfer it into a resealable bag for transportation.
- 10.2.3. Transport the sheet to the TAPPI room, in the PDC, to adjust to the humidity for 24 hours and measure the thickness using the benchtop digital micrometer
- 10.2.4. Measure the sheet thickness at several points across the width of the sheet
- 10.2.5. Repeat this process as you move perpendicular to the measurement direction, measuring 3 rows of 4 data points each (12 points total)
- 10.2.6. Calculate the average thickness and standard deviation of the measurements
- 10.2.7. Place the sheet in a labeled bag as described in CNF-SOP-10 (Labeling Procedure for Stocks, Samples, and Products)

10.3. Cleaning and Maintenance

- 10.3.1. Clean the station as outlined in CNF-SOP-09. Record all maintenance and cleaning performed in the maintenance and cleaning logs at the station.

CNF-SOP-08 CNF CONDUIT PRODUCTION

Nanocellulose Conduit Production
Standard Operating Procedure #08
Cellulose Nanofiber Conduit Fabrication

Rev	Date	Description
1	1/19/2017	Draft Development Document-Nicklaus Carter
2	7/28/2017	Revision-Mary Bourque
3	8/14/17	Revision – Nicklaus Carter

Approved by:	Signature	Date
Originator	Nicklaus Carter	
Manager	David Neivandt	
Quality Assurance	David Neivandt and Caitlin Howell	

1.0 Purpose

- 1.1. To fabricate a neural conduit using a CNF sheet

2.0 Definitions

- 2.1. CNF: Cellulose Nanofibrils
- 2.2. DIW: Deionized distilled water (17.45-17.46 Megaohms-cm)

3.0 Health and Safety Warnings

- 3.1. Blades are sharp and can cause cuts: Use caution when using razor blades.
- 3.2. Use appropriate personal protective equipment PPE (laboratory coats, gloves, safety glasses when applicable) while working in the laboratory.
- 3.3. Work in a well-ventilated laboratory area.
- 3.4. PPE is worn only in laboratory areas and removed before entering non-laboratory areas.
- 3.5. Hazardous waste must be disposed of in the designated waste container.
- 3.6. Be familiar with the MSDS/SDS for all chemicals being used in this procedure.

4.0 Cautions

- 4.1. Take care not to damage the CNF sheets employed for the fabrication of conduits.
- 4.2. Do not process recovered, re-conciliated, or damaged materials or equipment. Visually inspect all materials, and make note of any damaged or lost material in the corresponding QC checklist as well as reporting the loss to Dr. Neivandt.
- 4.3. Ensure filters have been on and running for at least 24 hours. If the filters have not been on for at least 24 hours, turn the filters on and wait until a full 24 hours has passed before entry to prevent contamination due to airborne particles.
- 4.4. If the clean room pressure is not twice that of the gowning room, do not enter the clean room, for this may indicate end of the filter life.

5.0 Interferences

- 5.1. Visually inspect conduits after dipping in slurry: Ensure there is no buildup of slurry on the top and bottom ends of the cylinder.

6.0 Personnel Responsibilities and Qualifications

- 6.1. Supervisor:
 - Ensure operators are trained on this procedure.
 - Ensure operators conduct procedures as instructed.
- 6.2. The Operator:

- Must be trained on all equipment and procedures prior to operation.
- Complete this procedure as instructed.
- Report any deviations to this procedure to Dr. Neivandt.
- Follow Safety and Environmental Management (SEM) lock-out tag-out procedure for equipment that needs repair. Remove broken equipment from the room.

7.0 Equipment and Materials

7.1. Equipment

- 7.1.1. 1 mL disposable syringe (Fisher Scientific, 14-823-30)
- 7.1.2. 20-gauge blunt tip needle, 304SS, 2" length (Fisher Scientific, 14-815-608)
- 7.1.3. Plastic mandrel, OD 1.6 mm (Vendor, Cat #XXXXXX)
- 7.1.4. Utility knife (Fisher Scientific, 18-999-28)
- 7.1.5. Tubing Cutter (Fisher Scientific, 11-187-15)
- 7.1.6. Microspatula (Fisher Scientific, 14-357Q)
- 7.1.7. Acrylic Template (McMaster-Carr, 8589K41)
- 7.1.8. Rotating drying rack (Fisher Scientific, 05-450-127)

7.2. Materials (as listed or equivalent)

- 7.2.1. CNF sheet (CNF-SOP-07)
- 7.2.2. CNF slurry (CNF-SOP-04)

8.0 Quality Control and Quality Assurance

- 8.1. Visually inspect all equipment prior to use: If equipment does not pass visual inspection, clean using protocol outlined in CNF-SOP-09, General Maintenance and Cleaning Protocol.
- 8.2. Visually inspect slurry prior to use: If slurry shows signs of mold or microbial contamination, DO NOT USE. Label with red tape and remove from operation area for proper disposal. Slurry may be used for up to 6 months after refinement.
- 8.3. Record the following data in the accompanying quality control checklist CNF-QCC-08, Conduit Production:
 - 8.3.1. Sheet Used
 - 8.3.2. Slurry Used for Seal/Dip
 - 8.3.3. Date rolled
 - 8.3.4. Type of Seal

- 8.3.5. Inner diameter
- 8.3.6. Number of layers
- 8.3.7. Length of conduit
- 8.3.8. End use
- 8.3.9. Additional Notes
- 8.3.10. Initials and Date

9.0 References

- 9.1. CNF-SOP-07 (CNF Sheet Fabrication)
- 9.2. CNF-QCC-08 (Processed Roll Quality Control Checklist)
- 9.3. CNF-SOP-09 (General Maintenance and Cleaning Protocol)
- 9.4. CNF-SOP-10 (Labeling Procedure for Stocks, Samples, and Products)

10.0 Procedures

10.1. Creating an acrylic template

- 10.1.1. Measure and draw out the desired conduit pattern on the acrylic platform
- 10.1.2. Score the template over the lines drawn on the acrylic with a utility knife (as presented in Appendix 11.1)
- 10.1.3. Repeat the above step until a continuous notch is made around the designated template
- 10.1.4. The utility knife must be able to freely travel within the notches of the template for consistent cutting of the pattern from CNF sheets

10.2. Cutting a CNF conduit pattern

- 10.2.1. Place the sheet over an acrylic template of conduit size specifications (1.5 x 2.5 cm rectangular pattern)
- 10.2.2. Position the sheet such that the direction of casting is in alignment with the longer edge of the pattern.
- 10.2.3. Cut the CNF sheet using a utility knife and follow the notches in the acrylic template. Blades are sharp and have potential to injure the operator: Use caution when using razor blades
- 10.2.4. If the template requires intricate geometrical entities to be removed from inside the rectangular outer shape, cut the interior geometry prior to the border

10.3. Rolling a CNF conduit

- 10.3.1. Place the long edge of the conduit cutout over the plastic mandrel. This edge will be noted as the starting edge, and the opposite edge will be the finishing edge
- 10.3.2. Roll the finishing edge overtop the start edge
- 10.3.3. Keep the successive wraps tight to the mandrel
- 10.3.4. Prior to completion of the final wrap, a seal of slurry is applied, via blunt tip needle, to the last half of the wrap to prevent unraveling. Visually inspect slurry prior to use: If slurry shows signs of mold or microbials, DO NOT USE. Label with red tape and remove from operation area

10.4. Sealing a CNF conduit

- 10.4.1. Fill a 1 mL syringe connected to a 20 gauge blunt tip needle with CNF slurry
- 10.4.2. Apply the slurry to the interior facing side of the finishing edge in a zig zag pattern
- 10.4.3. Fold the flap over and onto the conduit and gently press to seal the conduit
- 10.4.4. Gently wipe off excess slurry from the seal with a microspatula
- 10.4.5. Leave conduit on the mandrel and let dry for 24 hours in a secluded area. Record the batch of slurry used on the respective QCC

10.5. Coating a CNF conduit

- 10.5.1. Allocate the respective slurry into a separate container (100 mL beaker) such that the depth of the slurry in the container exceeds the length of the conduit. Designate this container as CNF slurry for conduit coating
- 10.5.2. Submerge the dried and sealed conduit in the designated container of CNF slurry
- 10.5.3. Remove conduit from the slurry, removing excess coating with a microspatula if uneven
- 10.5.4. Repeat dipping thrice until a consistent coating can be attained
- 10.5.5. Leave the coated conduit on the mandrel and relocate to a secluded area. Rotate the conduit during the drying process by fixing mandrel to the rotating drying rack.

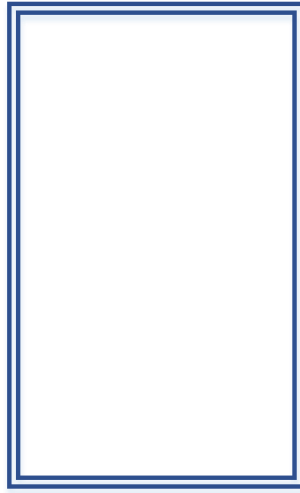
10.6. Removing the CNF conduit

- 10.6.1. Cut the conduits to length, still on the mandrel, using tubing cutters
- 10.6.2. Inspect each conduit for a clean-edge cut and ensure there is no delamination of the outer layer
- 10.6.3. Package in a sealable bag and label, as per CNF-SOP-10

10.7. Cleaning and Maintenance

- 10.7.1. Clean the station as outlined in CNF-SOP-09. Record all maintenance and cleaning performed in the maintenance and cleaning logs at the station.

11.0 Example of Notched Template on Acrylic platform



CNF-SOP-09 GENERAL MAINTENANCE AND CLEANING

Nanocellulose Conduit Production
Standard Operating Procedure #09
General Maintenance and Cleaning Protocol

Rev	Date	Description
1	1/19/2017	Draft Development Document-Nicklaus Carter
2	7/28/2017	Revision-Mary Bourque
3	8/14/17	Revision – Nicklaus Carter

Approved by:	Signature	Date
Originator	Nicklaus Carter	
Manager	David Neivandt	
Quality Assurance	David Neivandt and Caitlin Howell	

1. Purpose

- 1.1. To outline routine cleaning and maintenance procedures and schedule

2. Definitions

- 2.1. CNF: Cellulose nanofibrils
- 2.2. DIW: Deionized distilled water (17.45-17.46 Megaohms-cm)
- 2.3. Fines: Cellulose nanofibrils that are less than 200 μm in length
- 2.4. SMC: Super mass colloid

3. Health and Safety Warnings

- 3.1. Acidic cleaning solution can cause irritation to eyes and skin.
- 3.2. Take care when lifting or carrying either large or heavy loads: Improper form or the inability to lift heavy loads can cause strains and sprains.
- 3.3. Use appropriate personal protective equipment PPE (laboratory coats, gloves, safety glasses when applicable) while working in the laboratory.
- 3.4. Work in a well-ventilated laboratory area.
- 3.5. PPE is worn only in laboratory areas and removed before entering non-laboratory areas.
- 3.6. Hazardous waste must be disposed of in the designated waste container.
- 3.7. Be familiar with the MSDS/SDS for all chemicals being used in this procedure.

4. Cautions

- 4.1. Follow instructions for dilution of alkaline and acidic cleaners: Failing to do so may cause corrosion or damage to equipment.
- 4.2. Ensure filters have been on and running for at least 24 hours. If the filters have not been on for at least 24 hours, turn the filters on and wait until a full 24 hours has passed before entry to prevent contamination due to airborne particles.
- 4.3. If the clean room pressure is not twice that of the gowning room, do not enter the clean room, for this may indicate end of the filter life.

5. Interferences

- 5.1. Producing a cleaning solution that is too dilute may not clean and sanitize the equipment properly.

6. Personnel Responsibilities and Qualifications

- 6.1. Supervisor:
 - Ensure operators are trained on this procedure.

- Ensure operators conduct procedures as instructed.

6.2. The Operator:

- Must be trained on all equipment and procedures prior to operation.
- Complete this procedure as instructed.
- Report any deviations to this procedure to Dr. Neivandt.
- Follow Safety and Environmental Management (SEM) lock-out tag-out procedure for equipment that needs repair. Remove broken equipment from the room.
- Must be able to lift up to 50 pounds.

7. Equipment and Materials

7.1. Equipment

- 7.1.1. 2 - 116 Qt. storage totes (Home Depot, SKU #1000030696)
- 7.1.2. PBW-Alkali Cleaner (Northern Brewer Homebrew Supply, SKU#U005)
- 7.1.3. Star San (Northern Brewer Homebrew Supply, SKU#U001)
- 7.1.4. 1 - 32 oz. Spray Bottle (Home Depot, SKU#255852)
- 7.1.5. Cleanroom Wipe – part of a cleaning kit, (NCI, WW-MAINTK-1)

7.2. Materials (as listed or equivalent)

- 7.2.1. Deionized Water (17.45-17.46 Megaohms-cm)

8. Quality Control and Quality Assurance

- 8.1. This procedure is to be used for all dirty surfaces and stainless steel equipment. It should be repeated after every station use.

9. References

- 9.1. All QC checklists and SOPs in the master binder

10. Procedures

10.1. Preparation of alkaline scrub solution - Tote mix

- 10.1.1. Fill the tote marked “alkaline” with 10 gallons of water
- 10.1.2. Weigh 10 ounces of PBW powder and mix into the water

10.2. Preparation of acidic sanitary solution - Tote mix

- 10.2.1. Fill the tote marked “acidic” with 10 gallons of water
- 10.2.2. Measure 2 ounces of Star San (Bettix bottle) and mix into the water

10.3. Preparation of acidic sanitary solution - Spray bottle mix

10.3.1. Fill spray bottle with mix from tote if available

10.3.2. Fill the 32 oz spray bottle with water (0.25 gallons)

10.3.3. Mix 0.05 oz of Star San with the water

10.4. Cleaning stainless steel surfaces

10.4.1. Use the PBW solution to clean debris from surfaces.

10.4.2. Rinse surfaces with DIW and let dry

10.4.3. Apply the Star San via the 32 oz spray bottle solution

10.4.4. Let the Star San solution sit for 1-2 minutes, then wipe dry

10.4.5. Apply a DIW rinse

10.4.6. Fill out the station's cleaning log

10.5. Cleaning Walls of the Cleanroom

10.5.1. It is recommended that the walls of the cleanroom are cleaned weekly

10.5.2. Use a cleanroom wipe and DI water to wipe down the acrylic panels.

CNF-SOP-10 LABELING PROTOCOLS

Nanocellulose Conduit Production
Standard Operating Procedure #10
Labeling Procedure for Stock, Samples, and Products

Rev	Date	Description
1	4/25/2017	Draft Development Document-Nicklaus Carter
2	7/28/2017	Revision-Mary Bourque
3	8/14/17	Revision – Nicklaus Carter

Approved by:	Signature	Date
Originator	Nicklaus Carter	
Manager	David Neivandt	
Quality Assurance	David Neivandt and Caitlin Howell	

1.0 Purpose

- 1.1. To thoroughly label all materials, samples, and products to create a traceable account of all materials through a comprehensive log

2.0 Definitions

- 2.1. CNF: Cellulose Nanofibrils
- 2.2. DIW: Deionized distilled water (17.45-17.46 Megaohms-cm)
- 2.3. Fines: Cellulose Nanofibrils that are less than 200 μm in length

3.0 Health and Safety Warnings

- 3.1. Take care when lifting or carrying either large or heavy loads: Improper form or the inability to lift heavy loads can cause strains and sprains.
- 3.2. Use appropriate personal protective equipment PPE (laboratory coats, gloves, safety glasses when applicable) while working in the laboratory.
- 3.3. Work in a well-ventilated laboratory area.
- 3.4. PPE is worn only in laboratory areas and removed before entering non-laboratory areas.
- 3.5. Hazardous waste must be disposed of in the designated waste container.
- 3.6. Be familiar with the MSDS/SDS for all chemicals being used in this procedure.

4.0 Cautions

- 4.1. Ensure filters have been on and running for at least 24 hours. If the filters have not been on for at least 24 hours, turn the filters on and wait until a full 24 hours has passed before entry to prevent contamination due to airborne particles.
- 4.2. If the clean room pressure is not twice that of the gowning room, do not enter the clean room, for this may indicate end of the filter life.

5.0 Personnel Responsibilities and Qualifications

5.1. Supervisor:

- Ensure operators are trained on this procedure.
- Ensure operators conduct procedures as instructed.

5.2. The Operator:

- Must be trained on all equipment and procedures prior to operation.
- Complete this procedure as instructed.
- Report any deviations to this procedure to Dr. Neivandt.

- Follow Safety and Environmental Management (SEM) lock-out tag-out procedure for equipment that needs repair. Remove broken equipment from the room.
- Must be able to lift up to 50 pounds.

6.0 Equipment and Materials

6.1. Equipment

- 6.1.1. Brady BBP33 Label Printer (Brady, BBP33-C)
- 6.1.2. Brady Workstation Labeling Software (Brady, Free Online)

6.2. Materials (as listed or equivalent)

- 6.2.1. Adhesive Paper Label Roll, 2in x 1in (Brady, B33-17-424)
- 6.2.2. Black Thermal Transfer Print Ribbon (Brady, B30-R4300)

7.0 References

- 7.1. All QC checklists and SOPs contained in master binder. Labeling procedure applies to all stations of operation.

8.0 Procedures (Refer to respective quality control checklists)

8.1. Labeling raw material – in bags

- 8.1.1. Label the raw material as presented in Appendix 9.2.1
- 8.1.2. In respective log entry: source, lot#, quantity/mass, visual inspection results, etc. as presented in Appendix 9.3.1

8.2. Labeling cellulose pulp solutions - in buckets

- 8.2.1. Label solution as “unrefined,” as presented in Appendix 9.2.2
- 8.2.2. In respective log entry: pulp type, amount of pulp/water, etc.

8.3. Labeling cellulose slurries - in buckets

- 8.3.1. Label slurry as “refined,” as presented in Appendix 9.2.3
- 8.3.2. In respective log entry: % fines, cumulative energy, etc. as presented in Appendix 9.3.2

8.4. Labeling cellulose sheets - in bags

- 8.4.1. Label sheets as presented in Appendix 9.2.4
- 8.4.2. In respective log entry: % fines, thickness, material composition, etc.
- 8.4.3. as presented in Appendix 9.3.3

8.5. Labeling cellulose conduits - in bags/vials

8.5.1. Label conduits as presented in Appendix 9.2.5

8.5.2. In respective log entry: inner diameter, number of layers, length, etc. as presented in Appendix 9.3.4

8.6. Labeling various other products

8.6.1. Material dependent, follow the examples seen in Appendix 9.2

8.7. Packaging cellulosic materials

8.7.1. Dry materials are stored individually in plastic bags that are sealable

8.7.2. Wet materials are stored in appropriate containers with sealable covers

8.8. Labeling Compromised Materials

8.8.1. Label any materials that do not pass visual inspection or materials that are past their expiry date (6 months post-inception) with red tape; record the reason for product removal and the date applied. Report to Dr. Neivandt.

8.9. Creating Labels

8.9.1. Turn on the printer and the connected laptop

8.9.2. Data from the QCC's are entered into the Labeling Excel file, in the respective sections.

8.9.3. Open the respective labeling file from the Brady Workstation profile.

8.9.4. Ensure that the Excel Import tool is refreshed by reopening the Excel file and importing the data from the Labeling file.

8.9.5. Select the labels needed to print through the print menu, and select print

9.0 Labeling Examples

9.1. Sample Labeling Method

Sample: % fines and refinement	Date
Short Description/Name of Product	
Code: (trace through log)	Initials

9.2. Examples of Sample Labeling for Tracking

9.2.1. Labeling Pulp Samples

Sample: Pulp - Eucalyptus	5/1/17
Bleached Eucalyptus Pulp 200 g	
Code: P01	NRC

9.2.2. Labeling Solution Samples

Sample: Pulp/Water - Eucalyptus	5/1/17
Eucalyptus Suspension, 200g in 14 L	
Code: P01 – Unrefined	NRC

9.2.3. Labeling Slurry Samples

Sample: 89% fines and 2%wt	5/1/17
Eucalyptus CNF Slurry (E-89)	
Code: P01 – R01	NRC

9.2.4. Labeling Sheet Samples

Sample: 52 micron	5/2/17
E-89 CNF Sheet – No visible defects	
Code: P01 – R01 – S01	NRC

9.2.5. Labeling Conduit Samples

Sample: 2WD Conduit	5/2/17
Two Layered Conduit – Slurry Sealed/ Dipped	
Code: P01 – R01 – S01 – C01	NRC

9.3. Examples of Sample Logs for Tracking

9.3.1. Log for Raw Pulp

Sample from lot "P"	Storage Conditions in TAPPI room	Mass of Sample	Moisture Content (%) Of Aliquot	Visual Inspection	Notes	Employee Initials and Date
P01	25 °C 50% Humidity	200 grams	10%	No discoloration of any sort	Eucalyptus	NRC 5-1-17

9.3.2. Log for CNF Slurry

Sample # "R"	Pulp Sample Used (QCC-01)	Date CNF was Produced	Cumulative Energy	Time Spent Refining	Final % Fines	Weight % of Solids (SOP-04)	Volume of Slurry Collected (Estimation)	Notes	Employee Initials and Date
R01	P01	5-1-17	4300 kW-hr	1.5 hrs	89%	2.01%	15 Liters		NRC 5-1-17

9.3.3. Log for CNF Sheet

Sample # "S"	Slurry Used (QCC-06)	Date/Time Spread	Date/Time Lifted	Volume of Slurry Spread	Casting Thickness	Dried Thickness (Avg. ± St. Dev. Of 15pts)	End Use (Destination)	Notes	Employee Initials and Date
S01	R01	9 am 5-1-17	10 am 5-2-17	120 mL	1.9 mm	52 µm ± 1.7 µm	Shipped to Harvard Mouse Trial		NRC 5-2-17

9.3.4. Log for CNF Conduit

Sample # "C"	Sheet Used (QCC-07)	Slurry Used for Seal/Dip (QCC-06)	Date Rolled	Type of Seal	Inner Diameter	Number of Layers	Length of Conduit	End Use (Destination)	Notes	Employee Initials and Date
C 01	S01	R01	5-2-17	CNF seal and dip	0.65mm	2 layers	2.5 cm	Shipped to Harvard Mouse Trial		NRC 5-2-17

CNF-SOP-11 STABILITY STUDIES

***Nanocellulose Conduit Production
Standard Operating Procedure #11
Material Stability Studies***

Rev	Date	Description
1	6/30/2017	Draft Development Document-Nicklaus Carter
2	7/28/2017	Revision-Mary Bourque
3	8/14/17	Revision – Nicklaus Carter

Approved by:	Signature	Date
Originator	Nicklaus Carter	
Manager	David Neivandt	
Quality Assurance	David Neivandt and Caitlin Howell	

1. Purpose

- 1.1. To test the material stability of all materials, samples, and products

2. Definitions

- 2.1. CNF: Cellulose Nanofibrils
- 2.2. DIW: Deionized distilled water (17.45-17.46 Megaohms-cm)
- 2.3. Fines: Cellulose Nanofibrils that are less than 200 μm in length

3. Health and Safety Warnings

- 3.1. Take care when lifting or carrying either large or heavy loads: Improper form or the inability to lift heavy loads can cause strains and sprains.
- 3.2. Use appropriate personal protective equipment PPE (laboratory coats, gloves, safety glasses when applicable) while working in the laboratory.
- 3.3. Work in a well-ventilated laboratory area.
- 3.4. PPE is worn only in laboratory areas and removed before entering non-laboratory areas.
- 3.5. Hazardous waste must be disposed of in the designated waste container.
- 3.6. Be familiar with the MSDS/SDS for all chemicals being used in this procedure.

4. Cautions

- 4.1. Ensure stable conditions when storing each material for a predetermined amount of time. Changing conditions may invalidate results.
- 4.2. Ensure filters have been on and running for at least 24 hours. If the filters have not been on for at least 24 hours, turn the filters on and wait until a full 24 hours has passed before entry to prevent contamination due to airborne particles.
- 4.3. If the clean room pressure is not twice that of the gowning room, do not enter the clean room, for this may indicate end of the filter life.

5. Interferences

- 5.1. All conditions must be carefully monitored and recorded.

6. Personnel Responsibilities and Qualifications

6.1. Supervisor:

- Ensure operators are trained on this procedure.
- Ensure operators conduct procedures as instructed.

6.2. The Operator:

- Must be trained on all equipment and procedures prior to operation.

- Complete this procedure as instructed.
- Report any deviations to this procedure to Dr. Neivandt.
- Must be able to lift up to 50 pounds.

7. Equipment and Materials

7.1. Equipment

7.1.1. Shaker Table (Fisher Scientific, 11-676-339)

7.2. Materials (as listed or equivalent)

7.2.1. 50 ml centrifuge tubes (Fisher Scientific, 22170265)

8. Quality Control and Quality Assurance

8.1. Repeat tests to ensure no outliers in conditions. The stability studies in this SOP are meant to ensure high quality products that can withstand different environments.

9. References

9.1. All SOPs and QC checklists in the master binder

10. Procedures

10.1. Slurry Stability

10.1.1. Dispense the desired amount of CNF slurry into a new sealed container and label accordingly

10.1.2. Leave the slurry undisturbed for a predetermined amount of time in a predetermined environment

10.1.3. Visually inspect the slurry for contaminants/growth

10.2. Sheet Stability - Dry Stability

10.2.1. Leave sheets of CNF in a predetermined environment for a designated amount of time and label accordingly

10.2.2. Analyze sheets visually and record observations

10.2.3. Measure sheet thickness at each temporal observation

10.3. Sheet Stability - In Liquid

10.3.1. Submerge CNF sheets in desired solution and label accordingly

10.3.2. Visually inspect the sheets for degradation

10.3.3. Visually inspect the solution for increase in particulate concentration

10.4. Conduit Stability - Dry Test

10.4.1. Leave CNF conduits in a predetermined environment for a designated amount of time and label accordingly

10.4.2. Analyze conduits visually and record observations

10.4.3. Measure conduit diameter at each temporal observation

10.5. Conduit Stability - In Liquid

10.5.1. Fill centrifuge tubes with at least 3 inches of the predetermined solution to ensure coverage of the conduit and label accordingly

10.5.2. Visually inspect conduits for degradation

10.5.3. Observe the solution for increase in particulate concentration

10.5.4. Leave tubes stationary or place on shaker table

10.6. Conduit Stability - Bending Test

10.6.1. Leave conduits in predetermined solution for a predetermined amount of time and label accordingly

10.6.2. Remove conduit and fix at both ends using a mandrel: The mandrel is placed within the conduit ends $\frac{1}{4}$ " in

10.6.3. Place the conduit with mandrels assembly on a smooth platform where the conduit can be bent by moving the mandrel ends

10.6.4. Bend the conduit and record the angle at the point of outer layer tearing or collapse of the middle region

CNF-SOP-12 PRODUCT PACKAGING

***Nanocellulose Conduit Production
Standard Operating Procedure #12
Packaging Products Prior to Distribution***

Rev	Date	Description
1	4/25/2017	Draft Development Document-Nicklaus Carter
2	7/28/2017	Revision-Mary Bourque
3	8/14/17	Revision – Nicklaus Carter

Approved by:	Signature	Date
Originator	Nicklaus Carter	
Manager	David Neivandt	
Quality Assurance	David Neivandt and Caitlin Howell	

1.0 Purpose

- 1.1. To ensure all products are properly packaged and the log reflects complete characterization prior to distribution

2.0 Definitions

- 2.1. CNF: Cellulose nanofibrils
- 2.2. DIW: Deionized distilled water (17.45-17.46 Megaohms-cm)
- 2.3. Fines: Cellulose nanofibrils that are less than 200 μm in length

3.0 Health and Safety Warnings

- 3.1. Take care when lifting or carrying either large or heavy loads: Improper form or the inability to lift heavy loads can cause strains and sprains.
- 3.2. Use appropriate personal protective equipment PPE (laboratory coats, gloves, safety glasses when applicable) while working in the laboratory.
- 3.3. Work in a well-ventilated laboratory area.
- 3.4. PPE is worn only in laboratory areas and removed before entering non-laboratory areas.
- 3.5. Hazardous waste must be disposed of in the designated waste container.
- 3.6. Be familiar with the MSDS/SDS for all chemicals being used in this procedure.

4.0 Cautions

- 4.1. Improper storage of materials could result in damage or degradation of samples.
- 4.2. Do not process recovered, re-conciliated, or damaged materials or equipment. Visually inspect all materials and make note of any damaged or lost material in the corresponding QC checklist as well as reporting the loss to Dr. Neivandt.
- 4.3. Ensure filters have been on and running for at least 24 hours. If the filters have not been on for at least 24 hours, turn the filters on and wait until a full 24 hours has passed before entry to prevent contamination due to airborne particles.
- 4.4. If the clean room pressure is not twice that of the gowning room, do not enter the clean room, for this may indicate end of the filter life.

5.0 Interferences

- 5.1. Be sure all materials are packaged properly with the correct labels and log sheets included.

6.0 Personnel Responsibilities and Qualifications

- 6.1. Supervisor:
 - Ensure operators are trained on this procedure.
 - Ensure operators conduct procedures as instructed.

6.2. The Operator:

- Must be trained on all equipment and procedures prior to operation.
- Complete this procedure as instructed.
- Report any deviations to this procedure to Dr. Neivandt.
- Follow Safety and Environmental Management (SEM) lock-out tag-out procedure for equipment that needs repair. Remove broken equipment from the room.
- Must be able to lift up to 50 pounds.

7.0 Equipment and Materials

7.1. Equipment

7.1.1. Tabletop impulse sealer with cutter (ULINE, H-161)

7.2. Materials (as listed or equivalent)

7.2.1. Pre-designed labels (CNF-SOP-10)

7.2.2. Flat sealable polypropylene bags, 4mil 4x6" (ULINE, S-11585)

7.2.3. Resealable plastic bags, 2mil 10x13" (ULINE, S-596)

7.2.4. Glass jar with metal lids, 16 oz. or ~500mL (ULINE, S-17984M)

7.2.5. Glass jar with metal lids, 32 oz. or ~1L (ULINE, S-19316M)

8.0 Quality Control and Quality Assurance

8.1. Quality Assurance Supervisor MUST approve all QC checklists prior to distribution.

8.2. Visually inspect all packaging and storage materials prior to use: If packaging materials are dirty or damaged, discard immediately and report to Dr. Neivandt.

9.0 References

9.1. All QC checklists and SOPs contained in master binder.

10.0 Procedures (Refer to respective quality control checklists)

10.1. Packaging cellulose pulp slurries

10.1.1. Fill screw top glass containers with slurry (500mL or 1L container depending on the amount of slurry being packaged)

10.1.2. Cover and label containers accordingly

10.1.3. If the log corresponding to the slurry is complete, notate in the log the amount removed and the receiving organization in the "end use" column

10.2. Packaging cellulose sheets

10.2.1. Label bag accordingly

10.2.2. Package cellulose sheets in resealable plastic bag

10.2.3. If the log corresponding to the sheet is complete, notate the receiving organization in the end use column

10.3. Packaging cellulose conduits

10.3.1. Label bag accordingly

10.3.2. Place one conduit in the unsealed bag

10.3.3. Seal the bag using the impulse heat sealer, making sure to not crimp the conduit

10.3.4. If the log corresponding to the conduit is complete, notate the receiving organization in the end use column

10.4. Distribution of Products

10.4.1. When an order is received, the products are procured in the order in which they were made (line clearance methodology).

10.4.2. All log sheets must be collected for the procured products

10.4.3. Ensure that the log sheets are filled out thoroughly

10.4.4. Ensure that all products of acceptable quality (yields, visually inspect, etc.)

10.4.5. Final approval of shipment must be given by Dr. Neivandt.

10.5. Recalled/Defective Products

10.5.1. Recalls will be dealt with on a case-to-case basis with Dr. Neivandt to establish an acceptable procedure for future occurrences.

A4: GLUCOSE DIFFUSION COEFFICIENT

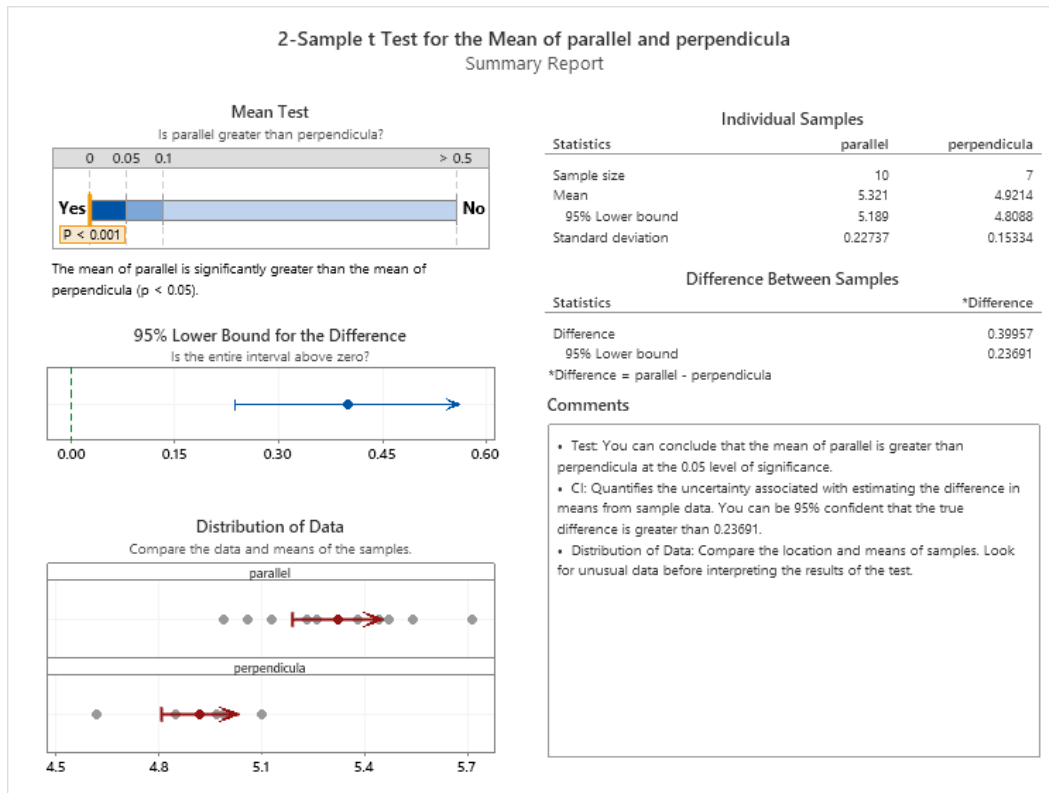
The glucose concentration in the receiver chamber of the bi-chambered tanks was measured as a function of time until either failure of the CNF sheet was observed, or the concentration approached that of the donor chamber. Aliquots of receiver chamber solution (50 μ L) were taken at a given time and the absorbance of the samples measured employing a UV-Visible spectrometer (Thermo Scientific, GENESYS 10S) at a wavelength of 340 nm. The glucose concentration of each sample was obtained employing the calibration curve of Section 3.11, see below.

Tank	Time	Absorbance	Concentration (mmol/L)
#1	3hrs	0.033	0.107
#2	3hrs	0.023	0.073
	6hrs	0.216	0.729
	9hrs	0.145	0.488
	3days	0.870	2.955
	4days	0.953	3.237
#3	3hrs	0.131	0.440
	6hrs	0.194	0.655
	9hrs	0.404	1.369
	27hrs	0.714	2.424
	33 hrs	0.754	2.560
#4	3hrs	0.114	0.382

A5: STATISTICAL ANALYSES FOR COMPARISONS

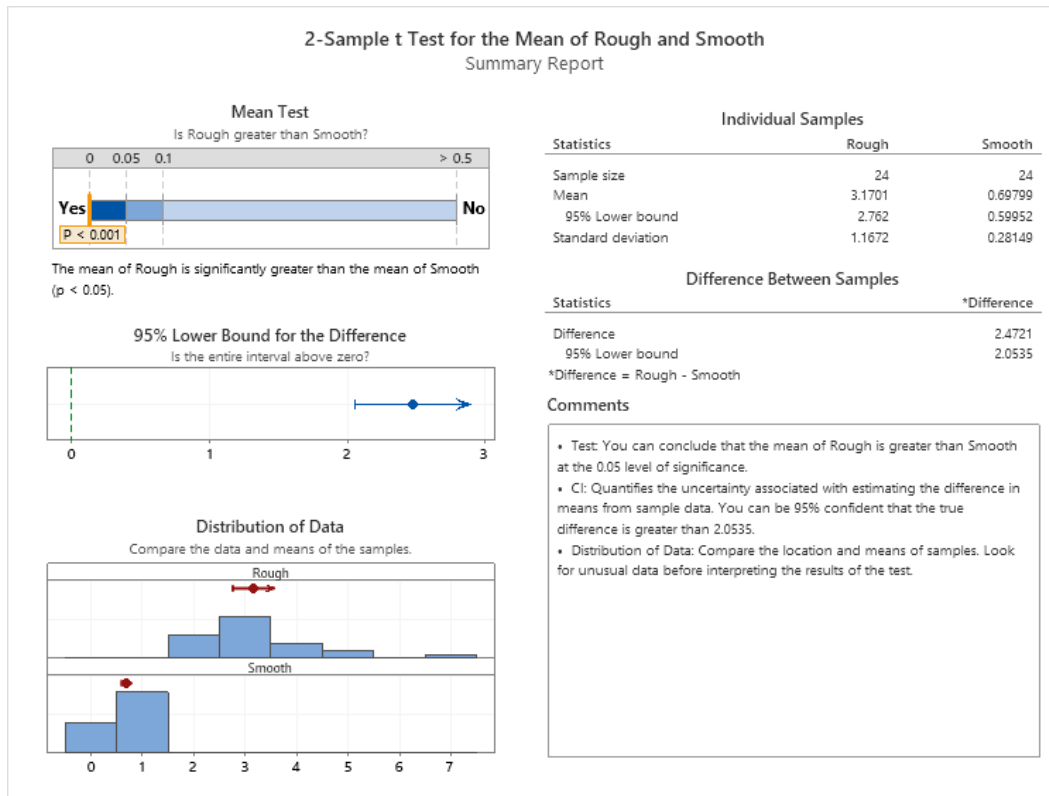
Statistical analyses were performed in Minitab 19 Statistical Software. Several comparisons were made regarding CNF sheets in both the tensile testing and surface roughness measurements. In tensile testing samples were taken both the with and cross to the direction of sheet casting. Surface roughness analysis compared the two surfaces of CNF sheets when plated on a stainless-steel plate: the air-exposed surface versus the steel contacting surface. The following readouts are resultant of Minitab's assistant function for statistical hypothesis testing.

STATISTICAL ANALYSIS FOR COMPARISONS OF TENSILE STRENGTH

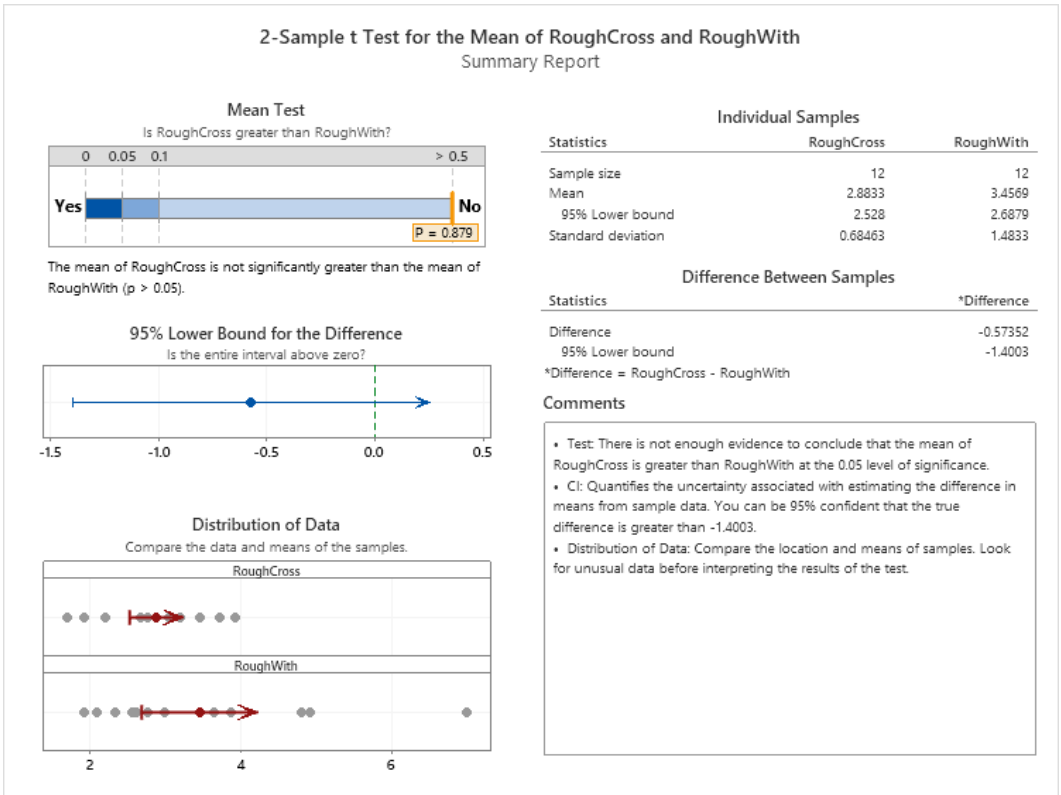


Samples used for tensile testing were taken from both with and cross to the direction of sheet casting, noted as parallel and perpendicular respectively. From the t test directly above, it can be confirmed that samples taken in the parallel direction statistically had a higher Young's modulus value than those taken in the perpendicularly.

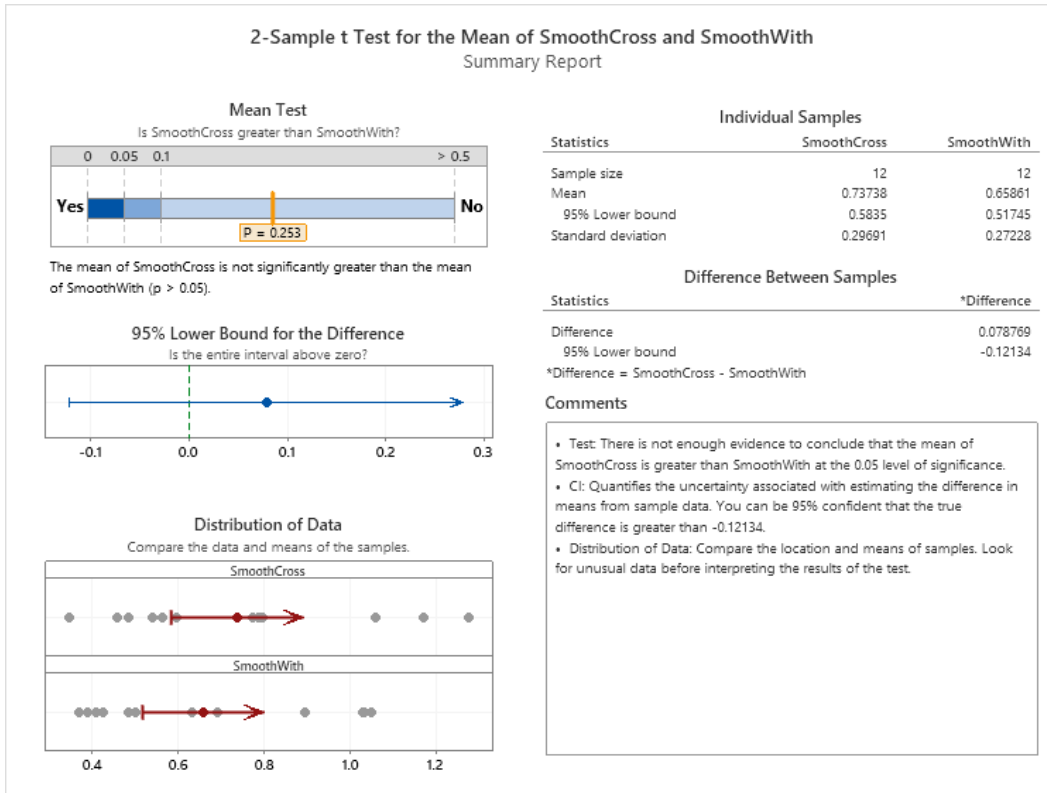
STATISTICAL ANALYSIS FOR COMPARISONS OF SURFACE ROUGHNESS



Duplicate CNF samples were taken from two sheets in both with and cross casting directions and mounted on glass slides with either the presumed rough or smooth side exposed. Each combination of variables was measured in triplicate resulting in 48 total measurements. All samples with the rough side exposed were grouped, regardless of other parameters, and compared to group of samples with the smooth side exposed. From the readout directly above, the average roughness of the air-exposed surface (rough side of the sheet) was statistically greater than the average roughness of the steel-contacting surface (smooth side of the sheet).



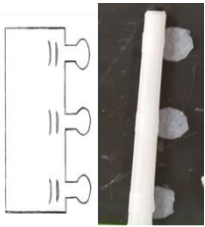
Duplicate CNF samples were taken from two sheets in both with and cross casting directions and mounted on glass slides with either the presumed rough or smooth side exposed. Each combination of variables was measured in triplicate resulting in 48 total measurements. All samples with the air-exposed surface were grouped (24), and comparisons were made between samples taken cross-casting direction against those taken with-casting direction (12 each). From the readout directly above, the average roughness of the air-exposed surface samples did not significantly differ as an effect of casting direction.



Duplicate CNF samples were taken from two sheets in both with and cross casting directions and mounted on glass slides with either the presumed rough or smooth side exposed. Each combination of variables was measured in triplicate resulting in 48 total measurements. All samples with the steel contacting surface (smooth) were grouped (24), and comparisons were made between samples taken cross-casting direction against those taken with-casting direction (12 each). From the readout directly above, the average roughness of the steel-contacting surface samples did not significantly differ as an effect of casting direction.

A6: VARIOUS CNF CONDUIT DESIGNS AND CNF RELATED DEVICES

Over the course of conduit development a range of sealing techniques and device designs were reduced to practice for a range of potential applications, see the table below.

Title	Image	Production	Potential Application
Simple Conduit		4.5x2.5cm rectangle of CNF sheet was rolled onto a mandrel and then sealed with CNF	Severed nerves
Mechanical Interlock Conduit		Uses various slits and tabs to reinforce the closure of the conduit for increased stability within solution. The tabs are inserted through the slits during rolling. This allows for the sealing method to be applied as in previous conduits	Physically 'locked' conduit for severed nerves with increased stability
Collared Conduit		4.5x2.5cm rectangle of CNF sheet with two integral rectangles with triangular tops removed, then rolled onto a mandrel and sealed with CNF	Reinforces suturing of severed nerves
Web and Guiding Cable Conduit		Simple conduit rolled and sealed accordingly. It was then threaded with a needle and thread to add webs to both ends and then an inner connecting thread	Directional guidance of nerve regeneration, severed nerves
Suture Conduit		Created a wet sheet of CNF as established. The wet sheet was then shaped into a 4.5x2.5cm rectangle. Sutures were added across the top of the wet sheet and then the sheet was left to dry.	Directional guidance of nerve regeneration, severed nerves

		It was then rolled and sealed with CNF	
Branched Conduits		Three simple conduits were produced and then the ends were trimmed to form the branch. CNF was used to seal the conduits and the point of branching. Branching can be used to create tees, 90-degree bends, etc.	Experimental
Curved Conduits		Wrapped a rectangular sheet of CNF around a curved mandrel and sealed with CNF. Alternatively, a mold could be used, and the two halves could be sealed together with CNF	Experimental
Hinged Conduits		Simple conduit cut down the middle, then a strip of a CNF sheet was sealed along the inside of the conduit which left two flaps that, when pulled on, would open the conduit	Nerve crush injuries
Windowed Conduits		Simple conduit with squares removed equidistant from one another. When rolled on a mandrel, the cut-out squares line up perfectly with each other and create a window	Visualization of regeneration or aid in surgery

<p>Double-Layer Conduits</p>		<p>Simple conduit made of one material rolled and dried on a mandrel, then a second layer is wrapped around the dried conduit of a different material to create a conduit with two different layers</p>	<p>Enhance regeneration by use of two materials</p>
<p>Tapered-End Conduits</p>		<p>Created a simple conduit and then fused the two ends together by wetting with water and then sealed the ends together with CNF. To reduce sharp edges, once dried the edges were trimmed and the slurry seal reapplied.</p>	<p>Drug delivery</p>
<p>Capsules</p>		<p>Using hermetic alodined pans as molds, CNF was poured over the pans to create sheets with indents when dried. Two sheets were then sealed together with DNF and the edges were cut away to create a capsule.</p>	<p>Drug delivery</p>

A7: MURINE STUDIES AVERAGE DATA

To gauge functional recovery in both murine studies, grip strength analysis was performed. Grip strength was measured in grams for both the control hindlimb and the hindlimb which had been operated upon. Measurements were recorded in triplicate; the following data represents the averages of the triplicate measurements.

MURINE STUDY 1 – AVERAGE GRIP STRENGTH DATA

Data below are those available from the first murine study. All recorded grip strength measurements are in grams.

Group	Week 2	Week 6	Week 8
<i>Conduit</i>	16.36	39.08	42.82
<i>Sham</i>	9.16	18.86	19.84

MURINE STUDY 2 – GROUP 1 AVERAGE GRIP STRENGTH DATA

'Week' denotes operated leg data, 'wk' denotes control leg data. All measurements reported in grams.

Animal ID	Group	Week 0	wk 0	Week 1		Week 2		Week 4		Week 6		Week 8		Week 10	
				1	wk 1	2	wk 2	4	wk 4	6	wk 6	8	wk 8	10	wk 10
2188	1	27.50	24.90	1.70	21.90	1.20	18.00	2.50	24.00	1.07	23.30	1.37	28.30	1.67	34.77
2189	1	31.80	24.50	0.80	18.00										
2192	1	36.50	36.90	1.20	20.20	1.70	26.20	1.20	36.50	1.37	34.20	1.37	48.27	1.40	48.23
2194	1	27.30	30.50	3.40	17.60	1.70	21.00	1.20	17.60	1.50	24.03	0.80	37.33	1.83	36.17
2199	1	35.20	39.00	0.40	34.30	1.70	23.60	0.80	27.90	1.40	28.30	1.59	37.27	1.70	37.90
2183	1	37.30	22.80	1.20	25.30	1.20	20.60	1.20	32.60	3.67	36.30	2.50	41.10	3.67	45.80
4	1	24.00	15.40	1.20	23.60	1.70	30.90	0.80	45.90	1.27	28.90	1.23	33.50	1.07	36.20
25	1	32.60	37.80	3.80	35.20	0.80	16.30	2.10	34.07	1.07	32.60	1.53	40.63	1.10	37.07
32	1	23.20	20.60	1.20	17.60	1.70	30.90	2.23	27.60	1.83	21.73	1.80	26.17	1.20	31.03
39	1	38.10	37.80	1.20	34.80	1.27	38.07	1.40	35.63	2.23	35.20	1.70	36.63	1.53	42.23
46	1	31.80	27.50												
53	1	42.10	41.20	1.53	28.60	2.37	38.80			3.27	31.90	5.83	39.20	5.27	44.10
54	1	39.50	41.60	1.63	20.47										
55	1	36.10	40.80	1.97	18.00	1.40	29.63			2.23	41.93	0.53	34.90	0.93	39.20
67	1	48.50	37.80	0.93	28.03	1.53	53.40	1.80	37.90	1.50	49.20	0.40	45.67	2.53	43.67
68	1	45.50	39.50	0.80	34.63	1.07	36.93	1.23	34.33	1.63	47.10	0.97	46.40	2.10	47.67
70	1	55.00	36.90	1.37	33.47	1.70	43.43	2.37	33.33	1.37	39.50	1.97	39.80	1.20	37.80
98	1	45.93	41.23	1.23	35.77	0.93	41.90	3.67	44.37	9.97	33.07	12.83	41.47	9.27	45.10
103	1	41.73	43.10	1.67	31.63	1.23	34.90	2.40	38.63	1.23	38.47	6.70	41.63	7.10	39.23
105	1	40.93	28.17	1.23	31.43	0.80	34.77	0.97	37.33	1.70	41.50	1.40	36.20	1.47	45.63
116	1	48.40	42.07	0.80	43.23	1.77	35.03	2.10	39.77	1.83	35.37	1.23	40.07	1.83	40.93

MURINE STUDY 2 – GROUP 1 AVERAGE GRIP STRENGTH DATA (CONT.)

'Week' denotes operated leg data, 'wk' denotes control leg data. All measurements reported in grams.

Animal ID	Group	Week 12		Week 14		Week 16		Week 18		Week 20	
		Week	wk								
2188	1	1.23	35.03	1.53	11.55	1.53	14.68	0.67	18.28	1.10	42.73
2189	1										
2192	1	2.40	46.67	0.80	10.95	1.07	24.82	0.80	23.73	0.93	44.83
2194	1	3.67	37.77	4.80	9.65	5.40	19.42	3.67	21.28	6.27	46.37
2199	1	1.23	40.03	0.93	18.00	1.53	19.33	1.80	20.48	1.67	42.07
2183	1	9.70	35.63	10.13	13.25	5.40	22.38	7.40	22.88	1.67	35.47
4	1	0.53	41.67	0.97	12.65	1.07	17.38	1.53	21.32	0.93	32.33
25	1	0.80	37.80	0.93	18.00	1.50	20.85	1.23	19.37	0.67	41.37
32	1	1.37	16.33	0.83	9.65	1.97	14.00	0.83	8.58	0.67	22.43
39	1	1.80	40.63	2.10	18.03	2.10	19.43	2.53	21.37	1.67	37.20
46	1										
53	1	2.27	44.67								
54	1										
55	1	1.93	44.77	1.10	9.70	1.93	18.57	1.80	22.93	1.80	36.77
67	1	7.27	48.97	10.83	14.78	7.70	23.58	4.67	29.90	7.10	42.37
68	1	1.40	41.07	1.37	17.85	1.37	24.02	0.97	21.22	1.93	54.03
70	1	4.53	40.90	4.27	17.58	4.23	20.58	5.10	22.58	2.23	35.90
98	1	12.40	45.33	10.00	18.35	11.27	25.72	8.97	27.67	11.40	43.53
103	1	7.83	38.07	11.10	16.43	5.97	21.43	2.23	24.58	1.67	31.93
105	1	1.67	40.07	1.80	16.12	1.53	18.95	1.67	20.93	1.50	38.77
116	1	1.53	49.07	1.70	22.50	4.73	20.95	1.53	25.38	1.23	44.63

MURINE STUDY 2 – GROUP 2 AVERAGE GRIP STRENGTH DATA

'Week' denotes operated leg data, 'wk' denotes control leg data. All measurements reported in grams.

Animal ID	Group	Week 0	wk 0	Week 1	wk 1	Week 2	wk 2	Week 4	wk 4	Week 6	wk 6	Week 8	wk 8	Week 10	wk 10
2190	2	43.80	24.00	1.70	26.60	1.20	23.60	1.70	32.20	1.23	42.20	1.53	28.90	1.07	41.97
2191	2	27.90	30.50	1.20	22.30	1.20	14.10	2.10	32.20	1.07	30.03	1.20	33.20	1.83	41.67
2198	2	32.60	33.50	1.20	29.60	0.80	18.00	2.10	34.80	1.40	30.33	2.40	37.07	4.77	38.63
5	2	15.40	12.80	1.20	15.40	1.20	29.20	0.80	39.20	1.53	26.30	3.10	33.03	2.37	39.67
31	2	30.50	33.90	3.00	37.80	1.70	42.10	1.80	41.20	6.27	31.47	8.70	45.07	2.70	42.80
34	2	33.90	30.90	1.20	30.90	3.00	33.00	3.13	30.00	11.57	39.23	8.97	34.77	8.53	40.90
36	2	41.60	33.50	1.70	29.60	1.53	33.77	2.97	35.93	9.57	45.93	11.70	37.00	14.27	34.50
41	2	36.50	29.60			1.80	27.30	1.07	36.17	1.80	41.80	2.37	35.90	1.97	40.93
43	2	34.30	23.20												
44	2	32.60	36.50			2.93	41.07	0.97	37.20	2.13	41.50	1.83	46.77	1.07	43.93
49	2	40.40	33.50	1.63	27.30	1.23	24.60			1.50	38.77	1.23	43.77	1.23	46.30
52	2	34.80	45.20	1.53	27.90	2.27	26.60			2.80	43.97	5.40	42.50	3.67	40.90
56	2	40.80	44.70			0.53	26.00			1.93	44.20	1.23	42.50	1.97	35.77
66	2	37.80	28.30	0.93	24.57	1.23	39.20	2.37	37.63	1.50	44.53	2.70	41.93	3.53	41.50
72	2	49.40	36.50	0.93	28.33	1.67	41.77	3.67	39.07	4.97	39.10	7.83	45.53	1.80	39.20
75	2	46.80	39.50	0.97	28.77	1.37	38.10	0.97	35.63	1.83	37.07	1.83	38.20	1.67	41.47
108	2	45.27	43.93	0.67	39.20	1.07	43.63	2.67	48.23	1.83	41.07	2.67	50.23	2.57	41.80
111	2	39.07	37.33	0.97	35.47	2.10	37.50	1.80	45.50	3.53	49.23	5.97	39.50	8.23	41.80
115	2	42.77	30.83	0.97	35.90	1.23	35.03	3.40	32.47	8.13	38.07	9.73	48.63	8.40	49.10

MURINE STUDY 2 – GROUP 2 AVERAGE GRIP STRENGTH DATA (CONT.)

'Week' denotes operated leg data, 'wk' denotes control leg data. All measurements reported in grams.

Animal ID	Group	Week 12	wk 12	Week 14	wk 14	Week 16	wk 16	Week 18	wk 18	Week 20	wk 20
2190	2	1.37	44.10	0.80	13.90	1.23	15.07	0.80	22.45	1.20	44.20
2191	2	1.53	33.17	1.23	11.75	1.40	17.13	0.97	17.20	1.70	37.90
2198	2	4.23	40.63	3.40	15.20	4.23	19.23	3.67	22.02	3.37	20.17
5	2	4.23	47.77	3.10	8.30	3.67	17.28	6.53	25.43	5.10	53.97
31	2	1.67	46.77	2.10	19.75	3.23	25.67	2.67	24.43	2.67	44.10
34	2	2.93	40.37	1.93	16.95	1.93	23.17	2.23	21.15	2.97	39.93
36	2	15.30	34.47	14.30	15.57	18.43	23.28	19.60	24.38	23.43	39.77
41	2	1.93	37.07	2.37	1.80	3.97	18.85	3.23	19.72	2.10	35.03
43	2										
44	2	1.97	46.93	4.07	2.93	3.80	24.45	4.80	25.50	4.83	47.23
49	2	0.80	38.10								
52	2	4.13	45.07								
56	2	2.37	38.93	2.80	0.53	1.37	22.22	1.67	20.87	4.40	48.40
66	2	3.83	40.80	5.97	12.90	5.37	21.72	5.83	23.38	6.97	48.13
72	2	13.80	46.20	14.13	15.00	11.13	25.25	11.77	30.17	12.70	40.37
75	2	3.80	33.77	7.57	15.07	4.40	20.02	3.97	20.67	3.70	41.33
108	2	4.23	36.30	6.23	20.13	4.57	26.03	3.67	21.27	2.53	38.20
111	2	8.13	40.50	9.67	18.78	7.83	21.52	8.70	25.08	4.53	36.63
115	2	7.53	41.50	10.40	18.57	8.30	28.38	10.83	25.95	11.35	47.10

MURINE STUDY 2 – GROUP 3 AVERAGE GRIP STRENGTH DATA

'Week' denotes operated leg data, 'wk' denotes control leg data. All measurements reported in grams.

Animal ID	Group	Week 0	wk 0	Week 1		Week 2		Week 4		Week 6		Week 8		Week 10	
				1	wk 1	2	wk 2	4	wk 4	6	wk 6	8	wk 8	10	wk 10
2193	3	32.20	24.90	1.20	27.90	0.80	18.90	1.70	24.50	2.23	34.47	1.70	32.17	1.40	37.07
2195	3	34.80	28.70	1.70	20.20	0.40	26.20	3.00	25.30	2.27	29.90	1.50	39.27	1.67	37.80
2196	3	27.90	30.00	0.40	17.60	0.00	28.70	1.70	33.50	1.63	30.03	2.63	38.37	6.83	43.23
2184	3	34.30	37.80	1.70	23.20	2.50	25.30	2.50	26.60	2.13	25.03	10.00	37.50	12.47	38.37
3	3	32.20	21.00	0.80	26.20	1.20	36.50	2.50	46.80	3.53	29.17	5.83	43.10	8.53	35.93
26	3	33.90	38.60	3.70	41.20	2.10	46.80	1.67	29.33	1.40	36.03	2.40	46.37	3.97	41.47
28	3	42.50	30.00	3.00	40.50	1.20	35.60	2.23	27.77	5.53	37.77	6.53	37.50	7.10	41.67
29	3	29.20	27.90	0.80	31.30	1.70	31.80	2.10	27.30	2.27	32.33	2.50	38.90	3.50	41.50
33	3	22.30	35.20	3.00	36.50	2.10	38.20	1.83	41.07	3.37	29.57	5.00	35.77	3.97	35.60
37	3	25.30	35.60	1.70	25.80	1.37	34.13	1.67	41.93	4.93	40.20	5.97	37.20	8.97	35.03
42	3	21.40	35.20												
50	3	44.20	40.80	1.23	24.03	0.67	30.63			4.33	35.33	5.83	37.97	6.53	38.33
60	3	34.80	34.80	1.83	20.00	1.40	27.17			6.70	34.93	8.57	33.60	8.40	39.63
61	3	43.40	47.20	1.97	24.77	0.83	29.60			1.23	38.50	0.93	42.37	1.40	42.60
63	3	35.20	39.90	0.67	30.33	1.97	41.33	2.80	42.00	3.80	47.23	5.57	49.37	4.80	49.67
65	3	39.50	36.90	0.67	31.30	1.23	44.20	1.50	41.67	1.80	36.63	1.20	39.23	6.27	47.80
71	3	42.10	47.70	0.97	24.30	1.23	38.07	3.67	36.20	5.13	40.23	6.23	38.50	6.10	40.77
80	3	34.82	34.82	1.23	39.50	2.70	43.07	3.27	44.77	0.93	36.20	13.83	41.50	11.80	43.07
84	3	36.07	32.86	1.23	42.07			2.10	43.63	2.93	37.33	4.50	46.10	5.53	43.50
87	3	36.72	35.49	1.70	38.63	1.67	35.47	1.67	42.80	2.23	40.20	3.23	41.67	4.23	45.63
107	3	52.93	45.40	1.07	40.63	1.07	30.87	1.50	37.20	7.83	42.07	10.00	42.07	15.00	37.03
112	3	36.77	42.80	1.37	28.77	1.37	36.80	2.13	46.53	1.67	43.93	1.67	32.73	2.10	45.80

MURINE STUDY 2 – GROUP 3 AVERAGE GRIP STRENGTH DATA (CONT.)

'Week' denotes operated leg data, 'wk' denotes control leg data. All measurements reported in grams.

Animal ID	Group	Week 12		Week 14		Week 16		Week 18		Week 20	
		Week	wk								
2193	3	1.93	30.17	0.83	14.35	0.67	17.20	0.93	15.50	0.97	39.03
2195	3	2.10	40.07	0.80	10.30	1.23	20.77	1.40	20.43	1.67	46.93
2196	3	9.13	49.97	7.10	8.80	4.50	20.00	3.67	28.53	4.97	45.97
2184	3	14.40	41.77	7.93	12.85	12.97	19.82	9.70	24.85	5.97	41.10
3	3	8.83	39.63	8.97	13.70	8.13	23.32	10.10	24.30	12.30	47.07
26	3	1.97	45.77	2.10	21.65	2.10	23.88	3.50	23.93	4.37	49.83
28	3	11.13	35.90	10.40	20.85	12.43	21.52	12.43	23.15	11.13	37.93
29	3	1.93	37.20	3.23	16.50	4.10	20.58	4.53	20.22	2.67	40.63
33	3	1.97	40.93	2.40	19.30	1.80	19.57	2.10	21.67	5.10	38.37
37	3	8.10	46.80	9.83	13.58	5.97	21.07	10.70	28.32	8.13	40.37
42	3										
50	3	5.70	39.20	4.83	12.35	10.70	21.15		22.02	13.27	43.93
60	3	6.67	38.93	6.40	10.70	8.53	20.15	7.13	22.67	9.53	37.03
61	3	1.10	36.33	1.50	12.80	2.27	21.80	1.97	18.92	3.10	44.20
63	3	5.67	49.50	5.37	16.15	8.27	26.58	8.27	27.43	5.23	54.40
65	3	2.97	34.63	2.40	16.27	3.07	20.52	4.97	18.52	4.27	53.37
71	3	10.10	38.50	7.97	12.77	11.27	21.82	9.13	23.23	11.70	40.37
80	3	23.73	46.80	21.43	21.10	25.03	21.22	23.47	34.12	29.33	41.53
84	3	10.70	46.83	7.23	42.07	7.27	24.52	11.15	27.03	5.27	38.77
87	3	5.97	47.40	6.83	20.15	2.80	21.95	6.10	27.12	4.50	51.23
107	3	14.27	39.23	12.57	20.85	8.43	24.95	15.57	25.90	6.53	32.17
112	3	2.13	34.90	1.80	15.07	2.10	17.20	2.40	18.35	2.67	38.70

MURINE STUDY 2 – GROUP 4 AVERAGE GRIP STRENGTH DATA

'Week' denotes operated leg data, 'wk' denotes control leg data. All measurements reported in grams.

Animal ID	Group	Week 0	wk 0	Week 1		Week 2		Week 4		Week 6		Week 8		Week 10	
				1	wk 1	2	wk 2	4	wk 4	6	wk 6	8	wk 8	10	wk 10
2197	4	29.20	24.50	1.20	22.70	0.40	18.90	1.70	32.20	1.10	27.17	2.80	43.37	5.43	43.17
2185	4	38.20	31.30	0.80	28.30	0.80	26.60	1.20	27.00	1.53	26.20	4.23	43.67	6.67	35.80
1	4	22.70	19.30	0.80	24.50	1.20	26.60	0.80	38.60	5.10	28.73	12.83	45.80	12.00	42.67
2	4	22.70	17.10	1.70	19.70	1.20	27.00	1.20	34.80	2.07	29.17	2.97	42.80	5.67	41.93
27	4	42.90	31.30	2.80	34.30	2.50	28.70	2.23	37.27	1.63	35.20	2.40	40.63	5.40	36.63
30	4	38.20	35.60	3.00	34.80	1.70	26.60	1.73	32.47	5.53	36.77	4.40	37.93	8.27	39.20
35	4	30.90	30.00	1.70	48.10	2.10	38.33	1.23	37.37	3.37	38.77	2.13	37.93	4.43	42.83
38	4	34.80	37.80	1.70	33.50	2.23	38.33	0.67	38.50	4.10	42.53	6.97	40.90	6.97	39.27
40	4	29.20	36.50	1.20	27.00	2.37	29.33	0.67	36.77	1.97	31.60	2.40	34.73	2.07	37.77
45	4	35.60	43.40	2.10		1.97	36.63	1.20	44.97	3.10	42.07	4.23	48.77	8.70	50.97
51	4	43.80	39.10	1.10	31.73	0.93	39.63			2.40	42.50	1.53	42.63	2.10	41.07
59	4	25.30	30.50	1.67	16.30	1.07	22.30			1.07	31.43	1.97	33.17	1.40	29.20
62	4	41.20	47.20	1.83	22.43	1.10	31.17			1.93	45.50	4.23	43.93	3.40	50.23
64	4	39.00	25.70	1.10	32.30	1.53	35.60	2.53	40.93	2.53	39.20	2.50	38.63	4.40	46.10
69	4	39.90	39.50	0.67	29.77	1.23	47.53	1.80	32.77	1.93	36.90	1.80	37.63	5.67	34.07
74	4	36.10	28.30	0.93	25.77	1.23	36.20	1.80	40.93	1.93	39.77	4.97	43.23	7.53	41.77
81	4	31.46	32.62	1.67	39.33	2.13	38.63	1.83	40.53	7.80	38.50	3.27	44.80	9.83	41.37
85	4	31.66	35.42	1.53	40.07			1.67	39.50	2.40	38.37	2.10	37.03	4.53	42.07
89	4	34.48	36.78	2.10	31.83	1.93	36.60	1.20	40.93	1.93	36.17	2.27	39.37	2.83	39.60
90	4	32.96	32.99												
106	4	50.80	43.63	0.80	35.50	1.23	36.20	2.27	46.67	2.93	39.80	4.13	39.63	5.10	37.33
114	4	42.50	45.97	1.67	40.93	1.53	41.93	3.83	36.33	1.53	39.17	2.83	45.80	3.23	49.57

MURINE STUDY 2 – GROUP 4 AVERAGE GRIP STRENGTH DATA (CONT.)

'Week' denotes operated leg data, 'wk' denotes control leg data. All measurements reported in grams.

Animal ID	Group	Week 12	wk 12	Week 14	wk 14	Week 16	wk 16	Week 18	wk 18	Week 20	wk 20
2197	4	5.80	41.93	5.83	11.55	1.67	22.23	2.10	23.88	2.80	41.50
2185	4	5.70	36.60	8.70	14.55	4.80	22.60	6.53	22.65	7.53	39.37
1	4	10.53	49.50	8.10	12.85	6.23	25.45	8.53	28.80	7.27	44.07
2	4	7.70	44.67	9.57	10.45	13.27	22.43	9.00	27.12	15.10	39.37
27	4	6.67	48.80	3.40	18.40	10.97	21.13	13.57	26.10	12.97	50.83
30	4	2.80	41.50	5.23	18.25	2.53	21.73	2.97	23.37	3.80	43.93
35	4	2.83	40.80	2.23	25.10	4.23	20.65	3.10	21.52	3.67	45.73
38	4	5.80	34.37	4.37	17.87	4.70	22.50	7.27	19.37	7.10	37.63
40	4	2.53	35.20	1.53	14.68	2.23	18.35	2.23	18.37	2.37	37.47
45	4	11.57	51.53	12.67	1.97	12.57	25.93	10.57	32.10	12.60	43.90
51	4	1.80	41.63	2.97	16.33	4.50	22.52	3.13	22.30	3.27	37.50
59	4	4.80	42.37	13.40	8.68	2.20	17.12	1.40	27.88	7.37	44.20
62	4	5.53	45.23	7.70	11.77	4.50	22.93	5.23	26.47	15.00	45.83
64	4	4.50	37.47	2.80	16.92	3.67	20.58	3.67	20.13	6.20	49.53
69	4	5.27	40.73	6.13	15.50	5.70	19.78	6.97	23.43	9.70	51.27
74	4	8.97	39.93	13.27	13.50	14.83	22.58	12.00	26.60	14.27	52.10
81	4	13.00	44.77	22.10	20.73	18.13	26.30	12.40	33.43	15.70	42.90
85	4	8.70	34.50	11.00	40.07	7.53	19.72	4.53	22.75	6.93	35.77
89	4	8.13	41.77	9.53	16.88	4.83	20.65	11.70	25.65	9.67	45.40
90	4										
106	4	8.27	27.73	10.83	18.37	5.07	21.28	5.10	19.28	4.40	35.90
114	4	2.67	38.90	3.10	21.23	1.53	23.67	3.07	21.00	2.80	40.37

MURINE STUDY 2 – GROUP 5 AVERAGE GRIP STRENGTH DATA

'Week' denotes operated leg data, 'wk' denotes control leg data. All measurements reported in grams.

Animal ID	Group	Week 0	wk 0	1		2		4		6		8		10	
				Week	wk 1	Week	wk 2	Week	wk 4	Week	wk 6	Week	wk 8	Week	wk 10
78	5	34.14	31.56	1.97	36.37	1.67	28.97	1.70	41.63	2.50	35.63	3.67	42.63	8.57	47.17
79	5	33.58	34.79	1.83	43.43	2.23	24.30	1.50	42.07	1.67	40.07	2.67	44.93	1.40	44.07
82	5	31.53	32.33	1.37	39.20	1.70	37.07	1.53	42.40	1.37	40.53	1.67	47.97	2.27	44.07
83	5	35.21	35.62	1.50	32.47			1.53	44.67	6.40	34.60	5.43	47.80	14.83	44.80
86	5	36.61	32.53	1.10	39.07	1.97	40.20	1.23	41.10	3.53	42.63	5.37	33.47	4.37	40.90
88	5	33.60	35.47	1.23	33.20	2.07	36.67	1.07	36.90	3.23	43.93	5.10	43.23	8.40	46.10
91	5	44.84	38.87	1.53	37.20	1.67	38.93	7.23	42.23	21.87	33.20	1.97	38.67	19.43	41.63
94	5	44.93	39.07	1.53	35.17	0.67	25.77	2.10	35.63						
95	5	44.53	39.47	1.67	36.07	0.93	33.90	4.53	44.10	7.87	54.43				
96	5	47.10	40.07	2.53	40.50	1.10	31.03	1.67	46.37						
97	5	55.67	50.40	1.23	37.63	1.53	36.07	4.40	44.67						
99	5	47.37	45.23	1.07	32.33	0.53	35.63	1.23	41.20	2.67	37.07	3.80	48.67	5.40	42.93
100	5	42.97	45.23	0.27	39.07	0.80	39.57	1.37	43.67	3.80	37.93	7.27	45.53	8.00	49.07
101	5	45.23	39.93	1.07	43.93	0.80	36.90	1.53	43.67	7.27	36.47	11.00	44.23	9.87	45.80
102	5	37.80	50.33	1.97	34.73	1.37	34.73			3.13	41.63	4.40	45.93	3.10	46.53
104	5	35.77	37.50	1.23	30.40	0.67	34.47	1.50	41.50	4.80	41.63	6.40	51.10	6.27	45.80
109	5	48.40	38.03	1.10	34.60	1.07	33.03	2.97	38.47	2.80	44.10	4.80	40.20	2.53	43.67
110	5	44.07	41.63	1.67	33.73	1.53	34.17	2.80	44.23	5.97	45.23	9.30	55.00	12.40	46.77
113	5	47.67	32.77	0.97	32.47	1.40	37.20	1.67	33.47	1.67	37.07	1.37	35.73	1.20	37.20

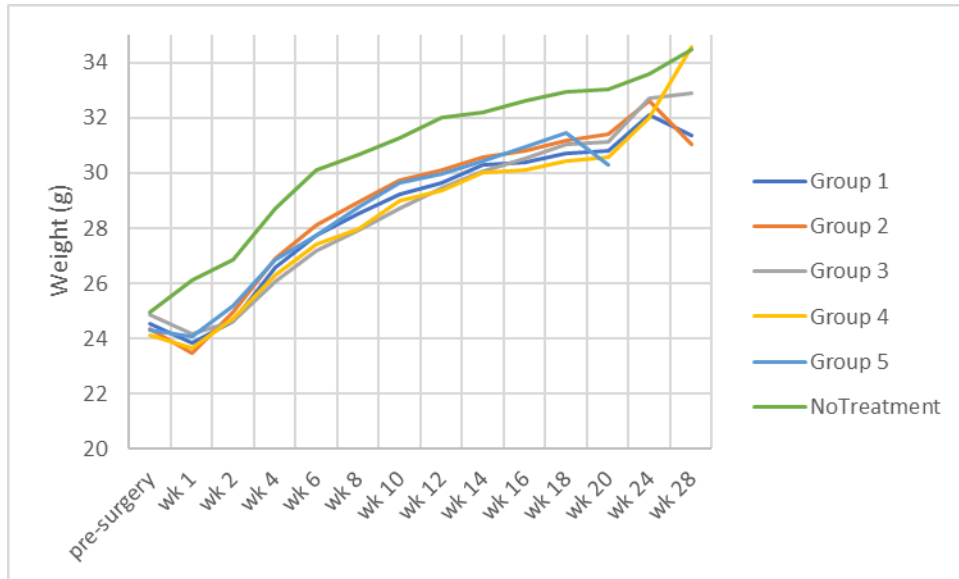
MURINE STUDY 2 – GROUP 5 AVERAGE GRIP STRENGTH DATA (CONT.)

'Week' denotes operated leg data, 'wk' denotes control leg data. All measurements reported in grams.

Animal ID	Group	Week 12	wk 12	Week 14	wk 14	Week 16	wk 16	Week 18	wk 18	Week 20	wk 20
78	5	13.70	48.53	11.27	19.02	10.40	22.57	8.37	29.90	7.83	36.03
79	5	9.97	43.97	12.73	22.83	7.97	23.30	8.97	28.35	7.70	37.10
82	5	0.67	40.77	1.93	20.45	1.07	24.67	1.23	21.35	1.93	44.93
83	5	20.17	40.80	17.00	32.47	20.60	27.10	19.47	28.90	19.70	43.23
86	5	9.13	50.53	10.57	20.52	11.57	18.50	11.53	30.55	9.13	36.90
88	5	10.83	38.77	10.53	17.63	10.80	23.23	11.83	24.65	10.87	41.80
91	5	20.60	44.67	24.60	19.43	22.30	30.27	21.90	34.63	22.30	42.20
94	5										
95	5										
96	5										
97	5										
99	5	7.40	38.77	9.67	16.43	15.00	25.67	7.70	24.22	3.97	48.10
100	5	12.57	46.37	10.57	19.93	11.40	24.67	6.83	28.47	8.27	45.93
101	5	12.13	34.77	9.40	22.37	12.60	25.75	9.83	22.08	8.53	44.07
102	5	3.23	41.00	4.10	18.05	3.37	24.53	2.80	22.55	2.10	39.63
104	5	5.67	46.53	11.23	15.53	7.27	27.95	6.97	28.88	5.40	44.80
109	5	5.53	48.67	3.67	17.83	2.53	21.50	2.67	26.17	2.80	41.20
110	5	10.40	39.20	5.40	17.63	11.40	30.48	7.10	22.30	15.13	38.07
113	5	1.10	44.33	2.10	16.93	1.10	18.70	1.23	23.22	1.20	40.90

MURINE STUDY 2 – WEIGHT TRENDS

The weights of subjects in the 2nd murine study were measured at the same time as grip strength measurements were made. Weights were averaged per group for each week and trends were plotted, see below. At the pre-surgery time point, weights were grouped closely. The no treatment group showed steadily increasing weights over the course of 28 weeks. Groups 1-5 showed a slight initial decrease in the first week after surgery, but thereafter recovered and all groups maintained similarly increasing trends in weight as the no treatment group for the remainder of the study duration.



BIOGRAPHY OF THE AUTHOR

Nicklaus Carter was born in Blue Hill, Maine, on January 14th, 1993. He was raised in Franklin, Maine, and graduated from Sumner Memorial High School in 2011. During his four years at the University of Maine Nick was enrolled as part of the Honors College, majored in Bioengineering, and attained a minor in Chemistry. In his senior year he was invited to and joined the national engineering society, Tau Beta Pi. Nick graduated in May of 2015 magna cum laude and with high honors.

In September of 2015, Nick enrolled in a master's program in Bioengineering at the University of Maine. Before completion of the master's program, Nick transferred to a PhD program in Biomedical Engineering as part of the Graduate School of Biomedical Science and Engineering in January of 2017. After two years, January 2019, Nick became a PhD Candidate after defending his grant titled *Cellulosic Subdermal Implants for Narcotic Delivery*. Upon successful defense of his present work, *Nanocellulose Conduits for Enhanced Regeneration of Peripheral Nerve Injury*, and graduation in May of 2021 Nick aims to pursue a career in the biomedical device industry continuing to perform research and contribute to the field of science. Nick is a candidate for the Doctor of Philosophy degree in Biomedical Engineering from the University of Maine in May 2021.